Theoretical and Experimental Development of Bipolar Based Fluorescence Detection for Microchip Electrophoresis

by

Manjula B. Wijesinghe

Submitted to the graduate degree program in the Department of Chemistry and the Graduate Faculty of the University of Kansas in partial fulfillment of the requirements for the degree of Doctor of Philosophy.

_____
Chairperson- Prof. Susan Lunte

_____
Prof. Robert Dunn

_____
Prof. Michael Johnson

_____
Prof. James Blakemore

_____
Prof. Karen Nordheden

Dissertation Defense: April 25th, 2019

The Dissertation Committee for Manjula B. Wijesinghe certifies that this is the approved version of the following dissertation:

Theoretical and Experimental Development of Bipolar Based Fluorescence Detection for Microchip Electrophoresis

_____

Chairperson- Prof. Susan Lunte

Date approved: April 25th, 2019

Acknowledgements

There have been a lot of kind individuals who supported my thesis dissertation throughout the duration of my time here. I would like to express my sincere gratitude to all of them.

First and foremost, I would like to express my sincere gratitude to Prof. Susan M. Lunte. I will always be beholden to her for her immense support, exceptional kindness, and invaluable guidance during my dissertation work. Prof. Lunte gave me the opportunity to join her research group in January 2014. At that point, I was encouraged to carry out a challenging research project through her way of scientific thinking and mentoring. I would not have succeeded in that regard without her patience and guidance throughout the projects that I have performed during my doctoral studies here at KU. I must specifically mention that the flexibility that we are given in the lab inspired us to think critically and perform well as developing independent researchers. I have presented my research work as podium presentations and posters both nationally and internationally in 10 conferences. I was able to explore many areas of science, make lasting connections with other scientists in the field, and develop my presentation skills through these conferences. Full credit for paving the way to provide me with those invaluable opportunities should undoubtedly go to Dr. Lunte. Her support was enormous in editing abstracts and conference papers for submission. At the same, I would like to thank her for the funding support she arranged for all the conferences that I have attended. Dr. Lunte has nominated me for several travel grants in the department and from conferences to further support attending these conferences. I have also been nominated for departmental awards as well. I believe I don't have enough words to thank and acknowledge all the immense support and recognition that she provided me. The comments, suggestions, and corrections that Dr. Lunte gave me through my dissertation writing are sincerely appreciated and I thank you very much for helping me reach the end of my dissertation work.

Dr. Lunte, I sincerely apologize if I make you even a little bit sad by bringing your memories here. Even after she had a shocking loss in her family life, she consistently supported our research work through both group meetings and individual meetings. I was never able to imagine, even to this day, "How does Sue manage time to work on so many dissertations during last few years along with a ton of meetings, and handling Co-facilities". Again, thank you so very much for your kindness and support and all the guidance.

Dr. Craig Lunte was the chair of the Department of Chemistry at the time of our recruitment. I would like to express my sincere gratitude to you for selecting me as a graduate student to the department. At the moment of selection, I was in a very bad predicament and had almost given up doing a PhD because of the loss of 5 years of graduate studies. I do not intend to state the reason which put me in that situation here but I would like to state that it was even after I became a PhD candidate with a GPA of 4.0 together with a research publication and couple of departmental awards. Looking back at all these things, I cannot find sufficient vocabulary to thank Dr. Craig Lunte for giving me this invaluable opportunity to carry out my graduate studies at KU. Additionally, I will not forget the separations class that I had with Dr. Craig Lunte till his death. I am very sad that I do not have an opportunity to say "Thank you" to you. In my way of blessing to you, I would like to bless you as "Dr. Craig Lunte, may you attain nibbana".

I would like to thank the generosity of my oral comprehensive examination committee, which includes Prof. Michael Johnson, Prof. Heather Desaire, Prof. Yong Zeng, Prof. Chris Elles and Prof. Prajna Dhar, for giving valuable feedback on my research work. It was an honor for me to have such a prestigious set of individuals in my committee; Prof. Susan Lunte, Prof. Robert Dunn, Prof. Michael Johnson, Prof. James Blakemore, Prof. Chris Elles, and Prof. Karen Nordheden, I thank you very much and greatly appreciate your time, corrections and support.

I have been awarded the Bailey Memorial Scholarship from the Department of Chemistry at recruitment. I would like to greatly appreciate and thank the graduating recruiting chair Prof. Chris Elles and the other committee members at the time of my recruitment. Also, I have been awarded the Burton & Cheryle Mackenzie Scholarship from the Department of Chemistry and two travel awards: Kuwana Travel Award and Craig Lunte Memorial Travel Fellowship. I would like to express my special thanks to the department and both travel fund facilitators.

I was a teaching assistant for the first two years and it was a great pleasure for me to work with Prof. Mario Rivera, Prof. Heather Desaire, and Prof. Yong Zeng. Particularly, it was a great opportunity to work with the project-based learning class and hence I would like to thank you all. I should not forget to appreciate the enormous support I have received from Dr. Travis Witte, the director of the analytical and physical laboratory during teaching these classes. Thank you very much, Dr. Travis.

I have been a research assistant for more than 3 years supported by NSF and the University of Kansas funding. I greatly appreciate and thank both funding sources for giving me an opportunity to be a Jayhawk graduate student.

The work that I carried out required microfabrication in the clean room. All the support, guidance, and suggestions provided by Ryan Grigsby were enormous. He was my major resource person for microfabrication of devices for my research work. This is the time to express my special thanks to him for being such a great instructor. Additionally, I would like thank COBRE funding for the work carried out in the microfabrication lab.

The person who always takes care of our ordering, travelling, and various problems with a ton of kindness, i.e Cady Bush, you did an exceptional job for us in all directions. I know by now you even got interested in learning about our research work while being involved in editing,

document checking, and ordering. I would like to express my sincere gratitude to you as well. Also, I would like to thank Jan Akers as well.

Nancy Harmony supported the editing of many abstracts and manuscripts throughout my dissertation work. Thank you very much for your time, comments and edits. You are very familiar with the Lunte group's research work and that was very convenient for me in editing my work.

Dr. Dulan Gunasekara, one of my best friends from 2003, was my senior graduate student mentor in Dr. Lunte's group and I would like to express my sincere gratitude to him as well. I always say that "I am a follower of Dr. Dulan" in humor; well, it was true for many years and may be true in the future as well. The exceptional support that he gave me to get into graduate studies at the University of Kansas right after New Mexico State University is sincerely appreciated.

In 2014, I joined Dr. Lunte's group and found a nice and scientific environment to perform research. I would like to thank Dr. Joseph Siegel and Dr. Nathan Oborny for all the kind guidance that helped my work in the lab. Also, I would like to specially thank Joe for the support in editing, comments, and suggestions given during my oral comprehensive examination. I would also like to thank Dr. Rachel Saylor and Dr. Jessica Creamer for all support that I have been given particularly at the start of my work in Lunte's group. Abdullah, you were a brother to me in the lab; thank you very much to you for all the support, comments and suggestions that you provided me.

Giuseppe Caruso and Claudia Fresta, our Italian family in the group, it was a great pleasure to work with you two for the ~2 years that you both were with us. I would like to thank you two for collaborating with me for your work and supporting me to get several publications with you.

Kelci Schilly, the most popular and supportive person to the Sri Lankan graduate student community, I should deliver my sincere gratitude to you as well. You were the editor of most of

my writing including this dissertation. Thank you very much Kelci, you have always supported me like a sister, a friend, and a colleague. I wish you all the best with your future endeavors.

Shamal Gunawardhana, you were with me in the same research group for 10 years! I shall never forget the times that you made us laugh with funny stories as well as other times where your comments relaxed our minds. Also, your support during my comprehensive examination needs to be thankfully and sincerely acknowledged. At the same time, valuable research discussions, support in the lab as well as the support given by you and your wife Mihiri in general life was enormous. I wish you all the best to your future success. My blessing to you, "attain nibbana or the way to the nibbana within this life".

I would like to specially thank my artistic colleague Dhanushka Weerasekara for all the support on editing figures whenever I needed help, and in my research. Specially, your massive support to me in finishing my dissertation nice and fast is truly appreciated. Also, you and your wife Chamalee were my neighbors for several years and both of you have supported me in general life apart from professional life. Again, thank you so very much again to both of you and wish you two all the best.

You two, Galina and Emily, thank you very much for all the support in the group. Indika Warnakula, you are the official follower of my work. I have received a great support from you even though you just joined the group. Thank you very much and I gratefully acknowledge you as well. I wish you all will succeed throughout your graduate carrier.

Our visiting professors Leena and Ebru, it was a great pleasure to work with you and thank you very much for all the support. Our undergraduate researchers Anton, Garet, Alexis, Paige, and Esha, thank you all. Anton, your support to my research is thankfully acknowledged.

Now, it is the moment to thank all of whom that are part of the Sri Lankan community. First, I would like to mention my friend Dr. Kasun Imaduwage, who was with me in graduate school since 2008. You and your wife Malika's support with my studies and particularly in general life was substantial. I will never forget any of it. Everyone in the Sri Lankan community, starting from my great teaching assistant from 16 years ago Dr. Chamani, Nalin, Dr. Kumuditha, Loshini, Dr. Susanthi, Rohan, Kavisha, Sasanka, Nilan, Shiwanthi, Thilina, Sumudu, Thilanga, Achala, Harshani, Nishantha, Milani, Gihan, Dimuthu, Pubudu, Indeewara, Uditha, Hasini, Chanaka, Priyanka, Sachini, Pamodha, Sanjaya, Chathurika, Charuni, Sachindra and Dilupa. Thank you all very much for all of your support to make my life happy and smooth in Lawrence. You all are great and did not make me feel alone in Lawrence.

I should not forget to thank and sincerely express my gratitude to several professors at New Mexico State University including Prof. Gluhen Kuhen, Prof. Amudhu Gopalan, Prof. David Smith, Prof. Garry Eiceman, and Prof. James Herndon. You all supported us to recover after a huge loss of time in my life and to find a better place, which is thankfully appreciated. Prof. Antonio Lara and Dr. Nicholas Beltran, thank you very much for keeping me in your group during my transit from NMSU to KU.

Also, I want to thank all my Professors at University of Peradeniya. First, I would like to thank Dr. Athula Bandara, my undergraduate research advisor for all the support and guidance. Also, I would like to thankfully acknowledge Prof. Veranja Karunarathne for keeping me as a teaching assistant for 2 additional years. I should also thank Prof. Namal Priyantha, Prof Ayanthi Navarathne, Prof. Needra Karunarathne, Prof. Chandrani Perera, Prof. Rathnayake Bandara, Prof. Gamini Rajapakse, Dr.Champika Vithana, and Dr. Vajira Senevirathne.

Now, all these would not be possible if not for my parents, Mr. Heenbanda and Mrs. Swarna Menike. I know I was the physically weakest child in the family and gave the most pain particularly in my childhood to both of you. The debt that I owe to you is difficult to pay off during the rest of my life. The effort that you two took during my childhood is substantial. However, My Dad, you decided to leave my Mom, Sisters and Me 19 years ago solely at your decision to start a new family of your own. I am stating this not to blame you but to ensure that I am giving a fair respect to Mom's efforts after the year 2000. Dear Dad, I thank you and appreciate your financial support to us during the period of my undergraduate university education. Dear Mom, I know that a huge responsibility fell on you after 2000, with so many difficulties and problems. After the year 2005 our lives got much better and I feel now we have a more stable life. My sisters, Subhashini and Sagarika, and my brother-in-law, thank you so much for your contributions and support to the family. I would like to specially thank both my sisters, particularly Sagarika for taking care of our mom for many years now and I am dying to get back to you all!!

I tried my best to acknowledge everyone who supported me throughout my career here at KU. If, I forgot someone, I greatly apologize.

Abstract

Methods for the separation and detection of reactive oxygen and nitrogen species (RNOS) at the cellular level can be useful tools for the study of the biochemical mechanisms of neurodegenerative diseases. Microchip electrophoresis (ME) is a promising analytical separation technique that can be used to separate these short-lived RNOS since it offers sub-minute analysis times, low sample volumes, and the ability for single cell analysis.

Amperometric detection is one of the most popular detection methods for ME and has been used for the detection of RNOS and related antioxidants. In this thesis, a dual-channel/dual-parallel electrode system is developed to identify electroactive species based on their redox properties without the need for complicated data correction procedures. This new strategy was applied to distinguish nitrite from azide in a cell sample. Azide is a contaminant that is introduced by the filters used to remove cell debris.

Microchip electrophoresis can also be coupled to fluorescence detection (FL) for the investigation of RNOS production in macrophage cells using different fluorescent dyes for specific RNOS that exhibit similar excitation and emission wavelengths. Using ME-FL, the effect of engineered carbon nanoparticles on ROS production by microglia and lung epithelial cells was investigated.

In this dissertation, a novel detection method for ME was developed that takes advantage of both electrochemical and fluorescence detection. This method involves transforming an electrochemical signal to a fluorescence signal using a bipolar electrode. The new method was evaluated with two model reducible analytes using 2,7-dichlorodihydrofluorescein ($DCFH_2$) as the fluorescence reporter. In addition, modeling of the ME-bipolar electrochemistry/ fluorescence experimental setup was performed using COMSOL Multiphysics. Programs were developed to

generate bipolar cell voltammograms and to model the effect of the flow rate on the size of the fluorescence plug formed at the detector electrode.

As a result of these studies, a bipolar fluorescence detection method was developed that was able to obtain low micromolar detection limits for reductive analytes. The method was further developed to obtain the bipolar fluorescence response without a potentiostat and with a simplified experimental setup. This development will be extended in the future to detect oxidizable analytes such as RNOS in cells. Additionally, chemiluminescence reporting can be used instead of fluorescence reporting to obtain better detection limits. Lastly, this system could be coupled to a miniaturized optical detection system to develop a portable microchip device capable of detecting electroactive species on-site.

Table of Contents

List of Figures

List of tables

1. Chapter 1: Fundamentals, design and applications of microchip electrophoresis coupled to amperometric detection

This chapter is based on the following publication.

Gunasekara, D. B.; Wijesinghe, M. B.; Saylor, R. A.; Lunte, S. M., Chapter 3 Principles and Strategies for Microchip Electrophoresis with Amperometric Detection. In *Electrochemical Strategies in Detection Science*, The Royal Society of Chemistry: 2016; pp 85-124.

1.1 Introduction

Electrophoresis in a microchannel format was introduced in the mid-1990s and became an influential separation technique with widespread use in lab-on-a-chip devices.[1-2] The principles of microchip electrophoresis (ME) are similar to that of electrophoretic separations performed in a fused silica capillary. ME separations are performed in micron- to submicron-sized channels fabricated in planar substrates composed of different materials. The small dimensions and the planar format of ME make it possible to integrate it with a variety of detection techniques, therefore expanding the applications of ME in separation science.

Detection techniques that are commonly used with CE, such as amperometry, conductivity and laser induced fluorescence (FL), can be easily adapted for use with ME. However, although UV detection is extensively used with CE, its integration with ME is complicated owing to the smaller dimensions of the microchip format and the difficulty of setting up the optics. The most widespread detection method for ME is FL, due to its low background, nanomolar to picomolar detection limits, and the ability to directly focus a laser beam onto the separation channel either through an inverted microscope or using fiber optics. However, FL generally requires derivatization of the analyte of interest with a fluorescent probe, which is an extra step during the sample preparation that can lead to selectivity issues depending on the specificity of the probe. Additionally, in order to extend the applicability of FL for a portable microchip device, further developments to miniaturize the FL optical detection system is necessary.

Electrochemical detection is an attractive detection method for ME because of the feasibility of miniaturization and the ability to detect many molecules directly. The ability to directly integrate electrodes into the microchip format is one of the primary advantages of ME with electrochemical detection (ME-EC). Microelectrodes fabricated directly on the substrate can be used without

sacrificing sensitivity or the limits of detection (LOD) obtained with macroelectrodes. In addition, many different types of materials, regardless of their optical transparency, can be used as substrates. The availability of low cost portable potentiostats enhances the miniaturization capability of ME-EC and its suitability for a point-of-care device. Moreover, many small biologically important molecules are electrochemically active; therefore, ME-EC has many applications in the field of bioanalysis.[3-9]

This chapter will discuss the fundamentals of ME separations followed by a discussion of theoretical and experimental aspects of the integration of ME with one of the most extensively used detection methods, *i.e.* electrochemical detection. In addition, the application of a variety of electrode materials and different electrode alignment strategies to enhance sensitivity and LODs will be described. Lastly several illustrative applications are provided.

1.2 Principles of microchip electrophoretic separations

The chip design shown in Figure 1.1 (a), the simple-t, is the most frequently used configuration for microchip electrophoretic separations. The simple-t consists of three side channels and one separation channel that are all filled with separation buffer. In a typical electrophoresis experiment, sample is loaded into the sample reservoir (S) and the analytes are separated by an applied electric field across the separation channel.

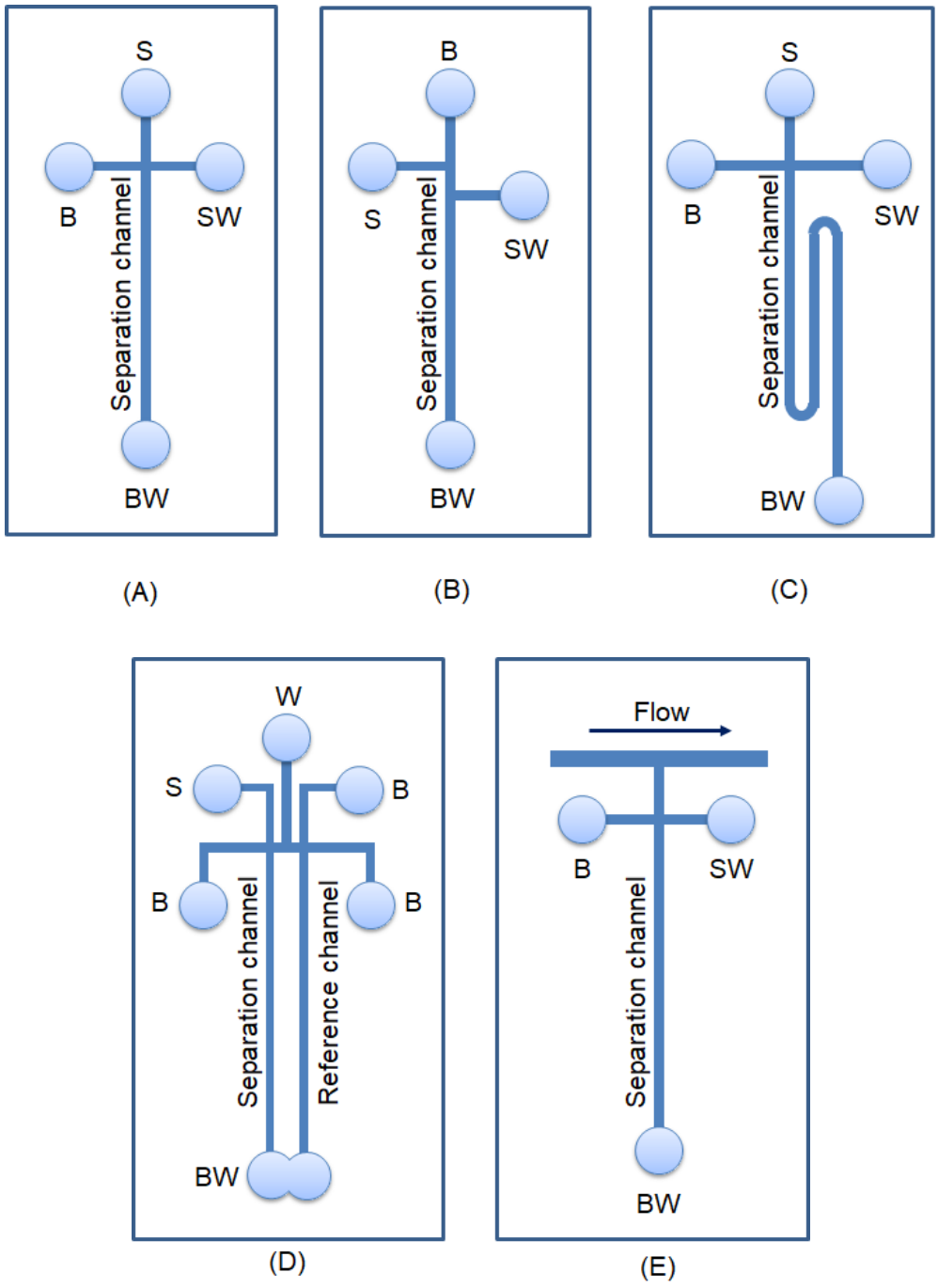

Figure 1.1 Schematics of various designs available for microchip electrophoresis (A) simple t design (B) offset-t design (C) serpentine design (D) dual-channel design (E) double-t design. S-sample, B-buffer, SW-sample waste, BW-buffer waste

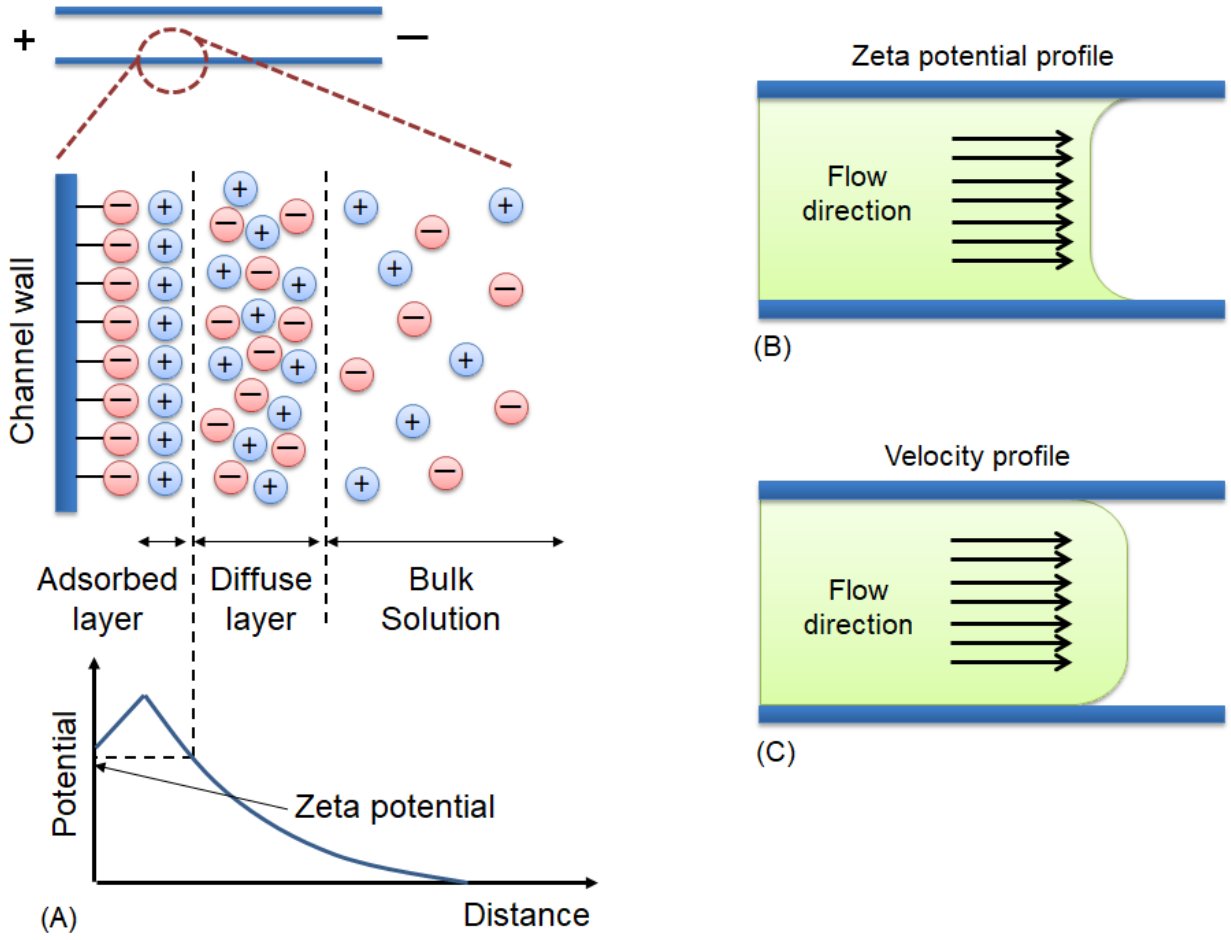

Figure 1.2 Schematic of electrical double layer (A) potential distribution with the distance from the channel wall (B) zeta potential profile along the cross section of the channel (C) shape of the electroosmotic flow along the cross section of the channel

Most ME-based separations are performed on silica or silicate-based substrates. The silanol groups on these surfaces have a pKa of 3-10; therefore, when using buffers with pH values higher than 3, protons are abstracted and negative charges are formed on the surface. These negative charges are partially balanced by oppositely charged counter ions available from the buffer solution. This immobile layer of oppositely charged ions is known as the adsorbed layer (Figure 1.2A). A diffuse layer of mobile cations that decays into the bulk solution neutralizes the remaining

charges on the capillary wall.[10-11] The distribution of these ions near the capillary wall forms the electrical double layer and the potential difference across this layer is known as the zeta potential (Figure 1.2A). Zeta potential decays exponentially towards the bulk solution and its magnitude depends on the thickness of the double layer and the charge density (σ).

The double layer thickness (δ) and the zeta potential (ξ) are governed by the following equations.

$$\delta = \left[\frac{\varepsilon_r \varepsilon_0 RT}{2cF^2}\right]^{\frac{1}{2}} \quad 1.1$$

$$\xi = \frac{\delta\sigma}{\varepsilon_0\, \varepsilon_r} \quad 1.2$$

where ε_r – relative permittivity of the medium, ε_0– permittivity of a vacuum, *R*- universal gas constant, *T* – absolute temperature, C – molarity, F- Faraday constant

Upon application of a positive voltage across the channel, ions in the diffuse layer migrate towards the cathode (ground electrode), dragging water molecules with them and causing flow. This flow, called electroosmotic flow (EOF), carries all the analytes present with the bulk solution toward the cathode, regardless of their charge. The EOF flow velocity is only sluggish at the channel surface and therefore the rest of the channel experiences plug flow (Figure 1.2C) and exhibits less band broadening compared to hydrodynamic flow.[10-11]

In microchip separations, a high voltage is applied relative to a ground by placing Pt leads in each sample reservoir, buffer reservoir, buffer waste reservoir, and sample waste reservoir. A net current flow through the solution due to the movement of ions is generated and its magnitude is based on the applied potential and the resistance of the solution. The resistance of the solution inside the channels is determined by both the conductivity of the buffer and the channel dimensions. Due to the high voltages applied across the channel and the current flow between the

ground and high voltage electrodes, it is possible for redox reactions to take place at each Pt electrode.[8] The nature of the reaction is dependent on the background electrolyte (BGE) composition. With aqueous BGEs, water oxidation can occur at the anode (positive electrode) and reduction at the cathode (negative electrode), generating hydrogen and oxygen gas, respectively.[12]

Cathode: $2H_2O + 2e^- \rightleftharpoons H_2 + 2OH^-$ (–0.828 vs. NHE)

Anode: $O_2 + 4e^- + 4H^+ \rightleftharpoons 2H_2O$ (+1.229 vs. NHE)

In an electric field, charged analytes are attracted towards the oppositely charged electrode by electrostatic forces (*Fc*), which are balanced by frictional forces generated due to the movement of analytes through the solution (*Fr*). The charged analytes reach a steady state velocity (υ) within a negligible amount of time. These forces and their effect on analyte velocity are described as follows:

$$Fc = qE \tag{1.3}$$

$$Fr = 6\pi\eta a\upsilon \tag{1.4}$$

$$\upsilon = \frac{q}{6\pi\eta a}E \tag{1.5}$$

$$\upsilon = \mu E \tag{1.6}$$

Where *E* is the electric field, *q* is the charge of the analyte, η is the viscosity of the medium, and *a* is the hydrodynamic radius. The quotient ($q/6\pi\eta a$) represents the electrophoretic mobility, denoted by μ_{ep}. The electrophoretic mobility of a given analyte depends only on two properties of the analyte. These are its charge (*q*) and hydrodynamic radius (*a*) since the viscosity is a constant for a specific BGE. Therefore, in the simplest form of microchip electrophoresis, called zone electrophoresis, the separation is based on the ratio of the charge to hydrodynamic radius of the ion. The migration time of an analyte is determined by both the electrophoretic mobility of the

ion and the electroosmotic flow generated in the channel (electroosmotic mobility). The net apparent mobility is given by the vector sum of these two terms as shown in Equation 1.7[10-11]

$$\mu_{app} = \mu_{ep} + \mu_{e0} \quad 1.7$$

$$\upsilon_{eof} = \left(\mu_{ep} + \mu_{e0}\right) E \quad 1.8$$

The velocity of the electroosmotic flow depends on the applied electric field strength (*E*) as shown in Equation 1.8. Therefore, the field strength is a major factor determining the time frame of the analysis.[11] Very fast (sub-minute) analysis times have been achieved with microchip electrophoretic separations with high field strengths (500-1000 V cm^{-1}).[13]

The applied electric field can be either positive or negative. Separations with positive polarity are known as "normal" polarity separations and negative polarity separations are known as "reverse" polarity separations. In the normal polarity mode, cations migrate towards the cathode and the electrophoretic mobility and electroosmotic flow mobility are in the same direction. Therefore, small cations elute first in this mode of separation. For anions, the direction of electrophoretic mobility and electroosmotic flow mobility are opposite, allowing more time for the establishment of separation. However, the magnitude of the electroosmotic flow must be higher than the electrophoretic mobility of the anion in order for it to be carried towards the detector. Therefore, small highly mobile anions, such as nitrite, may not be detected at the cathode under normal polarity owing to their high negative electrophoretic mobility. In zone electrophoresis, neutral analytes are carried with the electroosmotic flow and thus cannot be separated from one another.[10-11]

Anions with high negative charge density are often separated using the reverse polarity mode. In reverse polarity separations, the surface of the separation channel needs to be modified so that the electroosmotic flow mobility is towards the anode where the detector is placed. This

can be accomplished through the addition of cationic surfactants, such as tetradecyltrimethyl ammonium bromide (TTAB), tetradecyltrimethyl ammonium chloride (TTAC) and cetyl trimethyl ammonium bromide (CTAB) to the run buffer. A graphical representation of normal polarity and reverse polarity modes is given in Figure 1.3.

In reverse polarity separations, the mobile layer of the electrical double layer is composed of negative charges and thus the electroosmotic flow mobility is towards the ground electrode (ground is relatively positive). The apparent electrophoretic mobilities of small, negatively-charged analytes are the highest under these conditions and therefore these species reach the detector first. Small, positively-charged analytes elute last, given that their mobilities are lower than that of the electroosmotic flow mobility. This order of migration of analytes is opposite to the normal polarity separation order.[10-11]

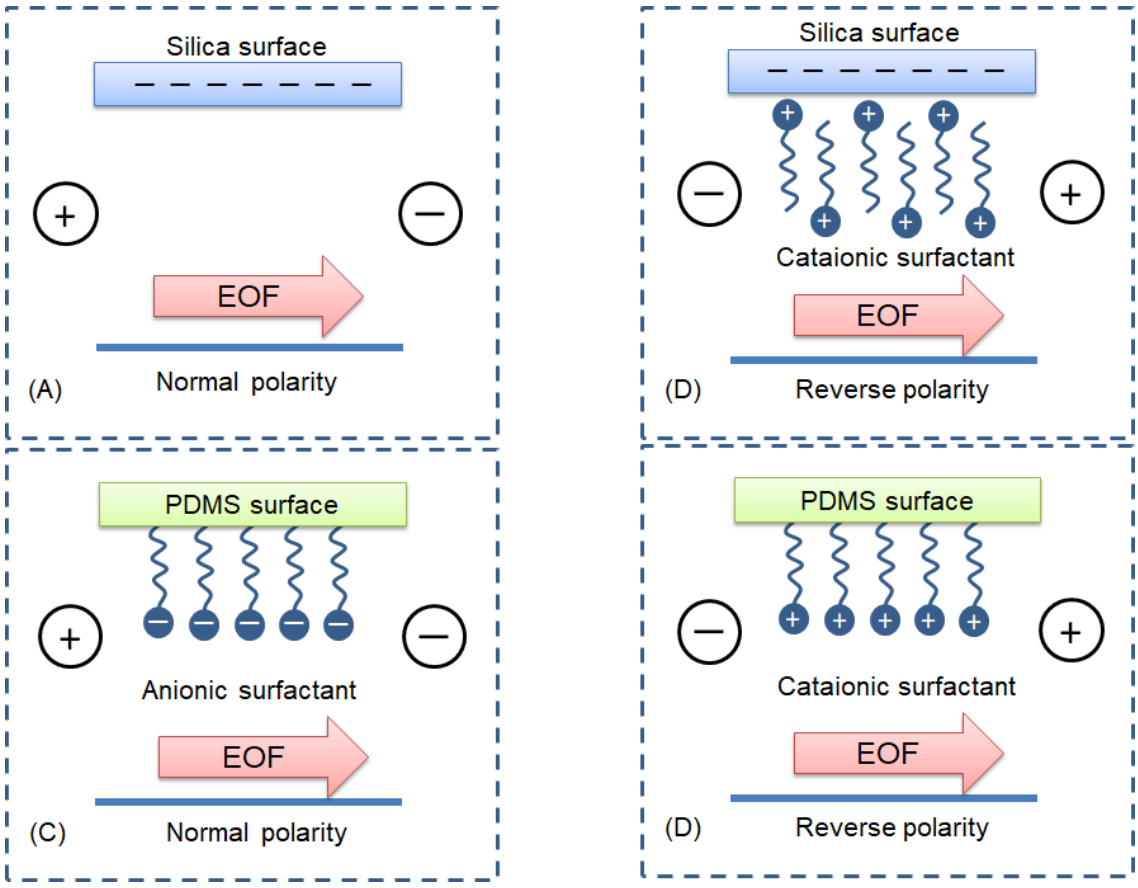

Figure 1.3 Surface charge and the direction of EOF of (A) unmodified silica surface or silica-based channel under normal polarity mode (B) silica surface modified with a cationic surfactant under reverse polarity mode (C) PDMS surface or a polymer modified with an anionic surfactant under normal polarity mode (D) PDMS surface or a polymer modified with a cationic surfactant under reverse polarity mode

Microchannels used for microchip electrophoresis can be fabricated in many different materials including glass, polydimethylsiloxane (PDMS), poly(methyl methacrylate) (PMMA), and ceramics.[14] A glass surface produces a substantial EOF at pH > 3 due to the presence of ionized silanol groups. However, modification of channels fabricated with polymer-based materials is often necessary as they do not contain a sufficient charge on their surface. Different techniques

have been used for the surface modification of polymer surfaces including dynamic modification with a surfactant, plasma oxidation, and inclusion of charged chemical moieties into the polymer matrix.[15]

1.3 Different electrokinetic injection methods with corresponding chip designs

The possibility for addition of numerous functionalities, such as sample preparation, preconcentration, microdialysis sampling, and on-chip cell lysis, is an inherent advantage of the microchip format. The simple -t format is the most uncomplicated and popular chip design for ME. Other chip formats including the double-t,[4] offset-t, serpentine channel and dual-channel have been described in the ME literature (Figure 1.1).[4, 16-19]

In general, electrokinetic gated injections have been used for the introduction of sample to the separation channel with all aforementioned chip designs except offset-T. This steps in the electrokinetic injection process are shown in Figure 1.4A-C.[16-17, 20] With this injection method, high voltages are applied to both the sample and buffer reservoirs to establish a gate. During injection, the buffer voltage is floated for a few seconds to allow sample to enter the intersection (Figure 1.4B). The gate is then reestablished (Figure 1.4C) and the separation is initiated when the buffer voltage is reapplied.

One drawback of using electrokinetic (EK) injection is that sample introduction into the separation channel is influenced by both the polarity of the applied voltage and electrophoretic mobility of the species. This phenomenon is known as electrokinetic bias and it is proportional to the difference of the electrophoretic mobilities of the analytes. Simply put, small cations are favorably introduced into the separation channel in normal polarity separations, while small anions are more favored in reverse polarity separations. This differentiation in injection among analytes is useful at times when a selectivity towards one analyte over an oppositely charged species is

desired. Minute changes in the EK injection conditions can change the sample injection volume as it depends on several factors, namely injection time, applied voltages, buffer pH, and ionic strength. The sample injection volume can be computed by knowing the electroosmotic flow velocity, injection time and the area of the channel.

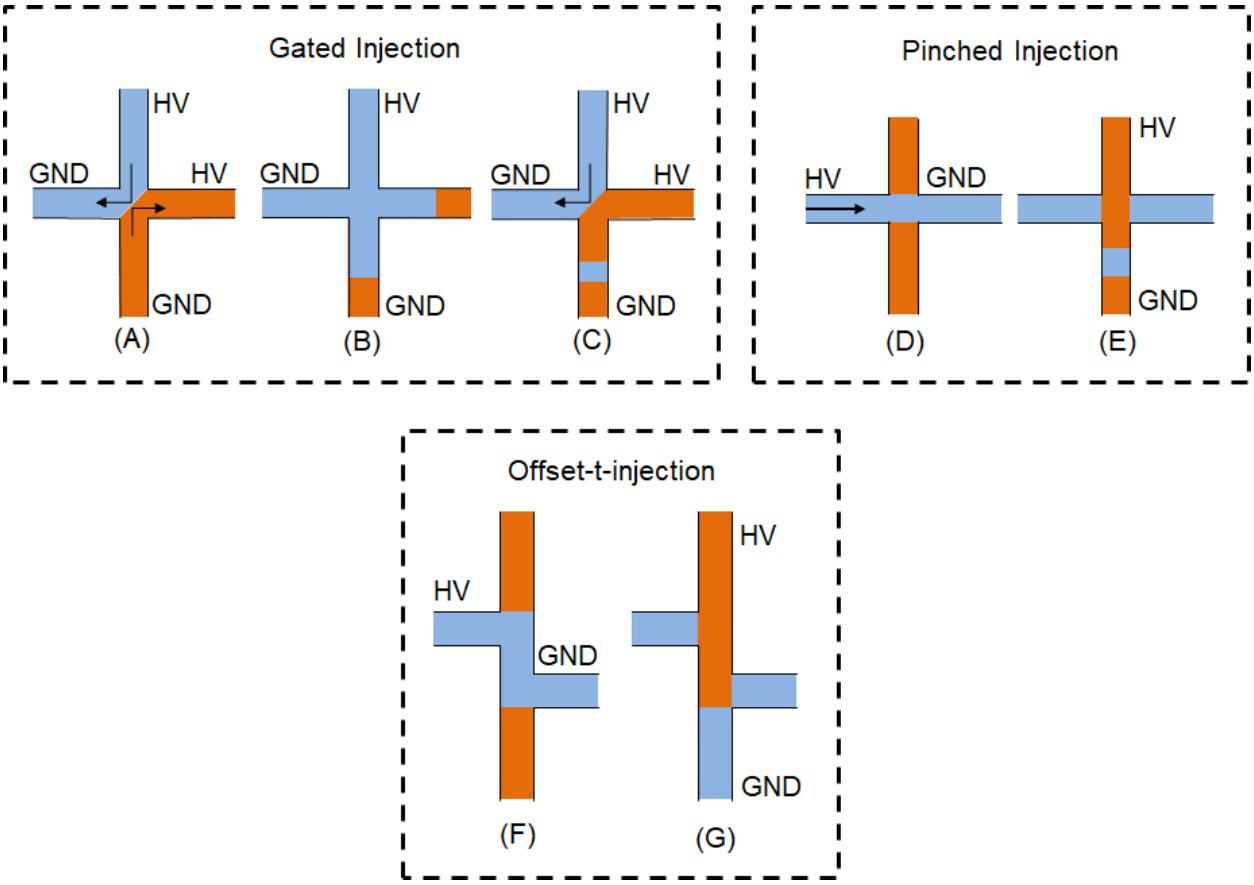

Figure 1.4 Sample injection for microchip electrophoresis. (A)–(C) Gated injection in a simple-t or serpentine channel device; (D) and (E) pinched injection in a simple-t or serpentine device; (F)–(G) defined volume sample injection using an offset-T device

When using electrochemical detection, an electrokinetic gated injection produces a characteristic signal in the electropherogram at the time of injection owing to the instantaneous change in the field strength and, therefore, the charging current at working electrode. This is

beneficial for the accurate determination of migration times of species that can be calculated relative to this reproducible signal at the injection point. The electric field strength across the separation channel is a function of the applied voltages and can be calculated by applying Kirchhoff laws (Figure 1.5).[18]

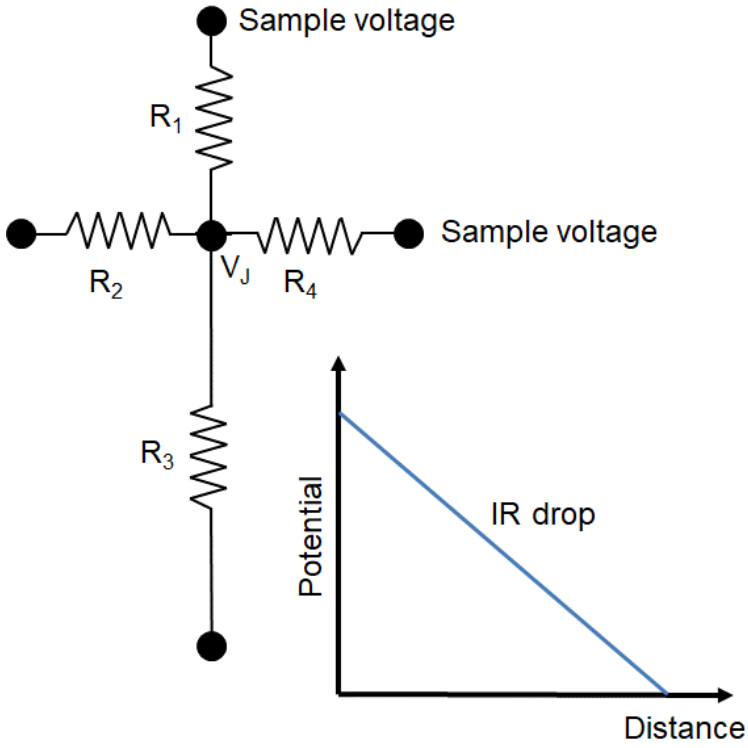

Figure 1.5 Equivalent electric circuitry that can be used for field strength calculations using the junction voltage (V_J)

A second popular injection mode is pinched injection. In this mode, the sample plug is defined by the geometric area of the chip intersection. For pinched injections, only one high voltage power supply is necessary. This is an advantage over the gated injection mode, where two separate power supplies are required. To make an injection, sample is loaded into one of the reservoirs located at the side channels perpendicular to the separation channel. A high voltage is

then applied to the sample-containing reservoir, while the oppositely-faced reservoir is grounded. This causes the horizontal channel to be filled with the sample (Figure 1.4D). A high voltage is then applied across the main separation channel, resulting in an injection of an analyte plug equivalent to the size of intersection, which then is followed by an electrophoretic separation (Figure 1.4E). This mode of injection can be used with both the simple-t and simple-t serpentine chip designs (Figure 1.1A and C).

The third injection approach is the offset-t chip design (Figure 1.4F). In this case, the injection volume is determined by the vertical distance between the two side channels, the channel depth and the channel width. The injection protocol for this chip design is similar to that of the pinched injection, in that a high voltage is applied across the horizontal channel to fully fill it with sample. After that, a voltage is applied across the separation channel to achieve the electrophoretic separation (Figure 1.4G)

Mixtures of analytes with close migration times can be difficult to resolve when using short (1-5 cm) microchannels. However, the fabrication of channels longer than 5 cm is a challenge due to the limitations in the wafer size of available substrates. The 4-inch silicon wafers that are commonly used in microelectronic device production are also used extensively for the fabrication of PDMS microchips using photolithography. The fabrication of long straight channels is therefore difficult. This has been addressed by designing serpentine channels as shown in Figure 1.1C.

One of the concerns that has arisen in the implementation of the serpentine channel design is band broadening owing to the use of the same channel width at the curved sections as of the straight section. This effect is termed the “race track effect” and results in lower peak efficiency and thus a decrease in the resolution. The race track effect has been modeled and the effect has been overcome by narrowing the channel widths around the corners in comparison to the straight

sections. Additionally, the lengths and the position of side arms must be designed to get an efficient injection with gated injection method.[21]

Another channel design approach that has a key advantage for electrochemical detection is shown in Figure 1.1 D. This dual-channel design has been used for electrochemical background subtraction for in-channel amperometric detection to improve the signal-to-noise ratio.[19, 22] Equal amounts of samples are introduced into two identical channels during the dual channel separation using two electrokinetic gates. More details about this approach is given in the sections 1.6.3 and 1.9.2.2.

Double-t chip designs have been developed (Figure 1.1 E) for coupling ME with the continuous flow of microdialysis sampling.[23-25] The mode of sample injection used with this design is known as flow-gated injection, as it is determined by both the hydrodynamic flow and the applied voltage. A continuous flow is established through the upper horizontal channel by means of a microsyringe pump. A high voltage is applied at one of the side-arm reservoirs while grounding at the opposite reservoir and the bottom reservoir at the channel end. A high voltage at the gate is then floated for a few seconds for sample introduction and then reapplied to reestablish the gate. ME has been successfully coupled to microdialysis sampling using this double-t design to facilitate both *in vitro* and *in vivo* monitoring of various biologically important molecules.[4]

As a substitute for flow-gated devices, valves have been used also to integrate microchip electrophoresis with continuous flow streams such as microdialysis.[26] Discrete sample injections into the separation channel are achieved by pneumatically-operated valves fabricated from PDMS. The first attempt to couple ME and microdialysis with amperometric detection was based on pneumatic valves. Advantageously, these devices do not introduce a bias in the sample injection as does electrokinetic gated injection.[27]

1.4 Electrochemical Detection

Amperometry is preferred over potential scanning methods such as voltammetry for electrochemical detection in ME due to its lower background currents, higher sensitivities, and low LODs, as well as its low cost.[28] However, the selectivity of amperometry towards different redox species at a single working electrode is determined by their formal potentials and the applied potential at the working electrode. In amperometry at a single electrode, analytes must be detected at different potentials using multiple ME injections in order to obtain voltammetric information. This inability to differentiate species based on redox potential is a disadvantage compared to voltammetric methods. However, this deficiency can be addressed through the use of multiple electrodes or modified electrodes. Fast scan voltammetry can provide better selectivity with sufficient temporal resolution to couple with ME, but advanced and expensive potentiostats and faraday cages are necessary to obtain a voltammetric response with reduced noise.

1.4.1 Amperometry

In amperometric detection, a constant potential sufficient to oxidize or reduce the electrochemically active analyte is applied to the working electrode with respect to the reference electrode. To maximize the current response, the applied potential should be at the steady state current plateau for the analyte of interest. Making the measurement in this region will also enhance the reproducibility of the peak currents obtained in ME-EC, as slight changes to the potential on the working electrode will not cause a significant change on the current response. This region can be estimated in two different ways. In one, a cyclic voltammogram (CV) is recorded for the analyte using the same electrode material and background electrolyte used for the microchip separation and the peak potential is determined. The optimal applied potential is a few tens of millivolts above the peak potential. However, one drawback of using CV to obtain the optimal detection potential

is that it does not take into account the effect of separation voltage on the applied potential. Therefore, this is not usually an ideal way of determining the optimal detection potential for ME-EC.

In the second, more rigorous approach, a hydrodynamic voltammogram (HDV) is constructed for each electroactive species of interest. First, peak currents are determined from electropherograms obtained for a range of working electrode potentials. The current (peak height) is then plotted against the applied potential to construct the HDV. The mass transport of analyte to the working electrode is determined by both the size of the electrode and the plug flow caused by the electroosmotic flow. All these factors lead to a steady state transport of species to the electrode and thus the HDV displays a sigmoidal shape.[29] The plateau potential can then be used as the optimal potential for the ME-EC detection.

The efficiency of amperometric oxidation or reduction of the analytes at the working electrode in ME-EC is typically in the range of 20-30%.[30] The highest current that can be obtained under the influence of convective flow can be calculated by adopting the Faraday equation as shown below.[29]

$$I_{limit} = nF(C_i - C_f)u \qquad 1.9$$

Where I_{limit} is the limiting current or the steady state current of the HDV, n denotes the number of electrons involved in the redox process, F is the Faraday constant, C_i is the initial concentration of the analyte in the sample plug, C_f is the final concentration after the redox process, and u is the linear velocity of the analyte.

The number of electrons involved, the linear velocity of the analyte, and the initial concentration of the analyte are all known quantities. The conversion efficiency must be known to calculate the C_f. The conversion efficiency can be computed by dividing the charge or current

produced at the electrode with ME-EC by the charge or current expected for the same amount of analyte according to Faraday's law.[29] It should be noted that the conversion efficiency for ME-EC under one set of conditions may differ significantly from another as it depends on several factors including electrode alignment, mode of injection, and changes in the flow rates. Thus, the conversion efficiency calculations must be performed cautiously.[29]

$$Q = nF \qquad 1.10$$

In coulometry, 100% electrolysis of the electroactive analyte is observed at the electrode. In this scenario, the number of moles in the analyte plug can be calculated directly by Faraday's law (Equation 1.10) given that the peak area (charge) due to full electrolysis is known as well as the number of redox electrons involved.

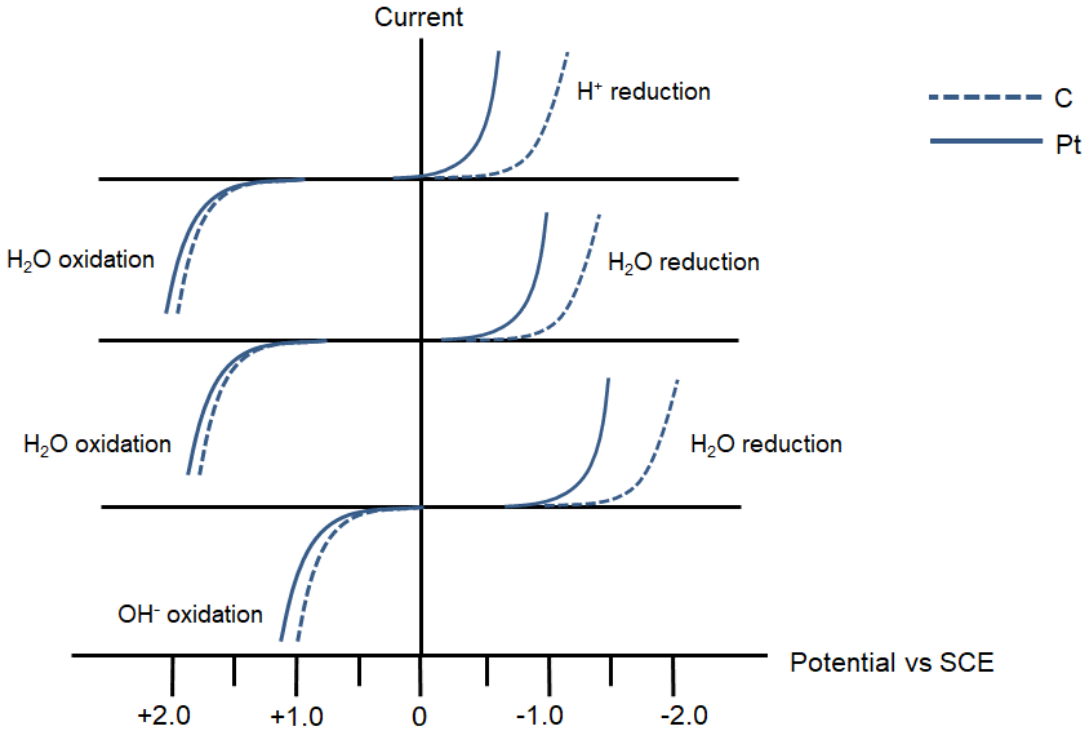

Figure 1.6 pH dependence on the potential window for carbon and platinum electrodes in aqueous media. Data for this figure were obtained from ref. 12, 31–33.

ME-EC is most frequently performed in the oxidative mode. The potential window for aqueous neutral solutions is limited primarily by the oxidation of water at positive potentials and reduction of oxygen at negative potentials. Both of these processes result in a high background current. Many important biomolecules are oxidizable but not reducible within this potential window. Therefore, ME-EC in the reductive mode can be challenging and requires proper degassing and isolation of the BGE from air. The actual active potential window depends on many factors including composition of the BGE, pH of the run buffer, and the type of electrode material used (Figure 1.6).[12, 31-33] Under acidic conditions, proton reduction is the determining factor for the cathodic potential window and hydroxide ion oxidation limits the anodic potential window for basic solutions. These limitations can be overcome by using modified electrodes or non-aqueous BGEs. With non-aqueous BGEs, the key factor determining the electrochemical potential window is the stability of the electrolyte at high potentials.

1.5 Interaction of Separation Field with the Working Electrode

In ME with amperometric detection, the working electrode needs to be placed at a position where the effect of the separation voltage will not damage the potentiostat or the working electrode. This issue has been addressed by developing different electrode alignment configurations and using battery-operated "isolated or floating" potentiostats. A theoretical discussion of the interaction of the separation field with the working electrode potential will be discussed first as it is useful in understanding the use of different electrode configurations later in this dissertation.

An electric field between 100 and 1500 V cm^{-1} is typically required for electrophoretic separations. The separation current generated due to the mobility of ions between the high voltage electrode and the ground electrode is in the range of microamperes. The magnitude of the current is determined by both the applied voltage and the conductivity of the solution according to Ohm's

law. The potential field across the solution interacts with the working electrode if it is placed inside the separation channel, thus changing the actual voltage felt by the electrode (effective voltage). This is the fundamental restriction of the integration of ME with EC.[34-35] The high voltage that is often powered by AC contains fluctuations and smoothing of these high voltage outputs are difficult due to the magnitude of the output. These fluctuations in the voltage output can cause small changes in the effective voltage felt by the electrode. This increases the noise observed in ME-EC compared to LC-EC and increases the LODs. Another potential problem is that Joule heating due to high separation currents can damage thin film electrodes that are used in the microchip format. In certain instances, the placing of working electrodes and the unexpected alignment changes during the experiment can cause the separation currents to ground through the potentiostat and damage it.

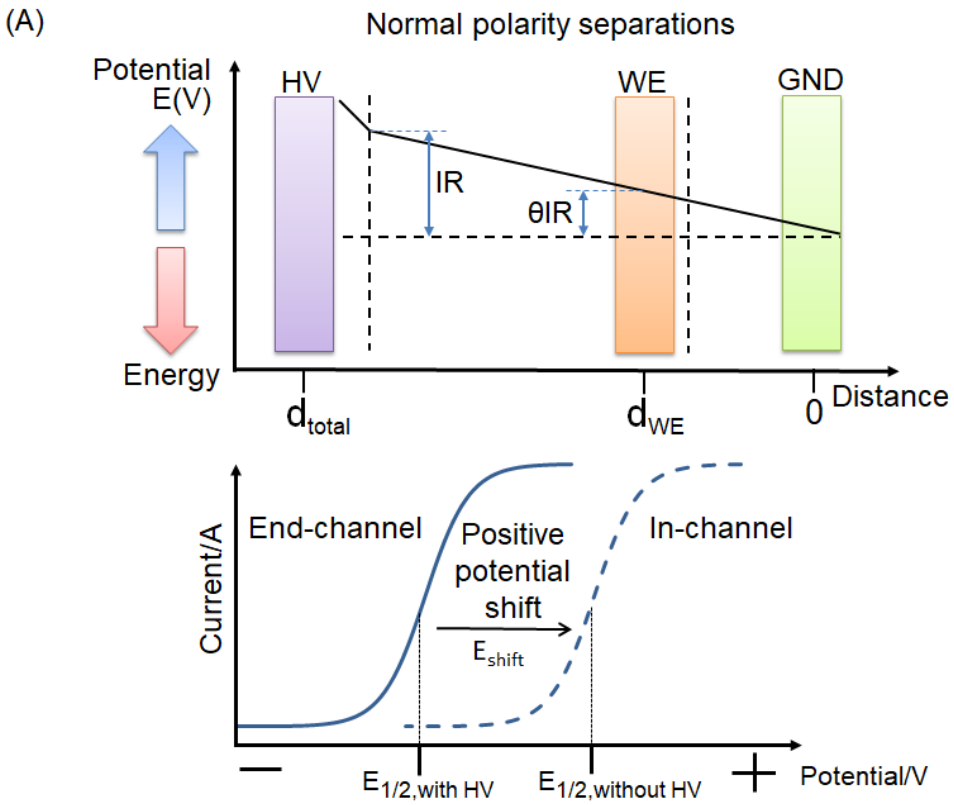

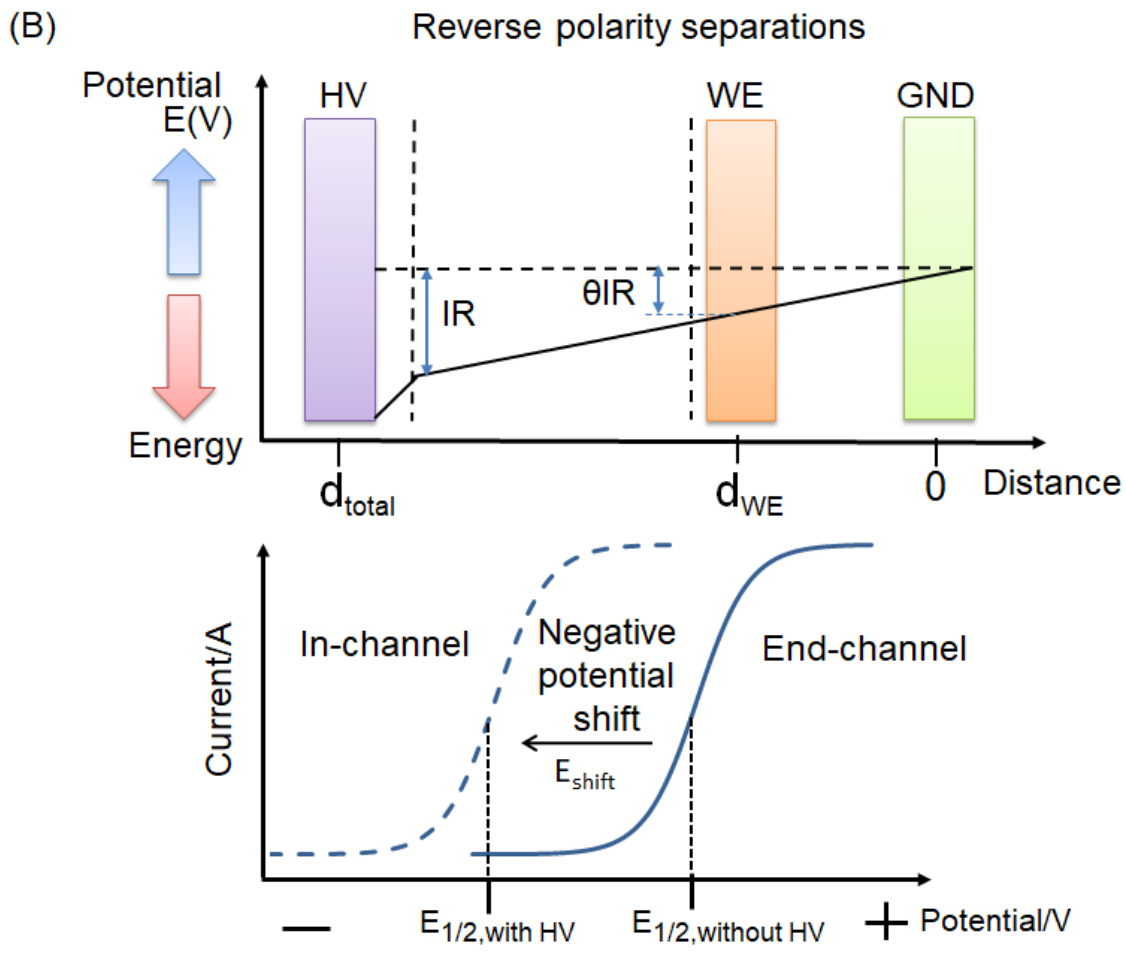

Figure 1.7 Potential versus distance diagram for normal and reverse polarity separations. The potential drop across the channel and representative potential shift in the HDV for (A) a normal polarity and (B) reverse polarity separation. (Reproduced with permission from ref. 36, with kind permission from Springer Science and Business Media.)

The effect of the separation voltage on the working electrode potential has been reported as shifts in the half-wave potential for both CE-EC and ME-EC.[34-35] Contento *et al.* and Forry *et al.* described the influence of separation voltage on the working electrode potential.[36-37] Bohn and coworkers used the model diagram shown in Figure 1.7A and B to show the effect of electric field on the working electrode potential.[36] There is a linear distribution of the separation voltage with

distance according to the solution resistance, as shown in Figure 1.7A and B. In this model, the ground electrode and the reference electrode are assumed to be placed at the same position at the end of the separation channel. Additionally, amperometric detection is accomplished in the oxidative mode and the conventional relation between the potential and energy is used.[36-37]

In normal polarity (Figure 1.7A) a positive voltage is applied across the separation channel that can lower the energy of the solution and its constituents. The magnitude of this energy is determined by the distance of the electrode inside the separation channel from the channel end. In an electrochemical oxidation reaction, electrons are transferred from the species in the solution to the electrode. The overpotential required to accomplish this is determined by the energy difference between the working electrode and the solution species. This energy gap increases upon decreasing the solution energy and, therefore, more overpotential is required to drive the oxidation process. Consequently, a higher apparent $E_{1/2}$ is required for oxidation compared to the $E_{1/2}$ of the species.[35] Therefore, the apparent half-wave potential is increased in the positive direction if the electrode is placed inside the separation channel.[36-37] The converse is true for reverse polarity mode. In that case, the energy difference between the electrode and the solution species is lowered and the apparent half wave potential is shifted towards less positive potentials as shown in Figure 1.7B.

The effective potential can be given by Equation 1.11, assuming that the separation voltage and the potential applied to the electrode are distinct (Forry *et al.)*.[37] In this equation, $E_{\text{eff,WE}}$ is the effective potential at the working electrode and $E_{\text{app,WE}}$ is the potential applied by the potentiostat. The E_{shift} can be computed according the equation below (1.12), where it is a function of the working electrode placement inside the channel (d_{WE}), the total channel length (d_{total}) and the IR drop. I is the separation current and the R is the resistance of the solution.[36-37]

$$E_{\text{eff,WE}}=E_{\text{app,WE}}+E_{\text{shift}} \qquad 1.11$$

$$E_{\text{shift}} = \theta IR \quad \theta = \frac{d_{\text{WE}}}{d_{\text{total}}} \tag{1.12}$$

This description can be used to explain the half-wave potential shifts in electrophoresis due to the placement of the electrode inside the separation channel. In positive polarity separations, the E_{shift} is positive as additional positive potential is required to drive the electrochemical oxidation as describe above. Therefore, the half-wave potential of the hydrodynamic voltammogram is shifted toward positive potentials when using the in-channel configuration compared to the end-channel configuration, *i.e.* compounds will appear to be "harder to oxidize." The reverse is true with negative polarity separations, where the half-wave potentials are shifted toward more negative (less positive) potentials, *i.e.* compounds will appear "easier to oxidize."

1.6 Different electrode configurations in ME-EC

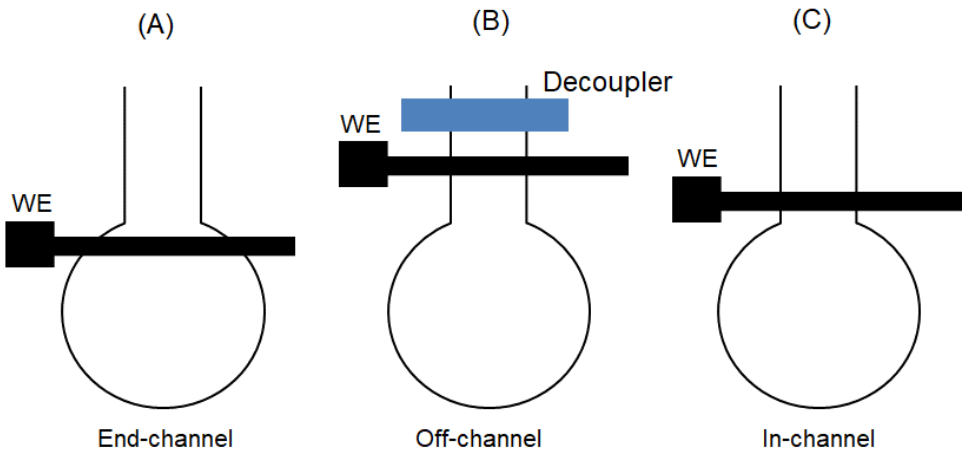

Figure 1.8 Different electrode alignment configurations in microchip electrophoresis. (A) End channel detection, (B) off-channel detection using a decoupler, and (C) in-channel detection using an isolated potentiostat.

There are essentially three distinct electrode placements relative to the separation channel end in ME-EC as shown in Figure 1.8. Two of these configurations, namely, end- and off-channel,

are two different approaches used to reduce or eliminate the effect of separation voltage on the working electrode potential.[38]

1.6.1 End-channel detection

End-channel detection is a very popular electrode alignment in which the working electrode is placed 5-15 μm from the channel end to minimize the applied electric field so that the electric field is dissipated before it reaches the working electrode.[9, 38] As the electric field dissipates at the channel end, the sample plug reaches the electrode because of the velocity that it gained while it was in the electric field. This velocity decreases as it travels towards the electrode due to the friction of the solution. This can cause band-broadening, reducing the separation efficiency and detection sensitivity.[9, 38] However, the reduction of noise due to the minimization of the interaction between the electrode and the electric field provides better LODs when compared to some other detection configurations.

A modification to this electrode alignment, designated as a "bubble cell" by Chuck Henry's group, has been used successfully to further dissipate the electric field. In this method, the channel end gets broader before it connects with the waste reservoir at the separation channel end.[39] The working electrode is sitting inside the broader channel and thus it feels a substantially lower electric field. In general, end-channel electrode alignment is an attractive approach to ME-EC because it permits the use of commercially available grounded potentiostats without any modification.

1.6.2 Off-channel detection

In off-channel detection, a metal decoupler (Figure 1.8B) is used to ground the high voltage prior to the placement of the working electrode.[9, 40] Palladium and platinum are the most commonly used metals and are fabricated as band electrodes. In this configuration, they are placed in the

channel prior to the working electrode, considering the direction of the separation. These materials have been successfully employed in normal polarity separations as they can adsorb the hydrogen gas produced at the cathode due to water reduction and they impede the development of bubbles inside the separation channel.[40-41] However, in reverse polarity separations, water oxidation occurs at the cathode, producing oxygen gas. Because a metal electrode that can adsorb the oxygen and be fabricated using photolithography is not known, this strategy has not been implemented successfully for reverse polarity separations. Another limitation of the off-channel configuration is that the thin film decoupler electrodes do not always tolerate the high electric fields desired for ME separation very well. This challenge has been overcome by the embedding of disk-shaped electrodes into epoxy-based substrates, replacing the microfabricated substrates.[42-43]

A decoupler was developed for CE using a laser to make a fracture in the capillary that is then filled with an ion permeable polymer membrane.[44] Membrane materials including cellulose acetate and Nafion have been used. The ground electrode is then placed outside of the membrane and the separation current is grounded by the movement of buffer ions through the membrane.[44-46] This decoupler design was adapted for ME by producing a series of laser-patterned holes on a thin glass substrate that was then aligned and bonded on the separation channel. The holes were covered with a cellulose acetate membrane and a ground electrode was then placed in the buffer reservoir over these holes along with the buffer. Noise levels less than 1 pA were observed with this approach and an exceptionally low LOD for dopamine (25 nM) was reported.[47]

The electrical isolation of a potentiostat or any other detector from the separation voltage is desirable since that should eliminate noise generation due to fluctuations in the separation voltage. Nonetheless, peak efficiencies may be significantly reduced in this configuration as the shape of the analyte plug changes from a plug flow prior to the decoupler to laminar flow after the

decoupler.[38] Band broadening can be minimized if a sufficiently high electroosmotic flow is generated by the separation system so that the analytes gain adequate velocity to reach the detector before very much diffusion occurs. However, low pH BGEs used with glass or fused silica substrates may not produce sufficient EOF, and thus will be accompanied by a significant loss in separation efficiency. To obtain the best results, the gap between the decoupler and detector should be kept at a minimum.

1.6.3 In-channel detection

A potentiostat isolated from earth ground ("floating potentiostat") is required for the in-channel configuration. These potentiostats are battery-operated and are not connected to the AC power outlet. The fact that they are not electrically grounded makes it possible to place the working electrode inside the separation channel (Figure 1.8C). A decade ago, most commercially available potentiostats were grounded and, therefore, not appropriate for use with in-channel ME detection. However, several commercial electrically isolated potentiostats have been developed during last decade with multiple functionalities in addition to amperometry.

Both reverse and normal polarity ME separations with in-channel amperometric detection have been carried out using isolated potentiostats.[34-35] In this electrode configuration, band-broadening is minimal compared to the other two electrode alignments. This is because the analyte plug is moving over the electrode with nearly the same velocity that it gains in the applied electric field. Peak efficiencies and sensitivities are therefore high. Nevertheless, noise introduced by the separation voltage fluctuations causes a decrease in the signal-to-noise ratio, affecting the LODs.

Particular care must be taken when using this configuration to determine the appropriate working electrode potential for an analyte since the apparent half-wave potential will be different than the formal half-wave potential (as discussed in Section 1.5) owing to the effect of separation

voltage. One way to overcome the noise issue is to use a dual-channel/dual-electrode design (Figure 1.1D).[22, 48] In this case, the chip contains two equivalent channels in a symmetric microchip. The symmetry of the microchip allows for similar voltage distributions across both channels and the same volume of sample and buffer injections. An electrode is aligned at each separation channel. One of the channels is used as the sample channel and the electrode at that end is the working electrode. The other channel becomes the blank/reference channel and the electrode at that channel end is the reference electrode. Sample reservoir and buffer reservoirs are selected according to the sample and blank channels. Since separation voltage fluctuations at both the working electrode and reference electrode should be very similar, much of the noise due to the separation voltage will be subtracted out.[22, 48]

1.7 Instrumentation for amperometric detection in microchip electrophoresis

Conventional three-electrode potentiostats are the most commonly employed detectors for electrochemical detection in ME. In these systems, the current flows through the counter (auxiliary) electrode and working electrode and there is negligible current flowing through the reference electrode. Most typically, the counter electrode potential is adjusted by the electronic circuitry such that the potential on the working electrode with respect to the reference electrode is at the required potential. The current produced by the oxidation or reduction of an analyte is then measured between the counter and working electrode, while the applied voltage is measured between the reference and working electrodes. Since there is negligible current flow through the reference electrode in this configuration, the potential of the working electrode does not experience a shift due to an ohmic drop (IR drop). However, there is a distance-related ohmic drop that depends on the distance between the reference and working electrodes and the solution

conductivity. Therefore, the working and reference electrodes need to be placed as close to each other as possible.

In the case of two-electrode systems, the voltage is applied between the working electrode and the reference/counter electrode. In this configuration, either large current measurements or high solution resistance can cause an ohmic drop, resulting in a potential change at the working electrode. Additionally, the large currents generated in this system can cause a change in the thermodynamic potential of the reference electrode. Therefore, two-electrode potentiostats are limited to low current measurements (low nA and pA), corresponding to low analyte concentration measurements or the use of microelectrodes.

For in-channel detection, an isolated or "floating" potentiostat must be used to avoid the separation voltage grounding through the potentiostat and destroying the electronics.[34-35] In contrast to most commercially available instruments, these potentiostats are completely electrically isolated and are usually battery-powered. Conventional commercially available grounded potentiostats cannot be employed for in-channel detection. Two prototypes isolated potentiostats have been evaluated by the Lunte group for in-channel detection in ME. The early version employed a three-electrode system, while a newer prototype employs a two-electrode configuration.[35] The latter was developed in collaboration with Pinnacle Technology, Inc.[34, 49]

When the two-electrode system is used with in-channel detection, a major concern is that it is difficult to determine the exact potential that is being applied to the working electrode, due to the combined effects of the separation voltage and the lack of a counter electrode.[34-35] Therefore, an HDV must be obtained for each analyte under the separation conditions of interest to determine the optimum detection potential. The interaction of the separation voltage with working electrode

is also possible in the end- and off-channel configurations. Therefore, it is also useful to generate HDVs for analytes in these electrode configurations to determine optimum potential.

There are several commercially available potentiostats that have been used in ME-EC. The Gamry Femtostat has been used for in-channel detection in the dual-channel/dual-electrode configuration.[22] The BASi Petit Ampere is battery-powered and could theoretically be used in the in-channel configuration. Additionally, modified BASi 4C-LC potentiostats that are electrically grounded have replaceable op-amps in case the separation current is grounded through the potentiostat.[50] If the separation voltage is grounded through the potentiostat, only the op-amp needs to be replaced. Micrux Technologies has developed hand-held battery powered instrumentation to perform both separation and detection for ME-EC. This is an ideal instrument to introduce ME-EC to undergraduate laboratories.[51-52] When using other commercially available grounded potentiostats, care needs to be taken to avoid grounding the separation voltage through the potentiostat. Damage to the instrumentation caused by a small oversight in electrode alignment can be very costly.

1.8 Signal, noise and limits of detection for ME-EC

1.8.1 Signal

One important benefit of amperometric detection for ME is that (under ideal conditions) the signal can be directly related to analyte concentration without the need for a calibration curve or standards. Signals generated by ME-EC are current vs. time profiles (i-t curves). Upon integration of peaks from i-t curves, charge (Q) is obtained. Using Faraday's equation (Equation 1.10) and knowing how many electrons are transferred in the oxidation/reduction, as well as taking into account the conversion efficiency, the number of moles of analyte that was injected into the

system can be calculated.[29, 38] If the volume of the injection plug is known, concentration can then be easily determined.

The current response and potential needed for an analyte in ME-EC is highly dependent on the type of working electrode that is employed. The molecular composition of the working electrode can have significant effects on the electron transfer kinetics. Additionally, the peak height and separation efficiencies are highly dependent on the electrode alignment with respect to the channel (in-, end-, or off-channel) and band broadening.

1.8.2 Noise

The high voltage power supply used for electrophoretic separation is the main source of noise in ME-EC. This noise is due to fluctuations in the potential applied by the high voltage power supply across the channel, as well as improper grounding of the separation voltage prior to detection.[22, 50, 53-54] The noise generated in an ME-EC experiment is usually greater than 25 pA, compared to the noise level of a typical amperometric experiment of less than 1 pA.[22, 50] The common components of noise observed during a typical ME-EC experiment are baseline drift, spikes, and oscillations.[53]

Low conductivity buffers, such as Good's buffers, are the best choice for ME-EC experiments. High conductivity buffers can contribute to non-Faradaic current that can cause additional noise. Fluctuations in the separation field can cause noise that increases as a function of voltage. This type of noise is most noticeable with the in-channel configuration. End- and off-channel configurations can also be affected by noise generated by the power supply if the working electrode is not fully decoupled from the separation field.

Any electrochemically active impurity in the sample or background electrolyte can cause generation of current at the working electrode and contribute to background noise. Therefore, the

noise is also dependent on the working electrode potential. In general, low positive working electrode potentials result in lower noise levels compared to high positive working electrode potentials. At electrode potentials above +1.00 V vs. Ag/AgCl, oxidation of water and generation of oxygen at metal working electrodes can cause increases in background current. The background current generated by solvent oxidation is highly dependent on pH and the type of the electrode that is used. The potential windows for metal and carbon electrodes were shown previously in Figure 1.6.[8] In particular, in the reductive mode, dissolved oxygen and hydrogen evolution from the reduction of water can generate high background currents and noise. For this reason, removal of oxygen is important in these applications.

The electrode configuration used for ME-EC also affects the amount of noise observed in the electropherogram. The in-channel configuration suffers from higher noise compared to the other two configurations, due to the interaction of the working electrode with the separation field, as discussed in Section 1.5. When an electrode is placed in the electric field, the voltage drop across the electrode can be calculated using the following equation.

$$\Delta E = (E/L)\, w \qquad 1.13$$

Where E is the separation voltage, L is the channel length, and w is the width of the electrode. Therefore, E/L is the separation field strength in V/cm. For 40 µm and 10 µm working electrodes in a –300 V/cm separation field, the voltage drops across the solution above the electrodes are –1.2 V and –0.45 V, respectively. This translates to an induced voltage of +1.2 V for the 40 µm electrode and +0.45 V for the 10 µm electrode. Under these conditions, oxidation of water can now occur at the 40 µm electrode and generate noise.[54]

To obtain better limits of detection for the in-channel configuration, a dual-channel microchip that contains separate reference and separation channels was reported by Hahn and

coworkers (Figure 1.1D) [19, 22] As discussed previously, this dual-channel configuration makes it possible to cancel the noise due to separation field since both the separation voltage fluctuations at the working and reference electrodes are identical. The noise levels observed using this configuration were low (around 4 pA).[19, 22, 50]

In the end-channel configuration, the working electrode is placed in the ground reservoir. For the off-channel configuration, the separation field is grounded before the working electrode. Therefore, the amount of noise that is observed is much lower in these configurations. The sensitivity of end-channel and off-channel configurations is lower than that of in-channel. However, lower LODs can be achieved with the end-channel and off-channel configurations due to the relatively low noise as compared to the in-channel configuration.[38] Hydrogen gas generated at Pt or Pd decouplers in off-channel configuration can eventually lead to bubbles that can generate noise at the working electrode or completely stop the separation process. In general, the LODs for end- and off-channel detection are lower than for in-channel detection due to the decrease in noise.

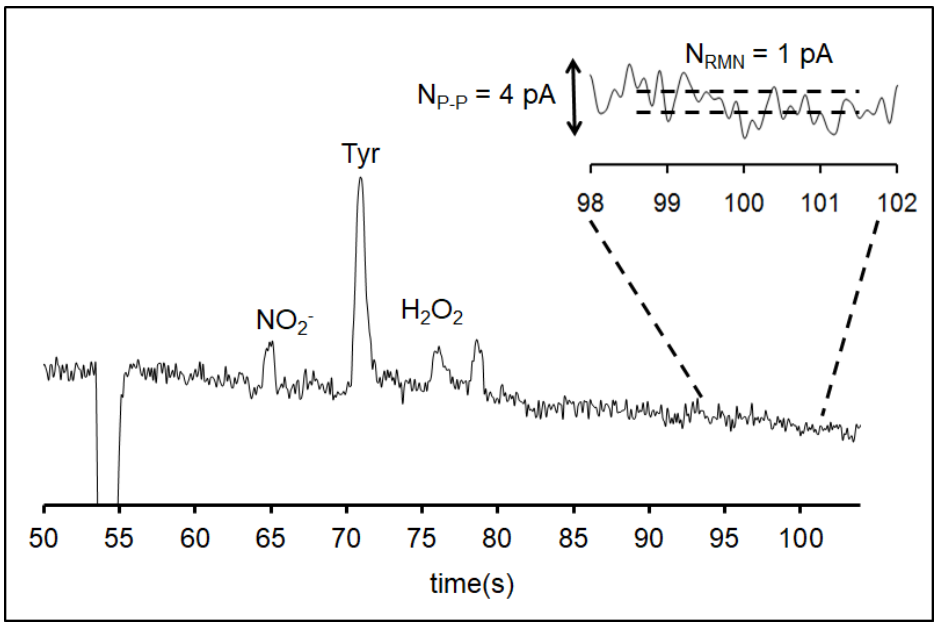

Figure 1.9 The signal and two types of noise measurement, root-mean noise (N_{RMN}) and peak-to-peak noise (N_{P-P}). This electropherogram was obtained for an equimolar (3.1 µM) mixture of nitrite, Tyr, H_2O_2, and an unknown, under reverse polarity conditions. (Reproduced with permission from ref. 50.)

1.8.3 Signal-to-noise ratio and LOD

To obtain the best LOD for an analyte of interest, both the signal and the noise need to be taken into consideration. Obviously, the ideal conditions are where there is a high signal and low noise so that S/N is at a maximum. The signal can be either current or charge, corresponding to peak height or area, respectively. The measurement of signal is straightforward in ME-EC. However, noise level measurements can be ambiguous. Figure 1.9 shows a signal and two types of noise measurements, root-mean noise (N_{RMN}) and peak-to-peak noise (N_{P-P}) that can be used to calculate S/N and LOD. Spikes and drifts in the baseline can be also be removed by filtering and/or baseline subtraction methods before calculating the LOD.[55-56] For a realistic determination of the LOD for an analyte, the best approach is to measure a concentration that is close to the LOD

and ensure that there is a S/N ratio greater than 3. This is important because as the signal decreases the noise becomes more apparent and it is easy to underestimate the noise if a peak with a S/N ratio greater than 10 is used. At analyte concentrations close to the LOD, drifts in the baseline, spikes, and baseline oscillations can be significant. These sources of noise are often not noticeable when higher concentrations (signals) are used to estimate the LOD.

1.9 Types of Electrodes

Generally, figures of merit obtained for amperometric detection are dependent on many other factors including the working electrode material (metal electrodes vs. carbon-based electrodes), size of the electrode, shape of the electrode, number of electrodes (*e.g.* an electrode array vs. a single electrode) and electrode setup (three-electrode vs. two-electrode system). Additional considerations come into play in the case of ME with amperometric detection, such as electrode configuration (off-channel vs. in-channel vs. end-channel) and type of the ME chip (dual-channel vs. single-channel)

1.9.1 Microelectrodes

Band electrodes of different sizes have been used for amperometric detection in ME. Width is the critical dimension of a band electrode. An electrode with a width less than 12.5 μm is considered an ultramicroelectrode and it becomes a nanoelectrode when the width is less than or equal to 100 nm. Mass transport to microelectrodes is governed by steady state diffusion and increases as the size of the electrode decreases. In general, the current response is proportional to the critical dimension (*e.g.* radius for a disk electrode, width for a band electrode) of the electrode, while the capacitive currents that contribute to the noise are proportional to the geometric area of the electrode. Therefore, as the size of the electrode decreases, the noise decreases at a faster rate than that of the signal, causing an enhancement of the signal-to-noise ratio.[57] Additionally, IR drop

and background current decrease with decreasing electrode size, leading to an improved amperometric signal.[58]

1.9.2 Multiple electrodes

A collection of micro-or nanoelectrodes can be utilized in an array format to improve the analytical performance including LODs, sensitivity and selectivity. Selectivity is achievable as different potentials can be applied to each electrode, resulting in voltammetric information about the analyte of interest.

1.9.2.1 Electrode arrays

The simplest multiple electrode system is a dual-electrode system. These systems are useful for extracting voltammetric information and thus for identifying peaks in an electropherogram. More complex formats, such as microelectrode or nanoelectrode arrays, can be used to further improve the signal-to-noise ratio and for peak identification. The reason for this is that the overall current response is determined by the geometric area of the array while the capacitive current depends on the active areas of electrodes. A carbon ink electrode array (8 electrodes) has been used by the Martin group with ME-amperometry to obtain improved LODs for catecholamines.[42, 59]

1.9.2.2 Dual-electrode systems

Dual-electrode systems in ME are either dual-series or dual-parallel. Solutions of run buffer or sample are running over both electrodes at the same time in dual-parallel electrode configuration. In dual-series configuration, the run buffer or sample plug interacts with the first electrode before it reaches the second electrode.

Voltammetric identification of compounds has been achieved using dual-series and dual-parallel configurations in many LC and CE amperometric detection studies.[60-63] Electrochemically

reversible analytes can be identified using dual-series electrodes in which a species is generated at the first electrode and then is collected at the second electrode.[64-66] In most of these studies, a sufficiently positive potential is applied to the first working electrode to oxidize the analyte and then it will be reduced at a more selective negative potential at the second electrode. This is a useful strategy as only a few reducible molecules exist in biological samples. This approach has been used for the identification of catecholamines.[64-66] Orthohydroxy-substituted phenols (catechols) oxidize to their orthoquinone products. These can then be reduced back to the catechol at the second electrode. The reduction of the oxidized product requires a less negative potential, thus imparting an added selectivity.

The generation-collection mode can also be used to identify redox active species that undergo chemically reversible reactions based on the collection efficiency. The percent reduction of the analyte at the second electrode relative to the first electrode is defined as the collection efficiency and is dependent on the chemical reversibility of the redox process. Electrochemically active species with different degrees of chemical reversibility can therefore be identified. For instance, the degree of chemical redox reversibility is different (unique) for classes of compounds such as phenols, trihydroxyphenols, methoxy substituted phenols and catechols. Therefore, this methodology has been utilized in many studies to identify catecholamines and phenolic acids.[64-66]

The dual-parallel configuration can be employed to extract voltammetric information based on the current ratio at two different potentials. This approach has been successfully utilized in CE,[67] with the first such studies in ME not reported until 2014. Challenges of fabricating dual-parallel electrodes in a microchannel were the cause for the delay of these studies. Recently, the dual-parallel electrode configuration was implemented within a dual-channel (Figure 1.1D)

microchip design in by Gunasekara *et al.* This method was successful in identifying impurities in peroxynitrite samples and peaks in macrophage cell lysates.[68-69]

Potential scanning methods, such as cyclic voltammetry and square wave voltammetry, are ideal for peak identification based on peak potential. However, the coupling of these methods with ME is difficult for several reasons. Sufficiently fast scan rates are needed to provide the high temporal resolution required by ME. Unfortunately, the high capacitive currents associated with these fast scan rates lead to poor S/N ratios and thus high LODs. Specialized potentiostats that can handle fast scan rates that are equipped with high noise filtering are required to address the mentioned challenges. Such potentiostats are commercially available but at a high price.[70-72]

1.9.3 Electrode materials

Care must be taken in selecting the electrode material for a particular analysis with ME-amperometry. Carbon-based electrodes and metal-based electrodes are two major categories of electrodes.

1.9.3.1 Carbon-based electrodes

Carbon-based materials are beneficial over metal electrodes as they are inexpensive and are simple to fabricate. Additionally, they have a relatively large potential window, low background currents and less fouling when compared to metal electrodes.[12] Most biologically important molecules of interest to our group are organic compounds and these generally exhibit better electrochemical activity on carbon-based versus metal electrodes. There are many types of carbon-based electrodes available, including carbon fibers, carbon nanotubes, carbon paste and boron doped diamond electrodes. These are different from one another by the composition of s, p character and arrangement of carbon atoms in the structure. Carbon-based electrodes are extensively used in ME and have been successfully integrated with PDMS-PDMS, PDMS-glass,

polymer-based, and plastic devices. However, the inclusion of a carbon-based electrode with an all-glass microchip device is difficult.

Carbon fiber electrodes have been extensively used for ME with amperometric detection.[73] In this case, a carbon fiber is placed in a trench and a Cu wire connection is establish using silver colloidal to use it as a working electrode. The trench is usually constructed on a PDMS substrate and has a similar width to that of the fiber. Care must be taken to avoid damaging the fiber while attempting to place it inside the trench. This process is often difficult and time-consuming; however, CF electrodes are generally durable if the user is sufficiently careful. The size of the CF electrodes used with ME are generally limited to diameters of 7 µm and 33 µm, owing to commercial accessibility.

Since its introduction by Ralph Adams in the 1950s,[74] carbon paste electrodes have been widely employed for electrochemical measurements. The first study that used carbon paste as the working electrode for ME-EC was in 2001 by Lunte's group.[75] The fabrication procedure is less complicated than using a carbon fiber, but photolithography cannot be used. Analogous to the carbon fiber electrode fabrication, a trench is created in glass, PDMS or another substrate material and a mixture of a carbon-based material (*e.g.* graphite, carbon nanotubes) with an adhesive oil is pressed into the trench.[76] The ability to introduce carbon paste into both flexible and rigid materials is an advantage compared to carbon fibers, which can only be integrated with malleable materials. For instance, a carbon paste electrode was integrated into a PMMA substrate for the ME separation and amperometric detection of dopamine and catechol using a PMMA/PDMS hybrid simple-t device.[76]

Micromolded or screen-printed carbon ink electrodes have been incorporated with different substrate materials such as PDMS,[38] glass[77] and epoxy[42] for amperometric detection with ME. In

one such study, an externally printed carbon electrode was successfully utilized on an all-glass microchip device with end-channel configuration.[78]

Pyrolyzed photoresist is another carbon electrode that has been used with microchip electrophoresis. Classical photolithography can be employed to fabricate these pyrolyzed photoresist film (PPF) electrodes as small as 10 μm.[79] To fabricate these electrodes, photoresist is spin-coated onto a quartz glass substrate and the features from the photo mask are copied to the thin photoresist film during exposure to a UV flood source. The plate is then developed to remove the excess photoresist. Next, the film is pyrolyzed under nitrogen/argon at a temperature of 1100 ^{o}C to generate the finished electrode. These PPF electrodes possess desirable properties similar to conventional glassy carbon electrodes, such as low background currents and a wide cathodic potential window. However, sluggish electron transfer rates, due to the low oxygen/carbon ratio, have been observed for some analytes, such as dopamine.[80]

The organization of carbon atoms on the planes of the lattice structure generally determines the electron transfer rates at the carbon surface.[81] A carbon nanotube structure is one allotropic form of carbon that is popular for electrochemical measurements due to its large surface area, substantial catalytic activity, and reduced surface fouling. The electrocatalytic activity may be enhanced further by the introduction of oxygen atoms as active sites using chemical or electrochemical methods. The redox response of these carbon materials for organic compounds may show an enhancement owing to the large surface area. All these factors lead to more signal enhancement relative to the noise and thus improve the attainable LODs with ME-amperometric detection.[82]

During the last two decades, significant attention has been given to developing different electrode materials such as boron-doped diamond. Diamonds exhibit high thermal conductivity

and electrical resistivity compared to other allotropes of carbon because of its crystalline structure and sp^3 hybridization. Diamond can be doped with boron to give a p-type semiconductor possessing sufficient electrical conductance.[83] Plasma-assisted chemical vapor deposition of both carbon and boron is used to fabricate thin film boron-doped diamond electrodes on silicon wafers. Chemical etching of the Si substrate is then used to recover the boron-doped diamond electrode film. An electrode film with the required length can be fixed onto a substrate of interest using a bonding agent.[84] Low capacitive currents, reduced electrode deactivation and a wide potential window are significant advantages of boron-doped diamond electrodes.[84-85] Additionally, when these electrodes are coupled with ME, they are rugged and give reproducible results.[86]

1.9.3.2 Metal-based electrodes

Metal electrodes such as Pt, Pd, Au, Cu and Ag are most commonly utilized for amperometric detection in ME. Conventional photolithography techniques can be employed to produce metal electrodes and thus it is possible to do mass fabrication of chips with electrodes (*e.g.* MicruX Technologies and Microliquid). Additionally, incorporation of metal electrodes into all glass devices is possible.[49, 87-88] Therefore, metal electrodes are advantageous over carbon-based electrodes in the sense of mass production and integration with all glass devices. However, the total production cost for metal electrodes is generally much higher than carbon electrodes due to the fabrication cost and use of precious metals. Frequently, an adhesive electrode layer (usually titanium, tantalum or chromium) is deposited prior to the desired metal as most of these precious metal electrodes do not adhere to substrates firmly. However, this adhesion layer can decrease the lifetime of the electrode if the separation field induces the formation of oxide layers in the adhesive metal via the process of grain boundary diffusion. Adsorption of gases, adsorption of organics and generation of oxide layers are some of the disadvantages of metal electrodes.

A photoplot containing desired electrode features is first drawn using AutoCAD software and printed on a transparency sheet with adequate resolution. Features from the photomask are then transferred to a chrome- and photoresist-coated glass substrate (*e.g.* borofloat or soda lime glass) using a UV flood source. The glass plate is then developed to remove the UV-exposed photoresist layer with a suitable developer followed by treatment with chrome etchant to remove the chrome layer beneath the UV exposed photoresist layer. A trench with a known depth is obtained by etching the glass in a buffered oxidant and then the glass is cleaned with the aid of plasma. A thin film of adhesive metal (typically about 40 nm) is sputtered under a vacuum on the glass followed by the deposition of the desired metal with desired thickness. The plate is then treated with acetone followed by chrome etchant to lift off the excess metal layer and the chrome layer, respectively.[49, 87]

As an alternative to metal deposition, wire electrodes can also be integrated into the microchip format in a similar manner to carbon fiber electrodes. In this case, a metal wire is firmly placed in a trench fabricated on a substrate with the aid of glue.[89] Protocols have been successfully developed to integrate a wire electrode in an epoxy substrate.[42]

1.10 Applications

Microchip electrophoresis with amperometric detection has been deployed in multiple areas of science. Size, portability, fast analysis capabilities, adoption of different designs, and low (nL to pL) sample and reagent volumes are fundamental advantages of ME that are not attainable with traditional benchtop instruments. The next section briefly summarizes some of the important applications of ME-EC in the areas of biological, environmental and food science.

1.10.1 Biological applications

Microchip electrophoresis with electrochemical detection (ME-EC) devices have been used for both *in vivo* and *in vitro* studies of biological systems, including on-animal sensing, analysis of reactive nitrogen species in cells, and release of catecholamines from PC12 cells.[4, 90] Analytes of interest in these studies can be broadly categorized as neurotransmitters,[38] reactive oxygen and nitrogen species,[34, 87, 91-92] cellular and non-cellular antioxidants,[87, 93] amino acids,[94-95] and pharmaceuticals. Bioanalytical applications of ME-EC have been reviewed widely and readers can find additional information in several recent review articles.[3-8] In this chapter, representative applications of ME-EC to microdialysis sampling, cellular analysis, and detection of amino acids are presented. Also, a brief account of carbohydrate detection is provided at the end of this section.

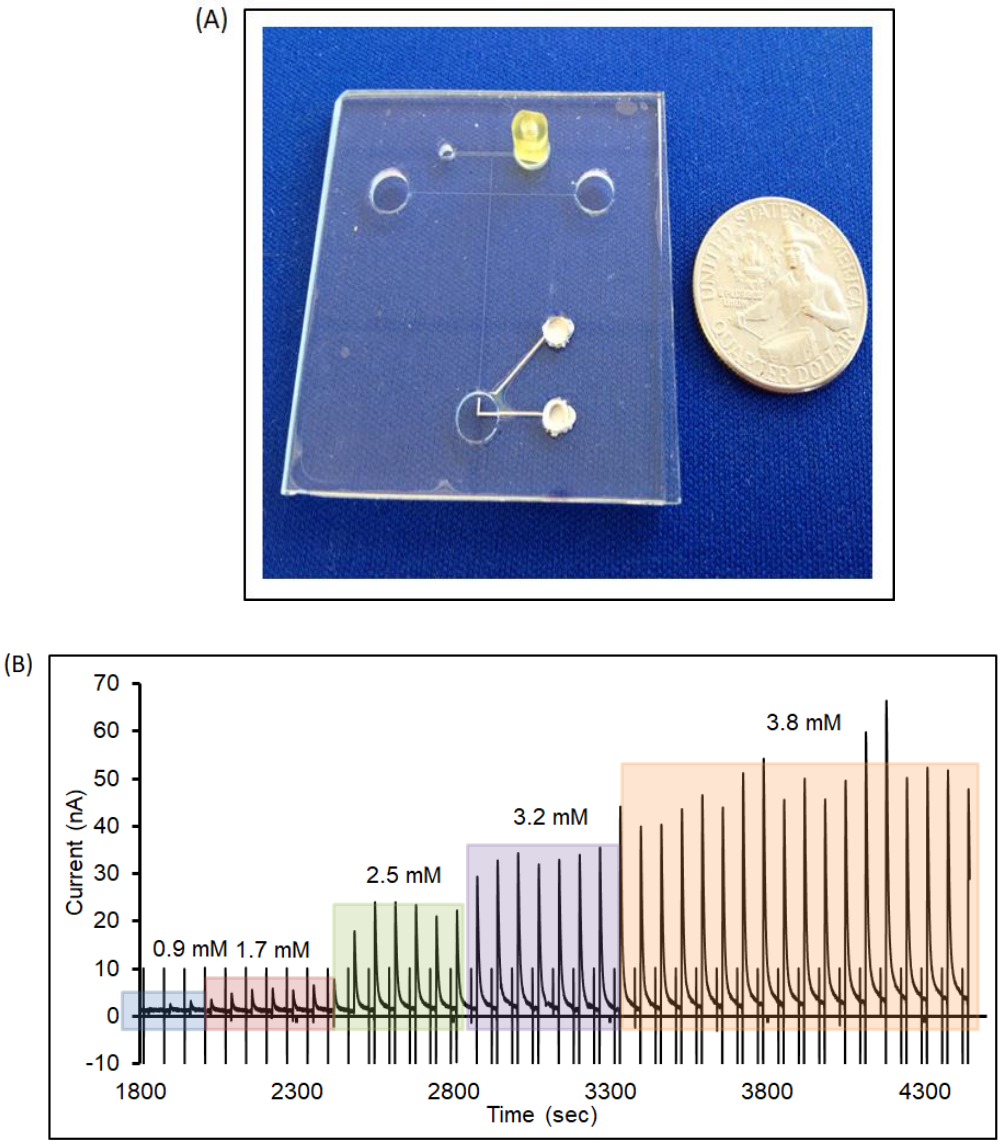

Figure 1.10 (A) Double-t all glass microchip with integrated platinum electrodes for coupling microdialysis sampling to ME–EC. (B) Continuous monitoring of H_2O_2 production following addition of glucose to a solution of glucose oxidase monitored by a linear microdialysis probe. (Reproduced with permission from ref. 49.)

Microdialysis (MD) sampling has been coupled to ME-EC for both *in vitro* and *in vivo* analysis of biological systems.[4] The combination of these two techniques allows for fast, near real-time monitoring of dynamic biological events such as neurotransmitter release and drug metabolism. In the first coupling of MD-ME-EC, Mecker *et al*. employed a pneumatically driven valving system to inject discrete microdialysis samples into the separation channel. This device was used to monitor the stimulated release of dopamine from PC12 cells *in vitro*.[27]

MD-ME-EC can also be used for *in vivo* monitoring of drug metabolism. Due to the small size and portability of the ME-EC devices, on-animal sensing is possible. The Lunte group developed a double-t all-glass microchip with integrated platinum electrodes for coupling MD to ME-EC (Figure 1.10A).[49] While the first application of this device was to monitor an enzymatic reaction *in vitro* (Figure 1.10B)[49] it has since been employed for on-sheep analysis to monitor subcutaneous nitrite production following nitroglycerin perfusion.[96] This exciting application paves the way for the development of on-animal sensors for neurotransmitters that can be used in freely roaming, freely behaving animals to correlate neurochemistry with behaviors.

ME-EC separation and detection of important biomolecules in cells has been successfully achieved and details can be found in review articles.[3] Martin's group developed an all on-chip ME-EC device integrated with a carbon ink electrode and multiple additional functionalities including immobilization of PC-12 cells on a collagen-coated micropallet, cell stimulation, sample injection, separation and detection.[97] Dopamine and norepinephrine were successfully separated and analyzed with this device. The same group developed a polystyrene-PDMS hybrid device incorporating on-chip cell culture to monitor the species releasing from cells.[98]

The human body produces various toxic pro-oxidants as a result of irregular metabolic processes and external effects such as environmental toxins, poor diet, and physical stress. These

pro-oxidants are frequently free radicals and include reactive nitrogen and oxygen species (RNOS). Antioxidants, such as glutathione, cysteine, and ascorbic acid, are endogenous intracellular species that reduce the activity of RNOS. The balance between pro-oxidants and antioxidants defines the redox status of cells and a redox imbalance can lead to diseases such as cancer, autoimmune disorders, cataracts, rheumatoid arthritis, and cardiovascular and neurodegenerative diseases. Therefore, the quantification of pro-oxidants and antioxidants in cells is very important and will facilitate a better understanding of these disease pathways.

ME-EC is a promising analytical tool for the separation and detection of short-lived species such as nitric oxide and peroxynitrite, as the ME format offers fast analysis times.[34, 91-92] A simple-t microchip aligned at a Pt electrode with in-channel configuration was successfully used to separate and detect nitrite, nitric oxide and antioxidants in macrophage cells (Figure 1.11).[87]

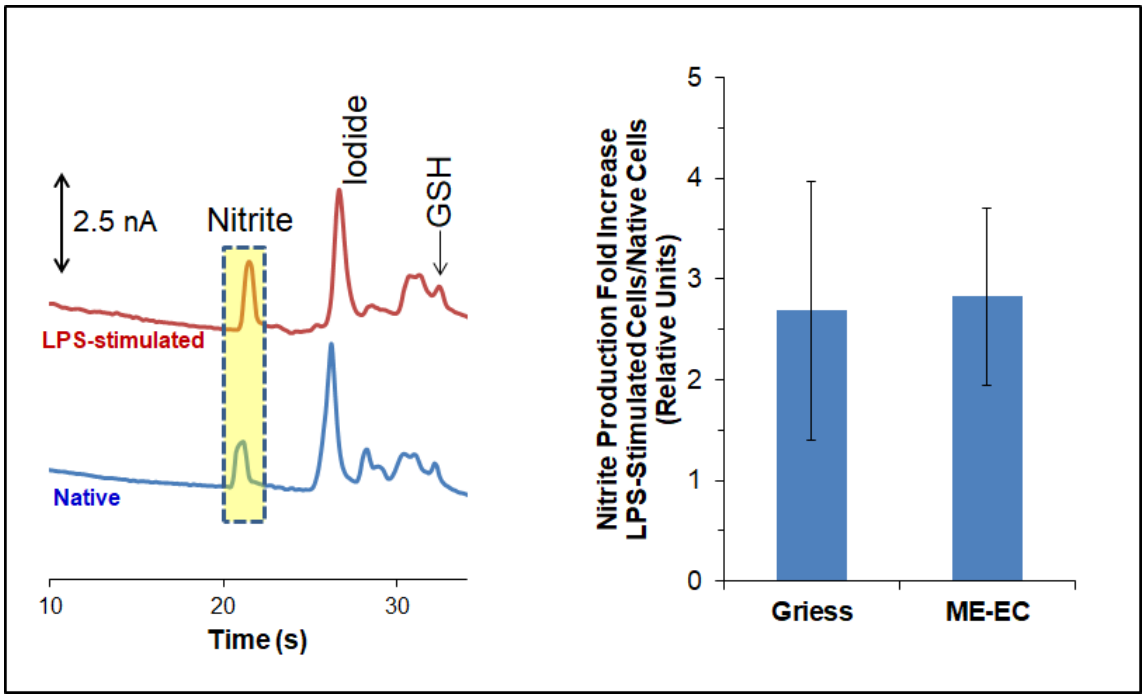

Figure 1.11 Separation and detection of intracellular nitrite and glutathione (GSH), in addition to an internal standard (iodide) in bulk cell lysates of native and LPS-stimulated macrophages. The bar graphs show a comparison of fold-increase production of nitrite levels following LPS stimulation measured using ME–EC and the Griess assay. (Reproduced with permission from ref. 87.)

Separation and detection of amino acids is usually accomplished by pre-column derivatization followed by FL detection; however, ME-EC has been employed successfully for such analysis. Using ME-EC, Swartz *et al.* successfully separated and detected tryptophan, histidine, and glycine without derivatization by performing direct electrochemical detection with a copper-coated Pt electrode.[95] An alternative strategy for the detection of amino acids by ME-EC is to derivatize the compounds with an electroactive tag. The products of both o-phthaldialdehyde (OPA) and naphthalene-2,3-dicarboxaldehyde (NDA) are isoindoles that are electrochemically active. ME was used to separate NDA/CN-derivatized citrulline and glycine, which were then

detected using the end-channel configuration with a carbon paste electrode.[75] Wang and co-workers developed an (OPA)/2-mercaptoethanol reagent-based on-chip derivatization method for the amino acids histidine, valine, isoleucine, leucine, glutamic acid, aspartic acid, arginine, and lysine.[99] The same chip has the capability to separate and detect them using a screen printed electrode aligned at end-channel configuration. Carbohydrates have also been detected directly using pulsed amperometric detection at a gold electrode or, under high pH conditions, by amperometry.[100]

1.11 Future Directions

Microchip electrophoresis with electrochemical detection is being utilized in various fields of science and become a popular separation and detection technique owing to its ability to accomplish rapid, near real-time, field portable analysis of many different analytes. The microchip format allows multiple processes to be integrated on-chip prior to separation and detection. Additionally, the small microchip format permits portable analysis. In the future, these benefits will continue to be exploited for applications such as cell cytometry, on-animal sensing, and portable diagnostics.

Chemical cytometry with FL detection has been used for peptide-based single cell assays and single cell nitric oxide assays.[101-103] Electrochemical cytometry has also been reported by the Ewing group; however, in that report, a short capillary connected to a microfluidic device was used to transport isolated vesicles into an electrode for coulometric detection of the vesicles' contents.[104] This is an important development for understanding neurotransmitter release but the report has not used the full potential of electrochemical cytometry. In the future, electrochemical cytometry could be used for measuring multiple cellular species and their by-products, drugs and their metabolites, and enzymatic activity.

The small and portable nature of microchip electrophoresis with electrochemical detection allows the device to be placed on-animal. Many behavioral studies employing animals involve tethering or restricting the animal to a small cage, seriously limiting the behaviors that can be studied. By placing the sampling, separation, and detection system on-animal, the animal can be in its natural environment, enabling better studies of behavior. On-animal sensing of analytes such as catecholamines and excitatory amino acids will permit better correlation between animal behavior and neurotransmitter concentration. This miniaturization capability of ME-EC will lead to the development of novel devices based on ME-EC in the future for the detection of explosives at airport security or food quality control in supermarkets. This portable nature can also be exploited for biomedical applications, in terms of point-of-care diagnostics. The ability to monitor analytes in near real-time will make it possible to make faster diagnosis of disease both in the doctor's office and at remote locations in developing countries. A detailed summary of applications of ME-EC can be found in Appendix 1.

1.12 Summary of thesis chapters

1.12.1 Chapter 1: Introduction

This chapter describes the principles of microchip electrophoresis followed by a discussion of different strategies to couple it to amperometric detection. The effect of separation voltage on the noise associated with ME-amperometric detection in different electrode configurations is described. In addition, the use of different electrode materials for the detection of different types of electroactive species is also described. Lastly, some representative applications of ME with amperometric detection described in the literature are discussed.

The details in this chapter have been published in the following book chapter

Gunasekara, D. B.; Wijesinghe, M. B.; Saylor, R. A.; Lunte, S. M., Chapter 3 Principles and Strategies for Microchip Electrophoresis with Amperometric Detection. In *Electrochemical Strategies in Detection Science*, The Royal Society of Chemistry: 2016; pp 85-124.

1.12.2 Chapter 2: Dual-channel/dual-parallel electrode configuration for the voltammetric identification of redox active species in cells

Voltammetric identification of compounds using a single electrode integrated into a microchip is a time consuming process not suited for short lived species. One approach to collect voltammetric data in microchip electrophoresis is to use a dual-series electrode configuration, with the two electrodes set at different potentials. However, with this configuration, a correction factor must be used to eliminate effect of electrode placement in the channel on the signal response. To obviate

this problem, a dual-channel chip was designed that integrates dual-parallel electrodes that can be used to obtain voltammetric data on the analyte of interest in a single run. This new approach was used for the identification of electrochemically active species in cell lysate samples.

This chapter is based on the following manuscript

Gunasekara, D.B.; Pichetsurnthorn, P.; Wijesinghe, M.B.; Lunte, S.M.; Evaluation of Dual-Electrode Configurations for Microchip Electrophoresis for Voltammetric Identification Electroactive Species

1.12.3 Chapter 3: Detection of reactive nitrogen and oxygen species using microchip electrophoresis coupled to fluorescence detection.

Inflammation and the production of reactive oxygen and nitrogen species is believed to be a major factor in neurodegenerative disease. The qualitative and quantitative analysis of these species produced due to external stimuli in cells can provide insights regarding the biochemistry of the disease pathways. Microchip electrophoresis provides an opportunity to detect more than one species in a single analysis. Toward this end, superoxide and nitric oxide were both detected in cell lysates using two different fluorescent probes. Microchip electrophoresis with fluorescence detection was also used to investigate the effect of nanoparticles on ROS production in lung endothelial cells and microglial cells.

This chapter is based on the following Publications:

1. Fresta, C. G.; Chakraborty, A.; Wijesinghe, M. B.; Amorini, A. M.; Lazzarino, G.; Lazzarino, G.; Tavazzi, B.; Lunte, S. M.; Caraci, F.; Dhar, P.; Caruso, G., Non-toxic engineered carbon nanodiamond concentrations induce oxidative/nitrosative stress, imbalance of energy metabolism, and mitochondrial dysfunction in microglial and alveolar basal epithelial cells. *Cell Death & Disease* **2018,** *9* (2), 245.

2. Caruso, G.; Fresta, C. G.; Siegel, J. M.; Wijesinghe, M. B.; Lunte, S. M., Microchip electrophoresis with laser-induced fluorescence detection for the determination of the ratio of nitric oxide to superoxide production in macrophages during inflammation. *Analytical and Bioanalytical Chemistry* **2017,** *409* (19), 4529-4538.

3. Siegel, Joseph M.; Schilly, K. M.; Wijesinghe, M. B.; Caruso, G.; Fresta, C. G.; Lunte, S. M., Optimization of a microchip electrophoresis method with electrochemical detection for the determination of nitrite in macrophage cells as an indicator of nitric oxide production. *Analytical Methods* **2019,** *11* (2), 148-156.

1.12.4 Chapter 4: Development of a bipolar fluorescence-based detector for microchip electrophoresis

Microchip electrophoresis-electrochemical detection is one of the most powerful analytical tools to separate and detect electroactive species. However, the detection limits are generally in the micromolar range. On the other hand, fluorescence detection usually provides nanomolar detection limits. However, fluorescence detection normally requires a derivatization step, particularly for small molecules. This additional step leads to selectivity issues. In this chapter, a

novel detection system was developed for microchip electrophoresis that combines amperometric detection with fluorescence detection using a bipolar electrode. The new detection method was demonstrated using two model analytes in the reductive mode.

This chapter is based on the following manuscript:
Wijesinghe, M.B.; Gunasekara, D.B.; Lunte, S.M. "Bipolar electrochemically-generated fluorescence detector for microchip electrophoresis," to be submitted to Analytical Chemistry

1.12.5 Chapter 5: Challenges of the new detection system and strategies employed to overcome them: Development of a bipolar detection system that does not require a potentiostat.

The major challenge of the new bipolar electrode-based detection system was achieving nanomolar detection limits in the presence of a high electrochemical background. In order to reduce this background, very small channels and electrodes were employed. In this case, better detection limits were obtained for bipolar fluorescence detection compared to bipolar electrochemical detection. However, the detection limits were still in the high micromolar range because the electrode response also decreased with small channels and small electrodes. It was then observed that the in-channel electrode alignment reduced the electrochemical background substantially and thus it was the ideal solution. Low micromolar detection limits were obtained with this strategy. In all these previous experiments, a hydrodynamic flow was used to flow the fluorescence probe. The use of electroosmotic flow was then tested and a strategy was identified to obtain the bipolar fluorescence response in the absence of a potentiostat.

1.12.6 Chapter 6: Modeling of the bipolar electrochemically-generated fluorescence system

It was of interest to find ways of optimizing the bipolar electrochemistry/fluorescence experimental system using computer modeling. In particular, it was of interest to determine how the flow rate influences the fluorescence plug forming at the electrode as it is sitting inside the flow channel. As the experimental set up is complicated, each part of the experiment was modeled first individually. Using COMSOL, voltammograms were generated at different flow rates. Also, a program was developed using coding and the model builder to generate bipolar cell voltammograms even for electrochemical systems with quasi reversible rate constants. The full system was modeled and the sample injection and separation were seen. Also, the effect of the flow rate on the detector response was explored.

1.12.7 Chapter 7: Future directions

Future goals for bipolar-based detection are described. The immediate goal is to use an optically transparent electrode such as indium tin oxide (ITO) as the reporter electrode. Then, this new method can be applied for the detection of electrochemically reducible nitroaromatic explosives. The long-term goal is to develop the novel detection method to quantitate electrochemically oxidizable species, such as antioxidants and reactive oxygen and nitrogen species, using resazurin as the fluorescence reporter. Lastly, the use of chemiluminescence as the reporting method to further improve the detection limits is discussed.

1.13 References

1. Manz, A.; Graber, N.; Widmer, H. M., Miniaturized total chemical analysis systems: a novel concept for chemical sensing. *Sens. Actuators, B* **1990,** *1*, 244-8.

2. Jacobson, S. C.; Hergenroder, R.; Koutny, L. B.; Ramsey, J. M., High-Speed Separations on a Microchip. *Anal. Chem.* **1994,** *66*, 1114-18.

3. Johnson, A. S.; Selimovic, A.; Martin, R. S., Microchip-based electrochemical detection for monitoring cellular systems. *Anal. Bioanal. Chem.* **2013,** *405*, 3013-3020.

4. Saylor, R. A.; Lunte, S. M., A review of microdialysis coupled to microchip electrophoresis for monitoring biological events. *J. Chromatogr.* **2015,** *DOI: 10.1016/j.chroma.2014.12.086*.

5. Chen, G.; Lin, Y.; Wang, J., Microchip capillary electrophoresis with electrochemical detection for monitoring environmental pollutants. *Curr. Anal. Chem.* **2006,** *2*, 43-50.

6. Martin, A.; Vilela, D.; Escarpa, A., Food analysis on microchip electrophoresis: An updated review. *Electrophoresis* **2012,** *33*, 2212-2227.

7. Mark, J. J. P.; Scholz, R.; Matysik, F.-M., Electrochemical methods in conjunction with capillary and microchip electrophoresis. *J. Chromatogr.* **2012,** *1267* (0), 45-64.

8. Kuban, P.; Hauser, P. C., Fundamentals of electrochemical detection techniques for CE and MCE. *Electrophoresis* **2009,** *30* (19), 3305-3314.

9. Lacher, N. A.; Garrison, K. E.; Martin, R. S.; Lunte, S. M., Microchip capillary electrophoresis/electrochemistry. *Electrophoresis* **2001,** *22*, 2526-2536.

10. Whatley, H. In *Basic principles and modes of capillary electrophoresis*, Humana Press Inc.: 2001; pp 21-58.

11. Giddings, J. C., *Unified Separation Science,* John Wiley & Sons, Inc., New York, 1st edn, **1991**.

12. Bard, A. J.; Faulkner, L. R., Fundamentals and Applications, John Wiley & Sons, Inc., New York, 2nd edn, **2001**.

13. Sandlin, Z. D.; Shou, M.; Shackman, J. G.; Kennedy, R. T., Microfluidic Electrophoresis Chip Coupled to Microdialysis for in Vivo Monitoring of Amino Acid Neurotransmitters. *Anal. Chem.* **2005,** *77* (23), 7702-7708.

14. Nge, P. N.; Rogers, C. I.; Woolley, A. T., Advances in Microfluidic Materials, Functions, Integration, and Applications. *Chem. Rev.* **2013,** *113* (4), 2550-2583.

15. Makamba, H.; Kim, J. H.; Lim, K.; Park, N.; Hahn, J. H., Surface modification of poly(dimethylsiloxane) microchannels. *Electrophoresis* **2003,** *24* (21), 3607-19.

16. Ermakov, S. V.; Jacobson, S. C.; Ramsey, J. M., Computer Simulations of Electrokinetic Injection Techniques in Microfluidic Devices. *Anal. Chem.* **2000,** *72* (15), 3512-3517.

17. Karlinsey, J. M., Sample introduction techniques for microchip electrophoresis: A review. *Anal. Chim. Acta* **2012,** *725*, 1-13.

18. Seiler, K.; Fan, Z. H.; Fluri, K.; Harrison, D. J., Electroosmotic pumping and valveless control of fluid flow within a manifold of capillaries on a glass chip. *Anal. Chem.* **1994,** *66* (20), 3485-3491.

19. Chen, C.; Hahn, J., Enhanced aminophenols monitoring using in-channel amperometric detection with dual-channel microchip capillary electrophoresis. *Environ. Chem. Lett.* **2011,** *9* (4), 491-497.

20. Slentz, B. E.; Penner, N. A.; Regnier, F., Sampling BIAS at channel junctions in gated flow injection on chips. *Anal. Chem.* **2002,** *74* (18), 4835-40.

21. Griffiths, S. K.; Nilson, R. H., Low-Dispersion Turns and Junctions for Microchannel Systems. *Anal. Chem.* **2001,** *73*, 272-278.

22. Chen, C.; Hahn, J. H., Dual-Channel Method for Interference-Free In-Channel Amperometric Detection in Microchip Capillary Electrophoresis. *Anal. Chem.* **2007,** *79*, 7182-7186.

23. Attiya, S.; Jemere, A. B.; Tang, T.; Fitzpatrick, G.; Seiler, K.; Chiem, N.; Harrison, D. J., Design of an interface to allow microfluidic electrophoresis chips to drink from the fire hose of the external environment. *Electrophoresis* **2001,** *22* (2), 318-327.

24. Lin, Y.-H.; Lee, G.-B.; Li, C.-W.; Huang, G.-R.; Chen, S.-H., Flow-through sampling for electrophoresis-based microfluidic chips using hydrodynamic pumping. *J. Chromatogr. A* **2001,** *937*, 115-125.

25. Huynh, B. H.; Fogarty, B. A.; Martin, R. S.; Lunte, S. M., On-Line Coupling of Microdialysis Sampling with Microchip-Based Capillary Electrophoresis. *Anal. Chem.* **2004,** *76*, 6440-6447.

26. Li, M. W.; Martin, R. S., Integration of continuous-flow sampling with microchip electrophoresis using poly(dimethylsiloxane)-based valves in a reversibly sealed device. *Electrophoresis* **2007,** *28*, 2478-2488.

27. Mecker, L. C.; Martin, R. S., Integration of Microdialysis Sampling and Microchip Electrophoresis with Electrochemical Detection. *Anal. Chem.* **2008,** *80*, 9257-9264.

28. Vandaveer, W. R.; Pasas-Farmer, S. A.; Fischer, D. J.; Frankenfeld, C. N.; Lunte, S. M., Recent developments in electrochemical detection for microchip capillary electrophoresis. *Electrophoresis* **2004,** *25* (21-22), 3528-3549.

29. Kissinger, P. T.; Heineman, W. R., *Laboratory Techniques in Electroanalytical Chemistry*, Marcel Dekker., Inc, New York, 2nd edn, **1996.**

30. Hulvey, M. K.; Lunte, S. M.; Fischer, D. J.; Kuhnline, C. D., Electrochemical Detection Methods Following Liquid Chromatography, Capillary Electrophoresis, and Microchip Electrophoresis Separations. *Encyclopedia of Analytical Chemistry*.

31. Creager, S.; Handbook of Electrochemistry, ed. Zoski, C. G.; Elsevier, San Diego, 1st edn, 2007, ch. 3, pp. 57–72.

32. Rieger, P. H.; *Electrochemistry*. Chapman & Hall, New York, 2nd edn, 1994.

33. Rocklin R. D.; A Practical Guide to HPLC Detection, ed. D. Parriott, Academic Press, Inc., San Diego, 1993, ch. 6, pp. 145–173.

34. Gunasekara, D. B.; Hulvey, M. K.; Lunte, S. M., In-channel amperometric detection for microchip electrophoresis using a wireless isolated potentiostat. *Electrophoresis* **2011,** *32* (8), 832-837.

35. Martin, R. S.; Ratzlaff, K. L.; Huynh, B. H.; Lunte, S. M., In-channel electrochemical detection for microchip capillary electrophoresis using an electrically isolated potentiostat. *Anal. Chem.* **2002,** *74* (5), 1136-1143.

36. Contento, N. M.; Bohn, P. W., Electric field effects on current–voltage relationships in microfluidic channels presenting multiple working electrodes in the weak-coupling limit. *Microfluid. Nanofluid.* **2014**, 1-10.

37. Forry, S. P.; Murray, J. R.; Heien, M. L.; Locascio, L. E.; Wightman, R. M., Probing electric fields inside microfluidic channels during electroosmotic flow with fast-scan cyclic voltammetry. *Anal. Chem.* **2004,** *76* (17), 4945-4950.

38. Fischer, D. J.; Hulvey, M. K.; Regel, A. R.; Lunte, S. M., Amperometric detection in microchip electrophoresis devices: Effect of electrode material and alignment on analytical performance. *Electrophoresis* **2009,** *30* (19), 3324-3333.

39. Guan, Q.; Henry, C. S., Improving MCE with electrochemical detection using a bubble cell and sample stacking techniques. *Electrophoresis* **2009,** *30*, 3339-3346.

40. Lacher, N. A.; Lunte, S. M.; Martin, R. S., Development of a microfabricated palladium decoupler/electrochemical detector for microchip capillary electrophoresis using a hybrid glass/poly(dimethylsiloxane) device. *Anal. Chem.* **2004,** *76* (9), 2482-2491.

41. Wu, C.-C.; Wu, R.-G.; Huang, J.-G.; Lin, Y.-C.; Chang, H.-C., Three-Electrode Electrochemical Detector and Platinum Film Decoupler Integrated with a Capillary Electrophoresis Microchip for Amperometric Detection. *Anal. Chem.* **2003,** *75* (4), 947-952.

42. Selimovic, A.; Johnson, A. S.; Kiss, I. Z.; Martin, R. S., Use of epoxy-embedded electrodes to integrate electrochemical detection with microchip-based analysis systems. *Electrophoresis* **2011,** *32* (8), 822-831.

43. Johnson, A. S.; Selimovic, A.; Martin, R. S., Integration of microchip electrophoresis with electrochemical detection using an epoxy-based molding method to embed multiple electrode materials. *Electrophoresis* **2011,** *32*, 3121-3128.

44. Osbourn, D. M.; Lunte, C. E., Cellulose acetate decoupler for on-column electrochemical detection in capillary electrophoresis. *Anal. Chem.* **2001,** *73* (24), 5961-5964.

45. Park, S.; Lunte, S. M.; Lunte, C. E., A perfluorosulfonated ionomer joint for capillary electrophoresis with on-column electrochemical detection. *Anal. Chem.* **1995,** *67* (5), 911-18.

46. O'Shea, T. J.; Greenhagen, R. D.; Lunte, S. M.; Lunte, C. E.; Smyth, M. R.; Radzik, D. M.; Watanabe, N., Capillary electrophoresis with electrochemical detection employing an on-column Nafion joint. *J. Chromatogr.* **1992,** *593* (1-2), 305-12.

47. Osbourn, D. M.; Lunte, C. E., On-column electrochemical detection for microchip capillary electrophoresis. *Anal. Chem.* **2003,** *75* (11), 2710-2714.

48. Chen, C.-P.; Teng, W.; Hahn, J.-H., Nanoband electrode for high-performance in-channel amperometric detection in dual-channel microchip capillary electrophoresis. *Electrophoresis* **2011,** *32*, 838-843.

49. Scott, D. E.; Grigsby, R. J.; Lunte, S. M., Microdialysis Sampling Coupled to Microchip Electrophoresis with Integrated Amperometric Detection on an All-Glass Substrate. *Chemphyschem* **2013,** *14* (10), 2288-2294.

50. Meneses, D.; Gunasekara, D. B.; Pichetsurnthorn, P.; da Silva, J. A.; de Abreu, F. C.; Lunte, S. M., Evaluation of in-channel amperometric detection using a dual-channel microchip electrophoresis device and a two-electrode potentiostat for reverse polarity separations. *Electrophoresis* **2014**.

51. Fernández-la-Villa, A.; Sánchez-Barragán, D.; Pozo-Ayuso, D. F.; Castaño-Álvarez, M., Smart portable electrophoresis instrument based on multipurpose microfluidic chips with electrochemical detection. *Electrophoresis* **2012,** *33* (17), 2733-2742.

52. Fernández-la-Villa, A.; Pozo-Ayuso, D. F.; Castaño-Álvarez, M., New analytical portable instrument for microchip electrophoresis with electrochemical detection. *Electrophoresis* **2010,** *31* (15), 2641-2649.

53. Kuldvee, R.; Kaljurand, M.; Smit, H., Improvement of Signal-to-Noise Ratio of Electropherograms and Analysis Reproducibility with Digital Signal Processing and Multiple Injections. *J. High. Resolut. Chromatogr.* **1998,** *21* (3), 169-174.

54. Lu, W.; Cassidy, R. M., Background noise in capillary electrophoretic amperometric detection. *Anal. Chem.* **1994,** *66* (2), 200-204.

55. Laude, N. D.; Atcherley, C. W.; Heien, M. L., Rethinking data collection and signal processing. 1. Real-time oversampling filter for chemical measurements. *Anal. Chem.* **2012,** *84* (19), 8422-8426.

56. Mohammadi, B.; Bharadwadj, R.; Santiago, J., Design and optimization of on-chip capillary electrophoresis. *Electrophoresis Journal* **2002,** *23* (16), 2729-2744.

57. Wightman, R. M., Detection technologies. Probing cellular chemistry in biological systems with microelectrodes. *Science* **2006,** *311* (5767), 1570-4.

58. Cahill, P. S.; Walker, Q. D.; Finnegan, J. M.; Mickelson, G. E.; Travis, E. R.; Wightman, R. M., Microelectrodes for the Measurement of Catecholamines in Biological Systems. *Anal. Chem.* **1996,** *68*, 3180-3186.

59. Mecker, L. C.; Filla, L. A.; Martin, R. S., Use of a Carbon-Ink Microelectrode Array for Signal Enhancement in Microchip Electrophoresis with Electrochemical Detection. *Electroanalysis* **2010,** *22*, 2141-2146.

60. Lunte, C. E.; Ridgway, T. H.; Heineman, W. R., Voltammetric-amperometric dual-electrode detection for flow injection analysis and liquid chromatography. *Anal. Chem.* **1987,** *59* (5), 761-6.

61. Lunte, C. E.; Kissinger, P. T.; Shoup, R. E., Difference mode detection with thin-layer dual-electrode liquid chromatography/electrochemistry. *Anal. Chem.* **1985,** *57* (8), 1541-6.

62. Roston, D. A.; Shoup, R. E.; Kissinger, P. T., Liquid chromatography/electrochemistry: thin-layer multiple electrode detection. *Anal. Chem.* **1982,** *54* (13), 1417A-1418A, 1422A, 1424A, 1428A, 1430A, 1432A, 1434A.

63. Zhong, M.; Lunte, S. M., Tubular-Wire Dual Electrode for Detection of Thiols and Disulfides by Capillary Electrophoresis/Electrochemistry. *Anal. Chem.* **1999,** *71* (1), 251-255.

64. Fischer, D. J.; Vandaveer, W. R. I. V.; Grigsby, R. J.; Lunte, S. M., Pyrolyzed photoresist carbon electrodes for microchip electrophoresis with dual-electrode amperometric detection. *Electroanalysis* **2005,** *17* (13), 1153-1159.

65. Martin, R. S.; Gawron, A. J.; Lunte, S. M.; Henry, C. S., Dual-Electrode Electrochemical Detection for Poly(dimethylsiloxane)-Fabricated Capillary Electrophoresis Microchips. *Anal. Chem.* **2000,** *72* (14), 3196-3202.

66. Mecker, L. C.; Martin, R. S., Use of micromolded carbon dual electrodes with a palladium decoupler for amperometric detection in microchip electrophoresis. *Electrophoresis* **2006,** *27* (24), 5032-5042.

67. Dorris, M. K.; Crick, E. W.; Lunte, C. E., A parallel dual-electrode detector for capillary electrophoresis. *Electrophoresis* **2012,** *33* (17), 2725-2732.

68. Lunte, S. M.; Gunasekara, D. B.; Pichetsurnthorn, P.; Meneses, D.; Proceedings of mT The Chemical and Biological Microsystems Society, **2014**, pp. 39–42.

69. Gunasekara, D. B. Ph.D.Thesis, University of Kansas, 2014.

70. Ferris, S. S.; Lou, G.; Ewing, A. G., Scanning electrochemical detection in capillary electrophoresis. *J. Microcolumn Sep.* **1994,** *6*, 263-8.

71. Swanek, F. D.; Chen, G.; Ewing, A. G., Identification of Multiple Compartments of Dopamine in a Single Cell by Scanning Electrochemical Detection. *Anal. Chem.* **1996,** *68*, 3912-3916.

72. Fang, H.; Vickrey, T. L.; Venton, B. J., Analysis of Biogenic Amines in a Single Drosophila Larva Brain by Capillary Electrophoresis with Fast-Scan Cyclic Voltammetry Detection. *Anal. Chem.* **2011,** *83*, 2258-2264.

73. Gawron, A. J.; Martin, R. S.; Lunte, S. M., Fabrication and evaluation of a carbon-based dual-electrode detector for poly(dimethylsiloxane) electrophoresis chips. *Electrophoresis* **2001,** *22*, 242-8.

74. Adams, R. N., Carbon paste electrodes. *Anal. Chem.* **1958,** *30*, 1576.

75. Martin, R. S.; Gawron, A. J.; Fogarty, B. A.; Regan, F. B.; Dempsey, E.; Lunte, S. M., Carbon paste-based electrochemical detectors for microchip capillary electrophoresis/electrochemistry. *Analyst* **2001,** *126*, 277-80.

76. Regel, A.; Lunte, S., Integration of a graphite/poly(methyl-methacrylate) composite electrode into a poly(methylmethacrylate) substrate for electrochemical detection in microchips. *Electrophoresis* **2013,** *34*, 2101-2106.

77. Kovarik, M. L.; Torrence, N. J.; Spence, D. M.; Martin, R. S., Fabrication of carbon microelectrodes with a micromolding technique and their use in microchip-based flow analyses. *Analyst* **2004,** *129*, 400-405.

78. Wang, J.; Tian, B.; Sahlin, E., Micromachined electrophoresis chips with thick-film electrochemical detectors. *Anal. Chem.* **1999,** *71*, 5436-5440.

79. Ranganathan, S.; McCreery, R.; Majji, S. M.; Madou, M., Photoresist-derived carbon for microelectromechanical systems and electrochemical applications. *J. Electrochem. Soc.* **2000,** *147*, 277-282.

80. Ranganathan, S.; McCreery, R. L., Electroanalytical Performance of Carbon Films with Near-Atomic Flatness. *Anal. Chem.* **2001,** *73*, 893-900.

81. Pumera, M.; Escarpa, A., Nanomaterials as electrochemical detectors in microfluidics and CE: Fundamentals, designs, and applications. *Electrophoresis* **2009,** *30* (19), 3315-3323.

82. Wang, J., Electrochemical detection for capillary electrophoresis microchips: A review. *Electroanalysis* **2005,** *17* (13), 1133-1140.

83. Swain, G. M.; Ramesham, R., The electrochemical activity of boron-doped polycrystalline diamond thin film electrodes. *Anal. Chem.* **1993,** *65*, 345-51.

84. Shin, D.; Tryk, D. A.; Fujishima, A.; Muck, A., Jr.; Chen, G.; Wang, J., Microchip capillary electrophoresis with a boron-doped diamond electrochemical detector for analysis of aromatic amines. *Electrophoresis* **2004,** *25*, 3017-3023.

85. Strojek, J. W.; Granger, M. C.; Swain, G. M.; Dallas, T.; Holtz, M. W., Enhanced Signal-to-Background Ratios in Voltammetric Measurements Made at Diamond Thin-Film Electrochemical Interfaces. *Anal. Chem.* **1996,** *68*, 2031-2037.

86. Wang, J.; Chen, G.; Chatrathi, M. P.; Fujishima, A.; Tryk, D. A.; Shin, D., Microchip Capillary Electrophoresis Coupled with a Boron-Doped Diamond Electrode-Based Electrochemical Detector. *Anal. Chem.* **2003,** *75* (4), 935-939.

87. Gunasekara, D. B.; Siegel, J. M.; Caruso, G.; Hulvey, M. K.; Lunte, S. M., Microchip electrophoresis with amperometric detection method for profiling cellular nitrosative stress markers. *Analyst* **2014,** *139* (13), 3265-3273.

88. Woolley, A. T.; Lao, K.; Glazer, A. N.; Mathies, R. A., Capillary Electrophoresis Chips with Integrated Electrochemical Detection. *Anal. Chem.* **1998,** *70*, 684-688.

89. Henry, C.; Lunte, S.; Santiago, J., Ceramic microchips for capillary electrophoresis–electrochemistry. *Anal. Commun.* **1999,** *36* (8), 305-307.

90. Pasas, S. A.; Lacher, N. A.; Davies, M. I.; Lunte, S. M., Detection of homocysteine by conventional and microchip capillary electrophoresis/electrochemistry. *Electrophoresis* **2002,** *23* (5), 759-766.

91. Gunasekara, D. B.; Hulvey, M. K.; Lunte, S. M.; Fracassi da Silva, J. A., Microchip electrophoresis with amperometric detection for the study of the generation of nitric oxide by NONOate salts. *Anal. Bioanal. Chem.* **2012,** *403* (8), 2377-2384.

92. Hulvey, M. K.; Frankenfeld, C. N.; Lunte, S. M., Separation and Detection of Peroxynitrite Using Microchip Electrophoresis with Amperometric Detection. *Anal. Chem. (Washington, DC, U. S.)* **2010,** *82* (5), 1608-1611.

93. Antwi, C.; Johnson, A. S.; Selimovic, A.; Martin, R. S., Use of microchip electrophoresis and a palladium/mercury amalgam electrode for the separation and detection of thiols. *Anal. Methods* **2011,** *3*, 1072-1078.

94. Schwarz, M. A.; Hauser, P. C., Chiral on-chip separations of neurotransmitters. *Anal. Chem.* **2003,** *75* (17), 4691-4695.

95. Schwarz, M. A.; Galliker, B.; Fluri, K.; Kappes, T.; Hauser, P. C., A two-electrode configuration for simplified amperometric detection in a microfabricated electrophoretic separation device. *Analyst* **2001,** *126* (2), 147-151.

96. Scott, D. E.; Willis, S. D.; Gabbert, S.; Johnson, D.; Naylor, E.; Janle, E. M.; Krichevsky, J. E.; Lunte, C. E.; Lunte, S. M., Development of an on-animal separation-based sensor for monitoring drug metabolism in freely roaming sheep. *Analyst* **2015,** *140* (11), 3820-3829.

97. Bowen, A. L.; Martin, R. S., Integration of on-chip peristaltic pumps and injection valves with microchip electrophoresis and electrochemical detection. *Electrophoresis* **2010,** *31* (15), 2534-2540.

98. Johnson, A. S.; Mehl, B. T.; Martin, R. S., Integrated hybrid polystyrene-polydimethylsiloxane device for monitoring cellular release with microchip electrophoresis and electrochemical detection. *Anal. Methods* **2015,** *7*, 884-893.

99. Wang, J.; Chatrathi, M. P.; Tian, B., Micromachined separation chips with a precolumn reactor and end-column electrochemical detector. *Anal. Chem.* **2000,** *72*, 5774-5778.

100. García, C. D.; Henry, C. S., Direct determination of carbohydrates, amino acids, and antibiotics by microchip electrophoresis with pulsed amperometric detection. *Anal. Chem.* **2003,** *75* (18), 4778-4783.

101. Kovarik, M. L.; Shah, P. K.; Armistead, P. M.; Allbritton, N. L., Microfluidic Chemical Cytometry of Peptide Degradation in Single Drug-Treated Acute Myeloid Leukemia Cells. *Anal. Chem.* **2013,** *85* (10), 4991-4997.

102. Kovarik, M. L.; Dickinson, A. J.; Roy, P.; Poonnen, R. A.; Fine, J. P.; Allbritton, N. L., Response of single leukemic cells to peptidase inhibitor therapy across time and dose using a microfluidic device. *Integrative Biology* **2014,** *6* (2), 164-174.

103. Metto, E. C.; Evans, K.; Barney, P.; Culbertson, A. H.; Gunasekara, D. B.; Caruso, G.; Hulvey, M. K.; Fracassi da Silva, J. A.; Lunte, S. M.; Culbertson, C. T., An Integrated Microfluidic Device for Monitoring Changes in Nitric Oxide Production in Single T-Lymphocyte (Jurkat) Cells. *Anal. Chem.* **2013,** *85* (21), 10188-10195.

104. Omiatek, D. M.; Dong, Y.; Heien, M. L.; Ewing, A. G., Only a fraction of quantal content is released during exocytosis as revealed by electrochemical cytometry of secretory vesicles. *ACS Chem. Neurosci.* **2010,** *1* (3), 234-245.

2. Chapter 2: Development of a dual-channel/dual-electrode configuration for microchip electrophoresis to identify chemical species based on redox potentials

This chapter is based on the following manuscript

Gunasekara, D.B.; Pichetsurnthorn, P.; Wijesinghe, M.B.; Lunte, S.M.; Evaluation of Dual Electrode Configurations for Microchip Electrophoresis for Voltammetric Identification of Electroactive Species, to be submitted to Electrophoresis

2.1 Introduction

One of the most popular detection methods coupled to ME or CE is amperometry. Generally, amperometry provides better detection limits compared to voltammetry techniques as the amperometric signal is free of capacitive currents. The selectivity of amperometry can be improved through judicious selection of working electrode potential and composition. Different classes of compounds including catechols, phenolic acids, reactive nitrogen and oxygen species and their metabolites, and inorganic compounds have been separated and detected by ME coupled to amperometry.[1-4] Nonetheless, voltammetric information that leads to the identification of species based on their redox potentials cannot be achieved using a single electrode. This challenge has been addressed by using dual electrodes[5-14] to collect the voltammetric information.

Dual-series and dual-parallel electrode configurations are the two key categories of dual electrode systems. These two configurations have been applied extensively with LC-EC, CE-EC and ME-EC for the recognition of species and/or selective detection of species.[15-17] Generation-collection mode of the dual-series configuration has been primarily utilized for selective detection of electrochemically reversible analytes.[5, 7, 9, 12-13] In this mode, a stable product, typically an oxidized form of the original analyte, is generated at the first electrode followed by the reduction of the product formed at the second electrode. The generation-collection mode has been commonly used to detect catecholamines and phenolic acids.[7, 10] At the first working electrode, catechols are oxidized to their quinone form and then at the second electrode, the quinone product is reduced back, providing a selective method of detection for these substances.

The collection efficiency, or the percent amount of the redox product formed at the first electrode relative to the amount of the redox analytes reacted at the second electrode, is determined by the electrochemical rate constant of the analytes, the distance between the electrodes, and the

flow rate. Species having different heterogeneous kinetic rates can therefore be identified based on their collection efficiencies.

Redox cycling, leading to better detection limits, can be achieved using the dual-parallel electrode configuration. This has been implemented in CE by placing two cylindrical electrodes opposed to each other.[11, 14] Based on the redox potential of the analyte of interest, a potential is applied to one electrode to form its redox product at the maximum rate. The species is then regenerated by applying a suitable potential at the second electrode. This process can significantly enhance the mass transport of the species to the electrode given that the two electrodes are sufficiently close relative to their sizes.[14] The species travel by diffusion between the electrodes and the electrodes are placed at a short distance so that it takes only a few milliseconds to reach the opposite electrode.

Potential sweeping techniques, such as voltammetry, can be used to identify electrochemically active analytes based on their redox potentials. However, it is challenging to couple voltammetry with CE or ME owing to a couple of reasons. Capacitive charging currents result due to the scanning of potentials, leading to high background noise. Consequently, low LODs and high sensitivities are difficult to obtain in general with voltammetry coupled to CE or ME. Also, the temporal resolution is insufficient to couple with ME at slow scanning rates.[18-20] Nonetheless, there have been some reports of voltammetric detection for CE.[18, 20-24] Instead of using conventional voltammetry, two parallel working electrodes biased at two different potentials can be used to obtain voltammetric information.[25] This strategy has been employed with CE to obtain current ratios and thus voltammetric information.[14] The combination of the migration time with the voltammetric characterization using a current ratio increases the certainty of identification of the analytes.

Either dual-series or dual-parallel configuration can be utilized to obtain current ratios for analytes separated by ME. A simple-t microchip is most easily coupled to the dual-series configuration. Nevertheless, electrolysis of the analytes at the first electrode and the placement of electrodes must be optimized to generate good results with the dual-series configuration. Voltammetric identification of redox species with cylindrical electrodes integrated to CE using dual-parallel configuration has been reported.[14] In this mode, the analyte plug travels over the two working electrodes at the same time and, therefore, analyte depletion and the peak width differences at the two electrodes due to their relative placement need not be considered.[14]

To date, dual-series configuration integrated with ME in generation-collection mode has been employed most often to determine the redox identity. In contrast, dual-parallel configuration has not been used. In this chapter, the identification of intracellular redox species based on the current ratios obtained using both dual-parallel and dual-series electrode configurations is discussed. The use of modification factors in dual-series configuration to account for differences in response due to electrode placement and to produce more representative current ratios is also explained. A dual-channel electrode microchip was then developed to implement dual-parallel configuration that enables injection of the same amount of sample into two unique separation channels, each coupled to a detector electrode. This configuration is then assessed for the analysis of pro-oxidants and antioxidants present in macrophage cell lysates.

2.2 Materials and Methods

2.2.1 Materials and reagents

These chemicals and reagents were used as received: SU-8 10 photoresist and SU-8 developer (MicroChem Corp., Newton, MA, USA); AZ 1518 photoresist and 300 MIF developer (Mays Chemical Co., Indianapolis, IN, USA); photolithography film masks (50,000 dpi; Infinite

Graphics Inc., Minneapolis, MN, USA); N(100) 100 mm (4") silicon (Si) wafers (Silicon, Inc., Boise, ID, USA); chrome and AZ1518 positive photoresist-coated soda lime glass substrates (4"×4"×0.090", Nanofilm, Westlake, CA, USA); Sylgard 184 Silicone Elastomer Kit: polydimethylsiloxane (Ellsworth Adhesives, Germantown, WI, USA); Titanium (Ti) etchant (TFTN; Transene Co., Danvers, MA, USA); epoxy and 22 gauge Cu wire (Westlake Hardware, Lawrence, KS, USA); silver colloidal paste (Ted Pella, Inc., Redding, CA, USA); acetone, 2-propanol (isopropyl alcohol, IPA), 30% H_2O_2, H_2SO_4, HNO_3, NaOH and HCl (Fisher Scientific, Fair Lawn, NJ, USA); sodium nitrite, boric acid, tetradecyltrimethylammonium bromide (TTAB), tetradecyltrimethylammonium chloride (TTAC), tyrosine (Tyr), sodium azide, potassium iodide, NaCl, (Sigma, St. Louis, MO, USA); buffered oxide etchant (JT Baker, Austin, TX, USA) and peroxynitrite (ONOO-, Cayman Chemicals, Ann Arbor, MI, USA or EMD Millipore, Billerica, MA, USA). All water used was ultrapure (18.2 MΩ·cm) (Milli-Q Synthesis A10, Millipore, Burlington, MA, USA).

2.2.2 PDMS device fabrication

PDMS microchip devices were fabricated as described in the literature.[26] Microchannels were first drawn using AutoCad LT 2004 (Autodesk, Inc., San Rafael, CA, USA) and printed on a transparency sheet at a resolution of 50,000 dpi (Infinite Graphics Inc., Minneapolis, MN, USA). A simple-t design with a 5 cm×40 μm×15 μm separation channel and 0.75 cm×40 μm×15 μm side arms was used for the dual-series configuration. The dual-channel microchip design shown in Figure 2.1 was used for the dual-parallel electrode configuration. Both separation channels are 5 cm in length with a cross-section of 40 μm×15 μm and other dimensions are indicated in Figure 2.1A.

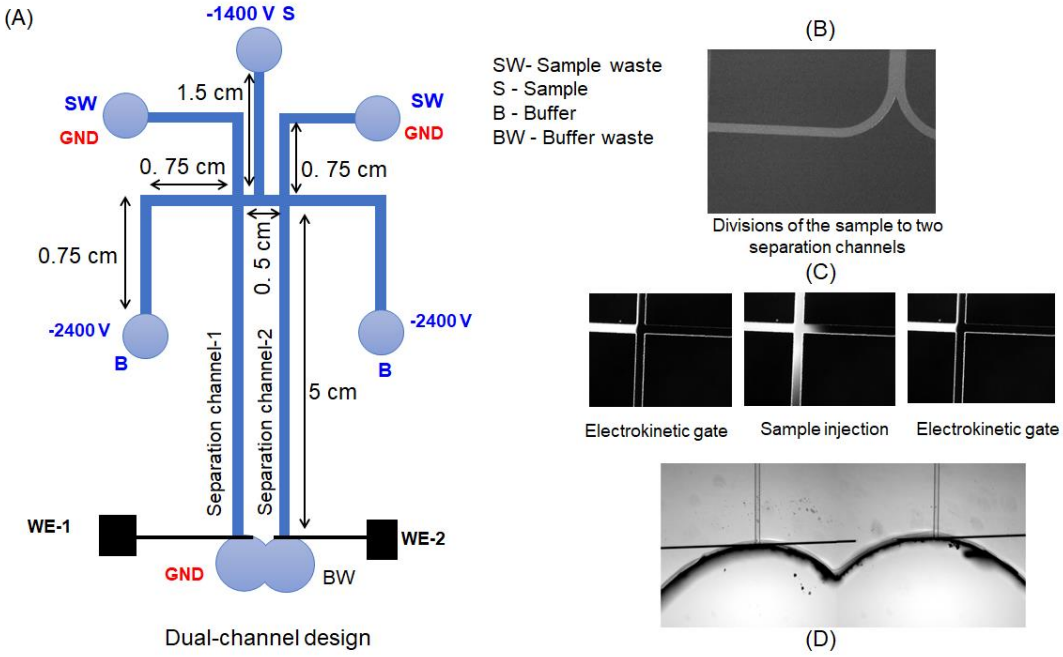

Figure 2.1 (A) Dual-channel design (B) equal amounts of sample injected to two separation channels (C) electrokinetic gated injection (D) electrode alignment

Channel structures from the developed transparency mask were then transferred to a 4-inch silicon wafer coated with SU-8 photoresist using a UV flood source. The wafer was then subjected to a soft bake and then it was developed to obtain the channel master. Hard bake of the wafer was then performed at 200 °C for 2 hours. A PDMS mixture containing the elastomer and the curing agent at a ratio of 10:1 was poured onto the master and was cured at 70 °C overnight. The PDMS device was punched using a 4 mm biopsy punch (Harris Uni-core, Ted Pella Inc., Redding, CA, USA) at the end of each channel to create reservoirs, as necessary.

2.2.3 Platinum electrode fabrication

All amperometric measurements were made using 15 μm electrodes fabricated on glass by photolithography. The fabrication procedure was described previously by the Lunte group.[27] Briefly, the designs were first drawn with a sufficient resolution using AutoCad LT 2004

(Autodesk, Inc., San Rafael, CA, USA) and printed on a transparency sheet (Infinite Graphics Inc., Minneapolis, MN, USA). 15 μm wide electrodes with a distance of 15 μm between the two electrodes were used for dual-series configuration and electrodes separated by a distance of 100 μm was used for the dual-parallel configuration (Figure 2.1A). Channel features were copied to a borofloat glass plate coated with chromium and photoresist using the mask and the UV flood source. The glass was then treated with developer followed by chrome etch to reveal the electrode features on the glass. A trench of 200-300 nm was then etched using buffered oxidant. The depth was measured with an Alpha-Step profiler (Alpha Step-200, Tencor Instruments, Mountain View, CA, USA).

The trench was then cleaned with oxygen plasma and the metals Ti (40 nm) and Pt (250 nm) were then sputtered onto the glass under a vacuum (AXXIS DC magnetron sputtering system, Kurt J. Lesker Co., Jefferson Hills, PA, USA). The excess metal and photoresist were then removed by treating with acetone and the chromium layer was removed using chrome etch to obtain the electrode.

2.2.4 Solution preparation

All solutions were prepared in 18 MΩ milliQ water (Millipore A10 system). Standard stock solutions of 10 mM sodium nitrite, 10 mM hydrogen peroxide, 5 mM potassium iodide and 5 mM sodium azide were prepared in milliQ water and stored at 4 °C. 10 mM tyrosine solution was prepared by acidifying the solution with 1 M HCl. Each solution was diluted in the run buffer as necessary at the time of the experiment. 10 mM borate separation buffer was prepared by first diluting a 50 mM boric solution followed by adjusting the pH to 11 with 10 mM or 1 M NaOH solution. TTAB was added to the run buffer to a final concentration of 2 mM.

2.2.5 Chip construction and electrophoresis procedure

Reversibly-sealed PDMS-glass hybrid devices were used for all separations. A two-electrode system was used for amperometric measurements with a Pinnacle isolated potentiostat (Pinnacle Technology Inc., Lawrence, KS, USA), a Ag/AgCl reference electrode (Bioanalytical Systems, West Lafayette, IN, USA) and 15 μm Pt working electrode fabricated as described above.

Electrophoretic separations were performed under reverse polarity mode and TTAB was used as the cationic surfactant to produce a stable electroosmotic flow. For each single-channel experiment, a Pt lead was placed in each reservoir (buffer, sample, buffer waste, sample waste) of a simple-t microchip (Figure 2.2A). High voltages of -2400 V and -2200 V were applied to the buffer and sample reservoirs, respectively, while other two reservoirs were grounded. For each dual-channel experiment, sample was placed in reservoir S and all other reservoirs and channels were filled with buffer. A high voltage of -1400 V was applied to the sample reservoir (S) and -2400 V was applied to buffer reservoirs (B) (Figure 2.1A). Reservoirs SW and BW were grounded to direct sample into the channels for injection to each channel. An electrokinetic gated injection procedure was applied for each dual-series and dual-parallel experiment with an injection time of 1 s. All these operations were controlled using home-built LabView software.

2.2.6 Electrochemical detection

Amperometric measurements were made using modified models of 8151BP, 8100-K6, or 9051 single- or dual-channel wireless, battery operated potentiostats (Pinnacle Technology Inc., Lawrence, KS, USA). Data sampling rates for the models 8151BP, 8100-K6, and 9051 are 5 Hz (Gain = 5,000,000 V/A, Resolution = 30 fA), 10 Hz (Gain = 5,000,000 V/A, Resolution = 27 fA), and 6.5 to 13 Hz (Gain = 5,000,000 V/A, Resolution = 47 fA), respectively. Data acquisition was carried out by Pal or Sirenia software (Pinnacle Acquisition Laboratory) in wireless mode through

Bluetooth technology. A potential of 1.1 V was applied to the working electrode against an Ag/AgCl reference electrode.

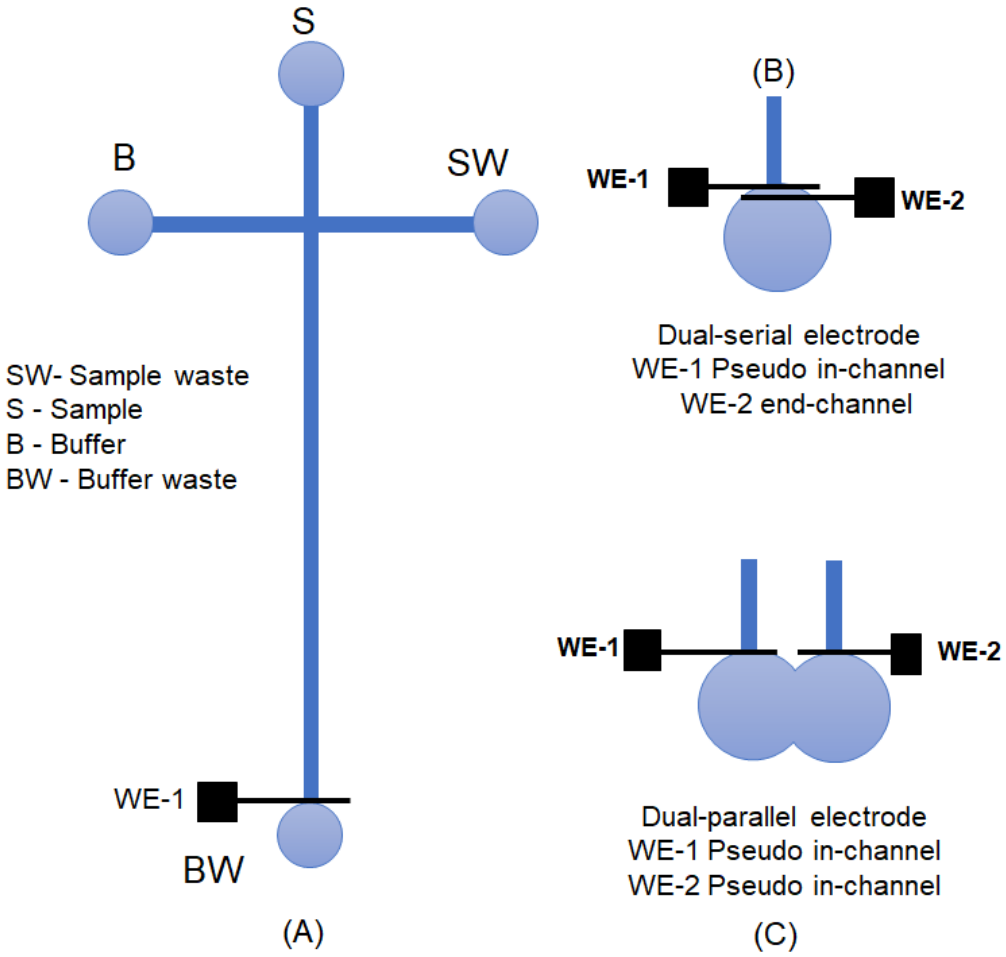

Figure 2.2 (A) Simple-t microchip design, pseudo in-channel alignment (B) dual-series electrodes, WE-1 – pseudo in-channel, WE-2– end-channel (C) dual-parallel electrodes, WE-1 – pseudo in-channel, WE-2– end-channel

2.3 Results and discussion

2.3.1 Theoretical background of generating current ratios for voltammetric identification

In general, a Pt ground lead is placed at the end of the separation channel and the reference electrode is placed behind the Pt lead to eliminate the influence of the separation voltage. This

strategy was used in this work for dual-series configuration with a simple-t microchip. However, it was observed that the reference electrode placement behind the ground electrode leads to low peak efficiencies in dual-channel design. This may be due to the common ground and reference electrode for both channels.

(A)

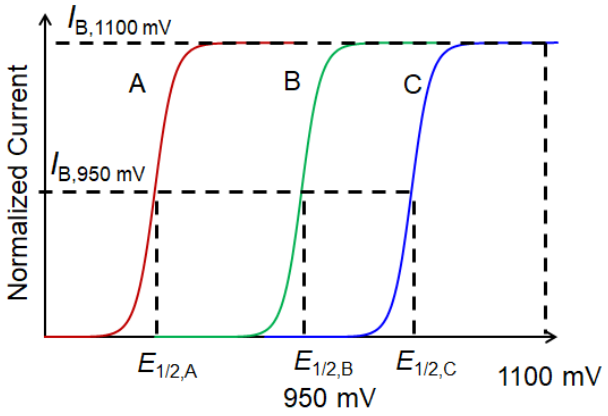

(B)

Species	I_{950}/I_{1100}
A	1.0
B	0.5
C	0.0

Figure 2.3 (A) Hypothetical voltammograms for species having different $E_{1/2}$ values (B) Current ratios for the species shown in Figure 2.3 A

2.3.2 Dual-series electrode configuration with ME

In dual-series configuration, two different potentials are applied to the two working electrodes and their respective electropherograms are recorded to obtain current ratios for analytes separated by ME or CE. A steady state plateau potential of the analyte is selected as one potential and the other one is selected at the vicinity of the half wave potential of the hydrodynamic voltammogram. The basis for the judicial selection of potentials for these measurements is shown in Figure 2.3A using characteristic voltammograms for three different species having distinct half wave potentials. Potentials can be selected as shown to produce unique current ratios for species of this kind. Current ratios are indicative of relative feasibility or difficulty of oxidation or reduction. In this example, 1.1 V and 0.95 V were selected as potentials. A current ratio of 1 is

obtained for species A, showing that it is the easiest to oxidize of them all, while a current ratio of 0 for species C shows that it is the most difficult to oxidize. Therefore, a scale of 0 to 1 can be used to classify the analytes.

A comprehensive analysis can be performed to identify the analytes by considering both voltammetric information and analyte migration times. A potential of 1.1 V vs Ag/AgCl was selected as the higher potential while 0.95 V was selected as the lower potential to obtain current ratios for abundant intracellular compounds such as nitrite, glutathione, ascorbic acid, tyrosine and nitrite. Nitrite cannot be oxidized to its steady state limit at 1.1V; however, this is the maximum potential that is allowed by the electrochemical window of the run buffer. 0.95 V was chosen for the second potential, as the nitrite signal significantly lessened at 0.95 V.

Current ratios can be generated using a single working electrode (Figure 2.2A). However, this procedure is time-consuming since twice as many injections compared to the dual-electrode configuration are necessary to generate current ratios. Therefore, this method is not preferred for short-lived species or volume-limited samples. Electropherograms at two different potentials can be easily generated by the dual-electrode approach in a single run (Figure 2.2B). This can be accomplished in CE and ME with two electrodes either in a dual-series (Figure 2.2B) or dual-parallel (Figure 2.2C) configuration.

A 5 cm simple-t microchip reversibly sealed to two 15 μm electrodes fabricated with a spacing of 15 μm on a glass plate was used for the dual-series electrode configuration. Current ratios generated using this configuration are not realistic due to two major factors. As the first electrode “sees” the analyte plug before the second, a considerable amount of analyte can be lost at the first electrode due to electrolysis. Additionally, the overlap of the diffusion layers of the two electrodes may lead to reduced mass transport to the second electrode and thus lesser current at

the second. This can be overcome by increasing the spacing between the two electrodes. However, that will decrease the peak efficiency and resolution of peaks at the second electrode.

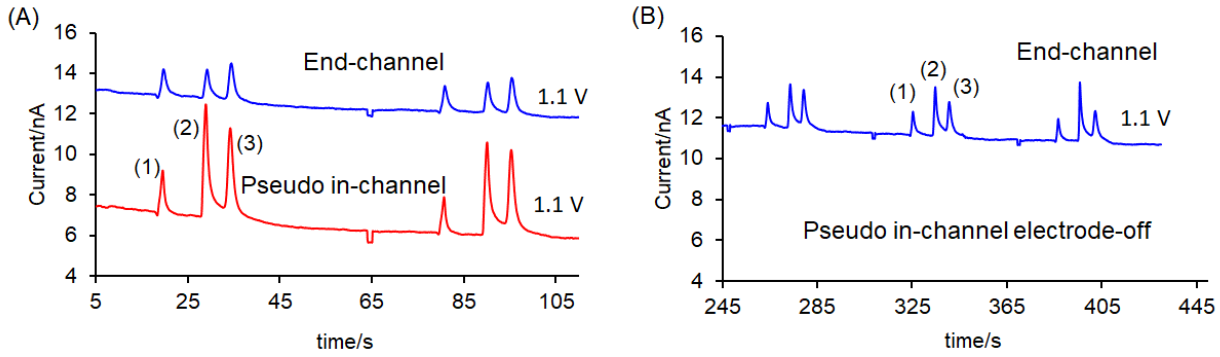

Figure 2.4 Electropherograms obtained for dual-series configuration for (1) nitrite, (2) tyrosine and (3) hydrogen peroxide with (A) both electrodes on and biased at 1.1 V (B) end-channel electrode on but pseudo in-channel electrode off

The difference of electrode response owing to the placement of the electrodes relative to the channel end is the second major influential factor for dual-series configuration. In this study, the first electrode is aligned at the exact end of the channel (pseudo in-channel) and the other electrode therefore is placed at end-channel configuration. It was reported that the electrode responses of pseudo-in-channel and end-channel differ by a factor of 2.[28] Therefore, the current ratios generated in the dual-series configuration must be adjusted to account for these factors. The current response for all analytes were measured at both electrodes biased at 1.1 V against a Ag/AgCl reference electrode to evaluate the correction factor. Three successive injections were made with the potential turned on at both electrodes (Figure 2.4A) and then the potential was turned off at the pseudo-in-channel electrode during next three injections (Figure 2.4B). In these two sets of data, peak heights for nitrite were not changed; however, a change was noticed for tyrosine. This difference can be explained based on the half-wave potentials of nitrite and tyrosine.

Nitrite has a half wave potential of 1.0 V and tyrosine has a half wave potential of 0.7 V and, therefore, the differences of overpotential required for the oxidation of analytes significantly impacts the current ratios. As shown in Table 2.1, the correction factor for the oxidation differences is large for some species but negligible for other compounds.

The difference of the electrode response due to the actual geometric area responsible for the electroactivity is more important for the correction of the current ratios compared to the correction factor for oxidation differences. The original and corrected current ratios are shown in Table 2.1. Tyrosine shows a current ratio of 1.11 after the correction has been made to the original value of 2.26 for the electrode sensitivity differences. The corrected current ratio for tyrosine is slightly above 1 because of the higher electrochemical current at the pseudo-in-channel electrode compared to the end-channel electrode. A correction factor of 1.33 is obtained for this difference in current response due to the loss of the analyte at the first electrode. A final current ratio of 0.85 was obtained for tyrosine.

Species	I_{950}/I_{1100}	Oxidation ratio[a] I_{1100}/I_{1100}	Sensitivity ratio[b] I_{1100}/I_{1100}	Corrected[c] I_{950}/I_{1100}
Nitrite	0.51 ± 0.01	-0.16 ± 0.03	1.65 ± 0.17	0.23 ± 0.00
Tyrosine	2.26 ± 0.02	1.33 ± 0.12	2.03 ± 0.57	1.11 ± 0.01
H_2O_2	2.33 ± 0.12	-0.04 ± 0.26	2.57 ± 0.16	1.61 ± 0.09

Table 2.1: Current ratios and correction factors for dual-series electrode configuration

[a]Oxidation ratio is the difference between the sensitivity ratio (at both electrodes 1100 V) and the current ratio when both pseudo-end-channel and end-channel electrodes were switched on (at both electrodes 1100 mV)

[b]Sensitivity ratio: Ratio of the peak heights obtained at the end-channel electrode while the pseudo end-channel electrode is disconnected to the peak heights obtained at the pseudo-end-channel electrode

[c]Corrected current ratios for electrode sensitivities

Ratios represented by mean and standard deviations for three consecutive injections in the same microchip.

As is shown in Table 2.1, electrode responses (oxidation ratio in Table 2.1) are similar for nitrite and hydrogen peroxide. The reason for this observation is different for the two species. For nitrite, this is caused by the difficulty of oxidation that renders the loss of analyte insignificant. A final corrected current ratio of 0.89 was obtained for hydrogen peroxide, which is less than the value obtained with dual-parallel configuration (Table 2.2). The reason can be explained by considering the effect of separation voltage in between dual parallel and dual-series configurations. Because of the effect of separation voltage, the apparent potential is much higher at the pseudo-in-channel electrode compared to the end-channel electrode. It was previously reported that

hydrodynamic voltammograms for hydrogen peroxide show a current decrease at higher potentials and thus a decrease in current at the pseudo-in-channel electrode is observed in dual-series configuration. This is not the case in dual-parallel configuration where both electrodes are similarly affected by the separation voltage. In summary, the assembly and operation of dual-series configuration is easier; nonetheless, the requirement of necessary corrections to provide current ratios for peak identification are time-consuming and complex, making it not very convenient.

2.3.3 Dual-parallel electrode configuration with ME

A microchip with two separation channels, as shown in Figure 2.1A, was used with two parallel electrodes fabricated on glass with a spacing of 100 μm for dual-parallel configuration experiments. The channel design was adapted from the study reported by Hahn's group.[29-30] In their experiments, two electrodes were aligned in pseudo-in-channel configuration in two unique separation channels. The study was aiming to cancel out the noise due to the separation voltage by using one electrode as the working electrode (aligned at the sample channel) and the other electrode as the pseudo-reference electrode (aligned at the reference channel). All the channels were filled with run buffer and the sample was injected only to the sample channel. Buffer was injected into the reference channel instead of the sample.

Two distinct reservoirs were employed to hold the sample and run buffer for injection in Hahn's configuration. In this study, a new approach was designed to place the sample in one reservoir (Figure 2.1A) and then equal amounts of sample were injected into two separation channels. Buffer and sample voltages were optimized to obtain a proper electrokinetic gate and ensure the injection of similar amounts to each channel. This was accomplished under normal polarity separation conditions using 10 mM borate with 2 mM SDS at pH 11 as the run buffer and fluorescein as the analyte. Sample voltage and buffer voltage were optimized to be 1400 V and

2400 V, respectively. This optimization was performed under normal polarity, as it is difficult to see the injection of fluorescein under reverse polarity.

For the reverse polarity experiments for the measurement of nitrite, TTAB was used as a channel modifier. The BGE consisted of 10 mM borate with 2 mM TTAB at pH 11. The sample and buffer voltages were -1400 V and -2400 V, respectively. It was found that the sample injection was reproducible and similar from injection to injection with the above conditions and injection and separation voltages. This implies that the same response for the sample is possible at each electrode placed in each channel.

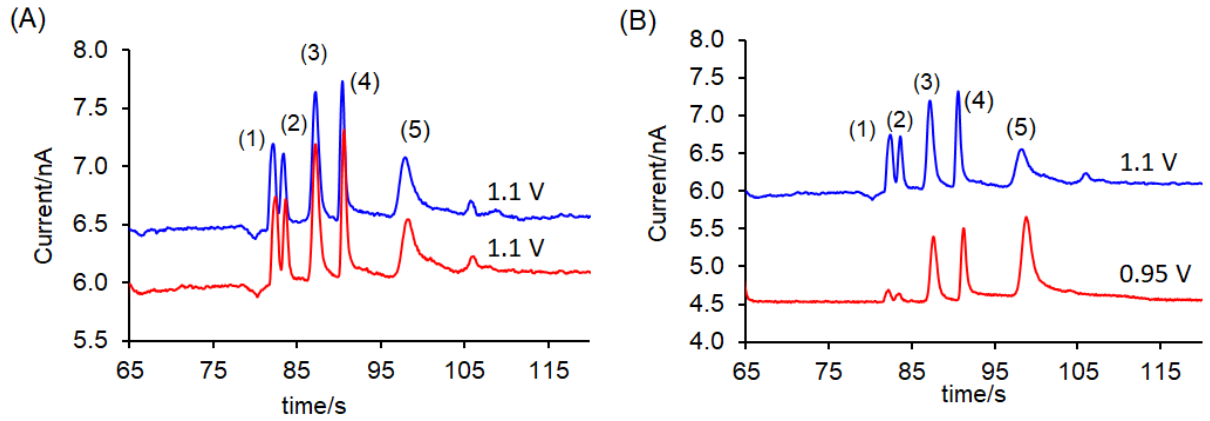

Figure 2.5 Electropherograms obtained for dual-channel/dual-parallel configuration for (1) nitrite, (2) azide, (3) iodide, (4) tyrosine, and (5) hydrogen peroxide with (A) both electrodes biased at 1.1 V and (B) one electrode biased at 1.1 V and the other at 0.95 V

Pseudo-in-channel alignment was used for the dual-parallel configuration. Electrode responses for the analytes were comparable at each electrode when they were biased at the same potential of 1.1 V against Ag/AgCl (Figure 2.5). As expected, the current response decreased upon setting the potential at one electrode to 0.95 V. Calculated current ratios without including correction factors are shown in Table 2.2. It can be seen that the current ratios are slightly varied

between the dual-series and dual-parallel configurations. These differences may be caused by the varied influences of separation voltage at the pseudo-in-channel electrode/dual-series configuration versus pseudo-in-channel electrode /dual-parallel configuration.

In some instances, it was also noted that there were variations in electrode responses even with the dual-parallel configuration. These differences are a result of variations introduced to the microchannels and electrodes during the microfabrication process. Such variation can be eliminated by including a correction factor. This can be accomplished by keeping both electrodes at 1.1 V and normalizing the current response accordingly. Because of these variations, both dual-series and dual-parallel microchip experiments were characterized using standards before running any biological samples. Nonetheless, the dual-parallel configuration is applicable with minor corrections to generate current ratios for peak identification.

Species	Migration time (s)	I_{1100}/I_{1100}	I_{950}/I_{1100}
Nitrite	17.4 ± 0.2	1.04 ± 0.06	0.20 ± 0.02
Azide	18.7 ± 0.2	0.87 ± 0.05	0.16 ± 0.02
Iodide	23.0 ± 0.1	0.98 ± 0.03	0.75 ± 0.02
Tyrosine	26.6 ± 0.0	0.92 ± 0.04	0.77 ± 0.04
H_2O_2	34.4 ± 0.3	1.04 ± 0.06	2.04 ± 0.09

Table 2.2 Dual-parallel electrode configuration for ME with amperometric detection, migration times and current ratios at different voltages as shown (n=3)

2.3.4 Comparison of dual-series and dual-parallel electrode configurations with ME

Microchip fabrication, electrode alignment and operation are comparatively easier for dual-series configuration. However, analyte depletion at the first electrode needs to be considered when calculating the current ratios for most compounds. Also, it can be difficult to identify species having close migration times with dual-series configuration because of the band broadening that can occur at the end-channel electrode. In contrast, realistic current ratios can be obtained using a much simpler procedure using dual-parallel configuration; however, the fabrication and electrode alignment require significant attention and care. The dual-channel microchip design described here makes it possible to obtain a current ratio from a single sample in one run, eliminating sample-to-sample variability and making it possible to obtain voltammetric information for short lived species with ME.

2.3.5 Use of dual-parallel configuration for better identification of intracellular electroactive species in macrophage cell lysates that have closer migration times

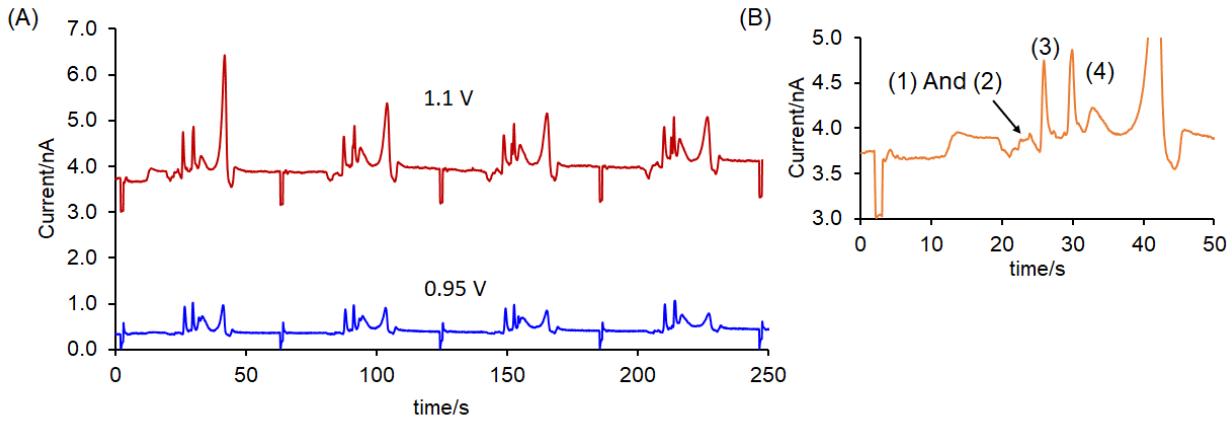

Figure 2.6 Electropherogram of macrophage cell lysates with an internal standard iodide (A) electropherograms at 1.1 V and 0.95 V (B) closer view – first injection of electropherogram at 1.1 V

As it is shown in Table 2.2, the migration times of nitrite and azide are close to each other; therefore, it is difficult to identify them by using only the migration times. Peak identification can be verified using current ratios. As shown in Table 2.2, the peak height for nitrite is higher than that for azide. As there is a considerable difference in the response at the two electrodes for azide when compared to the other species (Table 2.2), a correction has been made using I_{100}/I_{100} ratio for nitrite and azide for comparison; 0.20 ± 0.02 for nitrite and 0.16 ± 0.02 and are statistically different at 95% confidence limit. Therefore, these current ratios can be applied to resolve the azide from nitrite.

Species	Migration time (s)	Cells I_{950}/I_{1100}
1	19.6 ± 0.2	0.28 ± 0.08
2	21.0 ± 0.2	0.25 ± 0.08
3	23.6 ± 0.3	0.64 ±0.08
4	26.5 ± 0.2	1.26 ±0.02

Table 2.3 Current ratios for first three peaks of the electropherogram (n=5, fourth peak n=4)

Identification of electroactive species present in macrophage cell lysates was performed by a dual-channel/dual-parallel microchip. Previously, pseudo-in-channel amperometric detection coupled to a simple-t microchip was employed to identify nitrite, tyrosine, glutathione and NO from macrophage cell lysates based on the migration times. The background electrolyte was used to lyse the macrophage cells followed by filtering through a 3 kDa cut-off filter before the microchip analysis. As we have seen in our previous studies, several redox species appeared in the

electropherograms generated for the cell lysate using the dual-parallel/dual channel microchip system. Iodide was used as an internal standard and consistent peak heights were obtained, indicating good reproducibility of the analyte injection into the two channels and correct operation of the separation and detection system. The electropherogram obtained is shown in Figure 2.6. The current ratios and migration times were calculated for the first four species (Table 2.3). The third peak can be identified as iodide because its migration time and current ratio are close to the values obtained with standards. The current ratio alone cannot be used to confirm the peak identity of the first two peaks, as these current ratios are not statistically different. However, by using peak migration times, it can be justified that peak 1 is nitrite and peak 2 is azide. The peak height variabilities are high as the peak heights for the first two peaks are very small.

2.4 Conclusions:

It has been shown that the dual-series electrode configuration for identification of analytes based on current ratios requires a time consuming and comprehensive data analysis. A better method to collect voltammetric information to identify electroactive species has been developed. The dual-channel/dual-electrode configuration can identify electroactive compounds based on their current ratios with much simpler data analysis. The developed method was applied to identify species in macrophage cells. The internal standard peak, iodide, was identified based on both migration time and current ratios. Also, nitrite and azide have been identified using current ratios and migration times.

2.5 References

1. Lacher, N. A.; Garrison, K. E.; Martin, R. S.; Lunte, S. M., Microchip capillary electrophoresis/electrochemistry. *Electrophoresis* **2001,** *22*, 2526-2536.

2. Martin, A.; Vilela, D.; Escarpa, A., Food analysis on microchip electrophoresis: An updated review. *Electrophoresis* **2012,** *33*, 2212-2227.

3. Chen, G.; Lin, Y.; Wang, J., Microchip capillary electrophoresis with electrochemical detection for monitoring environmental pollutants. *Curr. Anal. Chem.* **2006,** *2*, 43-50.

4. Vandaveer, W. R.; Pasas-Farmer, S. A.; Fischer, D. J.; Frankenfeld, C. N.; Lunte, S. M., Recent developments in electrochemical detection for microchip capillary electrophoresis. *Electrophoresis* **2004,** *25* (21-22), 3528-3549.

5. Martin, R. S.; Gawron, A. J.; Lunte, S. M.; Henry, C. S., Dual-Electrode Electrochemical Detection for Poly(dimethylsiloxane)-Fabricated Capillary Electrophoresis Microchips. *Anal. Chem.* **2000,** *72* (14), 3196-3202.

6. Zhong, M.; Zhou, J.; Lunte, S. M.; Zhao, G.; Giolando, D. M.; Kirchhoff, J. R., Dual-Electrode Detection for Capillary Electrophoresis/Electrochemistry. *Anal. Chem.* **1996,** *68* (1), 203-207.

7. Zhong, M.; Lunte, S. M., Tubular-Wire Dual Electrode for Detection of Thiols and Disulfides by Capillary Electrophoresis/Electrochemistry. *Anal. Chem.* **1999,** *71* (1), 251-255.

8. Voegel, P. D.; Baldwin, R. P., Electrochemical detection in capillary electrophoresis with dual-parallel on-capillary electrodes. *Electrophoresis* **1998,** *19* (12), 2226-2232.

9. Mecker, L. C.; Martin, R. S., Use of micromolded carbon dual electrodes with a palladium decoupler for amperometric detection in microchip electrophoresis. *Electrophoresis* **2006,** *27* (24), 5032-5042.

10. Lin, B. L.; Colón, L. A.; Zare, R. N., Dual electrochemical detection of cysteine and cystine in capillary zone electrophoresis. *J. Chromatogr.* **1994,** *680* (1), 263-270.

11. Jin, W.; Li, X.; Gao, N., Simultaneous Determination of Tryptophan and Glutathione in Individual Rat Hepatocytes by Capillary Zone Electrophoresis with Electrochemical Detection at a Carbon Fiber Bundle−Au/Hg Dual Electrode. *Anal. Chem.* **2003,** *75* (15), 3859-3864.

12. Holland, L. A.; Harmony, N. M.; Lunte, S. M., Characterization of an Integrated On-Capillary Dual Electrode for Capillary Electrophoresis-Electrochemistry. *Electroanalysis* **1999,** *11* (5), 327-330.

13. Fischer, D. J.; Vandaveer IV, W. R.; Grigsby, R. J.; Lunte, S. M., Pyrolyzed Photoresist Carbon Electrodes for Microchip Electrophoresis with Dual-Electrode Amperometric Detection. *Electroanalysis* **2005,** *17* (13), 1153-1159.

14. Dorris, M. K.; Crick, E. W.; Lunte, C. E., A parallel dual-electrode detector for capillary electrophoresis. *Electrophoresis* **2012,** *33* (17), 2725-32.

15. Lunte, C. E.; Ridgway, T. H.; Heineman, W. R., Voltammetric-amperometric dual-electrode detection for flow injection analysis and liquid chromatography. *Anal. Chem.* **1987,** *59* (5), 761-766.

16. Lunte, C. E.; Kissinger, P. T.; Shoup, R. E., Difference mode detection with thin-layer dual-electrode liquid chromatography/electrochemistry. *Anal. Chem.* **1985,** *57* (8), 1541-1546.

17. Roston, D. A.; Shoup, R. E.; Kissinger, P. T., Liquid chromatography/electrochemistry: thin-layer multiple electrode detection. *Anal. Chem.* **1982,** *54* (13), 1417A-1434A.

18. Ferris, S. S.; Lou, G.; Ewing, A. G., Scanning electrochemical detection in capillary electrophoresis. *J. Microcolumn Sep.* **1994,** *6* (3), 263-268.

19. Swanek, F. D.; Chen, G.; Ewing, A. G., Identification of Multiple Compartments of Dopamine in a Single Cell by CE with Scanning Electrochemical Detection. *Anal. Chem.* **1996,** *68* (22), 3912-3916.

20. Fang, H.; Vickrey, T. L.; Venton, B. J., Analysis of Biogenic Amines in a Single Drosophila Larva Brain by Capillary Electrophoresis with Fast-Scan Cyclic Voltammetry Detection. *Anal. Chem.* **2011,** *83* (6), 2258-2264.

21. Gerhardt, G. C.; Cassidy, R. M.; Baranski, A. S., Square-Wave Voltammetry Detection for Capillary Electrophoresis. *Anal. Chem.* **1998,** *70* (10), 2167-2173.

22. Hebert, N. E.; Kuhr, W. G.; Brazill, S. A., Microchip capillary electrophoresis coupled to sinusoidal voltammetry for the detection of native carbohydrates. *Electrophoresis* **2002,** *23* (21), 3750-9.

23. Park, S.; McGrath, M. J.; Smyth, M. R.; Diamond, D.; Lunte, C. E., Voltammetric detection for capillary electrophoresis. *Anal. Chem.* **1997,** *69* (15), 2994-3001.

24. Wen, J.; Baranski, A.; Cassidy, R., Cyclic voltammetric detection in capillary electrophoresis with application to metal ions. *Anal. Chem.* **1998,** *70* (13), 2504-9.

25. Martin, R. S.; Gawron, A. J.; Lunte, S. M.; Henry, C. S., Dual-Electrode Electrochemical Detection for Poly(dimethylsiloxane)-Fabricated Capillary Electrophoresis Microchips. . *Anal. Chem.* **2000,** *72* (14), 3196-3202.

26. Hulvey, M. K.; Frankenfeld, C. N.; Lunte, S. M., Separation and Detection of Peroxynitrite Using Microchip Electrophoresis with Amperometric Detection. *Anal. Chem.* **2010,** *82* (5), 1608-1611.

27. Scott, D. E.; Grigsby, R. J.; Lunte, S. M., Microdialysis sampling coupled to microchip electrophoresis with integrated amperometric detection on an all-glass substrate. *Chemphyschem* **2013,** *14* (10), 2288-94.

28. Gunasekara, D. B.; Hulvey, M. K.; Lunte, S. M., In-channel amperometric detection for microchip electrophoresis using a wireless isolated potentiostat. *Electrophoresis* **2011,** *32* (8), 832-7.

29. Chen, C.; Hahn, J. H., Dual-channel method for interference-free in-channel amperometric detection in microchip capillary electrophoresis. *Anal. Chem.* **2007,** *79* (18), 7182-6.

30. Chen, C.; Teng, W.; Hahn, J. H., Nanoband electrode for high-performance in-channel amperometric detection in dual-channel microchip capillary electrophoresis. *Electrophoresis* **2011,** *32* (8), 838-43.

3. Chapter 3 Separation and detection of reactive oxygen and nitrogen species using microchip electrophoresis with fluorescence detection (ME-FL)

This chapter is based on the following publications:

1. Fresta, C. G.; Chakraborty, A.; Wijesinghe, M. B.; Amorini, A. M.; Lazzarino, G.; Lazzarino, G.; Tavazzi, B.; Lunte, S. M.; Caraci, F.; Dhar, P.; Caruso, G., Non-toxic engineered carbon nanodiamond concentrations induce oxidative/nitrosative stress, imbalance of energy metabolism, and mitochondrial dysfunction in microglial and alveolar basal epithelial cells. *Cell Death & Disease* **2018,** *9* (2), 245.

2. Caruso, G.; Fresta, C. G.; Siegel, J. M.; Wijesinghe, M. B.; Lunte, S. M., Microchip electrophoresis with laser-induced fluorescence detection for the determination of the ratio of nitric oxide to superoxide production in macrophages during inflammation. *Analytical and Bioanalytical Chemistry* **2017,** *409* (19), 4529-4538.

3. Caruso, G.; Fresta, C. G.; Martinez-Becerra, F.; Antonio, L.; Johnson, R. T.; de Campos, R. P. S.; Siegel, J. M.; Wijesinghe, M. B.; Lazzarino, G.; Lunte, S. M. Carnosine modulates nitric oxide in stimulated murine RAW 264.7 macrophagesMol. Cell. Biochem. 2017, 431, 197-210

3.1 Introduction

The human body constantly produces various free radicals including RNOS, referred as pro-oxidants, during normal essential metabolic processes and/or due to the environmental conditions such as microbial infections, excessive exercise, X-ray, environmental pollutants, cigarette smoke, alcohol, pesticides, and ozone.[1] Both mitochondrial and non-mitochondrial processes are endogenous sources of free radicals and RNOS production. The electron transport chain and nitric oxide synthase reaction are the mitochondrial sources, while the Fenton reaction, microsomal cytochrome P450 enzymes, peroxisomal beta-oxidation and respiratory burst of phagocytotic cells are the non-mitochondrial sources.[2] Superoxide anion and hydroxyl radical are examples of free radicals and they contain one electron in their outermost shell. Molecules such as hydrogen peroxide and singlet oxygen are examples of reactive oxygen species.[3-4] Certain forms of nitrogen, iron, copper and sulfur are also reactive and can contribute to an increase in the production of reactive oxygen species.[5-6] Nitric oxide and peroxynitrite are two important reactive nitrogen species that can lead to nitrosative stress. Molecules capable of donating an electron, thus neutralizing reactivity of free radicals, are known as antioxidants. They can defend against pro-oxidants in several different ways, for example as a radical scavenger, hydrogen donor, peroxide decomposer, singlet oxygen quencher, enzyme inhibitor, or metal chelating agent.[7] Some of the antioxidants, such as glutathione, ubiquinol, and uric acid, are synthesized in the body while other small molecule antioxidants, such as ascorbate, must be taken through the diet.

Excessive formation of RNOS in the cell creates an imbalance between pro-oxidants and antioxidants leading to both oxidative stress and nitrosative stress. It has been postulated that this imbalance may be the cause of more than 100 diseases in our body including neurological disorders (Alzheimer's disease, Parkinson's disease, muscular dystrophy), inflammatory diseases, (arthritis,

vasculitis, glomerulonephritis, lupus erythematous, adult respiratory diseases syndrome), cardiovascular diseases (atherosclerosis, congestive heart failure), hemochromatosis, emphysema, gastric ulcers, hypertension and preeclampsia, alcoholism and smoking-related diseases.[8-9] Therefore, the balance between pro-oxidants and antioxidants in cells is very important and quantification of these species will facilitate a better understanding of these disease pathways.

Fluorescence detection (FL) often provides the best detection limits for RNOS due to its characteristic low background and noise. Several fluorescent probes have been developed and many are available commercially. These have been used to detect and quantify pro-oxidants in cells by imaging.[10] Some fluorescent probes are selective for a specific molecule, while others are used to measure the total amount of reactive nitrogen species or reactive oxygen species present.[11] In certain instances, fluorescent detection alone is insufficient for the reliable measurement of RNOS. For example, there are fluorescent probes that are themselves weakly fluorescent and thus produce background fluorescence. Other probes also can react with other cellular species leading to side products and selectivity issues.[12] For such occasions, it is necessary to incorporate a separation step prior to fluorescence detection to distinguish the product of interest from interferences. Microchip electrophoresis is a good choice in this case because it features sub-minute analysis times, low volume requirements, and simple integration with fluorescence detection.[13]

Our group has investigated the production of NO in Jurkat cells following stimulation with lipopolysaccharide (LPS) using 4-amino-5-methylamino-2′,7′-difluorofluorescein diacetate (DAF-FM DA) and ME-FL. A 2.5-fold increase in NO production was found in the stimulated cells relative to the native cells.[12] Later, this technique was further extended to determine the effect of carnosine on NO production in macrophages.[14] It was demonstrated that there is a dramatic decrease in the NO

production in the presence of carnosine compared to control as shown in Figure 3.1A. The electropherograms showing NO production in the absence and presence of carnosine are shown in Figure 3.1B with interferon-γ used as the stimulant in this study.[14]

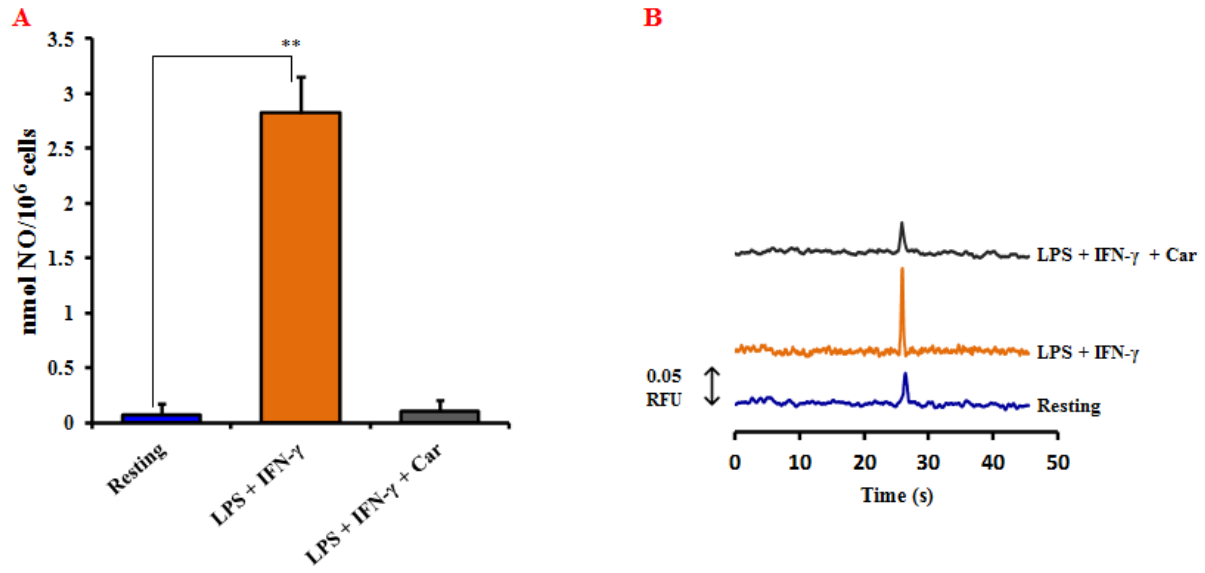

Figure 3.1: Production of NO in stimulated cells with LPS and IFN-γ in the presence and absence of carnosine (A) NO amounts produced compared to the native cells (B) comparison of electropherograms obtained using ME-fluorescence detection (Reproduced with permission from ref. 14.)

A different study was dedicated to studying superoxide production in RAW 264.7 macrophage cells. In that study, a 15-fold enhancement of superoxide production was detected on a per cell basis. Phorbol-12-myristate-13-acetate (PMA) was used to stimulate superoxide production. Mitochondrial superoxide indicator (MitoSOX Red), a fluorescent probe that specifically reacts with superoxide, was used as the fluorescence probe.[15] These studies further expanded the number of RNOS that could be determined by ME-FL. A ME-FL method was then developed to measure

both superoxide and nitric oxide in cell lysates using both DAF-FM DA and MitoHE.[15] The developed protocol and the electropherograms obtained with fluorescence detection is described in the methods section and the results section, respectively.

With these valuable and promising results, it was of interest to investigate oxidative stress in cell lines relevant to human biology using microglial and alveolar basal epithelial cells. Microglial cells are responsible for the immune response in the brain and are present in the brain and the spinal cord.[16] Therefore, these cells are relevant for the study of neurodegenerative disease. On the other hand, alveolar basal epithelial cells are present in human lung tissue and are responsible for the diffusion of water and electrolytes across alveoli of lungs. It has been shown that oxidative stress can cause damage to alveolar basal epithelial cells.[17]

In the last decade, the use of engineered nanoparticles has become widespread in many areas including renewable energy development,[18] various industrial developments[19] and biomedicine.[20-21] The accessibility of engineered nanoparticles to organs and tissues has led to its extensive use in biomedical research such as transport of drugs to tumors,[22-24] novel methods of killing bacterial cells,[25] non-invasive imaging method developments,[26] and scavenging of ROS.[27] However, the potential side effects of these engineered nanoparticles are still controversial and relevant studies have yet to be performed.[28-29]

In these studies, the effect of engineered carbon nanodiamonds (ECNs), one specific class of nanoparticles, on ROS production was investigated using 2′,7′dichlorodihydrofluorescein diacetate ($DCFH_2DA$). It had been shown previously *in vitro* that the anionic ECNs interact with the lipid domain of the cell membrane and cause changes in the phospholipid bilayer.[30] It is known that the toxic effects and the activity of carbon nanoparticles is dependent on their size and shape.[31]

The use of nanoparticles has dramatically increased over the past decade and nanoparticles are present in many industrial products (*e.g.* cosmetics, detergents), medicines and commercial laboratory products.[32] Therefore, there is a good chance that these nanoparticles will come in close contact with humans and end up in their lungs through respiration.[33-34] It has been reported that 10-200 nm nanoparticles and their agglomerates can interact with lung surfactants, leading to considerable accumulation in the alveolar regions of lungs.[35] Lung surfactants are composed of a complex mixture of lipids, proteins and carbohydrates. They act as a defense mechanism against foreign particles[36] entering the body by inhalation and keep lungs from collapsing[37-38] by generating a low surface tension.

Also, it is highly likely that the nanoparticles that are inhaled do not stay in the lungs but distribute through the bloodstream to other organs where they can exhibit cytotoxicity in other tissues. More attention needs to be given to this risk factor as it has been shown that ECN-based medicines are capable of transport through the blood brain barrier and have been used to treat diseases such as malignant brain gliomas[39] and Alzheimer's disease.[40]

Cell type	Target molecules	Fluorescent probe used
Jurkat cells	NO	DAF-FM DA
RAW 264.7 macrophages	NO	DAF-FM DA
RAW 264.7 macrophages	$O_2^{\bullet -}$	MitoSOX Red
Microglial cells	Total ROS	$DCFH_2DA$
Lung epithelial cells	Total ROS	$DCFH_2DA$

Table 3.1 A summary of different fluorescent probes used for various studies

The effect of ECN on cell toxicity was examined in the presence and absence of a model lung surfactant (LS), dipalmitoyl phosphatidylcholine (DPPC) and 1-palmitoyl-2-oleoyl-sn-glycero-3-phospho-(1′-rac-glycerol) (POPG) (7:3). A549 lung epithelial cells and BV-2 microglia were investigated as well as several different concentrations of ECNs. The selection of human epithelial A549 cells for this study was based on two criteria. First, the lung is the first organ that is exposed to the nanoparticles, where they can accumulate through inhalation,[35] and the A549 cells are a common model to study ROS-based cytotoxicity in the lung.[41-43] The BV-2 brain microglial cells were used, instead of primary microglia cultures, because BV-2 and primary microglia cells exhibit a similar response to inflammation and tropic factors.[44-45] The effect of ECNs on the amount of oxidative stress produced using selected cell models was determined at a concentration of ECNs that is reported to be non-cytotoxic. The different fluorescent probes used to study different RNOS are summarized in Table 2.1.

3.2 Materials and methods

3.2.1. Materials and reagents

Murine RAW 264.7 cells (ATCC® TIB-71™), alveolar basal epithelial A549 cells (ATCC® CCL185™), Dulbecco's modified Eagle's medium (DMEM), DMEM free of phenol red, trypsin-EDTA solution, fetal bovine serum, and penicillin–streptomycin antibiotic solution was purchased from American Type Culture Collection (ATCC, Manassas, VA, USA). Microglial BV-2 cells (ICLC ATL03001) were purchased from Interlab Cell Line Collection (ICLC, Genova, Italy). diethyldithiocarbamate (DDC), 2-methoxyestradiol (2-ME), PMA, anhydrous dimethyl sulfoxide (DMSO), phosphate-buffered saline (PBS), trypan blue solution, LPS, sodium dodecyl sulfate (SDS), calcium chloride, potassium chloride and bovine serum albumin (BSA) were all supplied by Sigma-Aldrich (St. Louis, MO, USA). 2′,7′dichlorodihydrofluorescein diacetate (DCF

H_2DA), phenol red-free RPMI-1640, N-acetyl-L-histidine, acetone, 2-propanol, Sodium hydroxide, hydrochloric acid, 25-mL polystyrene culture flasks, boric acid, ethanol (95%), and C-Chip disposable hemocytometers were obtained from Fisher Scientific (Pittsburgh, PA, USA). IFN-γ was supplied by Calbiochem (Gibbstown, NJ, USA). DAF-FM DA and MitoSOX Red were purchased from Life Technologies (Carlsbad, CA, USA). Poly (ether sulfone) membrane (3 kDa) centrifuge filters were purchased from VWR International (West Chester, PA, USA). Polydimethylsiloxane (PDMS) microdevices were prepared from a Sylgard 184 elastomer kit (Ellsworth Adhesives, Germantown, WI, USA). Organic (chloroform) mixtures of the phospholipids, dipalmitoyl phosphatidylcholine (DPPC, 25 mg/mL) and 1-palmitoyl-2-oleoyl-sn-glyc-ero3-phospho-(1′-rac-glycerol) (POPG, 10 mg/mL), used for this study were obtained from Avanti Polar Lipids Inc. (Alabaster, AL, USA). ECNs used in this research were obtained from Microdiamant (Lengwil, Switzerland). Nitrogen tanks for drying were supplied by Matheson TriGas Inc. All water used was ultrapure (18.2 MΩ cm, Milli-Q Synthesis A10, Millipore, Burlington, MA, USA).

3.2.2 Protocols for studying NO and $O_2^{\bullet -}$ production in RAW 264.7 macrophage cells

3.2.2.1 Cell culture and preparation of RAW 264.7 macrophage cells

DMEM culture medium composed of 10% (v/v) fetal bovine serum, L-glutamine (2 mM), penicillin (50 IU/mL), and streptomycin (0.3 mg/mL) was used to culture RAW 264.7 cells. 75 cm^2 polystyrene flasks were used to culture cells at a density of 5×10^6 cells/ flask in an incubator set to temperature of 37 ^{0}C with a supply of 5% CO_2 in a humidified environment. Cells were passaged every 3-5 days to eliminate overgrowth.

3.2.2.2 Stimulation protocol for the simultaneous detection of NO and $O_2^{\bullet -}$ in macrophage cells

RAW 264.7 macrophage cells were used for this study. Cell sample preparation was performed according to the protocol shown in Figure 3.2. Two cell flasks, one untreated native as a control and one stimulated, were used for the experiment. On the day of the experiment, cells were first harvested using a cell scraper followed by counting with a C-chip disposable hemocytometer. Cells were then plated on a flask at a cell density of 1.2×10^7. A LPS stock solution at 1 mg/mLwas prepared in 10 mM PBS. A 20,000 U/mL IFN-γ stock solution was prepared in 10 mM PBS containing 0.1 % BSA. These stock solutions were diluted in 5 mL cell culture medium to give 100 ng/mL LPS and 600 U/mL IFN-γ solutions. These solutions were added to one of the cell flasks after the macrophage cells adhered to the flask. Both untreated and stimulated cell flasks were then placed in an incubator at 37 ^{0}C and with 5% CO_2 supply for 20 h. A 5 mM DAF-FM DA solution was prepared in 99% sterile DMSO. This solution was diluted in 5 mM DMEM free of phenol red to give a DAF-FM DA concentration of 10 μM. After the incubation period, the cell medium in both cell flasks was substituted with the prepared 5 mL DAF-FM DA/DMEM phenol free solution.

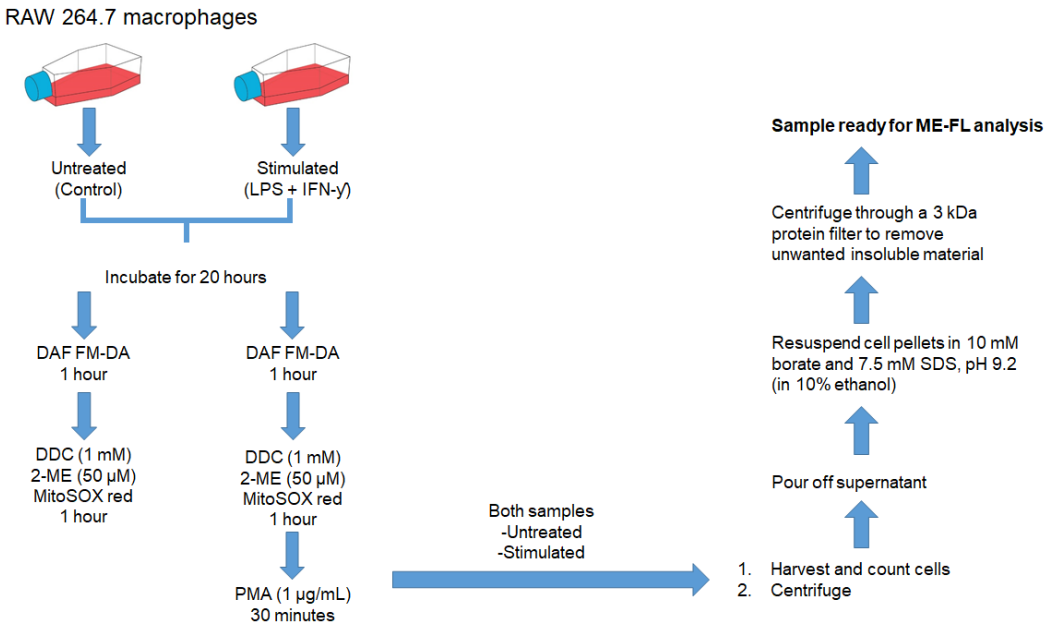

Figure 3.2 Diagram showing the cell stimulation protocol to study NO and $O_2^{\bullet -}$

Stock solutions of 100 mM DDC, 16.5 mM 2-ME, and 1 mg/mL PMA were prepared in 10 mM PBS, DMSO, and DMSO, respectively. The cytosolic SOD inhibitor DDC (final concentration 1 mM), the mitochondrial SOD inhibitor 2-ME (final concentration 50 µM) and MitoSOX Red (final concentration 10 µM) were combined and added to both cell flasks containing 5 mL followed by the incubation under the same conditions used above. After that, the stimulated cell flask (previously treated with LPS+IFN-γ) was also treated for 30 minutes with 1 µg/mL PMA. Photobleaching during the incubation time was minimized by covering it with aluminum foil.

An additional untreated native cell flask was prepared containing both SOD inhibitors to minimize the degradation of superoxide in the cell. Following treatments and the appropriate incubation times, cells were harvested and then counted by taking 100 µL aliquots of the cell suspensions. The cell suspension was centrifuged at 1137 g for 4 minutes to obtain the cell pellet. The pellet was washed with 1 mL of cold 10 mM PBS at pH 7.4 and then 50 µl pure ethanol was

used to lyse the cells. The resulting mixture was then centrifuged at 18690 g for 10 minutes in microcentrifuge tubes equipped with 3 kDa molecular weight cutoff filters. The cell filtrate was diluted in the run buffer (pH 9.2, 10 mM borate containing 7.5 mM SDS) at a ratio of 1:10 (10% final concentration of ethanol). The diluted cell sample was then analyzed using a simple-t microchip. Nitric oxide and superoxide peaks in the electropherogram were identified by employing the same protocol but with the cell incubation with either DAF-FM DA or MitoSOX only.

3.2.2 Cell culture and protocols to study cell viability and total ROS/ antioxidant activity for microglial cells and lung epithelial cells

3.2.2.1 Cell culture protocol for microglial cells and lung epithelial cells

RPMI 1640 media containing 10% (v/v) fetal bovine serum, streptomycin (0.3 mg mL^{-1}), and penicillin (50 IU mL^{-1}) was use to culture the alveolar basal epithelial A549 cells. 75 cm^2 polystyrene flasks were used to culture cells at a density of 5×10^6 cells/ flask in an incubator set to a temperature of 37 ^{0}C with a supply of 5% CO_2 in a humidified environment. Cells were passaged every 3-5 days to eliminate overgrowth.

3.2.2.2 Preparation of nanoparticle suspensions

A model lipid mixture to mimic the lung surfactant composition was prepared using DPPC:POPG in 7:3 molar ratio prepared in HPLC grade chloroform. This mixture was then subjected to drying using nitrogen and left under a vacuum overnight. The completely dried lipid mixture was resuspended in pH 7.4 PBS to give a concentration of 10 mg/mL by placing it in a precision water bath system at 45 ^{0}C (Thermo Fisher Scientific Inc., Pittsburgh, PA, USA). The temperature of the water bath was set at 45 ^{0}C as the phase transition of DPPC occurs at 41 ^{0}C. ECNs suspensions were prepared by suspending them first in pH 7.4 PBS followed by 2h of

sonication to eliminate nanoparticle aggregation. The ECNs solution was then mixed with the lipid mixture to give a concentration of 1 wt% of nanoparticles.

3.2.2.3 Nanoparticle characterization

ECNs were suspended in water and sonicated for 2 h and the size distribution of particles was determined using dynamic light scattering ((NanoBrook Omni, Brookhaven instruments Corporation, Holtsville, NY, USA). The effective particle size, polydispersity and zeta potential (in KCl medium) were measured to be 219 nm, 0.19, and -28 mV, respectively. TEM and AFM characterizations of ECNs were previously reported.[30]

3.2.2.4 Cell culture and treatment with LS/ECNs

Cells were harvested, counted and plated at a density 5×10^6 cells/flask before the experiment. Cell viability using MTT assay was performed by plating the cells on 48-well plates at 15×10^4 cells/well and after 2 h they were treated with ECNs or DPPC: POPG (7:3)/ECNs as necessary. After the treatment they were incubated for 24 h under similar conditions to those used for the cell passaging.

3.2.2.5 ROS/antioxidant activity

In experiments performed to examine the effect of antioxidants, the cells were first treated with N-acetyl-L-histidine or carnosine at final concentrations of 10 mM and incubated for 1 h. This was followed by the treatment with nanoparticles as stated above. The cell samples were then incubated for 24 hours under the conditions mentioned earlier. Intracellular ROS production was determined using $DCFH_2DA$. A 10 mM dye solution was freshly prepared in 99% sterile dimethyl sulfoxide. In these experiments, the cells were first washed twice with 5 mL of cold 10 mM PBS at pH 7.4 and then the cells were resuspended in phenol red-free RPMI-1640. The dye was then

added to generate a final concentration of 10 μM. The cell samples were incubated using the same conditions mentioned earlier for 1 h to allow the reaction between the dye and the ROS.

Prior to harvesting into a trypsin-EDTA solution (0.25% Trypsin/0.53 mM EDTA in Hank's Balanced Salt Solution without calcium or magnesium) cells were washed with 5 mL of cold pH 7.4 PBS. For cell counting purposes, 100 μl of the cell sample was used. The rest of the cell sample was subjected to centrifugation at 125×g for 5 min at 4°C. The cell pellet was washed two times with cold pH 7.4 PBS after the supernatant was removed. Fifty microliters of pure ethanol were used for cell lysis and cell lysate was filtered in centrifuge tubes with 3 kDa molecular weight cut-off filters by centrifugation at 18.690×g for 10 min at 4°C. The filtered lysate was then diluted 1:10 in the run buffer, pH 9.2 10 mM borate containing 7.5 mM SDS (final concentration of ethanol in the sample is 10%). The sample was then analyzed by microchip electrophoresis as described below in section 3.2.3. Native cells were used as the control.

Trypan blue exclusion assay was used to determine the live cell count. For this, the cells were diluted with 0.4% trypan blue solution at a ratio of 1:1 or 1:3, depending on the cell density. C-Chip disposable hemocytometers along with a manual counter were used to determine the live cell count.

3.2.2.6 MTT cell viability assay

MTT [3-(4,5 dimethylthiazol-2-yl)-2,5-diphenyltetrazolium bromide] assay was used to determine the cell viability with various preparations of nanoparticles (ECNs or DPPC:POPG(7:3)/ECNs).[48]

3.2.3 ME coupled to fluorescence detection

3.2.3.1 PDMS device fabrication

PDMS microchip devices were fabricated as described in the literature.[12, 46] Patterns for the microchannels were first drawn using AutoCad LT 2004 (Autodesk, Inc., San Rafael, CA, USA) and then printed on a transparency sheet at a resolution of 50,000 dpi (infinite Graphics Inc., Minneapolis, MN, USA). A simple-t design with a 5 cm×40 μm×15 μm was used for microchip electrophoresis.

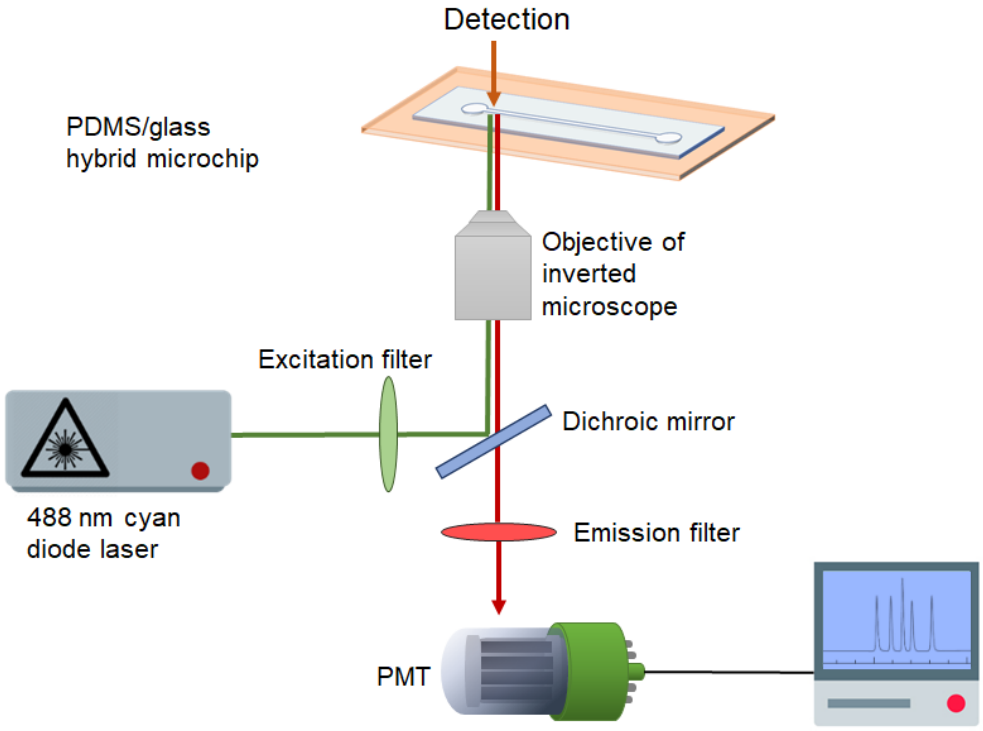

Figure 3.3 Instrumentation setup used for fluorescence detection

Channel structures from the developed transparency mask were transferred to a 4-inch silicon wafer coated with SU-8 photoresist using a UV flood source. The wafer was then subjected to a soft bake and was developed with SU-8 developer to obtain the channel master. Hard bake of

the wafer was then performed at 200 °C for 2 hours. A PDMS mixture containing the elastomer and the curing agent at a ratio of 10:1 was poured onto the master and was cured at 70 °C overnight. The PDMS device was punched using a 4 mm biopsy punch (Harris Uni-core, Ted Pella Inc., Redding, CA, USA) at the end of each channel to create reservoirs, as necessary. The PDMS simple-t was then reversibly bonded to a borofloat glass plate.

The PDMS-glass hybrid device was conditioned with 0.1 M NaOH followed by the run buffer (pH 9.2, 10 mM borate, 7.5 mM SDS). Separations were carried out under normal polarity conditions with a buffer reservoir voltage of +2400 V and a sample reservoir voltage of +2200 V. A 30 kV high voltage power supply (Ultravolt, Ronkonkoma, NY, USA) was used to apply these high voltages and the sample was injected using 1 s electrokinetic gated injection.[47] A 488 nm cyan diode laser was used as the excitation source and a photomultiplier tube (PMT) was used as the fluorescence detector (Figure 3.3). An effective separation distance of 3.5 cm was used in the simultaneous detection of NO and $O_2^{\bullet -}$ by positioning the laser. For the measurement of total ROS production, a 5 cm long separation channel was used. All measurements were made in a dark room. A low noise current amplifier was used to amplify the signal coming out from the PMT. The voltages, the injection times, and the data collection were operated using a home-built Labview program.[14]

3.3 Results and discussion

3.3.1 Detection of NO and $O_2^{\bullet -}$ in RAW macrophage cells simultaneously using ME with fluorescence detection

The simultaneous detection of NO and $O_2^{\bullet -}$ in native RAW macrophage cell lysate by ME-FL is shown in Figure 3.4A. Identification of these peaks was carried out by stimulating the cells in the presence of only one fluorescent probe, DAF- FM DA for NO and MitoSOX Red for $O_2^{\bullet -}$. The

reaction between DAF- FM DA and NO forms a triazolo-fluorescein analog (DAF- FM T) and the reaction of MitoOH with $O_2^{\bullet -}$ forms 2-OH-MitoE$^+$.[12, 47]

DAF-FM is highly selective for NO; however, it was previously reported that dehydroascorbate can also react with DAF-FM producing DAF-FM DHA.[49-51] This nonspecific peak was successfully separated from the NO-specific peak in earlier studies.[12] The peak due to the formation of DAF-FM DHA was only observed with simulated cell samples in this study (Figure 3.4C).[52]

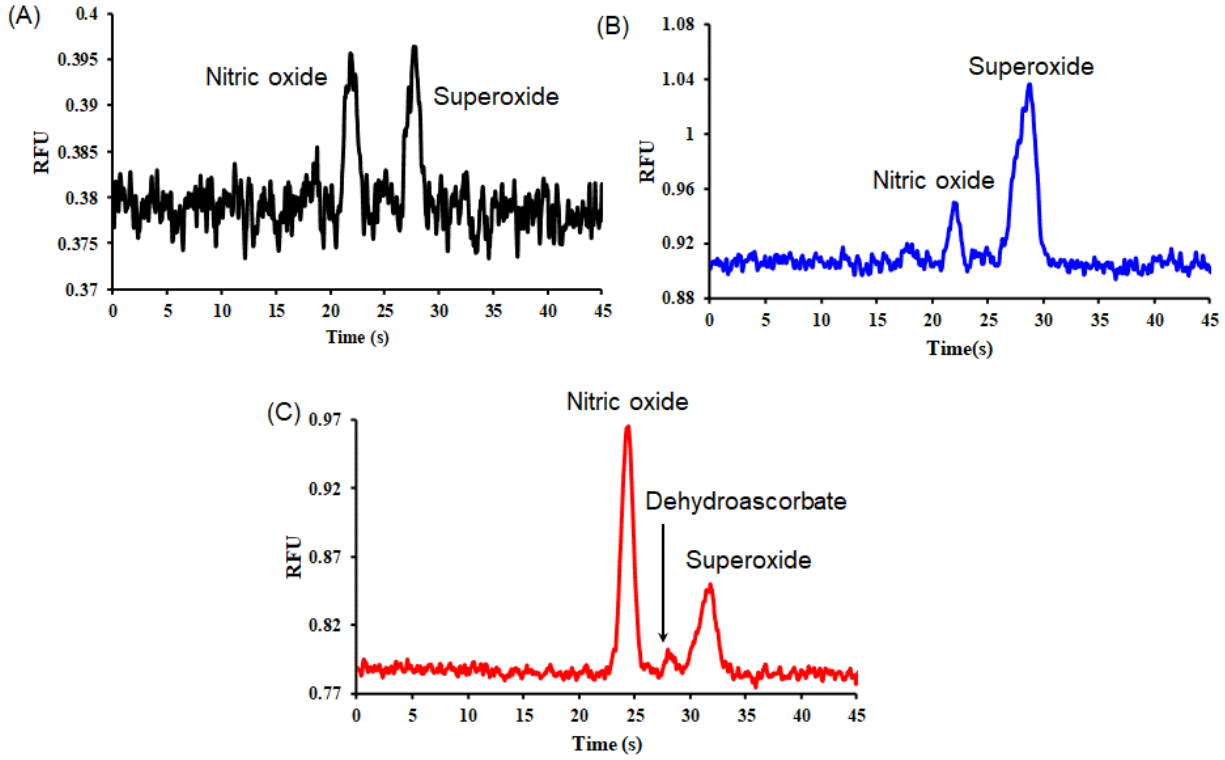

Figure 3.4 Nitric oxide and superoxide production under different stimulation conditions (A) for native cells (B) for native cells in the presence of SOD inhibitors 2-ME and DDC (C) stimulated cells with LPS+ interferon γ + PMA and SOD inhibitors 2-ME and DDC (Reproduced with permission from ref. 52.)

An electropherogram showing the production of NO and $O_2^{\bullet-}$ in native untreated cells is shown in Figure 3.4A. Endogenous enzymes that scavenge superoxide, such as SOD, are naturally present in the native untreated cells and thus low amounts of NO and $O_2^{\bullet-}$ were observed as shown in Figure 3.4A. It has been reported that it is difficult to detect $O_2^{\bullet-}$ in cell lysate samples since its intracellular concentration is controlled by cytosolic and mitochondrial SOD.[53] Therefore, two SOD inhibitors, 2-ME and DDC were added into the cells to diminish the effect of SOD. The cells were then incubated for 1 h with the fluorescent probe MitoSOX red. The electropherogram obtained under these conditions showed an increase in the 2-OH-MitoE^+ peak relative to the DAF-FM T peak (Figure 3.3B). Cells treated with LPS and IFN-γ followed by PMA with SOD inhibitors showed an increased production of intracellular NO and $O_2^{\bullet-}$ relative to the untreated cells, as expected (Figure 3.3C).

3.3.2 Investigation of the effect of engineered carbon nanoparticles on cell viability and total ROS production

3.3.2.1 Cell cytotoxicity at different preparations of DPPC:POPG (7:3)/ECNs on A549 and BV2 cells

In this study, the possible cytotoxic effect of different concentrations of ECNs on A549 and BV-2 cells was studied. This was carried out in the absence and presence of a model lung surfactant (LS, DPPC: POPG (7:3)), which was used to emulate the surfactants present in the lung. These surfactants are possible scavengers of nanoparticles once they enter the lungs. Both A549 and BV-2 cells at both high density and low density were utilized in this study. A picture of the cells is shown in Figure 3.5. The incubation of various ECNs concentrations (2, 5, 10, 50, or 100 μg/mL) with both A549 and BV-2 cells demonstrated a dose-related rise in cytotoxicity (Figure 3.6). The highest amount of cell death occurred at a dose of 100 μg/ml. The percent loss of viability

was found to be -53% and -65% in A549 and BV-2 cells, respectively, compared to the resting cells at a $p<0.01$. A significant protection from DPPC:POPG (7:3) was not observed with the doses of nanoparticles less than 50 µg/mL for both cell types.

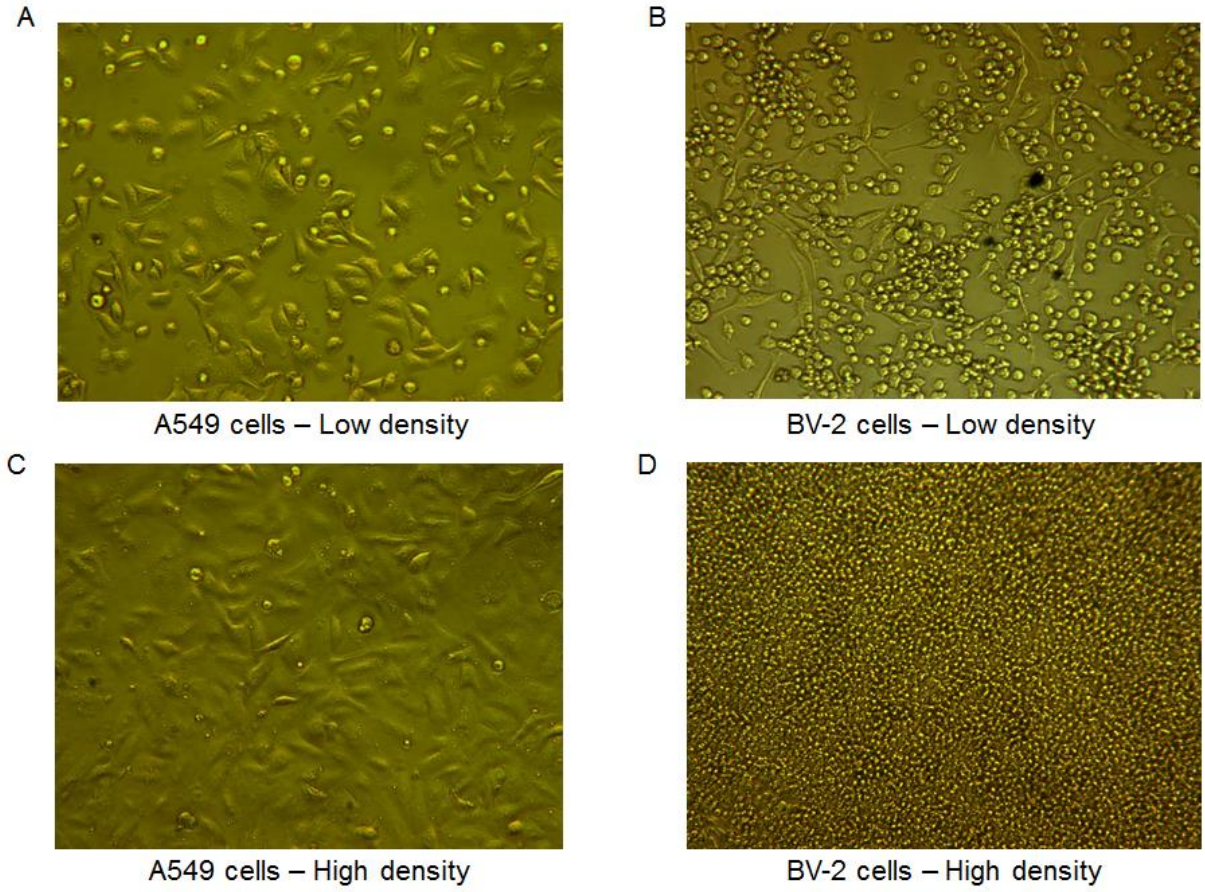

Figure 3.5: Representative cell lines of low density and high density (A) A549 cells-Low density (B) BV-2 cells-Low density (C) A549 cells- High density (D) BV-2 cells-High density (Reproduced from ref. 54, http://creativecommons.org/licenses/by/4.0/.)

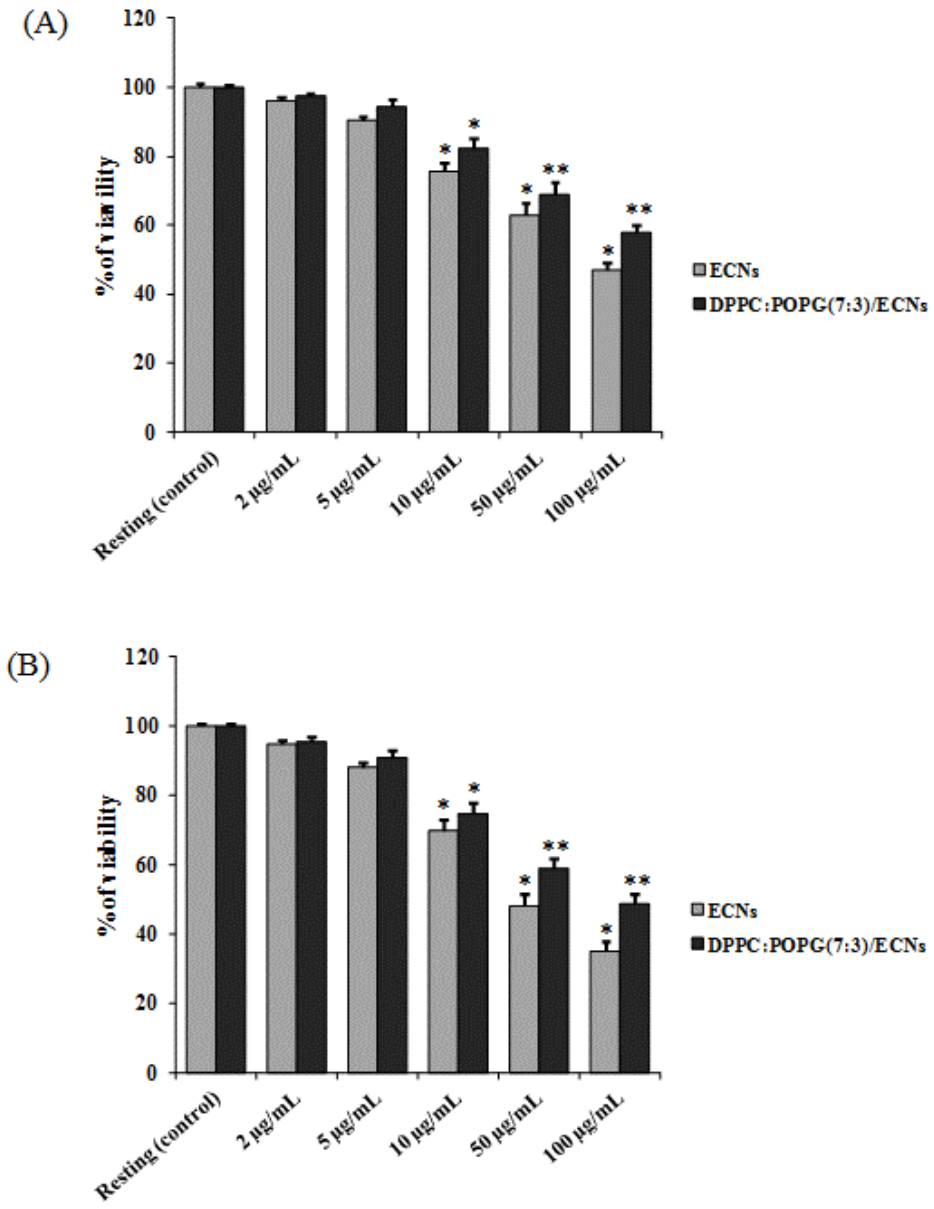

Figure 3.6: Cell viability with different doses of ECNs in the presence and absence of DPPC: POPG (7:3) (synthetic lung surfactant). Mean percent variations relative to the resting cells are shown. (A) A549 cells (B) BV-2 cells, Standard deviation has been used for the vertical error bars. * denotes a significant difference from resting cells, $p < 0.01$; ** denotes a significant difference at relevant ECNs in absence of DPPC: POPG (7:3), $p<0.01$ (Reproduced from ref. 54, http://creativecommons.org/licenses/by/4.0/)

It was observed in these experiments that at nanoparticle concentrations of 2 µg/mL for both cell types, the amount of cell death was less than 5%. Since there was no significant difference in cell viability between ECN exposed cells in the presence and absence of synthetic LS, the use of synthetic lung surfactant was no longer investigated.

3.3.2.2 Effect of non-cytotoxic levels of ECNs on the oxidative stress in cultured lung and microglial cells

The amount of ROS production was studied using $DCFH_2$-DA, a general probe for ROS, based on peak areas obtained using ME-fluorescence detection. A representative electropherogram of the fluorescent product (DCF) is shown in Figure 3.7. In these studies, it was found that at non-cytotoxic ECNs concentrations, there was a total increase in the ROS production of 57% and 83% ($p < 0.001$ compared to untreated cells) for A549 and BV-2 cells, respectively. The results obtained using ME-FL can be seen in Figure 3.8 and Figure 3.9. This implies that a significant increase of ROS production can occur in the presence of ECNs and is even higher in microglial cells than in lung cells. These results indicate that the accumulation of ECNs in these cells can cause significant cell death due to ROS production

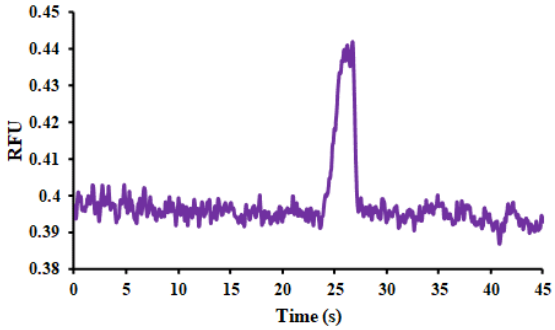

Figure 3.7 Electropherogram showing the ROS production in A549 lung cells in the presence of engineered carbon nanoparticles using $DCFH_2$-DA

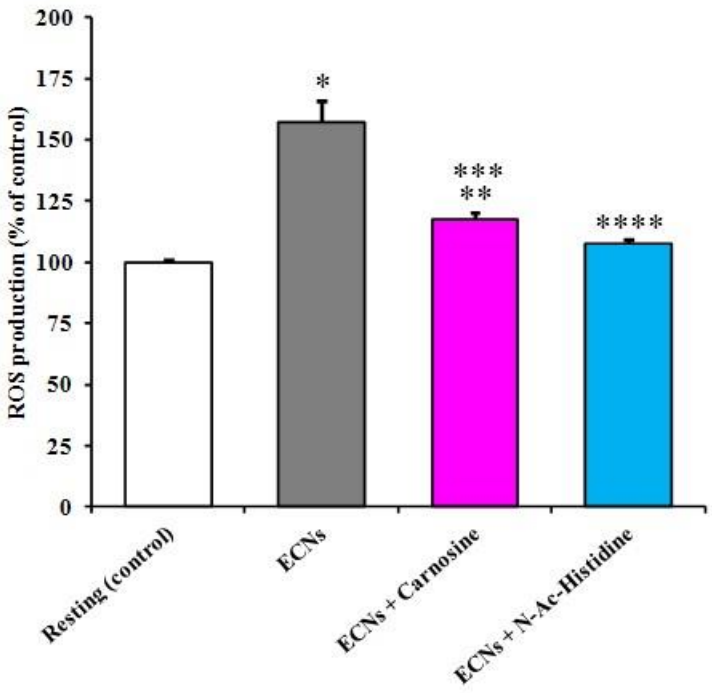

Figure. 3.8 Comparison of total ROS production in A549 cells the presence of ECNs, ECNs + carnosine, ECNs + N-AC-histidine, mean percent variations relative to the resting cells are shown. Standard deviation has been used for the vertical error bars. * denotes a significant difference from resting cells, $p < 0.001$; ** denotes a significant difference from resting cells, $p < 0.01$; *** denotes a significant difference in treated cells, $p < 0.01$, **** denotes a significant difference in treated cells, $p < 0.001$ (Reproduced from ref. 54, http://creativecommons.org/licenses/by/4.0/.)

Both N-acetyl-L-histidine and carnosine were evaluated as potential protective species to offset the ECNs-induced ROS overproduction. This was carried out by the pretreatment of both cell lines with 10 mM N-acetyl-L-histidine and carnosine for 1 h prior to the addition of 2 μg/mL ECNs. Based on these results, it was found that the N-acetyl-L-histidine can effectively reduce ECNs-induced ROS formation compared to carnosine for both cell types investigated in this study.

The ECNs mediated ROS production in cells pretreated with N-acetyl-L-histidine was not significant compared to the resting cells ($p < 0.001$), while a significant amount of ROS production (as large as 20%) compared to untreated cells was observed with carnosine-ECNs treatment ($p < 0.01$).

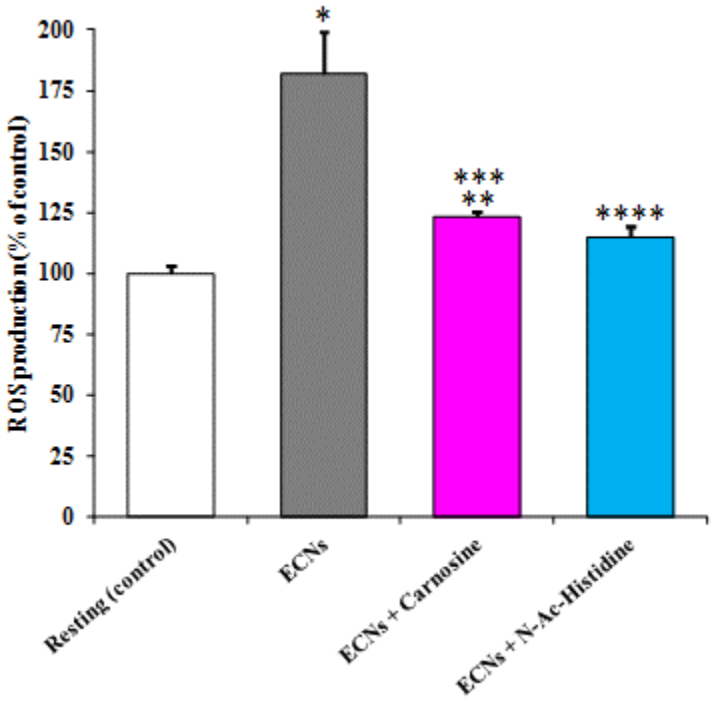

Figure. 3.9 Comparison of total ROS production in BV-2 cells the presence of ECNs, ECNs + carnosine, ECNs + N-AC-histidine, mean percent variations relative to the resting cells are shown Standard deviation has been used for the vertical error bars. * denotes a significant difference from resting cells, $p < 0.001$; ** denotes a significant difference from resting cells, $p < 0.01$; *** denotes a significant difference in treated cells, $p < 0.01$, **** denotes a significant difference in treated cells, $p < 0.001$ (Reproduced from ref. 54, http://creativecommons.org/licenses/by/4.0/.)

3.4 Conclusion

Microchip electrophoresis coupled to fluorescence detection was successfully used to separate and detect both nitric oxide and superoxide produced in macrophages. It was seen that the presence of SOD inhibitors results in increased superoxide accumulation in stimulated cells as detected by MitoSOX.

Nanotechnology has become an emerging methodology in many areas of both science and technology. Recently, it has been shown that the use of nanoparticles is a promising approach to deliver medicines to treat cancers as well as neurodegenerative diseases[55] such as Alzheimer's and Parkinson's disease.[56-57] It is therefore of utmost importance to study potential toxic side effects of these nanoparticles both *in vitro* and *in vivo*.[58] Toward this end, it is worthwhile to study the effect of the carbon nanoparticles on cell viability and ROS production. Several studies have been carried out to investigate the biosafety and toxicity of these nanoparticles and the effects of μantioxidants. As mentioned by previous reports, this study also shows that there can be serious side effects and cell death caused by these nanoparticles.

3.5 References

1. Lobo, V.; Patil, A.; Phatak, A.; Chandra, N., Free radicals, antioxidants and functional foods: Impact on human health. *Pharmacogn Rev.* **2010,** *4* (8), 118-26.

2. Gilca, M.; Stoian, I.; Atanasiu, V.; Virgolici, B., The oxidative hypothesis of senescence. *J. Postgrad. Med.* **2007,** *53* (3), 207-13.

3. Docampo, R., 9 - Antioxidant Mechanisms. In *Biochemistry and Molecular Biology of Parasites*, Müller, J. J. M., Ed. Academic Press: San Diego, 1995; pp 147-160.

4. Rice-Evans, C. A.; Gopinathan, V., Oxygen toxicity, free radicals and antioxidants in human disease: biochemical implications in atherosclerosis and the problems of premature neonates. *Essays Biochem.* **1995,** *29*, 39-63.

5. Riley, P. A., Free radicals in biology: oxidative stress and the effects of ionizing radiation. *Int. J. Radiat. Biol.* **1994,** *65* (1), 27-33.

6. Halliwell, B.; Gutteridge, J. M.; Cross, C. E., Free radicals, antioxidants, and human disease: where are we now? *J. Lab. Clin. Med.* **1992,** *119* (6), 598-620.

7. Frei, B.; Stocker, R.; Ames, B. N., Antioxidant defenses and lipid peroxidation in human blood plasma. *Proc. Natl. Acad. Sci. U. S. A.* **1988,** *85* (24), 9748-9752.

8. Stefanis, L.; Burke, R. E.; Greene, L. A., Apoptosis in neurodegenerative disorders. *Curr. Opin. Neurol.* **1997,** *10* (4), 299-305.

9. Rahman, K., Studies on free radicals, antioxidants, and co-factors. *Clin. Interv. Aging* **2007,** *2* (2), 219-36.

10. Wang, H.-S., Development of fluorescent and luminescent probes for reactive oxygen species. *TrAC, Trends Anal. Chem.* **2016,** *85*, 181-202.

11. Chen, X.; Wang, F.; Hyun, J. Y.; Wei, T.; Qiang, J.; Ren, X.; Shin, I.; Yoon, J., Recent progress in the development of fluorescent, luminescent and colorimetric probes for detection of reactive oxygen and nitrogen species. *Chem. Soc. Rev.* **2016,** *45* (10), 2976-3016.

12. Mainz, E. R.; Gunasekara, D. B.; Caruso, G.; Jensen, D. T.; Hulvey, M. K.; Fracassi da Silva, J. A.; Metto, E. C.; Culbertson, A. H.; Culbertson, C. T.; Lunte, S. M., Monitoring intracellular nitric oxide production using microchip electrophoresis and laser-induced fluorescence detection. *Anal Methods.* **2012,** *4* (2), 414-420.

13. Pasas, S.; Fogarty, B.; Huynh, B.; Lacher, N.; Carlson, B.; Martin, S.; Vandaveer, W. I. V.; Lunte, S. In *Detection on microchips: principles, challenges, hyphenation, and integration*, CRC Press LLC: 2006; pp 433-497.

14. Caruso, G.; Fresta, C. G.; Martinez-Becerra, F.; Antonio, L.; Johnson, R. T.; de Campos, R. P. S.; Siegel, J. M.; Wijesinghe, M. B.; Lazzarino, G.; Lunte, S. M., Carnosine modulates nitric oxide in stimulated murine RAW 264.7 macrophages. *Mol. Cell. Biochem.* **2017,** *431* (1-2), 197-210.

15. de Campos, R. P. S.; Siegel, J. M.; Fresta, C. G.; Caruso, G.; da Silva, J. A. F.; Lunte, S. M., Indirect detection of superoxide in RAW 264.7 macrophage cells using microchip electrophoresis coupled to laser-induced fluorescence. *Anal. Bioanal. Chem.* **2015,** *407* (23), 7003-7012.

16. Lenz, K. M.; Nelson, L. H., Microglia and Beyond: Innate Immune Cells As Regulators of Brain Development and Behavioral Function. *Front. Immunol.* **2018,** *9*, 698-698.

17. Aoshiba, K.; Nagai, A., Oxidative Stress, Cell Death, and Other Damage to Alveolar Epithelial Cells Induced by Cigarette Smoke. *Tob. Induc. Dis.* **2003,** *1* (1), 21-21.

18. Mu, Q.; Jiang, G.; Chen, L.; Zhou, H.; Fourches, D.; Tropsha, A.; Yan, B., Chemical Basis of Interactions Between Engineered Nanoparticles and Biological Systems. *Chem. Rev.* **2014,** *114* (15), 7740-7781.

19. Piccinno, F.; Gottschalk, F.; Seeger, S.; Nowack, B., Industrial production quantities and uses of ten engineered nanomaterials in Europe and the world. *J. Nanopart. Res.* **2012,** *14* (9), 11.

20. Murthy, S. K., Nanoparticles in modern medicine: State of the art and future challenges. *Int. J. Nanomed* **2007,** *2* (2), 129-141.

21. Zhang, L.; Gu, F. X.; Chan, J. M.; Wang, A. Z.; Langer, R. S.; Farokhzad, O. C., Nanoparticles in Medicine: Therapeutic Applications and Developments. *Clin. Pharmacol. Ther.* **2008,** *83* (5), 761-769.

22. Sun, T.; Zhang, Y. S.; Pang, B.; Hyun, D. C.; Yang, M.; Xia, Y., Engineered nanoparticles for drug delivery in cancer therapy. *Angew. Chem. Int. Ed. Engl.* **2014,** *53* (46), 12320-64.

23. Denora, N.; Lopedota, A.; Perrone, M.; Laquintana, V.; Iacobazzi, R. M.; Milella, A.; Fanizza, E.; Depalo, N.; Cutrignelli, A.; Lopalco, A.; Franco, M., Spray-dried mucoadhesives for intravesical drug delivery using N-acetylcysteine- and glutathione-glycol chitosan conjugates. *Acta Biomater.* **2016,** *43*, 170-184.

24. Lopedota, A.; Cutrignelli, A.; Laquintana, V.; Denora, N.; Iacobazzi, R. M.; Perrone, M.; Fanizza, E.; Mastrodonato, M.; Mentino, D.; Lopalco, A.; Depalo, N.; Franco, M., Spray Dried Chitosan Microparticles for Intravesical Delivery of Celecoxib: Preparation and Characterization. *Pharm. Res.* **2016,** *33* (9), 2195-2208.

25. Gao, L.; Liu, Y.; Kim, D.; Li, Y.; Hwang, G.; Naha, P. C.; Cormode, D. P.; Koo, H., Nanocatalysts promote Streptococcus mutans biofilm matrix degradation and enhance bacterial killing to suppress dental caries in vivo. *Biomaterials* **2016,** *101*, 272-84.

26. Mahmoudi, M.; Serpooshan, V.; Laurent, S., Engineered nanoparticles for biomolecular imaging. *Nanoscale* **2011,** *3* (8), 3007-3026.

27. Nelson, B. C.; Johnson, M. E.; Walker, M. L.; Riley, K. R.; Sims, C. M., Antioxidant Cerium Oxide Nanoparticles in Biology and Medicine. *Antioxidants* **2016,** *5* (2).

28. De Jong, W. H.; Borm, P. J. A., Drug delivery and nanoparticles:applications and hazards. *Int. J. Nanomed* **2008,** *3* (2), 133-149.

29. Love, S. A.; Maurer-Jones, M. A.; Thompson, J. W.; Lin, Y. S.; Haynes, C. L., Assessing nanoparticle toxicity. *Annu Rev Anal Chem* **2012,** *5*, 181-205.

30. Chakraborty, A.; Mucci, N. J.; Tan, M. L.; Steckley, A.; Zhang, T.; Forrest, M. L.; Dhar, P., Phospholipid Composition Modulates Carbon Nanodiamond-Induced Alterations in Phospholipid Domain Formation. *Langmuir* **2015,** *31* (18), 5093-5104.

31. Fiorito, S.; Serafino, A.; Andreola, F.; Togna, A.; Togna, G., Toxicity and biocompatibility of carbon nanoparticles. *J Nanosci Nanotechnol* **2006,** *6* (3), 591-9.

32. Oberdorster, G.; Castranova, V.; Asgharian, B.; Sayre, P., Inhalation Exposure to Carbon Nanotubes (CNT) and Carbon Nanofibers (CNF): Methodology and Dosimetry. *J. Toxicol. Environ. Health. B Crit. Rev.* **2015,** *18* (3-4), 121-212.

33. Zhao, J.; Castranova, V., Toxicology of nanomaterials used in nanomedicine. *J. Toxicol. Environ. Health. B Crit. Rev.* **2011,** *14* (8), 593-632.

34. De Volder, M. F.; Tawfick, S. H.; Baughman, R. H.; Hart, A. J., Carbon nanotubes: present and future commercial applications. *Science* **2013,** *339* (6119), 535-9.

35. Heyder, J., Deposition of inhaled particles in the human respiratory tract and consequences for regional targeting in respiratory drug delivery. *Proc. Am. Thorac. Soc.* **2004,** *1* (4), 315-20.

36. Zuo, Y. Y.; Veldhuizen, R. A.; Neumann, A. W.; Petersen, N. O.; Possmayer, F., Current perspectives in pulmonary surfactant--inhibition, enhancement and evaluation. *Biochim. Biophys. Acta* **2008,** *1778* (10), 1947-77.

37. Kapralov, A. A.; Feng, W. H.; Amoscato, A. A.; Yanamala, N.; Balasubramanian, K.; Winnica, D. E.; Kisin, E. R.; Kotchey, G. P.; Gou, P.; Sparvero, L. J.; Ray, P.; Mallampalli, R. K.; Klein-Seetharaman, J.; Fadeel, B.; Star, A.; Shvedova, A. A.; Kagan, V. E., Adsorption of

surfactant lipids by single-walled carbon nanotubes in mouse lung upon pharyngeal aspiration. *ACS Nano* **2012,** *6* (5), 4147-56.

38. Kendall, M.; Holgate, S., Health impact and toxicological effects of nanomaterials in the lung. *Respirology* **2012,** *17* (5), 743-758.

39. Xi, G.; Robinson, E.; Mania-Farnell, B.; Vanin, E. F.; Shim, K. W.; Takao, T.; Allender, E. V.; Mayanil, C. S.; Soares, M. B.; Ho, D.; Tomita, T., Convection-enhanced delivery of nanodiamond drug delivery platforms for intracranial tumor treatment. *Nanomedicine* **2014,** *10* (2), 381-91.

40. Faustino, C.; Rijo, P.; Reis, C. P., Nanotechnological strategies for nerve growth factor delivery: Therapeutic implications in Alzheimer's disease. *Pharmacol. Res.* **2017,** *120*, 68-87.

41. Uboldi, C.; Bonacchi, D.; Lorenzi, G.; Hermanns, M. I.; Pohl, C.; Baldi, G.; Unger, R. E.; Kirkpatrick, C. J., Gold nanoparticles induce cytotoxicity in the alveolar type-II cell lines A549 and NCIH441. *Part. Fibre Toxicol.* **2009,** *6* (1), 18.

42. Chairuangkitti, P.; Lawanprasert, S.; Roytrakul, S.; Aueviriyavit, S.; Phummiratch, D.; Kulthong, K.; Chanvorachote, P.; Maniratanachote, R., Silver nanoparticles induce toxicity in A549 cells via ROS-dependent and ROS-independent pathways. *Toxicol. In Vitro* **2013,** *27* (1), 330-8.

43. Escamilla-Rivera, V.; Uribe-Ramirez, M.; Gonzalez-Pozos, S.; Velumani, S.; Arreola-Mendoza, L.; De Vizcaya-Ruiz, A., Cytotoxicity of semiconductor nanoparticles in A549 cells is attributable to their intrinsic oxidant activity. *J. Nanopart. Res.* **2016,** *18* (4), 85.

44. Henn, A.; Lund, S.; Hedtjarn, M.; Schrattenholz, A.; Porzgen, P.; Leist, M., The suitability of BV2 cells as alternative model system for primary microglia cultures or for animal experiments examining brain inflammation. *Altex* **2009,** *26* (2), 83-94.

45. Kraft, A. D.; Harry, G. J., Features of microglia and neuroinflammation relevant to environmental exposure and neurotoxicity. *Int. J. Environ. Res. Public Health* **2011,** *8* (7), 2980-3018.

46. Gunasekara, D. B.; Hulvey, M. K.; Lunte, S. M.; da Silva, J. A. F., Microchip electrophoresis with amperometric detection for the study of the generation of nitric oxide by NONOate salts. *Anal. Bioanal. Chem.* **2012,** *403* (8), 2377-2384.

47. de Campos, R. P.; Siegel, J. M.; Fresta, C. G.; Caruso, G.; da Silva, J. A.; Lunte, S. M., Indirect detection of superoxide in RAW 264.7 macrophage cells using microchip electrophoresis coupled to laser-induced fluorescence. *Anal. Bioanal. Chem.* **2015,** *407* (23), 7003-12.

48. Caruso, G.; Distefano, D. A.; Parlascino, P.; Fresta, C. G.; Lazzarino, G.; Lunte, S. M.; Nicoletti, V. G., Receptor-mediated toxicity of human amylin fragment aggregated by short- and long-term incubations with copper ions. *Mol. Cell. Biochem.* **2017,** *425* (1-2), 85-93.

49. Kim, W.-S.; Ye, X.; Rubakhin, S. S.; Sweedler, J. V., Measuring Nitric Oxide in Single Neurons by Capillary Electrophoresis with Laser-Induced Fluorescence: Use of Ascorbate Oxidase in Diaminofluorescein Measurements. *Anal. Chem.* **2006,** *78* (6), 1859-1865.

50. Balcerczyk, A.; Soszynski, M.; Bartosz, G., On the specificity of 4-amino-5-methylamino-2',7'-difluorofluorescein as a probe for nitric oxide. *Free Radic. Biol. Med.* **2005,** *39* (3), 327-35.

51. Zhang, X.; Kim, W. S.; Hatcher, N.; Potgieter, K.; Moroz, L. L.; Gillette, R.; Sweedler, J. V., Interfering with nitric oxide measurements. 4,5-diaminofluorescein reacts with dehydroascorbic acid and ascorbic acid. *J. Biol. Chem.* **2002,** *277* (50), 48472-8.

52. Caruso, G.; Fresta, C. G.; Siegel, J. M.; Wijesinghe, M. B.; Lunte, S. M., Microchip electrophoresis with laser-induced fluorescence detection for the determination of the ratio of nitric

oxide to superoxide production in macrophages during inflammation *Anal. Bioanal. Chem* 2017, 409 (19), 4529-4538

53. Fukai, T.; Ushio-Fukai, M., Superoxide dismutases: role in redox signaling, vascular function, and diseases. *Antioxid. Redox Signal.* **2011,** *15* (6), 1583-606.

54. Fresta, C. G.; Chakraborty, A.; Wijesinghe, M. B.; Amorini, A. M.; Lazzarino, G.; Lazzarino, G.; Tavazzi, B.; Lunte, S. M.; Caraci, F.; Dhar, P.; Caruso, G., Non-toxic engineered carbon nanodiamond concentrations induce oxidative/nitrosative stress, imbalance of energy metabolism, and mitochondrial dysfunction in microglial and alveolar basal epithelial cells. *Cell Death Dis.* 2018, 9 (2), 245

55. Melita, E. D.; Purcel, G.; Grumezescu, A. M., Carbon nanotubes for cancer therapy and neurodegenerative diseases. *Rom. J. Morphol. Embryol.* **2015,** *56* (2), 349-56.

56. Yang, Z.; Zhang, Y.; Yang, Y.; Sun, L.; Han, D.; Li, H.; Wang, C., Pharmacological and toxicological target organelles and safe use of single-walled carbon nanotubes as drug carriers in treating Alzheimer disease. *Nanomedicine* **2010,** *6* (3), 427-41.

57. Li, H.; Luo, Y.; Derreumaux, P.; Wei, G., Carbon nanotube inhibits the formation of β-sheet-rich oligomers of the Alzheimer's amyloid-β(16-22) peptide. *Biophys. J.* **2011,** *101* (9), 2267-2276.

58. Gomes, A.; Sengupta, J.; Datta, P.; Ghosh, S.; Gomes, A., Physiological Interactions of Nanoparticles in Energy Metabolism, Immune Function and Their Biosafety: A Review. *J Nanosci Nanotechnol* **2016,** *16* (1), 92-116.

4. Chapter 4: Bipolar electrochemically generated fluorescence detector for microchip electrophoresis

This chapter is based on the manuscript written on Wijesinghe, M.B.; Gunasekara, D.B.; Lunte, S.M. “Bipolar electrochemically generated fluorescence detector for microchip electrophoresis,” to be submitted to Analytical Chemistry

4.1 Introduction

Microchip-based electrophoretic separations have gained popularity, as they offer fast analysis times, employ low volumes of sample and reagent, and are a key component of miniaturized analytical systems due to their small footprint.[1] The separation capability of microchip electrophoresis has been demonstrated in many different areas of science including biology,[2-9] environmental chemistry,[10-13] and food science.[14-19] Several different detection techniques, such as electrochemical detection (EC), fluorescence detection, and conductivity detection, have been coupled to microchip electrophoresis (ME). In particular, electrochemical detection offers several advantages for microchip electrophoresis, including direct detection of electroactive molecules, ease of miniaturization, integration of the detection system, and low cost. However, limits of detection (LOD) reported for analytes using ME-EC are generally in the micromolar range.[3,20]

Many different strategies have been investigated to improve the LODs of ME-EC, including the use of different electrode configurations,[21] decouplers,[21] electrode modifications,[22-23] sample stacking approaches,[24-25] and other sample pre-concentration methods.[26] However, most of these approaches are analyte-specific and cannot be applied to improve LODs of all electroactive compounds.

Signal enhancement and/or noise reduction are the ways to obtain better LODs. As discussed in Chapter 1, the amperometric signal can be enhanced by using different electrode materials or modified electrodes. On the other hand, careful experimental design, including the use of a Faraday cage, noise filters, shielded connections, and/or battery operated potentiostats, leads to noise reduction. However, an electrochemical measurement is fundamentally limited by two noise sources: shot noise and Johnson noise. A transfer of 10^4 electrons per second will

produce 1.6 fA of current according to Faraday's law. The shot noise accompanied with this measurement is given by the following equation.[27]

$$\delta I = \sqrt{2e\Delta f} \tag{4.1}$$

where e is the charge of an electron and Δf is the bandwidth of the measurement. By considering a bandwidth of 1 Hz, the S/N limited by shot noise can be calculated as,

$$\frac{I}{\delta I} = \frac{e\times 10^4}{\sqrt{2eI\Delta f}} = \frac{e\times 10^4}{\sqrt{2e\times e\times 10^4\times \Delta f}} \approx 71 \tag{4.2}$$

This implies that the S/N ratio is significant even with a current measurement as low as 1.6 fA. In addition, the diffusive scattering of electrons, known as Johnson noise, causes the noise to increase substantially, resulting in higher LODs. Johnson noise is estimated as described below:

Consider that the above current measurement (1.6 fA) is made with a 1 MΩ load and 1 Hz band width. Then, the signal is given by,

$$V = IR \qquad V = 1.6\, fA \times 1\ \text{M}\Omega\ = 1.6\ \text{nV} \tag{4.3}$$

and noise can be calculated using $\sqrt{4kTR\Delta f}$

Now, the S/N limited by Johnson noise is,

$$\frac{V}{\delta V} = \frac{IR}{\sqrt{4kTR\Delta f}} = \frac{1.6\times 10^{-9}}{\sqrt{4\times 1.38\times 10^{-23}\times 298.15\times 10^4\times 1}} = 0.012 \tag{4.4}$$

Therefore, it is difficult to measure single electron transfer events even with today's improved electronics. However, counting single photons is achievable and has been reported.[27]

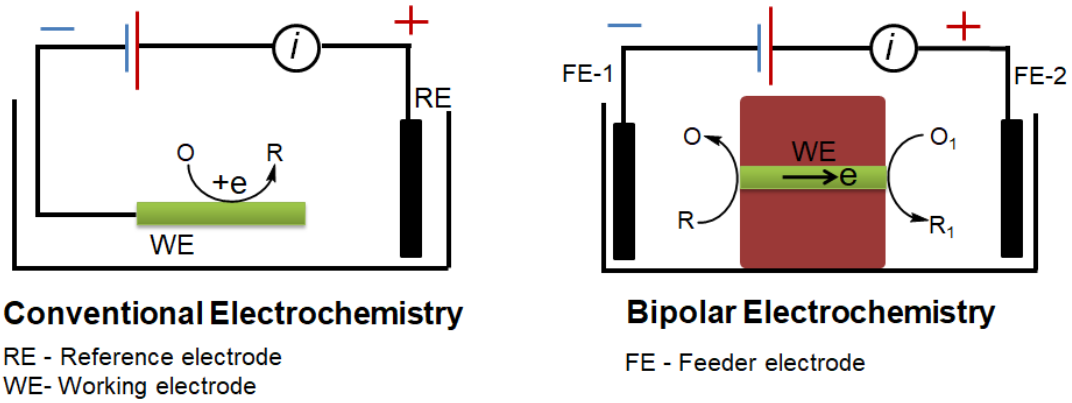

Figure 4.1 Comparison of electrochemical setups (A) Conventional electrochemical setup (B) Bipolar electrochemical setup

Luminescence measurements, such as fluorescence and chemiluminescence, are potential alternative detection methods to EC that offer picomolar LODs due to the low background signals characteristic of these techniques. However, these methods generally require derivatization of the compound of interest with a fluorescent/luminescent probe. Derivatization can lead to a lack of selectivity and sensitivity in the measurement, depending on the functional group that is targeted and the kinetics of the reaction.

A bipolar electrode, in which the electrochemical oxidation and reduction occur at the two extremities of the electrode without a direct ohmic contact, can be used to convert the current to an optical measurement such as fluorescence and chemiluminescence.[28-29] Quantitation of an analyte based on this coupling is possible, as the number of photons produced is proportional to the number of electrons transferred and thus to the analyte concentration. The principles of bipolar electrochemistry were described as early as the 1960s.[30] However, it did not gain significant attention as a detection method until 2000.[29]

Bipolar electrodes can provide several inherent advantages in terms of sensing and screening over conventional electrochemical detection. They can be operated without a direct electrical connection, which is one of the main differences between bipolar electrochemistry and conventional electrochemistry. It is also possible to concurrently control an array or ensemble of microscale or nanoscale electrodes using bipolar electrochemistry. As mentioned earlier, an electrochemical reaction occurs at each pole of the bipolar electrode simultaneously, making it very different from a conventional electrochemical setup (Figure 4.1).

There are two types of bipolar electrodes: open and closed. In "open mode," the entire electrode is floating inside a buffer or a conducting solution (Figure 4.2A). In "closed mode," part of the bipolar electrode is covered by an insulating material (Figure 4.2B). In "closed mode," the cathodic and anodic poles of the bipolar electrode are completely separated and therefore direct chemical reactions between the oxidized and reduced forms of reactant and products cannot occur.[29]

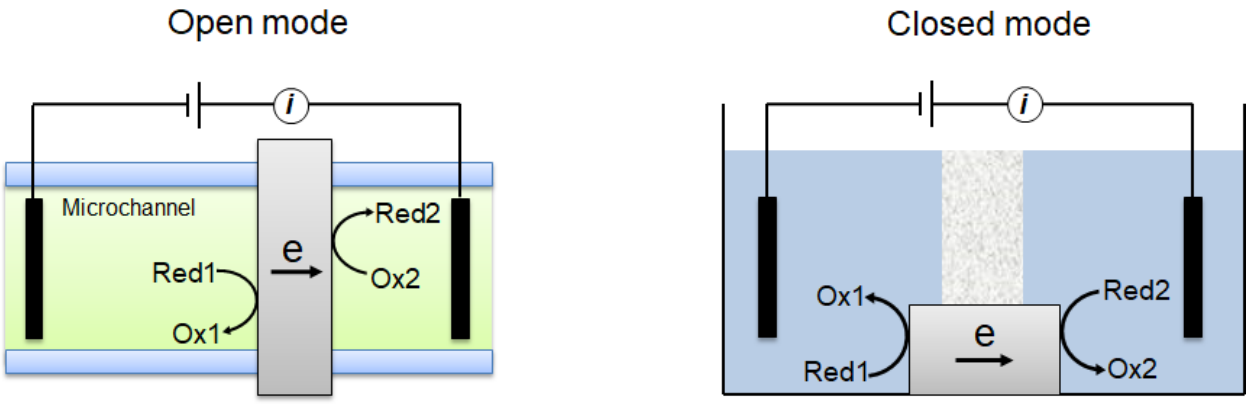

Figure 4.2 Bipolar electrode configurations (A) open mode (B) closed mode

The two major electrochemical parameters that are important in defining a closed bipolar cell are the limiting current and the $E_{1/2}$. According to the literature, the limiting current of the

bipolar cell is determined by the pole with the smallest current. The $E_{1/2}$ of the bipolar electrode depends on two major parameters: the $E_{1/2}$ values of the cathodic and anodic poles and the limiting currents of each cathodic and anodic pole of the bipolar electrode. The $E_{1/2}$ is simply the difference between the $E_{1/2}$ values of the cathodic and the anodic poles if the limiting currents at both poles are equal.[31] When the currents at two poles are not equal, a more rigorous approach is required to calculate the half wave potential of the bipolar cell.[31] Construction of a bipolar cell using two individual electrodes is shown in Figure 4.3.

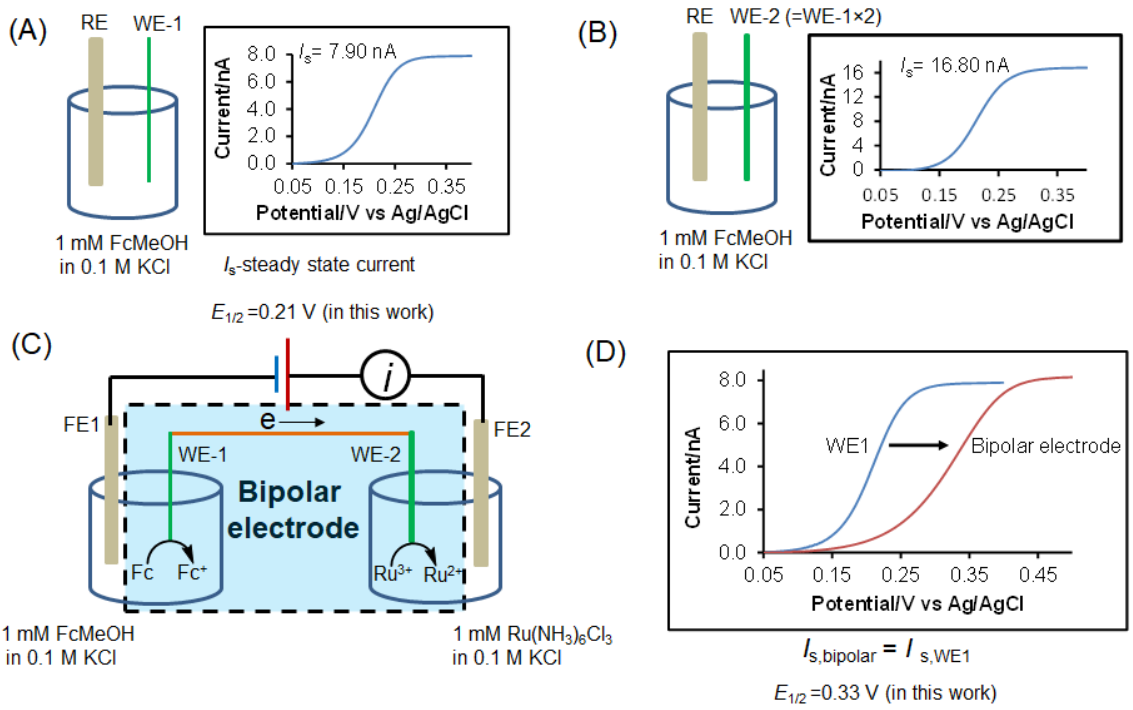

Figure 4.3 Construction of a bipolar electrode and comparison of its voltammogram with individual half-cell. Steady state voltammogram of 0.1 M ferrocene methanol solution with a disk-shaped working electrode (A) that has a radius of r (B) that has a radius of 2r. (C) Bipolar cell where one electrode is placed inside a solution of 0.1 M ferrocene methanol and the other electrode is placed inside a solution of 0.1 M ruthenium hexamine chloride solution (D) Comparison of steady state voltammograms between the bipolar cell and the individual working electrode.

In this experiment, a bipolar cell was constructed utilizing two individual disk-shaped working electrodes (WE). The radius of one of the electrodes is 2.1 times that of the other electrode and, therefore, the steady state current due to the electrochemical oxidation of ferrocene methanol at WE#2 (16.8 nA) is approximately twice that of WE#1 (7.90 nA). In the bipolar cell, the oxidation of ferrocene occurs at WE#1 and the reduction of ruthenium occurs at WE#2. Since the

concentrations of both solutions are the same, the current at the cathodic pole is twice that of the anodic pole. The current-limiting pole is therefore the anodic pole, as shown experimentally in Figure 4.3D. In this case, the half-wave potential of the bipolar cell is not simply the difference between the individual reactions because of the current differences at two poles. The following equations (Equation 4.5 and 4.6)[31] have been used to estimate the half-wave potential in such instances. A similar equation can be derived if the cathodic pole is limiting.

$E_{1/2}^{Fc/Fc^+} = 0.21\ V$ and $E_{1/2}^{Ru^{3+}/Ru^{2+}} = -0.15\ V$ vs Ag/AgCl in this study.

$$E_{1/2} = E_{1/2}^{Fc/Fc^+} - E_{1/2}^{Ru^{3+}/Ru^{2+}} - \frac{RT}{F} ln\left\{-2\left\{\frac{i_s^{Fc/Fc^+}}{-i_s^{Ru^{3+}/Ru^{2+}}}\right\} - 1\right\} \quad 4.5$$

$$E_{1/2} = 0.21 - (-0.15) - \frac{RT}{F} ln\left\{-2\left\{\frac{7.9}{-16.8}\right\} - 1\right\} \quad 4.6$$

$E_{1/2}$=0.33 V

As shown in Figure 4.3, the observed half-wave potential is equal to the potential estimated by the equation.

Three different types of measurements have been used in the literature as the reporting method for bipolar electrochemistry, namely fluorescence, chemiluminescence,[28] and the anodic dissolution of a silver layer. These are shown in Figure 4.4.[32] The use of fluorescence as the reporting method for a bipolar electrode to determine the concentration of dopamine in a static solution has been reported by the Zhang group, with a LOD of 1 μM.[33] However, the use of electrochemically-generated fluorescence or chemiluminescence using a bipolar electrode as an alternative detection method for microchip electrophoresis has not yet been reported. In this work, the development of a detector for microchip electrophoresis based on electrochemically-generated fluorescence (emission of fluorescence due to the excitation of electrochemically generated molecules) using a closed bipolar cell system is described.

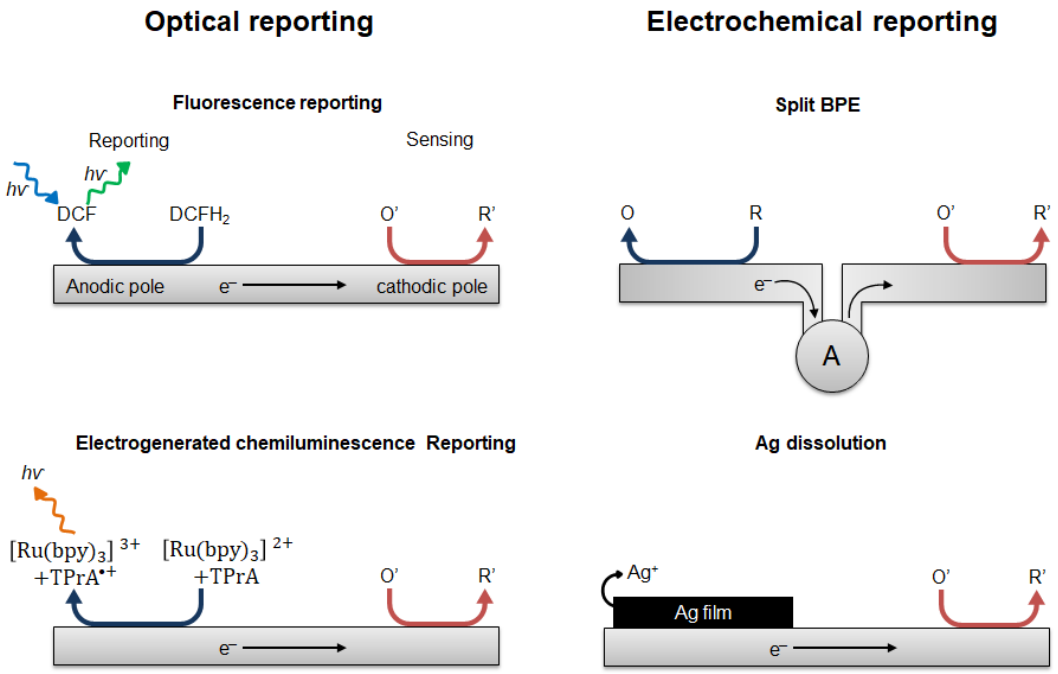

Figure 4.4 Different reporting methods for bipolar electrode-based reporting (A) fluorescence reporting (B) direct current measurement (C) electrochemically-generated chemiluminescence (D) Ag film dissolution

4.2 Experimental section

4.2.1 Chemicals and Reagents

SU-8 10 photoresist and SU-8 developer (MicroChem Corp., Newton, MA, USA); AZ1518 photoresist and 300 MIF developer (Mays Chemical Co., Indianapolis, IN, USA); photolithography film mask (40,000 dpi; Infinite Graphics Inc., Minneapolis, MN, USA); N(100) 100 mm (4″) silicon (Si) wafers (Silicon, Inc., Boise, ID, USA); chrome and AZ1518 positive photoresist coated Borosilicate float glass substrate (4″×4″×0.090″, Nanofilm, Westlake, CA, USA); Sylgard 184 Silicone Elastomer Kit: polydimethylsiloxane (Ells-worth Adhesives, Germantown, WI, USA); epoxy and 22 gauge Cu wire (Westlake Hardware, Lawrence, KS, USA); silver colloidal paste (Ted Pella, Inc., Redding, CA, USA); acetone, 2-propanol (isopropyl alcohol,

IPA), buffered oxide etchant (JTBaker, Austin, TX, USA); monosodium phosphate (Sigma Aldrich), disodium phosphate (Sigma Aldrich), sodium dodecyl sulphate (Sigma Aldrich), benzoquinone (BQ; 99% Sigma Aldrich), resazurin (99% ThermoFisher Scientific), dichlorodihydrofluorescein diacetate ($DCFH_2$; >95% Cayman chemicals), and lithium chloride (Sigma Aldrich) were used as received. All water used was ultrapure (18.2 MΩ cm, Milli-Q Synthesis A10, Millipore, Burlington, MA, USA).

4.2.2 Electrode fabrication

4.2.2.1 Pt electrode fabrication

A Pt electrode with a width of 15 μm was fabricated according to the procedure described earlier by our group.[1,34] Briefly, the design was drawn using AutoCad LT2004 (Autodesk, San Rafael, CA, USA) and printed on a transparency sheet (Infinite Graphics Inc., Minneapolis, MN, USA). After that, the design was transferred to the AZ 1518 photoresist and chrome coated borofloat glass substrate using a UV flood source. The electrode was then developed with AZ 300 MIF (Capitol Scientific, Inc., Austin, TX, USA) for 10 s. Next, the plate was subjected to chrome etch until the features were transparent. A trench 300-400 nm deep was generated using buffered oxidant (10% HF). The glass plate was then plasma cleaned for 50 s. A 40 nm Ti layer followed by a Au film with a thickness of 250-300 nm was then deposited using a Magnetron sputtering system (AXXIS DC magnetron sputtering system, Kurt J. Lesker Co., Jefferson Hills, PA, USA). After that, the plate was treated with acetone to remove excess Pt and then with chrome etch to obtain the Pt electrode fabricated on the glass.

4.2.2.2 Pyrolyzed photoresist film (PPF) electrode fabrication

The fabrication procedure of pyrolyzed photoresist film electrodes is described in detail in the literature.[35-36] Briefly, a cleaned quartz glass (to reuse the plate, it can be cleaned with acid and

base piranha solution) of 2.5 inches by 4 inches was baked at 200 ^{0}C for 2 h on a programmable hot plate. AZ 1518 positive photoresist was spin coated on the dried glass. Coated glass was then baked at 100 ^{0}C for 2 minutes on a programmable hotplate. Features from a positive mask design printed on a transparency were transferred onto the AZ1518 coated quartz glass using a UV flood source. The glass substrate was then developed using MIF-300 and rinsed with 18 MΩ water. The photoresist was then pyrolyzed in a tube furnace in a nitrogen environment with a temperature program up to 900 ^{0}C.

4.2.3 PDMS microchip fabrication

A simple-t PDMS microchip for electrophoresis containing a channel with dimensions of 5 cm×40 µm×15 µm was fabricated as previously described.[37] Briefly, the channel design was drawn with AutoCad LT2004 (Autodesk, San Rafael, CA, USA) software and printed on a transparency sheet at a resolution of 40,000 dpi. A 4" Si wafer was coated with SU-8 10 negative photoresist using a spin-coater to give a film thickness of 15 µm. The coated Si wafer was then soft baked at 65 ^{0}C for 2 minutes, followed by at 95 ^{0}C for 5 minutes on a programmable hotplate. Next, the features on the photomask were transferred to the spin-coated Si wafer using a UV flood source. SU-8 developer was used to develop the photoresist on the Si wafer and it was then rinsed with IPA. The wafer was transferred onto the hot plate for a hard bake for 2 h at 200 °C and then it was dried with nitrogen. 10.9 g of PDMS polymer and 1.1 g of curing agent (10:1) were mixed well, air bubbles were removed, and the PDMS was cast onto the Si-wafer mold. The PDMS microchip was peeled off the master after it was polymerized at 70 ^{0}C overnight. A simple-t PDMS chip containing the channel of 5 cm×40 µm×15 µm was used for the electrophoretic separation, while a straight channel of similar dimensions without side arms was used for the reporter channel.

4.2.4 Electrode configuration set-up for the bipolar fluorescence experiment

The electrode was aligned in either the pseudo in-channel configuration or the in-channel configuration with a simple-t PDMS microchip. Two silver wires were used to bias the working electrode as a bipolar electrode by connecting it to the potentiostat. In this work, the reference electrode lead of the potentiostat was connected with the Ag wire placed inside the sensing channel sample waste reservoir and the working electrode was placed in the reservoir in the flow channel. Potentials were applied either by an isolated potentiostat (Micrux) or a CHI potentiostat, as necessary for in-channel or end-channel alignment, respectively.

A broadband source or a 488 nm laser was used as the excitation source and a photomultiplier tube (PMT) was used for detection. All measurements were made in a dark room. A low noise current amplifier was used to amplify the signal coming from the PMT and the signal was recorded using a customized LabVIEW program. All bipolar electrochemically-generated fluorescence measurements were performed without a Faraday cage.

4.3 Results and Discussion: Preliminary results

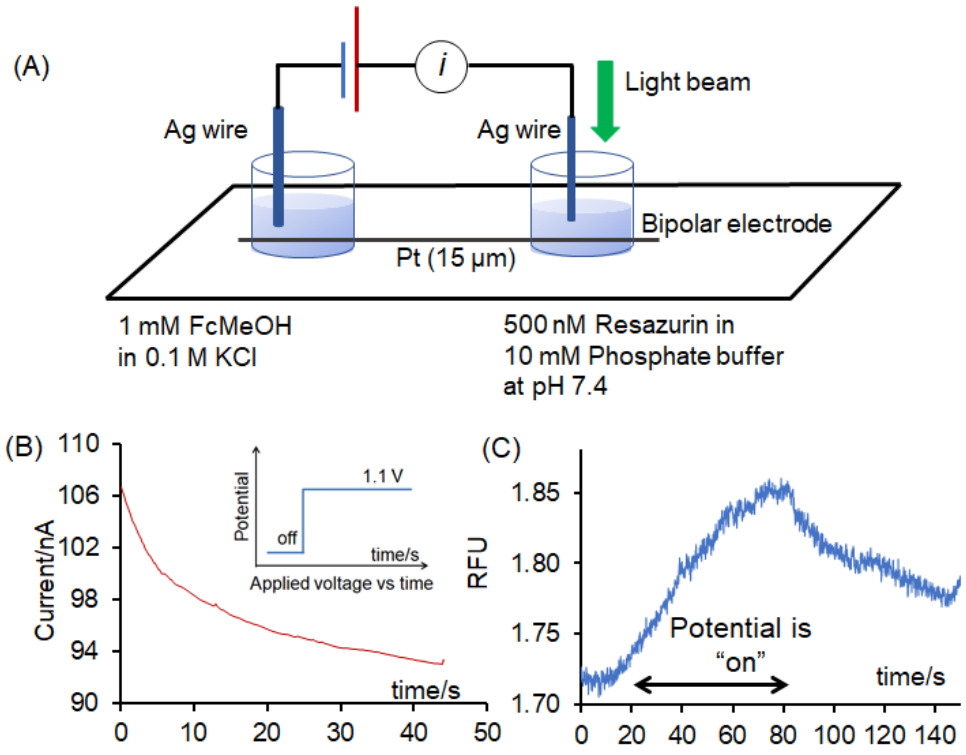

At the left-hand side of the bipolar electrode

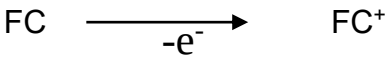

Ferrocene Ferrocenium

At the right-hand side of the bipolar electrode

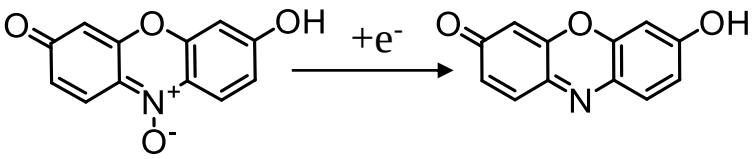

Resazurin Resorufin

Figure 4.5 (A) Experimental set up to study the feasibility of coupling a bipolar electrode-based fluorescence detection system with microchip electrophoresis (B) amperometric response with a biased potential of 1.1 V (C) fluorescence response results due to the reduction of resazurin

A few experiments were performed initially to understand the feasibility of coupling bipolar-based electrogenerated fluorescence with ME before being integrated with a microchip electrophoresis separation. The weakly fluorescent compound resazurin was used as the fluorescence reporter and ferrocene methanol was used as the analyte. Two pieces of PDMS were used to create two reservoirs sitting on a 30 µm wide Pt band electrode, as shown in Figure 4.5A, to hold the analyte solution and the fluorescent probe, respectively. A silver wire was placed in each reservoir to bias the Pt electrode externally as a bipolar electrode. The reference and counter leads of the potentiostat were connected to the silver wire sitting in the ferrocene methanol solution. The working electrode was connected to the Ag wire sitting in resazurin solution (Figure 4.5A). A biased voltage of 1.1 V was applied using a CHI potentiostat. The response of the bipolar system due to the oxidation of ferrocene to ferrocenium at the anodic pole and the reduction of resazurin to resorufin at the cathodic pole was recorded simultaneously using both amperometry and fluorescence (Figure 4.5B and 4.5C). A broad band light source was used as the excitation source and photomultiplier tube was used as the detector.

Under these static conditions, the decay of the fluorescence signal back to the background level took approximately 100 s. Therefore, it was determined that a flow system was necessary to improve the temporal resolution/response time of the system and allow for the determination of multiple analytes during a single analysis with ME. Additionally, a stronger excitation source was needed for an increased fluorescence signal intensity. A fluorescein-based oxidizable fluorescent probe (DCF) was used for the experiments after this for three reasons: DCF has a high quantum efficiency, its reduced form ($DCFH_2$) is non-fluorescent, and the reduced form is electrochemically oxidizable at low potentials.[38] These factors should make it possible to obtain low LODs with the bipolar fluorescence experiment.

A 488 nm cyan diode laser was used as the excitation source for $DCFH_2$ and a PMT was used to detect the fluorescence signal. $DCFH_2DA$ was dissolved in DMSO and diluted in methanol containing 2 mM NaOH and 5 mg/mL LiCl to yield a final probe concentration of 2 µM. The reason for the addition of NaOH is twofold: it hydrolyzes the acetate groups present on the molecule and it generates a pH above 10. DCF has the maximum quantum efficiency at very basic pHs and increases from 0.2 to 0.9 when the pH is increased from 8 to 10.[39] A straight channel was aligned with a Pt electrode in the channel and a hydrodynamic flow in the channel was generated using a vacuum pump. The applied potential of 1.1 V was turned on and off manually within a short time (for a few seconds) and the fluorescence response generated was recorded (Figure 4.6). This result indicated that the flow generated by the vacuum pump was sufficient for the initial investigation of coupling ME with bipolar electrogenerated fluorescence.

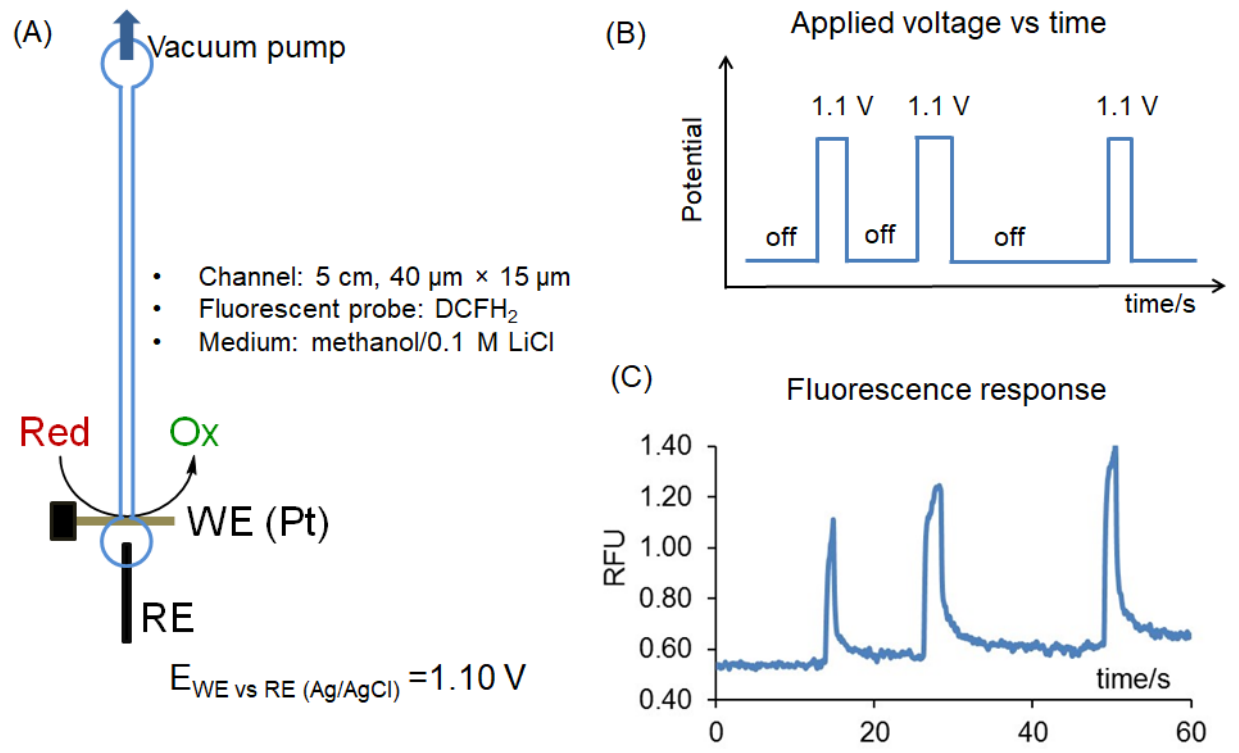

Figure 4.6 Investigation of the use of a vacuum pump as a flow generator for ME-Bipolar-EC-FL (A) experimental setup (B) applied potential program (C) resulting fluorescence response

4.3.1 Separation of two reducible analytes with microchip electrophoresis

Benzoquinone and resazurin were identified as two model analytes that were suitable for the initial evaluation of the bipolar-based detection system. Their half-wave potentials (cathodic peak potential of -0.245 V for benzoquinone[40] at pH 7.2 buffered solution and -0.21 at pH 6.2 for resazurin[41] vs Ag/AgCl) are more positive than the oxygen reduction potential. This is important since it eliminates the effect of oxygen reduction as a source of background during the amperometric detection step. Both of these species undergo two electron reduction reactions.

The separation of the two model analytes was achieved using ME in the normal polarity mode and a BGE consisting of 15 mM phosphate buffer pH 6.2 containing 2 mM SDS (Figure

4.7). SDS was added to the BGE to generate a stable electroosmotic flow with the PDMS substrate. Hydrodynamic voltammograms for both compounds were then generated to confirm the optimum potential that would be required to reduce the two analytes. These are shown in Figure 4.7. An electropherogram obtained using conventional amperometric detection coupled to ME is shown in Figure 4.7A. Peak widths for the two compounds were obtained as 1.45 ±0.00 s and 1.60±0.20 s.

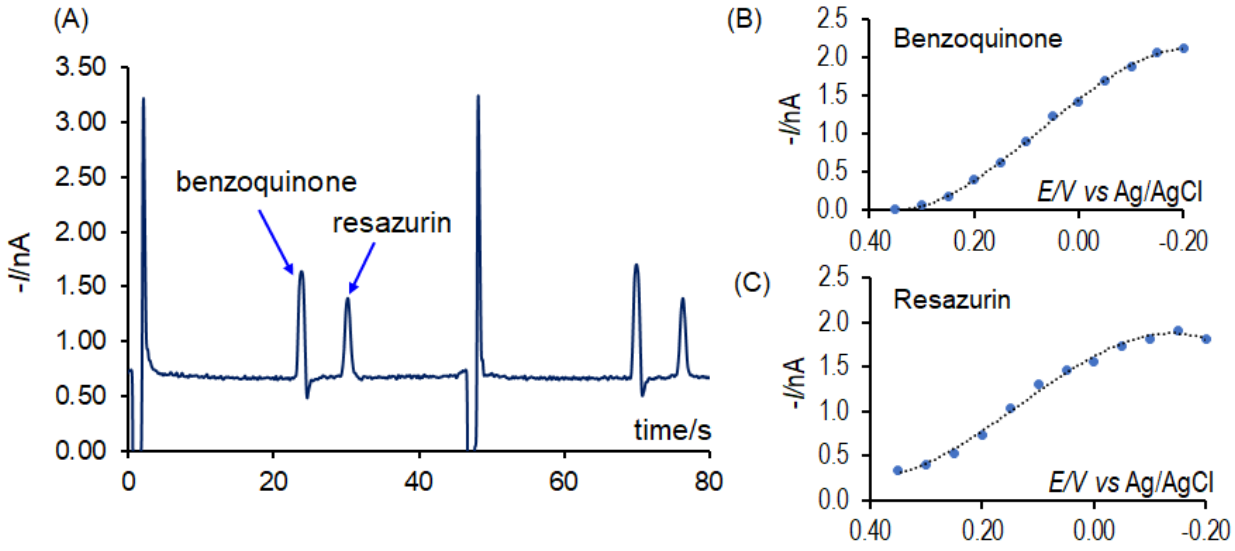

Figure 4.7 Separation and detection of (1) benzoquinone and (2) resazurin using ME-EC with a BGE consisting of 15 mM phosphate pH 6.2, 2 mM SDS (A) ME-EC electropherogram; hydrodynamic voltammograms for (B) benzoquinone (C) resazurin

4.3.2 ME separation channel coupled to bipolar fluorescence detection

For oxidizable analytes

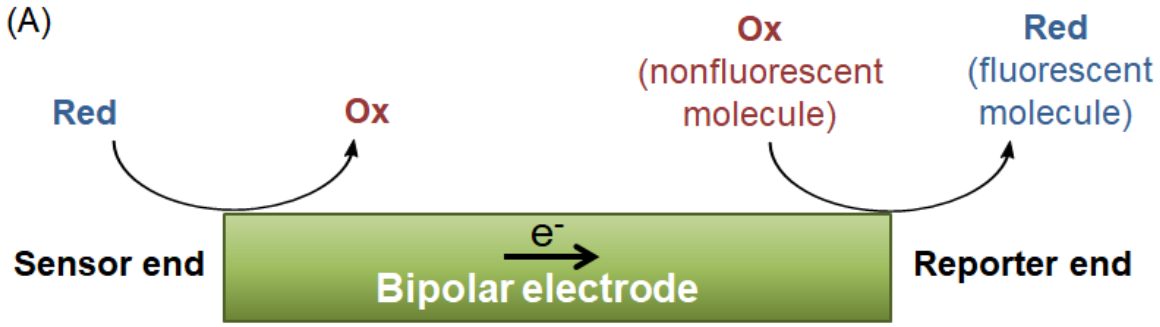

For reducible analytes

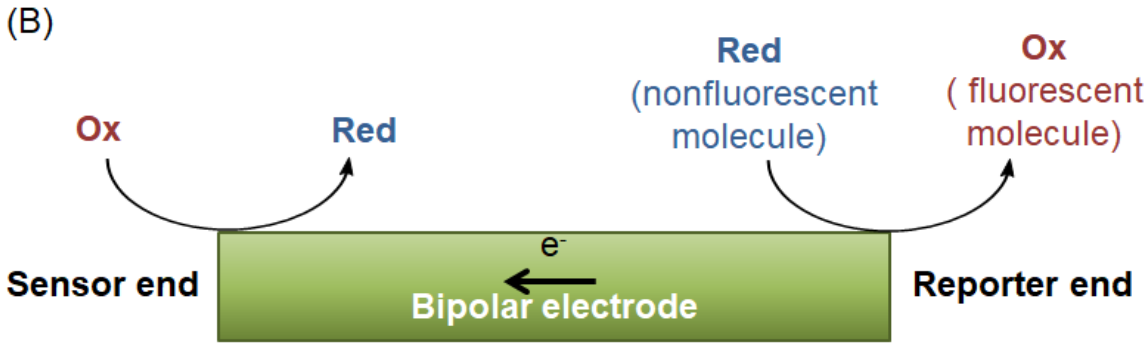

Figure 4.8 Bipolar electrode configuration (A) for oxidizable analytes (B) for reducible analytes

There are two configurations possible with bipolar fluorescence reporting. These are dependent on the redox chemistry of the analytes of interest and the fluorescent probe that is used. In the "oxidative mode", the current response due to oxidation of analytes can be reported by a reducible fluorophore. In the "reductive mode", the redox signal from reducible analytes is reported by an oxidizable fluorophore (Figure 4.8) In this chapter, we employed the second "reductive" mode and reducible analytes were separated by ME and detected by bipolar generated fluorescence (Figure 4.8B)

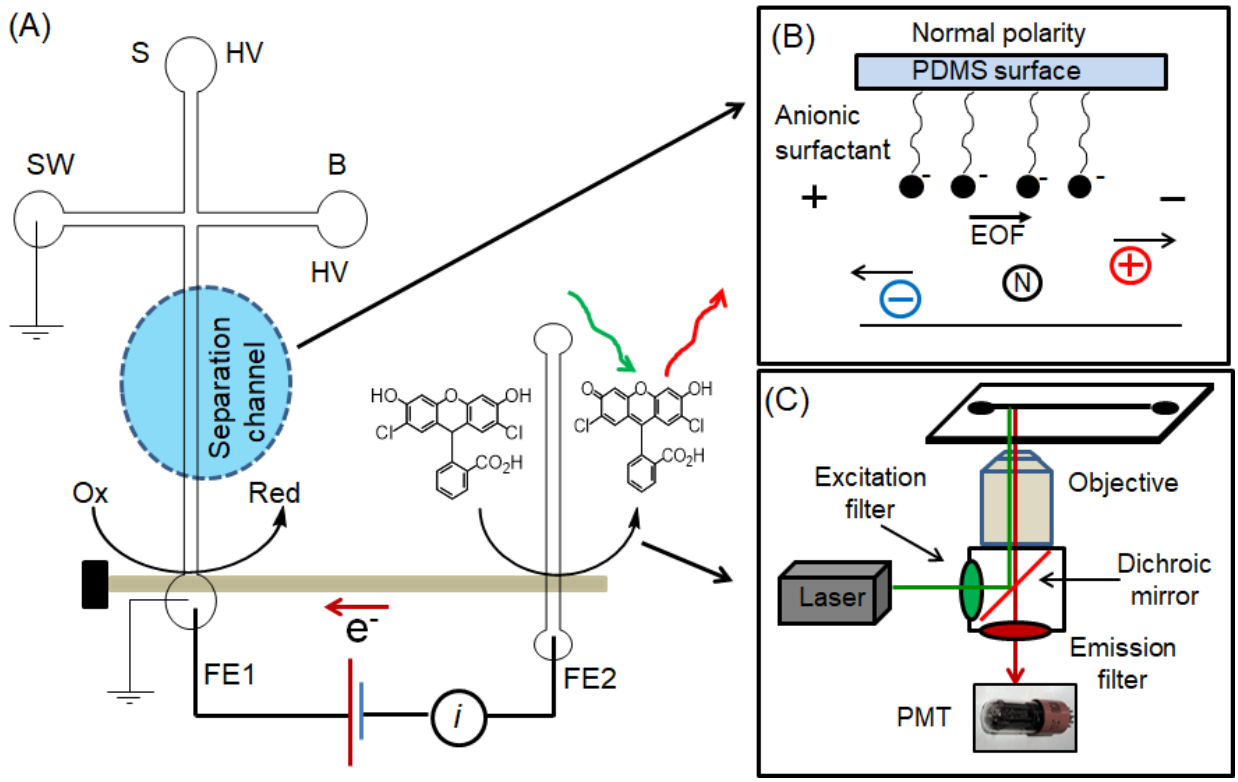

Figure 4.9 Experimental setup used for bipolar electrode-based fluorescence detection (A) simple-t microchip integrated with bipolar electrode and flow channel on a glass substrate (B) modification of the microchannel with an anionic surfactant and separation of charged species under normal polarity (C) fluorescence detection

A 5 cm long, 40 µm×15 µm simple-t microchip was used for the ME separation. The electrode was aligned with the separation channel using the pseudo-in-channel configuration and a 35 µm wide PPF electrode. A straight PDMS channel was used to flow a solution containing the fluorescent probe and was aligned onto the same electrode (Figure 4.9A). The PPF working electrode was biased as a bipolar electrode as shown in Figure 4.9 using a potentiostat. In this experimental configuration, the reference electrode and counter electrode connections were made at the end of the ME channel and the working electrode connection was at the end of the flow

channel as shown the Figure 4.9A. A bias voltage of -0.9 V was applied to the working electrode. The working principles of this closed bipolar electrode configuration have been well described in the literature.[42] Briefly, since the potential of the electrode end in the flow channel is sufficiently negative, electron transfer can occur from $DCFH_2$ to the bipolar electrode, leading to an oxidation current. The electrons can then flow through the electrode and be transferred to an oxidized analyte passing through the separation channel, causing its reduction. The resultant bipolar electrochemical and fluorescence responses are shown in Figure 4.10. Interestingly, the fluorescence signal shows a significant change in background at the injection which is different from a conventional ME-fluorescence electropherogram. This feature can be considered as a signature of the injection point for the bipolar fluorescence response. This feature is most likely due to the influence of the separation voltage change on the bipolar electrode at the time of injection. The field strength changes from 292 V/cm to 140 V/cm during the injection process causing a shift in the apparent applied potential at the sensor electrode towards a more positive potential. This leads to a smaller reduction background current and is translated at the detector end to a lower fluorescence background.

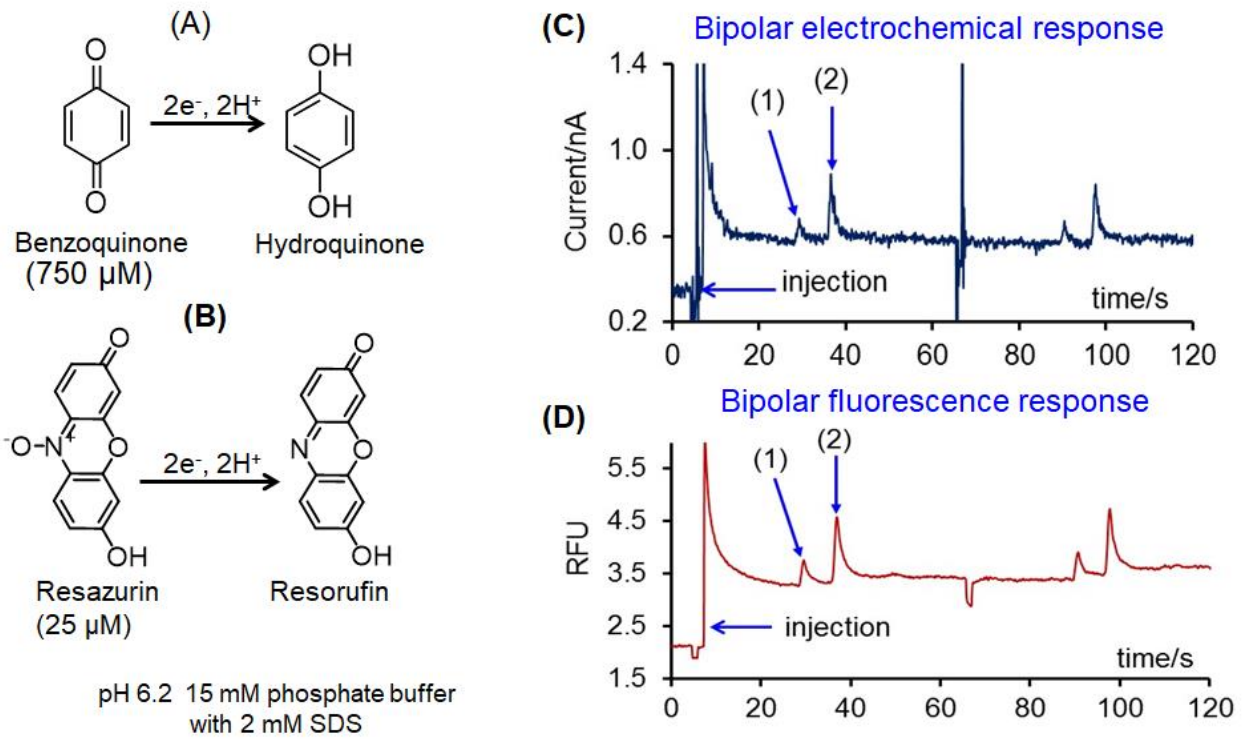

Figure 4.10 Microchip electrophoresis separation and detection of electrochemically reducible analytes (A) benzoquinone (750 µM) (B) resazurin (25 µM), using (C) bipolar electrochemical detection (D) bipolar fluorescence detection

A significant reduction in noise is observed with the bipolar fluorescence response compared to the bipolar electrochemical response. A comparison of S/N between bipolar electrochemical response and bipolar fluorescence response has not been made, as the electrochemical noise level for the ME-EC is much greater than normal. However, the ability of optical detection to eliminate the noise captured by electrochemical signal is significant. This proves that even in this preliminary experiment, there is promise for this new technique to provide better detection limits even though the actual concentrations used to record these electropherograms were high. Strategies to improve actual detection limits are discussed in the next section.

The migration time for benzoquinone with bipolar electrochemical detection was 23.44±0.48 s. The bipolar fluorescence response occurred at 23.60±0.60 s. This shows that the migration times are in good agreement within the two detection methods for the same run. The resazurin migration times show the same result; the migration time was 30.60±0.60 s with bipolar electrochemical detection and 31.46±0.71 s with bipolar fluorescence response. The slightly longer migration times in fluorescence measurements is most likely due to the larger detection window with fluorescence and that the detection was accomplished right after the electrode (as the electrode itself is not transparent). The variations and fluctuations in the migration time could also be due to small changes in the vacuum pump flow.

Peak widths of 2.2±0.4 s for benzoquinone and 3.3±0.7 s for resazurin were obtained with bipolar electrochemical detection. These values were approximately two times higher for the bipolar fluorescence detection (peak width of 4.3±1.1 s for benzoquinone and 7.5±0.7 s for resazurin). The peak widths obtained using bipolar fluorescence detection were also higher than those obtained by performing ME with conventional amperometric detection. As mentioned above, the reason for the increased peak width is a combination of the position of the fluorescence detection and the fluctuations in the flow of the fluorescence reporter solution by the vacuum pump. Additionally, the loss of separation efficiencies can be due to the hydrodynamic flow, compared to EOF, at the second channel. These factors lead to reduced efficiencies and resolution compared to that obtainable with conventional single-channel ME.

4.4 Conclusions

Preliminary experiments were performed to determine the best way to implement bipolar electrode-based fluorescence detection with the microchip format. It was revealed that a flow is necessary at the reporting channel to ensure the availability of a fresh solution at the reporting

electrode. A vacuum pump was used to successfully create a hydrodynamic flow in the flow channel. Separation and detection of two model analytes with the newly developed method was demonstrated. Though a comparison of bipolar fluorescence detection and bipolar electrochemical detection has not been made, it is clear that the fluorescence detection is less influenced by the environmental noise compared to the electrochemical detection. Optimization of the flow and limiting currents are necessary to obtain better detection limits with the newly developed method. These approaches are discussed in the next chapter.

4.5 References

1. Gunasekara, D. B.; Siegel, J. M.; Caruso, G.; Hulvey, M. K.; Lunte, S. M., Microchip electrophoresis with amperometric detection method for profiling cellular nitrosative stress markers. *Analyst* **2014,** *139* (13), 3265-3273.

2. Fischer, D. J.; Hulvey, M. K.; Regel, A. R.; Lunte, S. M., Amperometric detection in microchip electrophoresis devices: Effect of electrode material and alignment on analytical performance. *Electrophoresis* **2009,** *30* (19), 3324-3333.

3. Gunasekara, D. B.; Hulvey, M. K.; Lunte, S. M., In-channel amperometric detection for microchip electrophoresis using a wireless isolated potentiostat. *Electrophoresis* **2011,** *32* (8), 832-837.

4. Hulvey, M. K.; Frankenfeld, C. N.; Lunte, S. M., Separation and Detection of Peroxynitrite Using Microchip Electrophoresis with Amperometric Detection. *Anal. Chem.* **2010,** *82* (5), 1608-1611.

5. Fernandez-la-Villa, A.; Bertrand-Serrador, V.; Pozo-Ayuso, D. F.; Castano-Alvarez, M., Fast and reliable urine analysis using a portable platform based on microfluidic electrophoresis chips with electrochemical detection. *Anal. Methods* **2013,** *5* (6), 1494-1501.

6. Crevillén, A. G.; Pumera, M.; González, M. C.; Escarpa, A., Carbon nanotube disposable detectors in microchip capillary electrophoresis for water-soluble vitamin determination: Analytical possibilities in pharmaceutical quality control. *Electrophoresis* **2008,** *29* (14), 2997-3004.

7. Bani-Yaseen, A.; Kawaguchi, T.; Price, A.; Culbertson, C.; Jankowiak, R., Integrated microfluidic device for the separation and electrochemical detection of catechol estrogen-derived DNA adducts. *Anal. Bioanal. Chem.* **2011,** *399* (1), 519-524.

8. Wang, W.; Fu, F. F. u.; Xu, X.; Lin, J.-M.; Chen, G., Filmy channel microchip with amperometric detection. *Electrophoresis* **2009,** *30* (22), 3932-3938.

9. Ruecha, N.; Siangproh, W.; Chailapakul, O., A fast and highly sensitive detection of cholesterol using polymer microfluidic devices and amperometric system. *Talanta* **2011,** *84* (5), 1323-1328.

10. Piccin, E.; Dossi, N.; Cagan, A.; Carrilho, E.; Wang, J., Rapid and sensitive measurements of nitrate ester explosives using microchip electrophoresis with electrochemical detection. *Analyst* **2009,** *134*, 528-532.

11. Wang, J.; Zima, J.; Lawrence, N. S.; Chatrathi, M. P.; Mulchandani, A.; Collins, G. E., Microchip Capillary Electrophoresis with Electrochemical Detection of Thiol-Containing Degradation Products of V-Type Nerve Agents. *Anal. Chem.* **2004,** *76*, 4721-4726.

12. Yan, J.; Yang, X.; Wang, E., Electrochemical Detection of Anions on an Electrophoresis Microchip with Integrated Silver Electrode. *Electroanalysis* **2005,** *17* (13), 1222-1226.

13. Chen, C.; Hahn, J., Enhanced aminophenols monitoring using in-channel amperometric detection with dual-channel microchip capillary electrophoresis. *Environ. Chem. Lett.* **2011,** *9* (4), 491-497.

14. Chailapakul, O.; Korsrisakul, S.; Siangproh, W.; Grudpan, K., Fast and simultaneous detection of heavy metals using a simple and reliable microchip-electrochemistry route: An alternative approach to food analysis. *Talanta* **2008,** *74*, 683-689.

15. Godoy-Caballero, M. d. P.; Acedo-Valenzuela, M. I.; Galeano-Diaz, T.; Costa-Garcia, A.; Fernandez-Abedul, M. T., Microchip electrophoresis with amperometric detection for a novel determination of phenolic compounds in olive oil. *Analyst* **2012,** *137* (21), 5153-5160.

16. Dossi, N.; Toniolo, R.; Pizzariello, A.; Susmel, S.; Bontempelli, G., A modified electrode for the electrochemical detection of biogenic amines and their amino acid precursors separated by microchip capillary electrophoresis. *Electrophoresis* **2011,** *32*, 906-912.

17. Hervas, M.; Lopez, M. A.; Escarpa, A., Integrated electrokinetic magnetic bead-based electrochemical immunoassay on microfluidic chips for reliable control of permitted levels of zearalenone in infant foods. *Analyst* **2011,** *136*, 2131-2138.

18. Shiddiky, M. J. A.; Lee, K.-S.; Son, J.; Park, D.-S.; Shim, Y.-B., Development of Extraction and Analytical Methods of Nitrite Ion from Food Samples: Microchip Electrophoresis with a Modified Electrode. *J. Agric. Food Chem.* **2009,** *57*, 4051-4057.

19. Kovachev, N.; Canals, A.; Escarpa, A., Fast and Selective Microfluidic Chips for Electrochemical Antioxidant Sensing in Complex Samples. *Anal. Chem.* **2010,** *82* (7), 2925-2931.

20. Gunawardhana, S. M.; Lunte, S. M., Continuous monitoring of adenosine and its metabolites using microdialysis coupled to microchip electrophoresis with amperometric detection. *Anal. Methods* **2018,** *10* (30), 3737-3744.

21. Gunasekara, D. B.; Wijesinghe, M. B.; Saylor, R. A.; Lunte, S. M., Principles and strategies for microchip electrophoresis with amperometric detection. *RSC Detect. Sci. Ser.* **2016,** *6*, 85-124.

22. Lucca, B. G.; de Lima, F.; Coltro, W. K. T.; Ferreira, V. S., Electrodeposition of reduced graphene oxide on a Pt electrode and its use as amperometric sensor in microchip electrophoresis. *Electrophoresis* **2015,** *36* (16), 1886-1893.

23. Siegel, J. M.; Schilly, K. M.; Wijesinghe, M. B.; Caruso, G.; Fresta, C. G.; Lunte, S. M., Optimization of a microchip electrophoresis method with electrochemical detection for the determination of nitrite in macrophage cells as an indicator of nitric oxide production. *Anal. Methods* **2019,** *11* (2), 148-156.

24. Guan, Q.; Henry, C. S., Improving MCE with electrochemical detection using a bubble cell and sample stacking techniques. *Electrophoresis* **2009,** *30* (19), 3339-3346.

25. Kutter, J. P.; Ramsey, R. S.; Jacobson, S. C.; Ramsey, J. M., Determination of metal cations in microchip electrophoresis using on-chip complexation and sample stacking. *J. Microcolumn Sep.* **1998,** *10* (4), 313-319.

26. Lichtenberg, J.; Verpoorte, E.; de Rooij, N. F., Sample preconcentration by field amplification stacking for microchip-based capillary electrophoresis. *Electrophoresis* **2001,** *22* (2), 258-271.

27. Xu, W.; Zaino, L. P.; Bohn, P. W. In *Electrochemically modulated luminescence in nanophotonic structures*, Springer International Publishing AG: 2017; pp 79-104.

28. Mavre, F.; Anand, R. K.; Laws, D. R.; Chow, K. F.; Chang, B. Y.; Crooks, J. A.; Crooks, R. M., Bipolar electrodes: a useful tool for concentration, separation, and detection of analytes in microelectrochemical systems. *Anal. Chem.* **2010,** *82* (21), 8766-74.

29. Fosdick, S. E.; Knust, K. N.; Scida, K.; Crooks, R. M., Bipolar electrochemistry. *Angew. Chem. Int. Ed. Engl.* **2013,** *52* (40), 10438-56.

30. Blackhur.Jr; Coulson, J. M.; Goodridg.F; Plimley, R. E.; Fleischm.M, A preliminary investigation of fluidized bed electrodes. *J. Electrochem. Soc.* **1969,** *116* (11), 1600-&.

31. Cox, J. T.; Guerrette, J. P.; Zhang, B., Steady-state voltammetry of a microelectrode in a closed bipolar cell. *Anal. Chem.* **2012,** *84* (20), 8797-804.

32. Chow, K. F.; Chang, B. Y.; Zaccheo, B. A.; Mavre, F.; Crooks, R. M., A Sensing Platform Based on Electrodissolution of a Ag Bipolar Electrode. *J. Am. Chem. Soc.* **2010,** *132* (27), 9228-9229.

33. Guerrette, J. P.; Percival, S. J.; Zhang, B., Fluorescence coupling for direct imaging of electrocatalytic heterogeneity. *J. Am. Chem. Soc.* **2013,** *135* (2), 855-61.

34. Scott, D. E.; Grigsby, R. J.; Lunte, S. M., Microdialysis sampling coupled to microchip electrophoresis with integrated amperometric detection on an all-glass substrate. *Chemphyschem* **2013,** *14* (10), 2288-94.

35. Fischer, D. J.; Vandaveer IV, W. R.; Grigsby, R. J.; Lunte, S. M., Pyrolyzed Photoresist Carbon Electrodes for Microchip Electrophoresis with Dual-Electrode Amperometric Detection. *Electroanalysis* **2005,** *17* (13), 1153-1159.

36. Fischer, D. J.; Hulvey, M. K.; Regel, A. R.; Lunte, S. M., Amperometric detection in microchip electrophoresis devices: effect of electrode material and alignment on analytical performance. *Electrophoresis* **2009,** *30* (19), 3324-33.

37. Hulvey, M. K.; Frankenfeld, C. N.; Lunte, S. M., Separation and Detection of Peroxynitrite Using Microchip Electrophoresis with Amperometric Detection. *Anal. Chem.* **2010,** *82* (5), 1608-1611.

38. Wang, S. T.; Zhegalova, N. G.; Gustafson, T. P.; Zhou, A.; Sher, J.; Achilefu, S.; Berezin, O. Y.; Berezin, M. Y., Sensitivity of activatable reactive oxygen species probes by fluorescence spectroelectrochemistry. *Analyst* **2013**, 138 (15), 4363-4369.

39. Bouffier, L.; Doneux, T., Coupling electrochemistry with in situ fluorescence (confocal) microscopy. *Curr. Opin. Electrochem.* **2017**, 6 (1), 31-37.

40. Quan, M.; Sanchez, D.; Wasylkiw, M. F.; Smith, D. K., Voltammetry of Quinones in Unbuffered Aqueous Solution: Reassessing the Roles of Proton Transfer and Hydrogen Bonding in the Aqueous Electrochemistry of Quinones. *J. Am. Chem. Soc.* **2007,** *129* (42), 12847-12856.

41. Khazalpour, S.; Nematollahi, D., Electrochemical study of Alamar Blue (resazurin) in aqueous solutions and room-temperature ionic liquid 1-butyl-3-methylimidazolium tetrafluoroborate at a glassy carbon electrode. *RSC Advances* **2014,** *4* (17), 8431-8438.

42. Oja, S. M.; Guerrette, J. P.; David, M. R.; Zhang, B., Fluorescence-Enabled Electrochemical Microscopy with Dihydroresorufin as a Fluorogenic Indicator. *Anal. Chem.* **2014,** *86* (12), 6040-6048.

5. Chapter 5 Optimization of bipolar electrode based-fluorescence detection method for microchip electrophoresis

This chapter is based on the manuscript written on

Wijesinghe, M.B.; Gunasekara, D.B. and Lunte, S.M. Optimization of bipolar electrode based-fluorescence detection method for microchip electrophoresis, to be submitted to Analytical Chemistry

5.1 Introduction

Significant attention has been given to studies of bipolar electrochemistry[1-3] over the past two decades. One of the most important reports of this kind was published by Manz and coworkers using electrogenerated chemiluminescence with ($Ru(bpy)_3^{2+}$) as a bipolar electrode-based reporter.[4] After that, the Crooks group showed that there exists a quantitative relationship between the redox reactions occurring at the reporting and the sensing poles of the bipolar electrode.[5] These two fundamentals led researchers to explore many applications including bipolar electrode based biosensing,[6-14] analyte separation and enrichment,[15] and catalyst screening.[16-19] It was of our interest to evaluate bipolar electrode-based sensing with microchip electrophoresis (ME).

It was shown in Chapter 4 of this dissertation that it is possible to integrate bipolar electrode-based fluorescence detection with microchip electrophoresis. The separation and detection of two model compounds by ME-bipolar-EC-FL was successfully demonstrated. The next goal was to improve the LODs of this technique by optimizing the limiting current and minimizing band broadening at the two poles of the bipolar electrode integrated to the ME. The strategies to improve the bipolar electrode-based detector performance are discussed in this chapter. Also, at the end of this chapter the use of electroosmotic flow instead of hydrodynamic flow in the reporter flow channel is also discussed. Lastly, a method to obtain the bipolar fluorescence response with ME without the use of a potentiostat is described.

5.1.1 Challenges and strategies to improve the performance of bipolar detection method

Limiting currents available at the reporting pole (anodic pole) should be greater than that at the sensing pole (cathodic pole) to drive the electrochemical reduction of the analytes at the sensing pole to the highest possible value. Estimation of the limiting current available at the sensing pole in the system described in Chapter 4 yielded a value of approximately 3 nA. In those

experiments, the BGE was not totally inert over the potential window used for the experiment and thus generated a background current. Additionally, current due to the reduction of trace amounts of oxygen can also contribute to the background current. In contrast, the current at the reporting pole in the initial experiment was only 1 nA. This consisted of approximately 200 pA from the fluorescent probe and 800 pA from the solvent background (Figure 5.1). This implies that the current available at the sensor end is not sufficient to drive the analyte reductions to its maximum possible value.

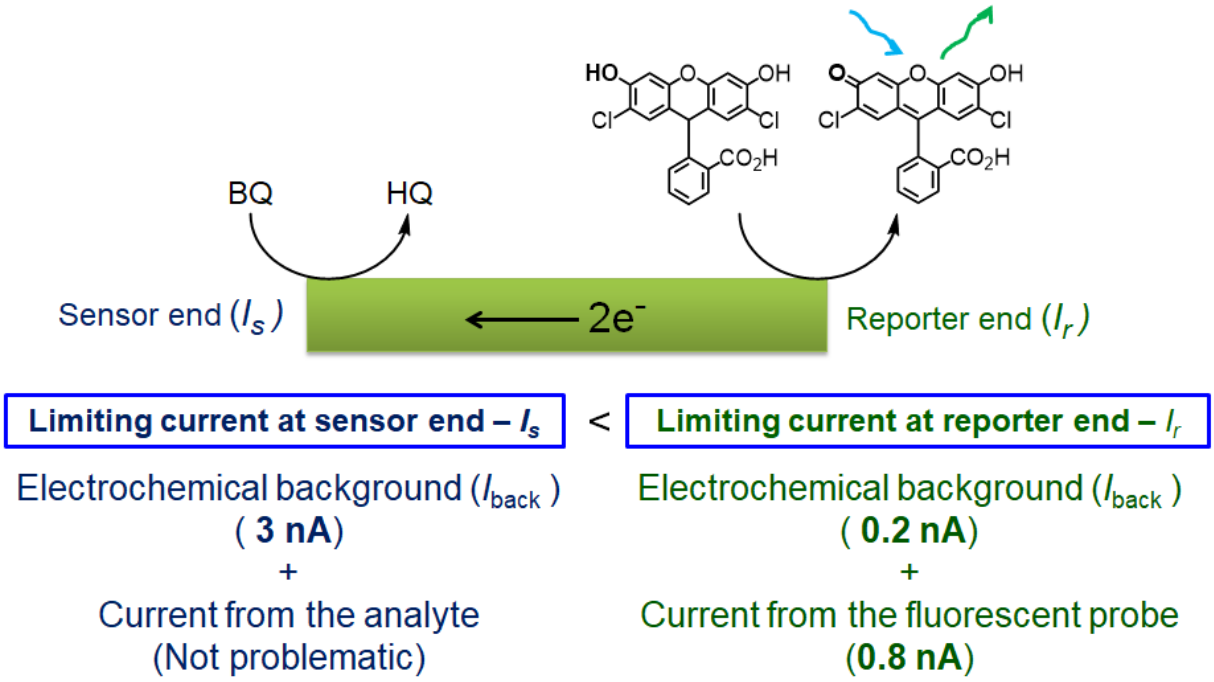

Figure 5.1 Amount of current at sensing and reporting poles

There are a few possible modifications that could be applied to circumvent the problem of low current at the anodic pole and/or high current at the cathodic pole. The simplest modification would be to use a higher fluorescent probe concentration. However, the probe concentration cannot be increased without limit for two main reasons. The first is that the fluorescence background will

increase due to the presence of trace amounts of the oxidized form of the fluorescent probe. The second reason is that transforming 3 nA of background signal to a fluorescent signal may not be ideal as it will generate a substantial fluorescence background. This will make the measurements more difficult and may lead to increased noise. We found that the probe concentration could be increased up to 10 μM without a significant increase of background noise.

An alternative approach is to increase the size of the electrode at the reporting pole. However, this need to be performed with a great care since a larger electrode can produce a wider zone of oxidized fluorescent probe. The optimum size, as far as we understand, is a size similar to that of the laser excitation beam. Therefore, in all the following experiments, a 30 μm electrode was used. Also, in these studies the electrode material used for the reporter electrode was changed from carbon to gold. Gold electrodes were found to be more stable and easier to operate with the flow system than the PPF electrodes. The flow system for the reporter channel was also changed from using negative pressure (vacuum) to a syringe pump. This helped maintain better control of the flow rate and minimized noise.

A third approach is to decrease the size of the separation channel and the size of the sensor electrode. This causes a decrease in the electrochemical background current due to the exposure of a lesser electrode area.

A different approach to decrease the electrochemical background at the simple-t microchip electrophoresis (sensor end) was also investigated. In this study, an in-channel electrode alignment was used instead of a pseudo-in-channel alignment. The details of this approach are discussed under results and discussion. The figures of merit and limits of detection for each of the modifications using bipolar ME-EC are also reported.

5.2 Experimental section

5.2.1 Chemicals and Reagents

SU-8 10 photoresist and SU-8 developer (MicroChem Corp., Newton, MA, USA); AZ1518 photoresist and 300 MIF developer (Mays Chemical Co., Indianapolis, IN, USA); photolithography film mask (40,000 dpi; Infinite Graphics Inc., Minneapolis, MN, USA); N(100) 100 mm (4″) silicon (Si) wafers (Silicon, Inc., Boise, ID, USA); chrome and AZ1518 positive photoresist coated borofloat glass substrate (4″×4″×0.090″, Nanofilm, Westlake, CA, USA); Sylgard 184 Silicone Elastomer Kit: polydimethylsiloxane (Ells-worth Adhesives, Germantown, WI, USA); epoxy and 22 gauge Cu wire (Westlake Hardware, Lawrence, KS, USA); silver colloidal paste (Ted Pella, Inc., Redding, CA, USA); acetone, 2-propanol (isopropyl alcohol, IPA), buffered oxide etchant (JTBaker, Austin, TX, USA) monosodium phosphate (Sigma Aldrich), disodium phosphate (Sigma Aldrich), sodium dodecyl sulphate (Sigma Aldrich), benzoquinone (BQ; 99% Sigma Aldrich), resazurin (99% ThermoFisher Scientific), dichlorodihydrofluorescein diacetate ($DCFH_2$; >95% Cayman chemicals), and lithium chloride (Sigma Aldrich) were used as received. All water used was ultrapure (18.2 MΩcm, Milli-Q Synthesis A10, Millipore, Burlington, MA, USA).

5.2.2 Electrode fabrication

5.2.2.1 Au electrode fabrication

A gold electrode with a width of 30 μm was fabricated according to the procedure described earlier by our group.[20-21] Briefly, the design was drawn using AutoCad LT2004 (Autodesk, San Rafael, CA, USA) and printed on a transparency sheet (Infinite Graphics Inc., Minneapolis, MN, USA). After that the design was transferred to the AZ 1518 photoresist and chrome coated borofloat glass substrate using a UV flood source. The electrode was then developed with AZ 300

MIF (Capitol Scientific, Inc., Austin, TX, USA) for 10 s. Next, the plate was subjected to chrome etch until the features were transparent. A trench of 300-400 nm was generated using buffered oxidant (10 % HF). The glass plate was then plasma cleaned for 50 s. A 40 nm Ti layer followed by a Au film with a thickness of 250-300 nm was then deposited using a Magnetron sputtering system (AXXIS DC magnetron sputtering system, Kurt J. Lesker Co., Jefferson Hills, PA, USA). After that, the plate was treated with acetone to remove excess Au and then with chrome etch to obtain the Au electrode fabricated on the glass.

5.2.2.2 Fabrication of the pyrolyzed photoresist film electrode (PPF)

The fabrication procedure for the pyrolyzed photoresist electrode has been described in detail in the literature.[22-23] Briefly, a clean quartz glass plate (to reuse, the plate can be cleaned with acid and base piranha solution) of 2.5 by 4 inch was baked at 200 ^{0}C for 2 h on a programmable hot plate. AZ 1518 positive photoresist was spin coated on the dried glass. Coated glass was then baked at 100 ^{0}C for 2 minutes using a programmable hotplate. Features from a positive mask design printed on a transparency were transferred onto the AZ1518 coated quartz glass using a UV flood source. The glass substrate was then developed using MIF-300 and rinsed with 18 MΩ water. The photoresist was then pyrolyzed in a tube furnace in a nitrogen environment with a temperature program up to a temperature of 900 ^{0}C.

5.2.3 PDMS microchip fabrication

A simple-t PDMS microchip containing a channel with dimensions of 5 cm × 40 µm×15 µm for the electrophoresis was fabricated as previously described.[24] Briefly, the channel design was drawn with AutoCad LT2004 (Autodesk, San Rafael, CA, USA) software and printed on a transparency sheet at a resolution of 40,000 dpi. A 4” Si wafer was coated with SU-8 10 negative

photoresist using a spin-coater to give a film thickness of 15 µm. The coated Si wafer was then soft baked at 65 ^{0}C for 2 minutes, followed by at 95 ^{0}C for 5 minutes on a programmable hotplate. Next, the features on the photomask were transferred to the spin coated silicon wafer using a UV flood source. SU-8 developer was used to develop the photoresist on the Si wafer and it was then rinsed with IPA. The wafer was transferred onto the hot plate for a hard bake for 2 h and then it was dried with nitrogen. 10.9 grams of PDMS polymer and 1.1 grams of curing agent (10:1) were mixed well, the air bubbles were removed, and it was cast onto the Si-wafer mold. The PDMS microchip was peeled off from the master after it was allowed to polymerize at 70 ^{0}C overnight. The simple-t PDMS chip containing the channel of 5 cm×40 µm×15 µm was used for the electrophoretic separation, while a straight channel of similar dimensions but without side arms was used for the reporter channel. A 6 mm thick PDMS chip (10:1 polymer to curing agent with a total mass of 84 g) was made containing the straight channel, resulting in a strong connection with the tubing from syringe pump.

A modified procedure has been used to fabricate a smaller simple-t microchip of 5 cm×5 µm×15 µm. A few additional steps in the fabrication of the corresponding simple-t master were necessary because the features are smaller. First, a layer of hexamethyl disilazane (HMDS) was applied before the photoresist coating. This provided better adhesion of the photoresist to the silicon wafer. The features were then transferred to the Si wafer as indicated earlier in the fabrication section. Generally, the development of the Si wafer is performed immediately after the UV exposure and soft bake step. However, in this fabrication, the Si wafer with features was kept in the dark overnight after the soft bake before the development. These modifications resulted in a fairly stable Si wafer master with smaller channel dimensions (Figure 5.2).

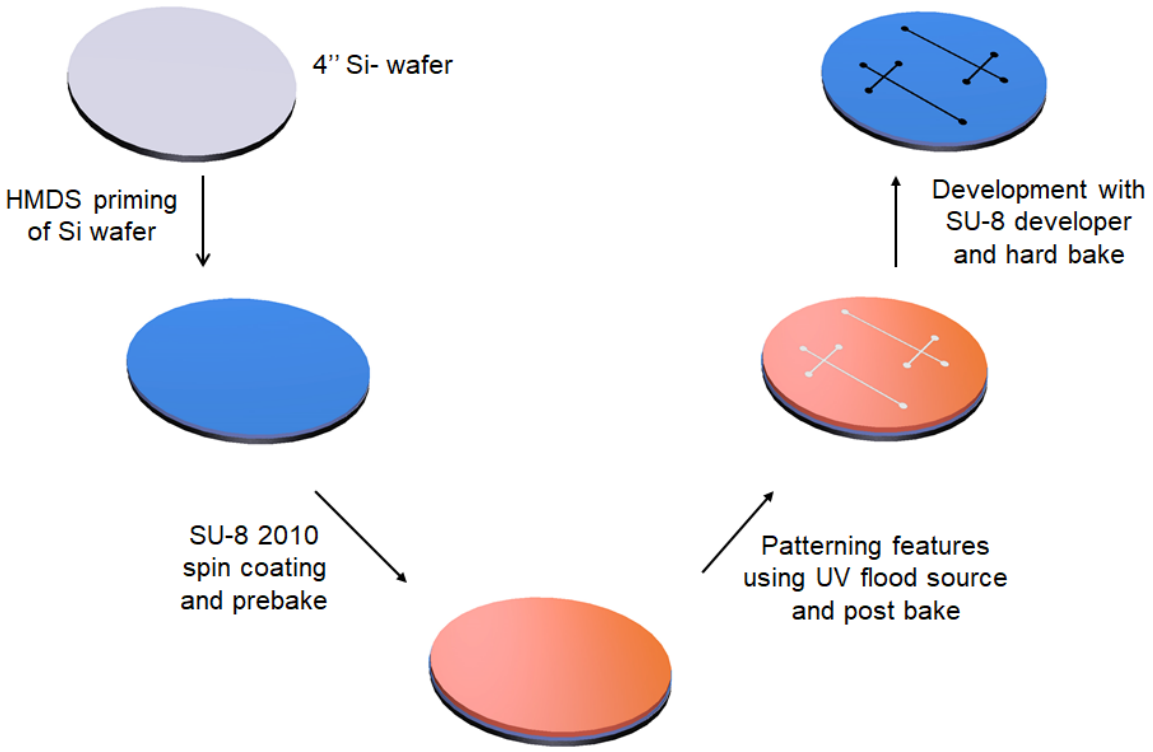

Figure 5.2 Procedure for fabricating a PDMS master with 5 μm-wide channels

5.2.4 PDMS simple-t/ quartz glass-PPF electrode and PDMS straight channel/ Au electrode combined device

In this configuration, a PPF electrode was used as the sensor electrode and a Au electrode was used as the reporter electrode. The two electrodes were fabricated on two different substrates and were connected using a Cu wire. The connection of the tubing to the flow channel was accomplished using a vacuum suction cup as shown in Figure 5.3. The combined working electrode setup consisted of PPF and Au electrodes that were biased by applying a potential as a bipolar electrode using the potentiostat as shown in Figure 5.4A.

The PDMS flow chip (reporter channel) was bonded irreversibly to the borofloat glass containing the Au electrode using a handheld plasma treater. Prior to bonding, this provided extra

strength to the chip's bond so it could withstand the hydrodynamic pressure generated at the site of connection to the tubing from the syringe pump. Bonding was accomplished with extra care to avoid damage to the electrode by plasma arcs.

The simple-t microchip was reversibly bonded to the quartz glass that contained a PPF electrode. The electrode was aligned in either the pseudo-in-channel configuration or the in-channel configuration with a simple-t PDMS microchip. Two silver wires were used to bias the working electrode as a bipolar electrode by connecting it to the potentiostat. In this work, the reference electrode lead of the potentiostat was connected with a Ag wire placed inside the sensing channel sample waste reservoir and the working electrode was placed in the flow channel reservoir. Potentials were applied using a Micrux isolated potentiostat.

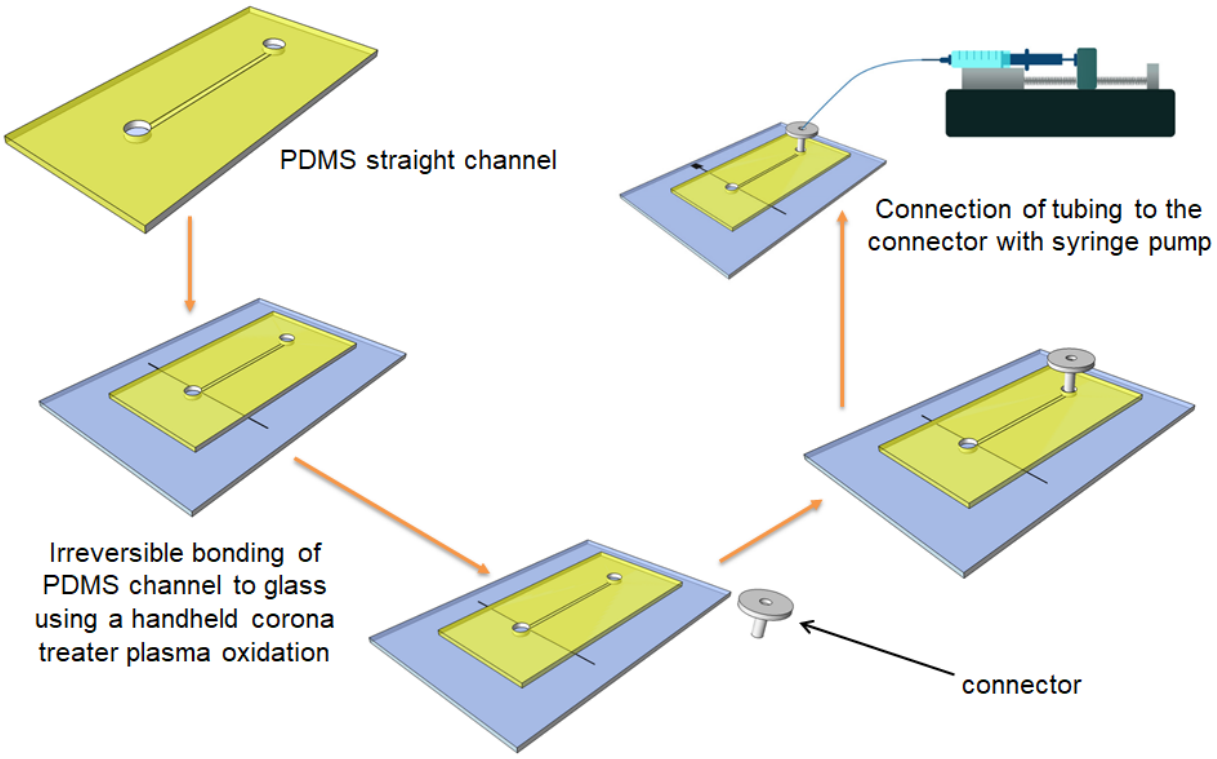

Figure 5.3 Connecting the flow channel to the syringe pump using a suction cup connector

5.2.5 Fluorescence measurements

A 488 nm diode laser was used as the excitation source and a photomultiplier tube (PMT) was used for detection. All measurements were made in a dark room. A low noise current amplifier was used to amplify the signal coming from the PMT and the signal was recorded using a customized LabVIEW program. All bipolar electrochemically generated fluorescence measurements were performed without a Faraday cage.

5.3 Results and discussion

5.3.1 Bipolar fluorescence detection using short separation channel (5 μm) and 10 μm PPF electrode

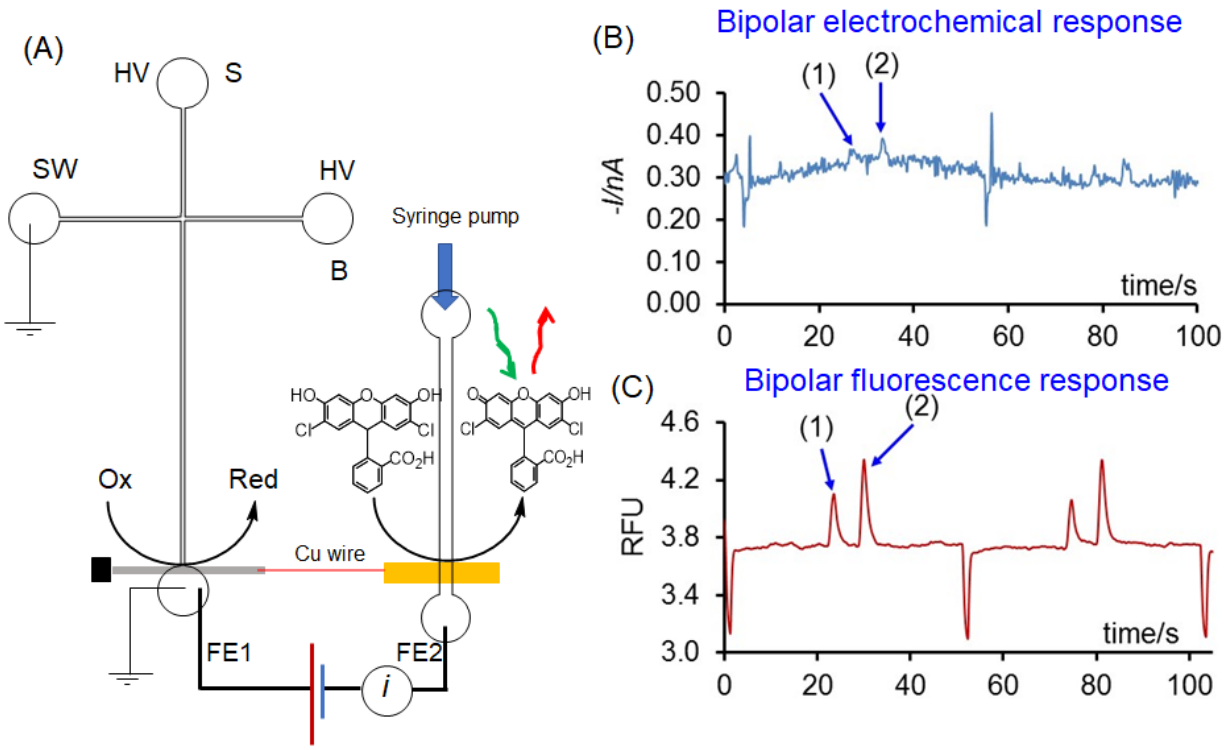

Figure 5.4 (A) Setup for bipolar electrochemically generated fluorescence detection of model analytes (1) benzoquinone (536 μM) (2) resazurin (12 μM) separated by ME (B) bipolar electrochemical response (C) bipolar fluorescence response

In this experiment, 10 μm-wide PPF electrodes were used with the simple-t microchip, as opposed to the 35 μm-wide electrodes used previously, for an approximately 3.5-fold decrease in electrode width. In addition, 5 μm flow channels were made, which are 8-fold narrower than the initial channels. Combined, these changes decreased the overall area of the electrode exposed to the solution by a factor of 28. The bipolar experimental setup with these modifications is shown in Figure 5.4.

The resultant bipolar electrochemical response exhibited an exceptionally high noise (about 30 pA), making it difficult to identify the peaks (Figure 5.4B and C). Amperometric currents for both benzoquinone and resazurin were 40 pA or below, meaning a signal-to-noise ratio of less than 2 for bipolar amperometric measurements. However, the noise level associated with the electropherogram shown in Figure 5.4B is higher than that of a conventional ME-EC electropherogram. This could be a result of the influence of the high voltage electrophoresis potential, lack of Faraday cage, and/or noise from the syringe pump. It may be possible to decrease this noise to 4 pA, which is the noise associated with a typical ME amperometry experiment. If this value is used to calculate the signal-to-noise ratio, a signal-to-noise ratio less than 10 is obtained for benzoquinone and resazurin at concentrations of 536 μM and 12 μM, respectively. However, fluorescence signals were clearly visible with S/N>25. Therefore, it is promising that the new spectro-electrochemical detection method should provide better LODs than conventional ME-EC. Additionally, calibration curves for both of the compounds were constructed and their R^2 values were greater than 0.99, demonstrating the ability of novel detection system to quantify the analytes being separated by ME.

In the bipolar fluorescence electropherogram, the peak widths of benzoquinone and resazurin are about 5 s and are therefore 3.5 times larger than those obtained using ME with

conventional amperometric detection. This could be due to the hydrodynamic flow and the use of a 3.5-fold larger reporter electrode compared to the sensor electrode. Additionally, it is possible that some of the oxidized probe adsorbed to the PDMS channel, leading to diminished peak efficiency.

The advantage of using smaller channels and electrodes at the sensor end is that this decreases the bipolar electrochemical background and thus leads to a lower fluorescence background. However, decreasing the dimensions of the electrode (width and the length) also reduces the available electrode area for the analyte reduction, leading to a decrease in the electrochemical response. Additionally, it is challenging to align a smaller electrode with a 5 μm channel and it is difficult to perform electrophoresis experiments using low micron size channels.

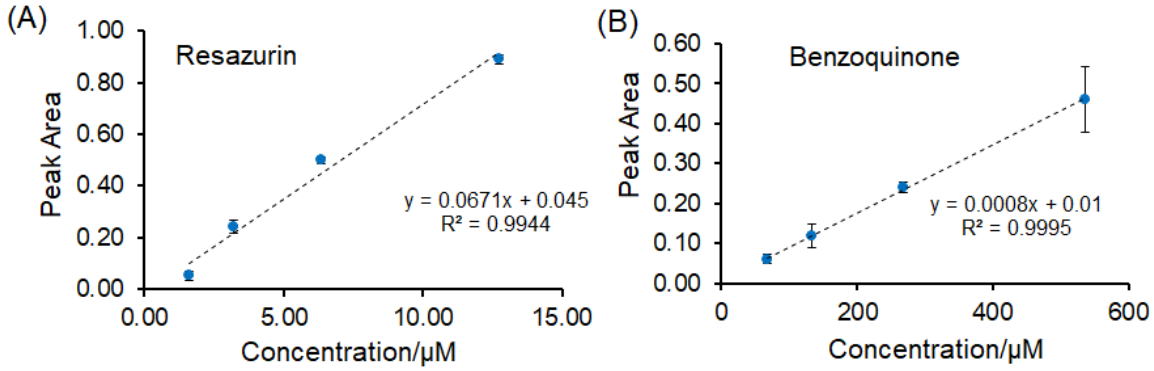

Figure 5.5 Calibration curves obtained with bipolar fluorescence detection using short separation channels (5 μm) and 10 μm PPF electrode for (A) benzoquinone and (B) resazurin

5.3.2 Use of in-channel electrode alignment to reduce the electrochemical background and its success in bipolar fluorescence-based detection

An alternative approach was investigated to overcome the high electrochemical backgrounds while still maintaining sufficient electrode area for reduction of the analytes. In this approach, the electrode was aligned in the in-channel configuration at the simple-t, which

improved separation efficiencies by reducing band broadening. Additionally, this configuration results in a lower electrochemical background. In both the end-channel and pseudo-in-channel configurations, additional surface area of the sensor working electrode is exposed to the solution that is not involved in the electrolysis of the analytes. This is due to the shape of the reservoir at the end of the channel. As shown in Figure 5.6, the analyte plug has the shape of the channel and, therefore, it only "sees" an electrode width equivalent to the channel width. Thus, the exposed electrode around the curved area of the reservoir does not contribute to analyte oxidation but does contribute to the background current. Hence, the in-channel electrode alignment provides a way to minimize the electrochemical background, while leaving enough electrode area for electrochemical analysis of analytes. This alignment allows a use of a general simple-t with 40 μm wide channels.

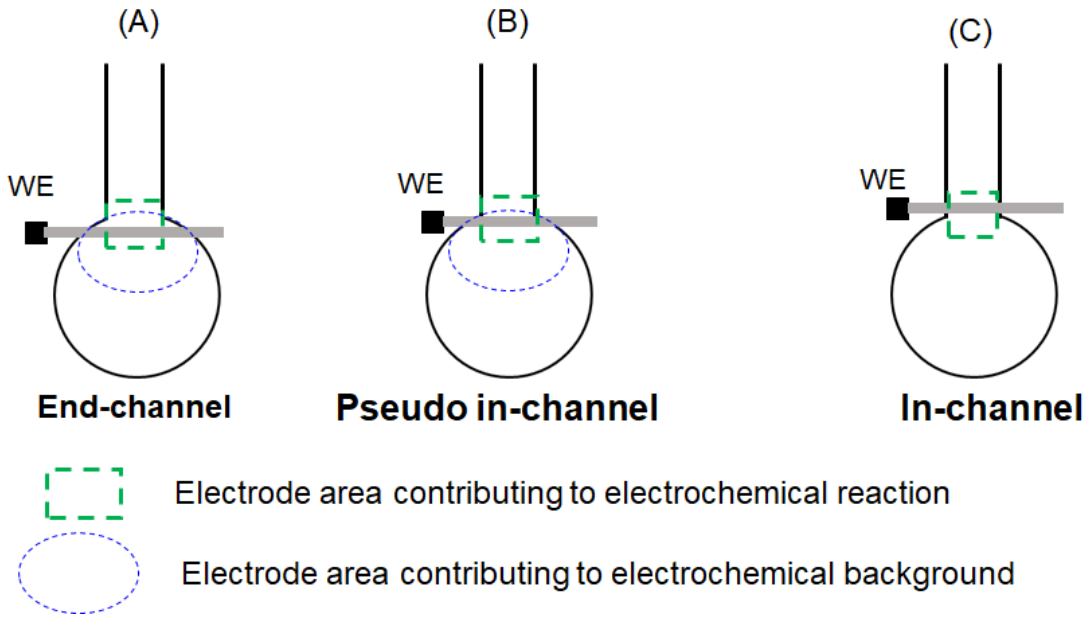

Figure 5.6 Comparison of electrode areas contributing to electrochemical background and the redox reaction of the analytes in (A) end-channel (B) pseudo-in-channel and (C) in-channel configuration

A 15 μm PPF electrode was aligned in the in-channel configuration with a 5 cm × 40 μm × 15 μm simple-t microchip and the electrode was connected using a copper wire to an Au electrode aligned in the flow "reporter" channel. A syringe pump was used to push a 10 μM solution of $DCFH_2$ prepared in MeOH/0.1 M LiCl through the channel at a flow rate of 0.1 μl min. The potential required for the bipolar experiment was optimized by determining the potential that generated the maximum response. The hydrodynamic voltammogram constructed based on the fluorescence peak areas is shown in Figure 5.7. The fluorescence response reached a maximum at a biased potential of -0.5 V vs Ag wire for both of the model compounds used in the study and decreased when the potential was shifted to more negative values.

It is important to experimentally determine the optimum potential in each experiment since it can vary from experiment to experiment due to a few reasons. As the electrode is aligned in the in-channel configuration, the apparent potential at the bipolar working electrode can vary as much as several 100 millivolts. This is not an issue if a method is developed that makes it possible to align the electrode at the exact same position relative to the channel end for each experiment. However, such a practice would be very difficult and time consuming if done manually. Solution resistance and junctional potentials can also contribute to the variation in maximum potential from experiment to experiment.

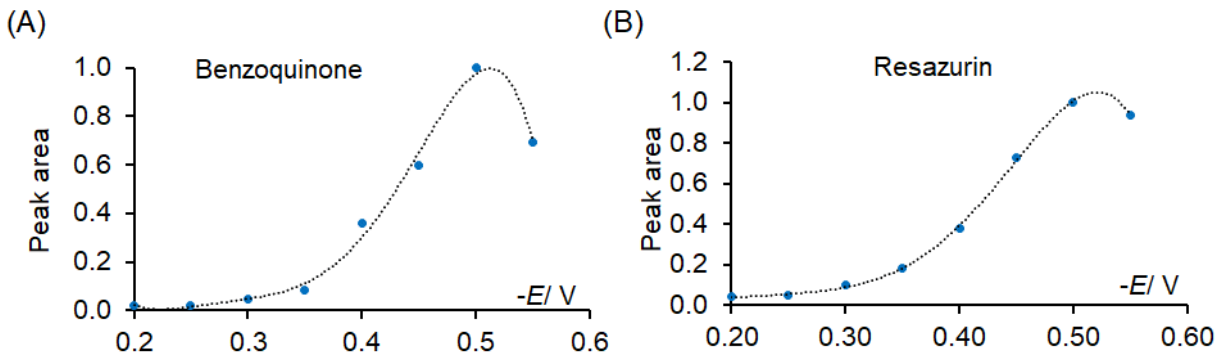

Figure 5.7 Hydrodynamic voltammograms for the bipolar detection system, where simple-t microchip (5 cm × 40 μm × 15 μm) aligned at in-channel configuration using fluorescence response (A) benzoquinone (C) resazurin

Experimental setup and resultant bipolar fluorescence and bipolar electrochemical response are shown in Figure 5.8. The peak widths were much smaller than those observed in Figure 5.4, as expected since this is in-channel configuration. Peaks widths of 2.2±0.4 s for benzoquinone and 2.3±0.3 s for resazurin were obtained for bipolar fluorescence detection. This is a factor of 2 smaller compared to pseudo-in-channel electrode alignment with this novel detection method. Peaks obtained with bipolar electrochemical detection were shorter than bipolar fluorescence detection, which can be attributed to the laser position at the electrode and adsorption of the dichlorofluorescein to the PDMS. Calibration curves showing the dependence of the bipolar fluorescence response are shown in Figure 5.9.

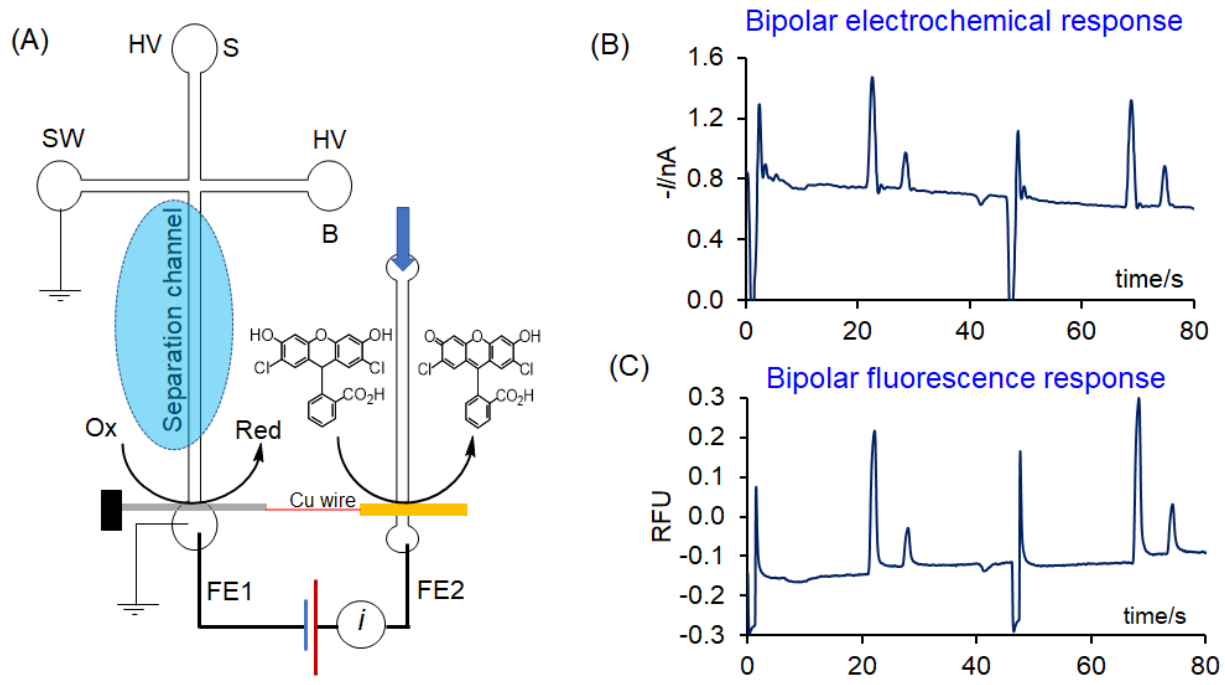

Figure 5.8 (A) Experimental setup for the bipolar electrochemically generated fluorescence detection system with in-channel electrode alignment at the separation channel (B) bipolar electrochemical response (C) bipolar fluorescence response

In this experiment, the bipolar electrochemical and fluorescence responses exhibited similar signal-to-noise ratios. This can be rationalized in two ways, either based on the flow rate or on solvent oxidation. The flow rate in the reporter channel is a critical factor in determining the analytical performance of this detection method. Therefore, optimization of the flow rate is essential. The above experiment was performed at the lowest flow rate possible with the syringe pump (0.04 μl min^{-1}). However, during these experiments, it was noticed that the methanol moved into the channel by capillary action in the first minute without any additional pumping. This provided evidence that the actual flow rate is much higher than what is programmed with the syringe pump. Additionally, since methanol can be oxidized along with the

dichlorodihydrofluorescein, changing the solvent may also need to be considered to obtain better detection limits.

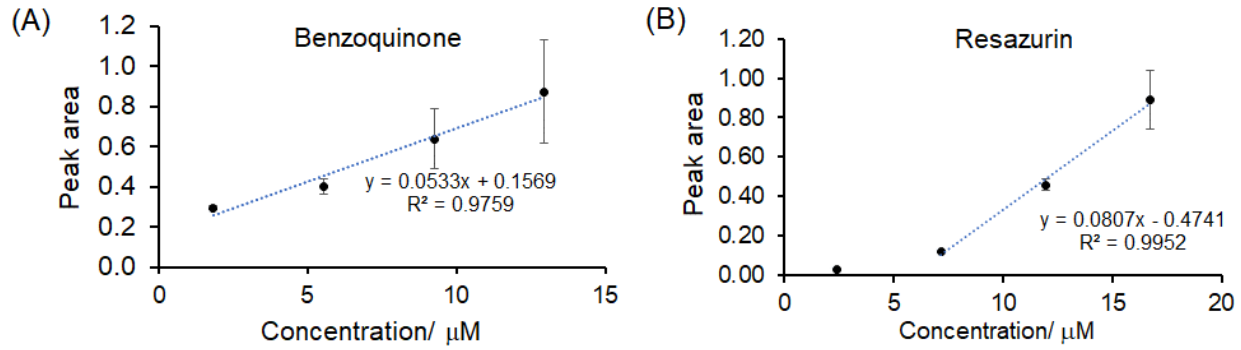

Figure 5.9 Calibration curves obtained with bipolar fluorescence detection using simple-t microchip (40 μm wide channels) and 15 μm PPF electrode for (A) benzoquinone and (B) resazurin

Therefore, it was decided to explore ethanol instead of methanol to dissolve the dye. Ethanol is more viscous and has higher oxidation potential than methanol. Another consideration regarding flow is that the tubing that was connected to the end of the flow channel can create a high back pressure that may lead to slow flow rates as shown in the Figure 5.10. Due to these considerations, the fluorescent probe was diluted in ethanol, keeping all other experimental conditions similar to previous experiments. The only other modifications were that the tube inserted at the channel end was filled with water/0.1 M LiCl and the pump was at a flow rate of 0.04 μl min. The bipolar fluorescence and electrochemical responses with this experimental setup are shown in Figure 5.10.

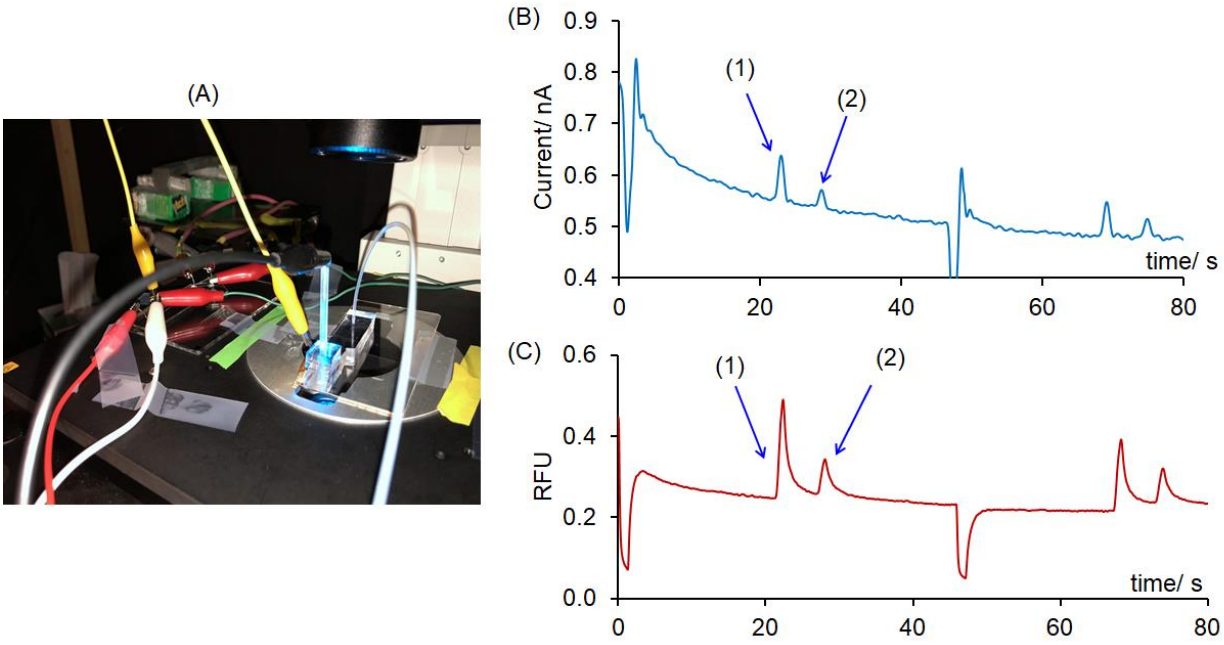

Figure 5.10 Use of a backpressure to better control the flow rate and use of ethanol instead of methanol as the solvent to dissolve fluorescent probe. (A) Experimental setup used for the bipolar electrogenerated fluorescence detection (40 μm wide separation channels and 15 μm PPF sensor electrode) of (1) benzoquinone (2) resazurin with (B) bipolar electrochemical response (C) bipolar fluorescence response

With these modifications, the bipolar fluorescence response exhibited a 4 times better S/N ratio compared to the bipolar electrochemical response. Additionally, as shown in the calibration plots below, both model analytes were detected at sub-micromolar concentrations (Figure 5.11). The peak widths were much broader for the bipolar fluorescence signal compared to the bipolar electrochemical signal. As mentioned earlier, this has to do with the position of the laser beam and the adsorption of the oxidized probe to the PDMS surface.

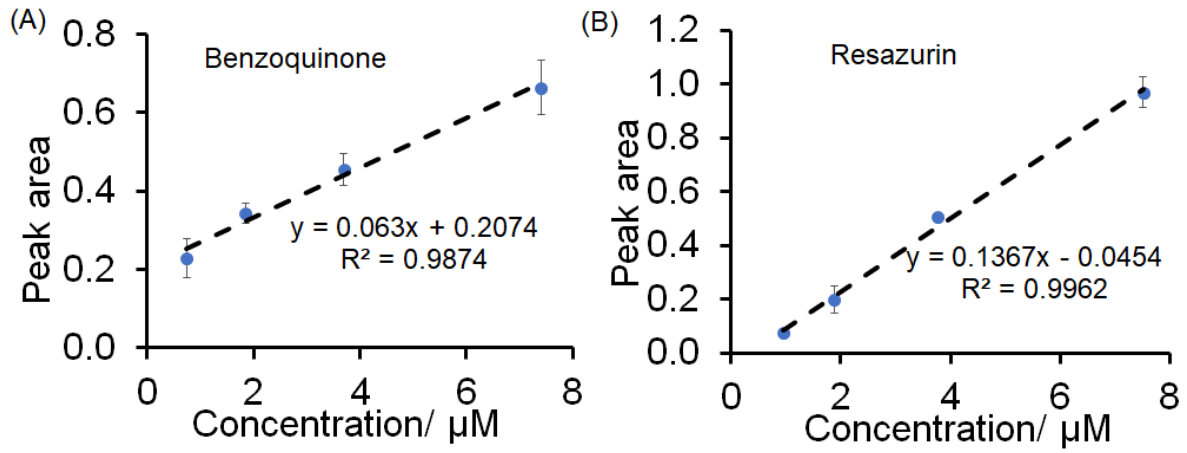

Figure 5.11 Calibration curves for (A) benzoquinone and (B) resazurin with the modified bipolar electrochemically generated fluorescence system

5.3.3 Bipolar fluorescence detection without a potentiostat

It was of interest to explore the use of an electroosmotic flow instead of hydrodynamic flow at the flow channel, as electroosmotic flow provides a plug flow profile and it can beneficial in improving the peak efficiency. Additionally, the applied voltage can be changed to control the flow rate more precisely than with the syringe pump. The major challenge of using electroosmotic flow for this study is the instability of the fluorescent probe in water. Therefore, the flow channel was first conditioned with a borate buffer of pH 10.2, 2 mM tetradecyltrimethylammonium chloride (TTAC). After that, the fluorescent probe solution was made, as in the other experiments, in methanol (10 µM $DCFH_2$ /LiCl). Voltages were applied as shown in Figure 5.12.

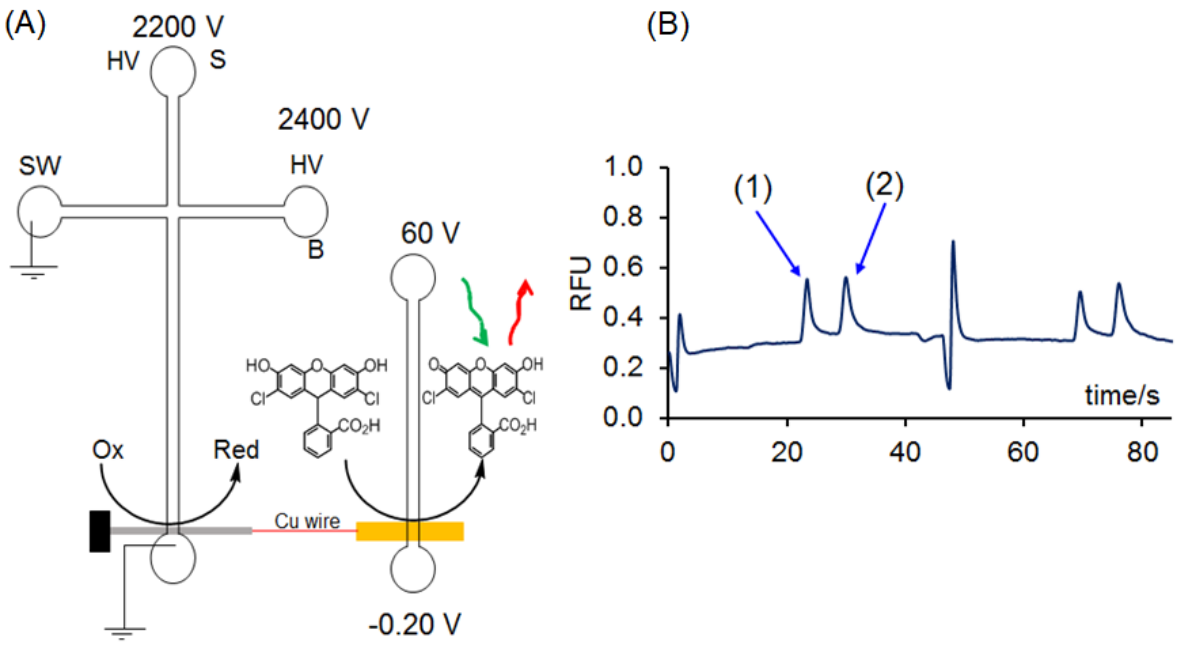

Figure 5.12 (A) The bipolar fluorescence set up for the potentiostat-free detection of (1) benzoquinone and (2) resazurin; (B) bipolar fluorescence electropherogram

In this experiment, the simple-t microchip (5 cm, 40 μm × 15 μm) was aligned on a glass substrate containing a PPF electrode (15 μm wide) at in-channel (15 μm inside the channel) configuration. Then, a flow channel was aligned on a glass containing an Au electrode (30 μm) at in-channel configuration (500 μm inside the channel) as shown in Figure 5.12A. The voltage at the sample end of the flow channel was adjusted to bias the electrode as necessary. The availability of a sufficient potential drop across the bipolar electrode to ensure the oxidation of the $DCFH_2$ at the reporter electrode and reduction of analytes at the sensor electrode based on the configuration in Figure 5.13. The potential distribution across the separation channel and the flow channel are shown in this figure. The average potential drop across the electrode is -530 mV.

Under these conditions, the electropherogram shown in Figure 5.12B was obtained. For both benzoquinone (7 μM) and resazurin (10 μM) a S/N of 100 was achieved. It was difficult to obtain a calibration curve with this set up since the buffer needed to be refreshed at the flow channel every 5 minutes from the start. This can be done 3-4 times, until the channel gets dirty with dust particles or through irreversible adsorption of the probe. However, this configuration is promising and can be developed further as the indicated issue is only relevant to this fluorescent probe. For example, resazurin is stable in an aqueous buffer and can be used to detect oxidizable analytes separated by ME.

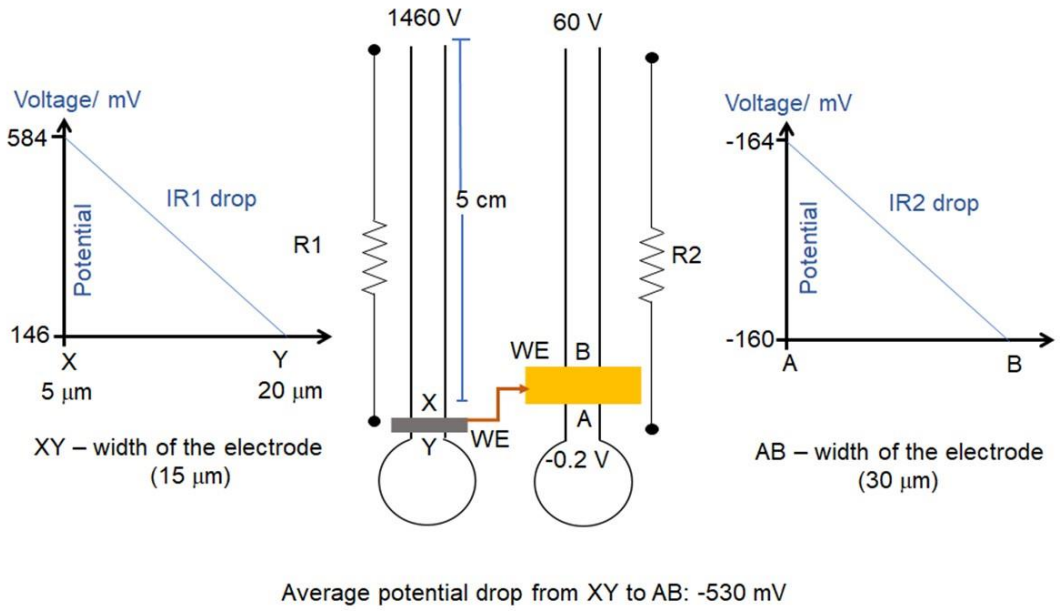

Figure 5.13 Potential distribution across the bipolar electrode

5.4 Conclusions

This chapter describes the successful demonstration of ME-EC coupled with bipolar electrochemically generated fluorescence. A better signal-to-noise ratio was obtained with the bipolar fluorescence detection compared to the bipolar electrochemical detection, except under

one set of experimental conditions. A better S/N was not obtained with the following conditions: 5 cm, 40 μm × 15 μm simple-t device aligned in-channel on a 10 μm-wide PPF sensor electrode, fluorescent probe prepared in methanol, 30 μm-wide reporter electrode, and syringe pump-induced flow. The reason that an improved bipolar fluorescence response was not achieved, compared to bipolar electrochemical response, can be explained due to the high electrochemical background in this experiment.

It has also been shown that calibration curves with high correlation coefficients can be obtained using the developed system and thus it is possible to use this as a quantitative method for ME. The influence of the separation voltage on the noise is usually high for the in-channel configuration but it is much less with the bipolar fluorescence detection. Additionally, in-channel configuration detection provided narrower peak widths and was thus most suitable for the novel detection method. In the future, the separation efficiency could be further improved using optically transparent electrodes such as ITO. However, it is very clear from these experiments that the electrochemical background and sensor channel flow rates are the major factors in determining the analytical performance of bipolar detection method. Lastly, it was shown that bipolar fluorescence detection for ME can also be performed without a potentiostat, using the separation voltage to set the working electrode potentials.

5.5 References

1. Mavre, F.; Anand, R. K.; Laws, D. R.; Chow, K.-F.; Chang, B.-Y.; Crooks, J. A.; Crooks, R. M., Bipolar Electrodes: A Useful Tool for Concentration, Separation, and Detection of Analytes in Microelectrochemical Systems. *Anal. Chem.* **2010,** *82* (21), 8766-8774.

2. Fosdick, S. E.; Knust, K. N.; Scida, K.; Crooks, R. M., Bipolar Electrochemistry. *Angew. Chem. Int. Ed.* **2013,** *52* (40), 10438-10456.

3. Anderson, R. M.; Yancey, D. F.; Zhang, L.; Chill, S. T.; Henkelman, G.; Crooks, R. M., A Theoretical and Experimental Approach for Correlating Nanoparticle Structure and Electrocatalytic Activity. *Acc. Chem. Res.* **2015,** *48* (5), 1351-1357.

4. Arora, A.; Eijkel, J. C. T.; Morf, W. E.; Manz, A., A Wireless Electrochemiluminescence Detector Applied to Direct and Indirect Detection for Electrophoresis on a Microfabricated Glass Device. *Anal. Chem.* **2001,** *73* (14), 3282-3288.

5. Zhan, W.; Alvarez, J.; Crooks, R. M., Electrochemical Sensing in Microfluidic Systems Using Electrogenerated Chemiluminescence as a Photonic Reporter of Redox Reactions. *J. Am. Chem. Soc.* **2002,** *124* (44), 13265-13270.

6. Chow, K.-F.; Mavré, F.; Crooks, R. M., Wireless Electrochemical DNA Microarray Sensor. *J. Am. Chem. Soc.* **2008,** *130* (24), 7544-7545.

7. Chow, K.-F.; Chang, B.-Y.; Zaccheo, B. A.; Mavré, F.; Crooks, R. M., A Sensing Platform Based on Electrodissolution of a Ag Bipolar Electrode. *J. Am. Chem. Soc.* **2010,** *132* (27), 9228-9229.

8. Wu, M.-S.; Xu, B.-Y.; Shi, H.-W.; Xu, J.-J.; Chen, H.-Y., Electrochemiluminescence analysis of folate receptors on cell membrane with on-chip bipolar electrode. *Lab on a Chip* **2011,** *11* (16), 2720-2724.

9. Wu, M.-S.; Qian, G.-s.; Xu, J.-J.; Chen, H.-Y., Sensitive Electrochemiluminescence Detection of c-Myc mRNA in Breast Cancer Cells on a Wireless Bipolar Electrode. *Anal. Chem.* **2012,** *84* (12), 5407-5414.

10. Wu, M.-S.; Yuan, D.-J.; Xu, J.-J.; Chen, H.-Y., Electrochemiluminescence on bipolar electrodes for visual bioanalysis. *Chemical Science* **2013,** *4* (3), 1182-1188.

11. Zhang, X.; Chen, C.; Li, J.; Zhang, L.; Wang, E., New Insight into a Microfluidic-Based Bipolar System for an Electrochemiluminescence Sensing Platform. *Anal. Chem.* **2013,** *85* (11), 5335-5339.

12. Bouffier, L.; Doneux, T.; Goudeau, B.; Kuhn, A., Imaging Redox Activity at Bipolar Electrodes by Indirect Fluorescence Modulation. *Anal. Chem.* **2014,** *86* (8), 3708-3711.

13. Zhang, X.; Li, J.; Jia, X.; Li, D.; Wang, E., Full-Featured Electrochemiluminescence Sensing Platform Based on the Multichannel Closed Bipolar System. *Anal. Chem.* **2014,** *86* (11), 5595-5599.

14. Zhang, X.; Chen, C.; Yin, J.; Han, Y.; Li, J.; Wang, E., Portable and Visual Electrochemical Sensor Based on the Bipolar Light Emitting Diode Electrode. *Anal. Chem.* **2015,** *87* (9), 4612-4616.

15. Anand, R. K.; Johnson, E. S.; Chiu, D. T., Negative Dielectrophoretic Capture and Repulsion of Single Cells at a Bipolar Electrode: The Impact of Faradaic Ion Enrichment and Depletion. *J. Am. Chem. Soc.* **2015,** *137* (2), 776-783.

16. Fosdick, S. E.; Crooks, R. M., Bipolar Electrodes for Rapid Screening of Electrocatalysts. *J. Am. Chem. Soc.* **2012,** *134* (2), 863-866.

17. Fosdick, S. E.; Berglund, S. P.; Mullins, C. B.; Crooks, R. M., Parallel Screening of Electrocatalyst Candidates Using Bipolar Electrochemistry. *Anal. Chem.* **2013,** *85* (4), 2493-2499.

18. Guerrette, J. P.; Percival, S. J.; Zhang, B., Fluorescence Coupling for Direct Imaging of Electrocatalytic Heterogeneity. *J. Am. Chem. Soc.* **2013,** *135* (2), 855-861.

19. Fosdick, S. E.; Berglund, S. P.; Mullins, C. B.; Crooks, R. M., Evaluating Electrocatalysts for the Hydrogen Evolution Reaction Using Bipolar Electrode Arrays: Bi- and Trimetallic Combinations of Co, Fe, Ni, Mo, and W. *ACS Catalysis* **2014,** *4* (5), 1332-1339.

20. Scott, D. E.; Grigsby, R. J.; Lunte, S. M., Microdialysis Sampling Coupled to Microchip Electrophoresis with Integrated Amperometric Detection on an All-Glass Substrate. *Chemphyschem* **2013,** *14* (10), 2288-2294.

21. Gunasekara, D. B.; Siegel, J. M.; Caruso, G.; Hulvey, M. K.; Lunte, S. M., Microchip electrophoresis with amperometric detection method for profiling cellular nitrosative stress markers. *Analyst* **2014,** *139* (13), 3265-3273.

22. Fischer, D. J.; Vandaveer IV, W. R.; Grigsby, R. J.; Lunte, S. M., Pyrolyzed Photoresist Carbon Electrodes for Microchip Electrophoresis with Dual-Electrode Amperometric Detection. *Electroanalysis* **2005,** *17* (13), 1153-1159.

23. Fischer, D. J.; Hulvey, M. K.; Regel, A. R.; Lunte, S. M., Amperometric detection in microchip electrophoresis devices: effect of electrode material and alignment on analytical performance. *Electrophoresis* **2009,** *30* (19), 3324-33.

24. Hulvey, M. K.; Frankenfeld, C. N.; Lunte, S. M., Separation and Detection of Peroxynitrite Using Microchip Electrophoresis with Amperometric Detection. *Anal. Chem.* **2010,** *82* (5), 1608-1611.

6. Chapter 6 COMSOL Modeling of the microchip electrophoresis bipolar electrode-based detection system

6.1 Introduction

In certain instances, it is valuable to predict the outcome of an experiment theoretically prior to the experiment, *e.g.* the heat energy from a system, the maximum current, or the optimum flow rate to operate a system. This prior knowledge supports better experimental design and the experimental data can then be compared to theoretical models to determine reliability. Gaining a theoretical understanding of an experimental system often requires solving partial differential equations. Sometimes, it is possible to solve these equations and reach an analytical equation. However, when it comes to complex systems, it is often difficult to find an exact solution to the problem and numerical modeling is a better option.

Computer modeling of experimental systems has become more popular during the last two decades due to the improvement of computer speed, random access memory (RAM) and increased storage capacity. Computer clustering with processing units of multiple cores is now available to perform complex computations within a short time. Many different programming languages including FORTRAN, Python, C, C++ and Java are available for researchers to use to develop their own code to run simulations. Also, there are several software packages available that are capable of running simulations. COMSOL Multiphysics is one such commercially available software package that features several different functionalities.

The COMSOL software package was first launched as FEMLAB in Stockholm Sweden in 1986. FEMLAB used the finite element method (FEM) to solve the physics problems of interest. After 15 years, the package was renamed COMSOL, which has been developed further through many versions, with a graphical user interface being introduced with version 4.0. The current version of the software is 5.4, which includes many modules that increase the ability of the software to couple many types of physical systems together. Additionally, the LiveLink

functionality is available to connect COMSOL with other data processing software such as MATLAB and Excel. Also, the COMSOL software package is compatible with AutoCAD drawing software to give the user an opportunity to draw complex designs and import them into the COMSOL modeling environment. Thus far, COMSOL Multiphysics has been used to perform numerical simulations in many different areas in science such as electromagnetics, structural mechanics and acoustics, fluid flow and heat transfer, and chemical engineering.

The physics of interest for the work in this thesis include electrochemistry, laminar flow, electrostatics, and transport of diluted species. Many electrochemical systems have been successfully modeled using COMSOL Multiphysics, including studies concerning voltammetry at both macro and microelectrodes, electrochemical behavior of electrode arrays,[1] positive and negative feedback curves and voltammetry in scanning electrochemical measurements,[2-3] and corrosion resistance studies. The flexibility of modeling various geometries is one of the key strengths of this software in the field of electrochemistry when compared to other software packages such as DigiElch.

COMSOL has shown success in simulating electroosmotic phenomena as well. Sample transport and electrokinetic injection in a flow cytometry device were successfully modeled using COMSOL by Kovarik *et al*.[4] In a different study, the optimization of a microfluidic fraction collection device was carried out by the Roper group.[5] Concentration enhancement of a sample in a microchannel facilitated by temperature gradient focusing was modeled by the Tang group.[6] They used COMSOL to determine the optimum electric field, solution velocity field, temperature field, and sample solute concentration field. Also, a chip design to obtain a 10,000-fold concentration increase using isotachophoresis has been developed through modeling with COMSOL Multiphysics.[7]

Our group has used COMSOL Multiphysics to model the injection plug and sample transport in a double-t microchip electrophoresis device to obtain a design that allows for a stable injection with a low separation background current.[8] Additionally, a microfluidic mixing device to carry out on-chip derivatization of amino acid neurotransmitters by NDA/CN has been modeled by Lunte's group.[9] Flow rates of the sample and reagent, channel dimensions, and applied voltages were all optimized to obtain the best mixing and reaction time resulting in better detection limits.[9] Because of all these examples of successful modeling with COMSOL within our group and in the literature, we were interested in investigating the ability of COMSOL to model the bipolar electrode-based fluorescence detection coupled to microchip electrophoresis device discussed in Chapter 4 and 5.

6.2 COMSOL Multiphysics modeling and results

The microfluidic system that was of interest is given in Figure 6.1 and is the experimental device that was described in chapter 4 and 5 of this dissertation. Briefly, a simple-t microchip (5 cm, 40 μm × 15 μm) was placed on a glass substrate that contains an electrode aligned at in- or pseudo-in-channel configuration. Additionally, another microchannel was aligned on another electrode on the same substrate and was used to flow the fluorescent probe solution (Figure 6.1). The electrode was biased in a manner to allow the reduction of the analytes separated by ME while causing the oxidization of the fluorescent probe in the flow "reporter" channel. This is quite a complicated system to be modeled and several COMSOL physical modules were necessary in combination to fully simulate the system. Therefore, the full model was separated first into several component models that were developed individually. The component models were as follows: (1) flow channel (Figure 6.1A) (2) bipolar electrode (Figure 6.1B) (3) simple-t microchip (Figure

6.1C) with electrokinetic gated injection and separation. Also, to further simplify the simulation, the effect of the electric field on the working electrode is ignored.

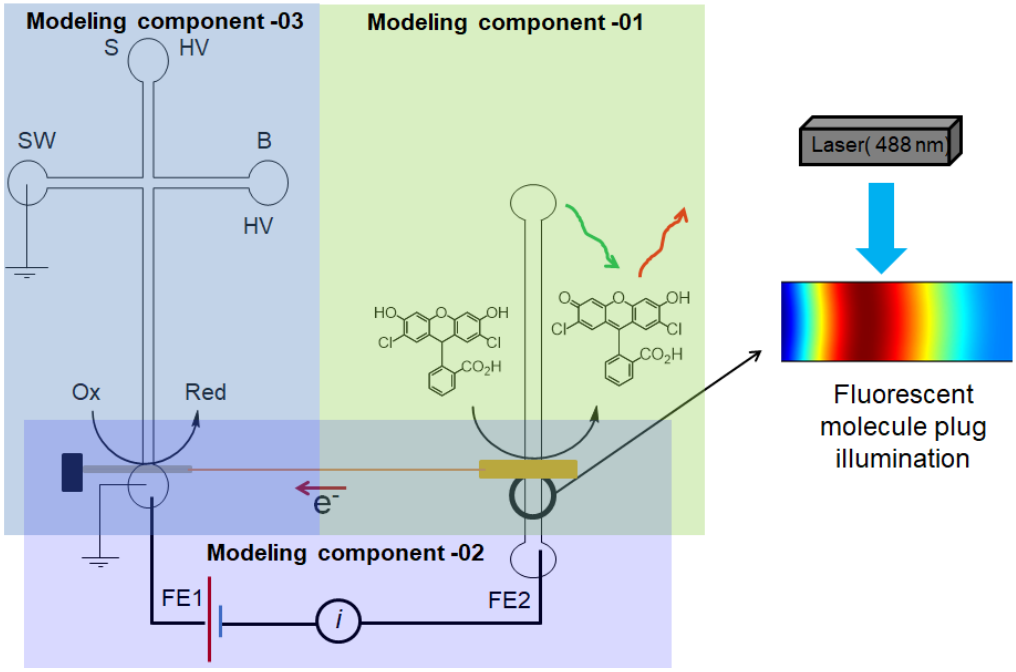

Figure 6.1. Schematic of the experimental setup to be modeled using COMSOL Multiphysics (A) Flow channel - modeling component -01 (B) Bipolar cell – modeling component – 02 (C) Simple-t separation channel – model component - 03

6.2.1 COMSOL Multiphysics modeling of the reporter flow channel

First, the flow channel containing the fluorescent probe was modeled to compute the oxidation current at various flow rates. A rectangular simulation domain representing a microchannel of 5 cm x 40 μm x 15 μm was used for this model (Figure 6.2). Both the laminar flow and the electroanalytical COMSOL modules were used for this simulation. Boundary conditions used for each module are shown in Figure 6.2.

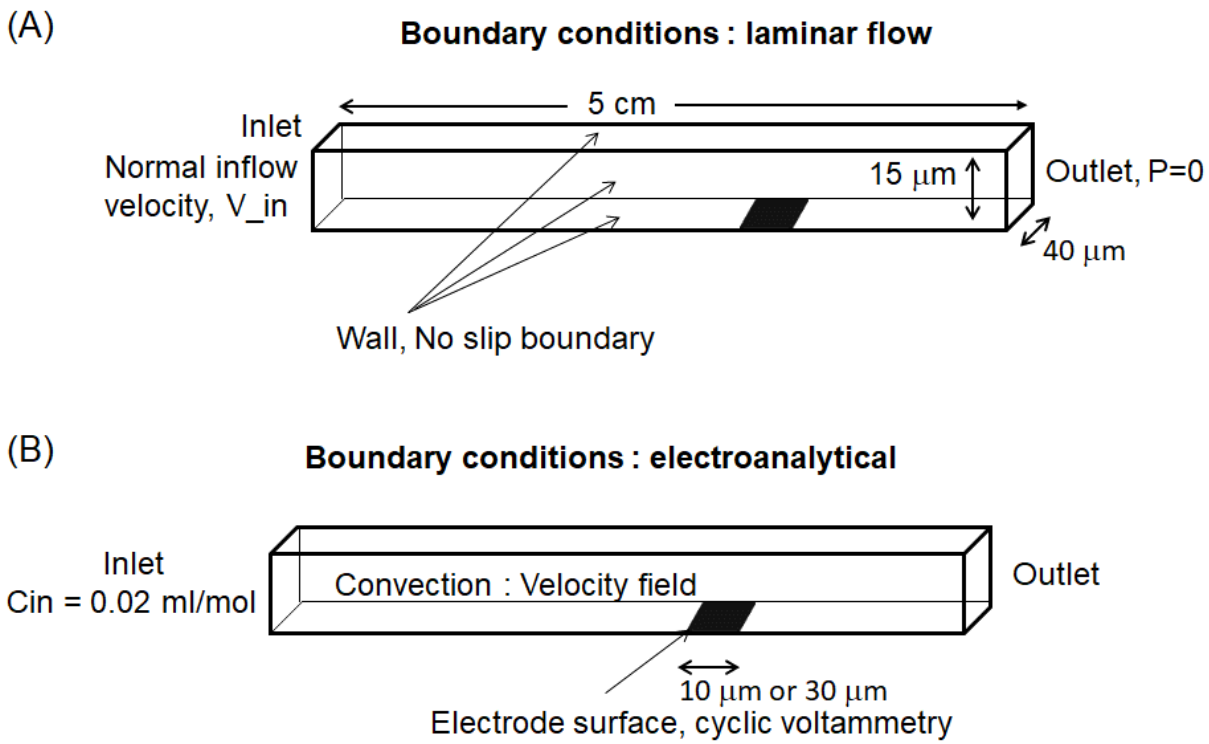

Figure 6.2. Simulation domain and boundary conditions used for the modeling of the fluorescence flow channel (A) laminar flow module (B) electroanalytical module

For the modeling, Butler-Volmer kinetics (Equations 1.1 to 1.6) were used at the electrode surface with a reversible electrochemical rate constant of 10 cm/s. A one electron electrochemical oxidation reaction was used for this study with a formal potential of 0.3 V vs Ag/AgCl. The diffusion coefficient of the species was assumed to be 1×10^{-5} cm^2/s.

$$O \underset{k_a}{\overset{k_c}{\rightleftharpoons}} R \tag{1.1}$$

$$[R] = c_R \quad [O] = c_O \tag{1.2}$$

$$\eta = E_{app} - E_{1/2} \tag{1.3}$$

$$k_a = k^o e^{(1-\alpha)\times n\times f\times \eta} \tag{1.4}$$

$$k_c = \ k^o e^{(-\alpha)\times n\times f\times \eta} \quad 1.5$$

$$\text{Exchange current density} = F(k_c \times c_O - k_a \times c_R) \quad 1.6$$

$\eta - over\,potential,\ f = \frac{F}{RT}\ ,\ \alpha - transfer\ coefficient,\ \ n - \#\ of\ electrons$
$k^0 - electrochemical\ rate\ constant\ \ F - Faraday\ constant$

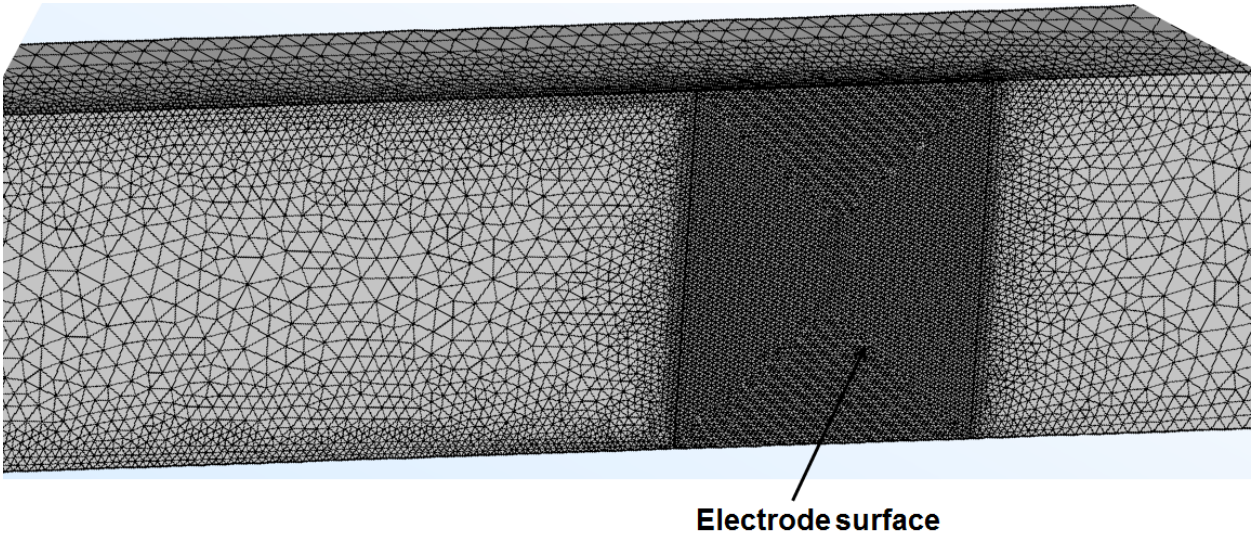

Figure 6.3. Distribution of mesh elements on and around the electrode

Meshing of the simulation domain, including the electrode surface, is important for modeling the system with high reliability. Free tetrahedral-shaped mesh elements of 1 μm were used in the entire domain and finer elements of 50 nm were used on and around the electrode surface. Fine elements were necessary in order to correctly determine the mass transport of the analyte to the electrode. Using COMSOL, a time-dependent study was conducted. The manual option was used to select time steps under the time dependent solver in order to obtain results within a short time, as the automatic option sometimes leads to unnecessarily long simulation times. An initial time step of one microsecond was used and it was set to increase gradually. A small initial time step is frequently required in these studies in order to obtain a convergent result

where a solution to the numerical problem that is closer to the exact solution at the specified error tolerance is reached. A relative tolerance of 1×10^{-7} was used to obtain smooth voltammograms without fluctuations. A direct solver known as PARDISO was used as it reduces the simulation time. However, it should be noted that these direct solvers often require a large amount of RAM.

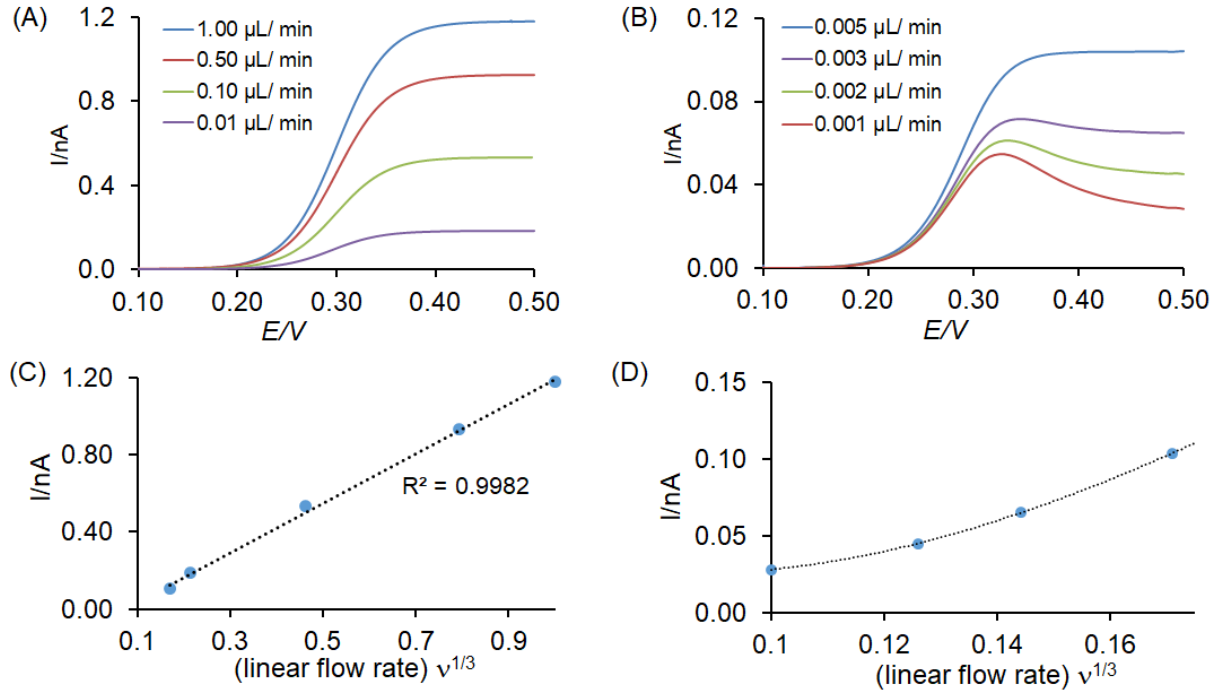

Figure 6.4 Linear sweep voltammograms at different (A) Flow rates from 0.01 µL/min to 1.00 µl/min and (B) Flow rates from 0.001 µL/min to 0.005 µL/min at a 10 µm-wide electrode placed in a 40 µm (width) × 10 µm (height) channel. Limiting currents against the cubic root of the linear flow rate (C) at flow rates ≥ 5 nl/min (D) at flow rates ≤ 5 nL/min

Linear sweep voltammograms simulated at a scan rate of 50 mV/s and at different flow rates are shown in Figure 6.4. An analyte concentration of 20 µM and a 10 µm-wide electrode was assumed for the modeling. As expected, as the flow rate is decreased, the current decreases and

deviates from steady state behavior. The mass transport to the electrode is governed by two mechanisms, diffusion and convection. The convection process is dominant at flow rates greater than or equal to 5 nL/min under these conditions, as shown in the Figure 6.4A. At lower flow rates, diffusion is the dominant process and, therefore, peak-shaped curves resulted (Figure 6.4B).

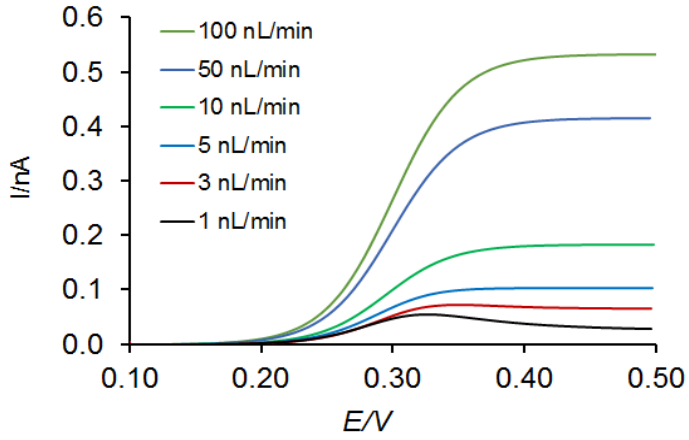

Figure 6.5. Linear sweep voltammograms at different flow rates for a 30 µm-wide electrode placed in a 40 µm (width) × 10 µm (height) channel

An analytical equation for channel electrodes is available in the literature assuming that the channel height is much higher than the channel width and that the channel width is larger than the electrode width in order to avoid edge effects and blocking the mass transport.[10] The dimensions of the channels and electrodes used in this study do not meet the indicated criteria since the electrode dimensions are 40 µm (length) × 10 µm (width) versus channel dimensions 15 µm (height) × 40 µm (width). However, the modeling results should obey the relationship between the limiting current and the flow rate given by the analytical equation in the literature.[10] Therefore, these modeling results were verified by plotting the limiting current against the cube root of the linear flow rate. A linear relation was obtained for flow rates higher than 5 nL/s and the relationship became nonlinear at flow rates below 5 nL/min, as expected. (Figure 6.4 C and D). These

simulations were also performed with a 30 µm-wide electrode size used in the experimental studies. The simulated voltammograms obtained for the 30 µm-wide electrodes are shown in Figure 6.5.

6.2.2 Development of a program to generate a voltammogram for a bipolar electrochemical cell

With these successful results, the next objective was to develop a program that could model and predict the $E_{1/2}$ of the bipolar cell based on the currents at the two ends of the bipolar electrode. The analytical equations available in the literature can only be utilized for electrochemical reactions obeying Nernstian behavior.[11] However, quasi-reversible and irreversible reactions are also encountered in our systems. Therefore, it was of interest to develop a model capable of predicting the $E_{1/2}$ of the bipolar cell and generating a linear sweep voltammogram.

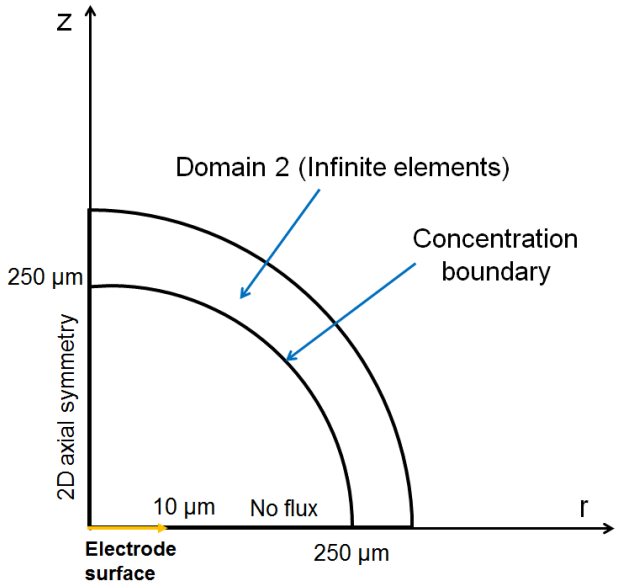

Figure 6.6 Simulation domain used to model the disk electrode response (radius 10 µm) with a total domain size of 250 µm

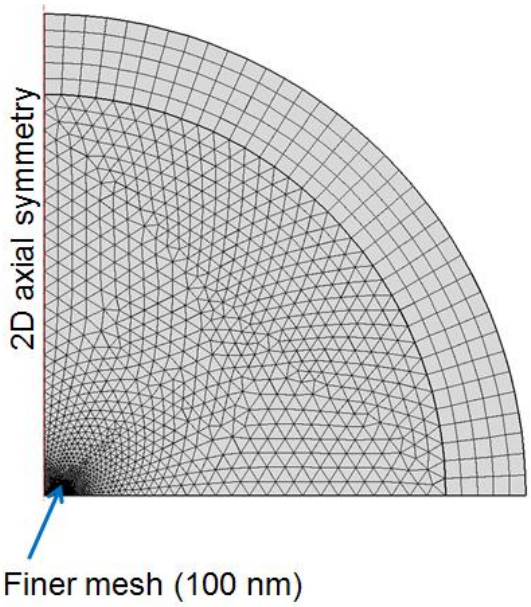

Figure 6.7 Distribution elements in the simulation domain

In this model, a disk electrode with a radius of 10 μm was modeled in the 2D axial symmetry mode of COMSOL, as shown in Figure 6.6. Domain 1 was represented by a quarter of a circle with a radius of 250 μm. A layer of "infinite elements" was used in domain 2 to correctly model the semi-infinite diffusion conditions. The electroanalytical module was used for this study with the boundary conditions as shown in Figure 6.6. Parameters used in this study are shown in Table 6.1. As indicated earlier in this chapter, a fine mesh of free triangular elements (100 nm) was used while the mesh was increased for the rest of the domain to have maximum element sizes of 10 μm (Figure 6.7). Parameters used for this modeling are given in Table 6.1.

The model builder itself is not sufficient to model the bipolar electrode, as an analysis of currents at each pole of the bipolar cell is required. A two-component system was used in this study to represent each end of the bipolar electrode and to calculate the potentials and currents separately. They were connected through coding in the application builder. This application

builder available in recent versions of the software is very flexible as it facilitates coding with loops and conditional statements. Also, variables can be defined as necessary to store and display data to use within the program.

Parameter	Value	Explanation
E_appl_1	-0.4[V]	Applied potential_01
Ef_01	-0.2[V]	Formal potential_01
c_bulk_1	1[mmol/L]	Reactant concentration
re	10[um]	Electrode radius
r_max	25*re	Size of simulation space
D1	1e-9[m^2/s]	Reactant diffusion coefficient
D2	1e-9[m^2/s]	Product diffusion coefficient
k01	1[m/s]	rate constant -01
E_start	-0.4[V]	Start potential
E_vertex	0.4[V]	Vertex potential
E_step	10[mV]	Potential step (output)
E_appl_2	0.4[V]	Applied potential _02
Ef_02	0.2[V]	Formal potential_02
c_bulk_2	10[mmol/l]	bulk concentration
k02	1[m/s]	rate constant -02

Table 6.1 Parameters used for the modeling of a bipolar cell voltammogram

The criteria to generate the bipolar electrochemical cell voltammogram is that the current at each potential should be equal to the smallest current of the two ends. In the developed method, the limiting currents at each half-cell were determined first to identify the half-cell that has the lower limiting current (limiting pole). The half-cell with the higher limiting current is known as the excess pole. The comparison was made for absolute values of currents as the current values at the two ends of the bipolar electrode are opposite in sign. After that, a potential (E_1) needed to be selected where the system produced nearly 0 A current, in actuality a few pA of current (I_x), at the limiting pole of the half-cell as shown in Figure 6.8A.

The potential (E_x) at which the same current I_x (within 1%) is produced by the excess pole then needed to be determined. For this, the full potential range ($E_{initial}$ to E_{final}) of the excess pole

was divided into two sections (Figure 6.8B). The current was then calculated at each potential ($E_{initial}$, E_{final}, and E_{middle}) to obtain $I_{initial}$, I_{final}, and I_{middle}. Then, the numerical value of the current I_x was compared to the numerical values of $I_{initial}$, I_{final}, and I_{middle} to find the region containing E_x. This is accomplished by using a conditional statement to consider the region containing E_x again in the next loop and eliminate the other region. For example, if E_x is between $E_{initial}$ and E_{middle}, the potential region of E_{middle} to E_{final} is eliminated. In the next loop, this retained potential region is again divided into two and the comparison is performed again to find which region contains E_x. This process is repeated in a loop for a total of 15 times (with 2^{15} divisions, as this is a binomial elimination) to obtain E_x with an error less than 2%. This full procedure is then repeated with the potential range at the limiting pole, *i.e.* E_1 to E_2. Coding for this process is given in Appendix 2.

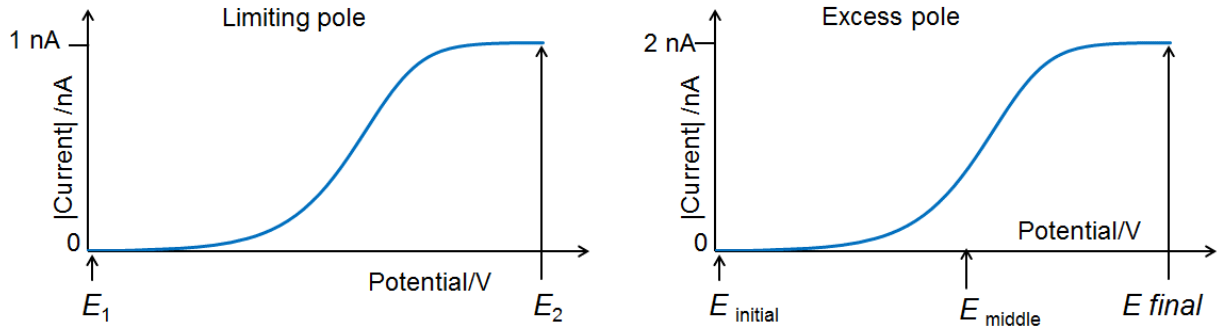

Figure 6.8 Hypothetical voltammograms for the (A) limiting pole and the (B) excess pole used in explaining the program written for the bipolar cell voltammogram

The bipolar voltammogram was obtained by assuming two half-cells with the same electrode size but different redox concentrations. A formal potential of 0.2 V was assumed for the half-cell where oxidation occurs while a potential of -0.2 V was assumed for the half-cell where reduction occurs (Table 6.1). A reversible rate constant (10 cm/s) was used at each half-cell to

verify the results against the equations given in the literature.[11] Bipolar cell voltammograms were generated for different concentrations at the excess pole, as shown in Figure 6.9. The $E_{1/2}$ values were compared to the values calculated using equations in the literature[11] and it was observed that they only differ by less than 2%. If a greater accuracy is required, the number of cycles used to find the bipolar potential can be increased. The developed program can be applied to electrodes of any shape and dimensions by changing only the model geometry used to represent the electrode of interest. Also, the same program can produce bipolar voltammograms for quasi-reversible and irreversible reactions.

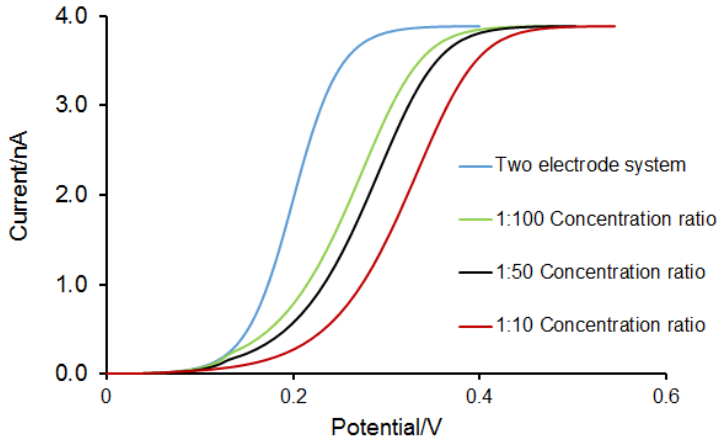

Figure 6.9 Comparison of two-electrode cell and bipolar cell voltammograms generated using the developed program

6.2.3 Modeling simple-t microchip to simulate gated injection and separation

The next step was to model the sample injection and separation in a simple-t microchip. This was carried out in 2D mode (Figure 6.10) as the computation times are less compared to those in 3D mode. The laminar flow module and Nernst-Planck module were used for this study. Under the laminar flow module, electroosmotic velocity was selected as the boundary condition for all

the inner walls of all the domains that represent the simple-t microchip. The electroosmotic velocity is calculated by the software according to the field strength defined by the user. The electric field in the x axis is defined as -dtang (V,x) and in the y axis it is defined as -dtang (V,y). Then, the electroosmotic mobility is calculated by the software. As inputs, -50 V was used as the zeta potential and 80 was used as the relative permittivity. A pressure of 0 was used at the inlets and outlets, as shown in Figure 6.10A.

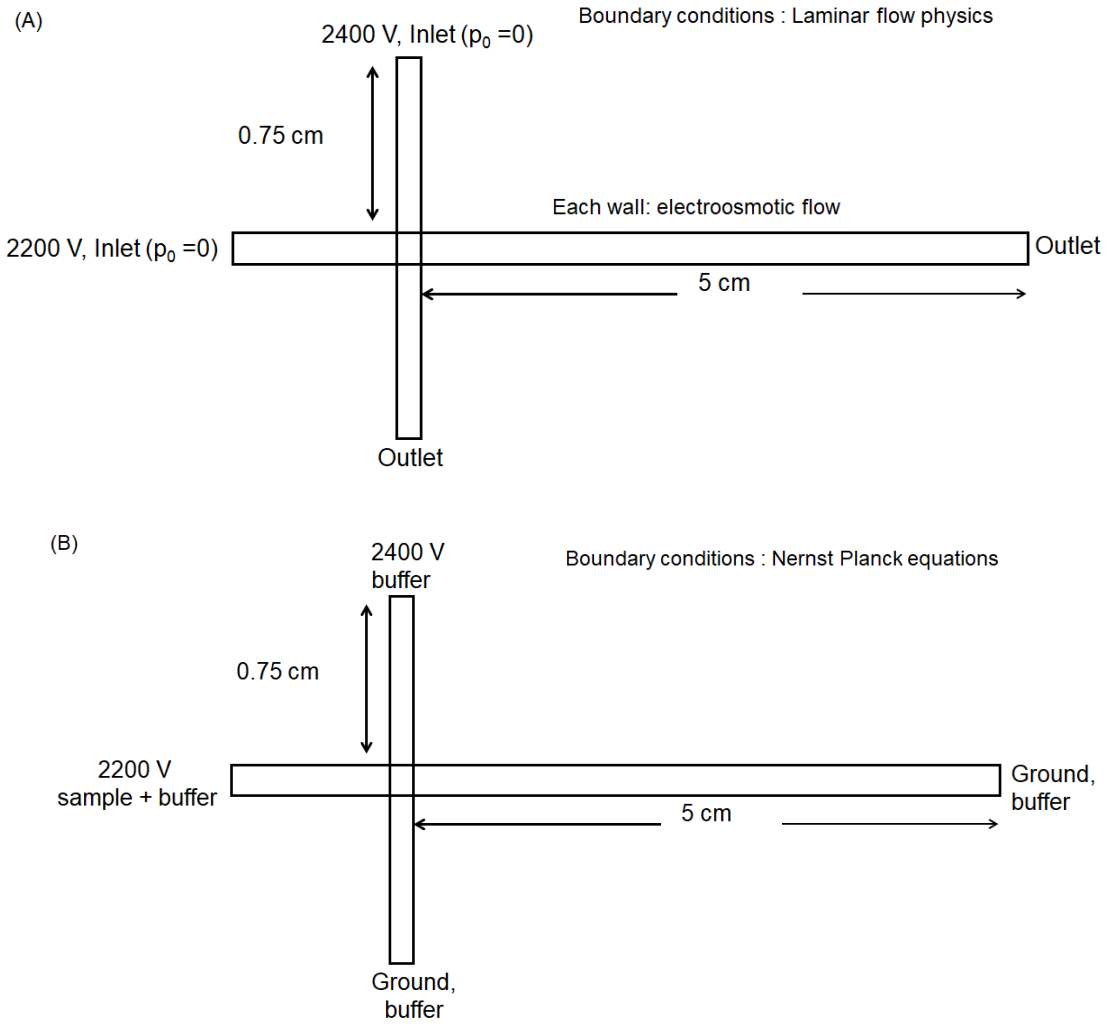

Figure 6.10 (A) Boundary conditions under laminar flow physics (B) boundary conditions under Nernst-Planck equations

The Nernst-Planck equations module was used to define the transport of species through the channel by convection, diffusion and migration. Convection is defined by the velocity field created by the electroosmotic flow under the laminar flow module. Variables defining the buffer and analytes species are shown in Table 2A and B. NaAcT (10 mM) was used as the buffer. Two species were defined as Sp1 and Sp2 with concentrations of 10 μM and 20 μM, respectively. Charges of species and diffusion coefficients were used as inputs and the electrophoretic mobilities were calculated within the program as shown in Table 2A. These diffusion coefficients and electrophoretic mobilities defined the diffusion and migration transport in the channel. It was considered that the channel walls are electrically insulated. Buffer, sample, potential and ground were included as boundary conditions at the channel ends as shown in Figure 6.10B.

(A)

Species	Values and definitions
DNa	1.332e-9[m^2/s]
DCl	2.034e-9[m^2/s]
DAc	1.089e-9[m^2/s]
pKaAc	4.76
pKw	14
pH	4.5
H3O	10^(-4.5)[mol/liter]
KaAc	10^(-pKaAc)[mol/liter]
zNa	1
zCl	-1
zAcm	-1
zAc0	0
zAcT	zAc0*H3O/(H3O+KaAc)+zAcm*KaAc/(H3O+KaAc)
uNa	DNa/T0/R_const
uCl	DCl/T0/R_const
uAcT	DAc/T0/R_const

(B)

Species	Values and definitions
DSp1	1e-9[m^2/s]
DSp2	1e-9[m^2/s]
uSp1	1.0e-4[cm^2/V/s]/zPr1/F_const
uSp2	0.2e-4[cm^2/V/s]/zPr2/F_const
zPr1	1
zPr2	4
Current	intop1(Pr1x+Pr2x)

Table 6.2 Values and variable definitions used to define the (A) buffer and (B) species

The sample injection was achieved using a rectangle function as shown in Figure 6.11. This is a time-dependent problem. In this study, the first 9 seconds were allowed for built-in solvers in COMSOL to find a stable converging result. This allowed a stable gate to be reached before the buffer voltage was brought to zero using the rectangle function to initiate the 1 s injection. This

function can take values of 1 or 0. The function has a value of 1 during the first 9 s and takes a value of 0 during the injection time to set the buffer voltage to 0 V and allow the injection. At 10 s, the value of the function returns to 1 and the buffer voltage returns to 2400 V and thus reestablishes the gate. Smoothing can be used at the initiation of the injection and at the end of the injection to get a close step function. However, very low values of smoothing relative to the difference of upper limit and lower limit may result in termination of the computations as it is difficult to define a step function that is taking 0-time steps between the lower limit and upper limit. A plot of buffer voltage during the simulation is shown in Figure 6.11B.

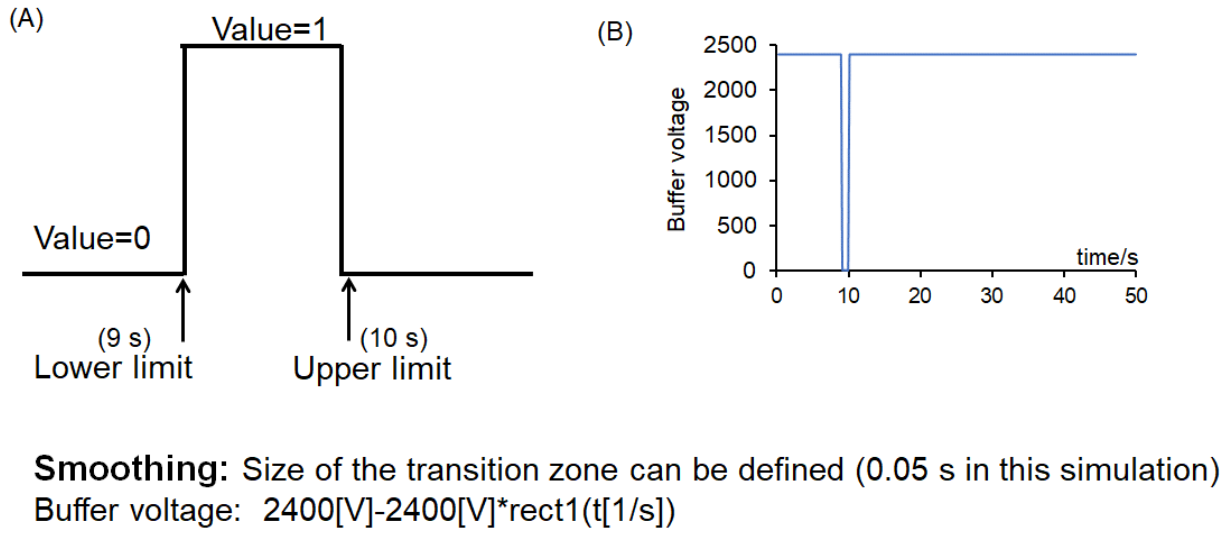

Figure 6.11 (A) Diagram showing the use of the rectangle function to bring the buffer voltage to 0 during the injection and set to 2400 V during the rest of the simulation time (B) buffer voltage before, during and after gated injection

A fine mesh was used for the injection cross-section to correctly define the injection plug. A minimum mesh size of 100 nm and maximum element size of 1 μm was used in the cross-section and edges of the cross section were meshed further by applying an edge mesh distribution. A

maximum element size of 8 μm and minimum element size of 100 nm were used for the rest of the domain. The distribution of mesh elements is shown in Figure 6.12.

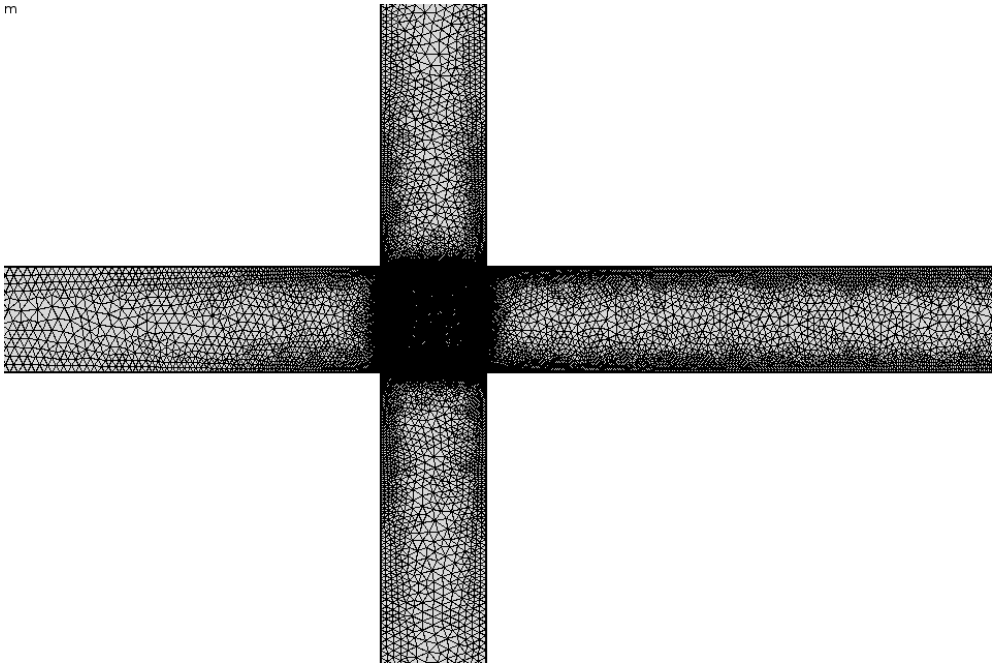

Figure 6.12 Distribution of mesh elements in the cross section

This is a time-dependent study and a relative tolerance of 0.001 was used. A maximum time step of 0.1 s was defined while the software automatically determined the minimum time step. The minimum time step should be sufficiently small to define the injection time which is 1 s in this study, otherwise the rectangular function may not be considered by the solvers resulting in an injection failure. The injection of the sample and the separation were successfully modeled as shown in Figure 6.13.

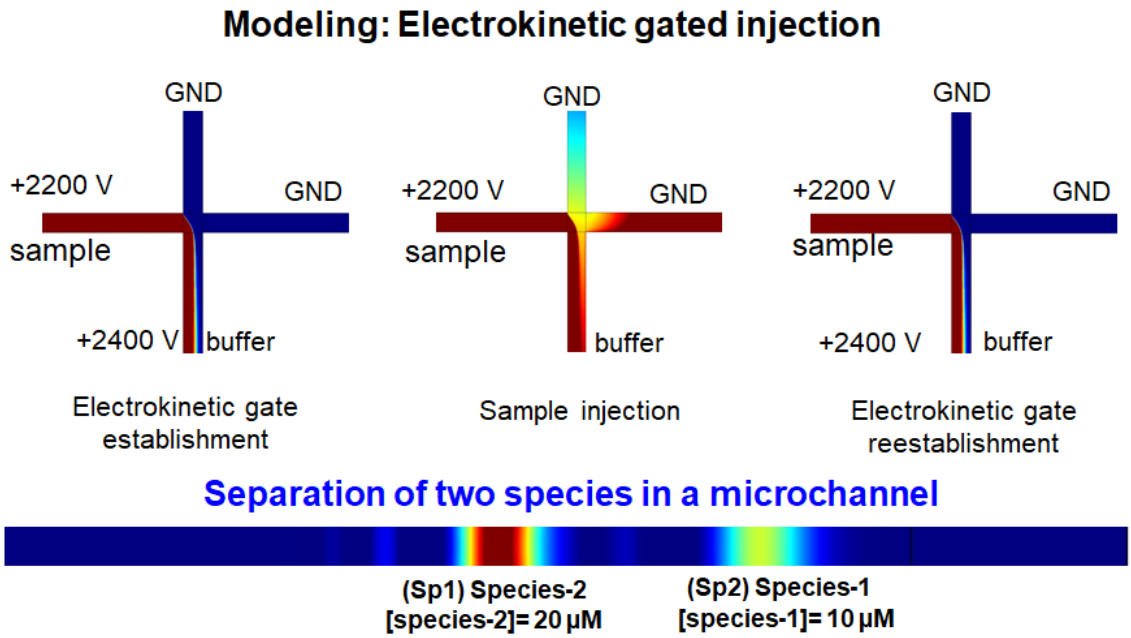

Figure 6.13 Modeling of gated injection and separation of species

This study was further extended to couple the flow channel to this simulation and thus model the full experimental system. An electrode was defined inside the separation channel by a line as shown in Figure 6.13. The flow channel was implemented using a rectangle and a vertical line was used to represent the electrode in the flow channel. Both electrodes were kept in-channel and the effect of placing them in-channel was not considered. This implementation cannot be used to calculate the exact current produced by an experiment as the channel height and electrode sizes cannot be accounted for in this 2D model. However, it is sufficient to find the concentration gradient at the electrode (Table 2, intop1(Pr1x+Pr2x)) and that can be transformed to the second channel to show the effect of the flow. The effect of the flow rate was successfully modeled as shown in Figure 6.14.

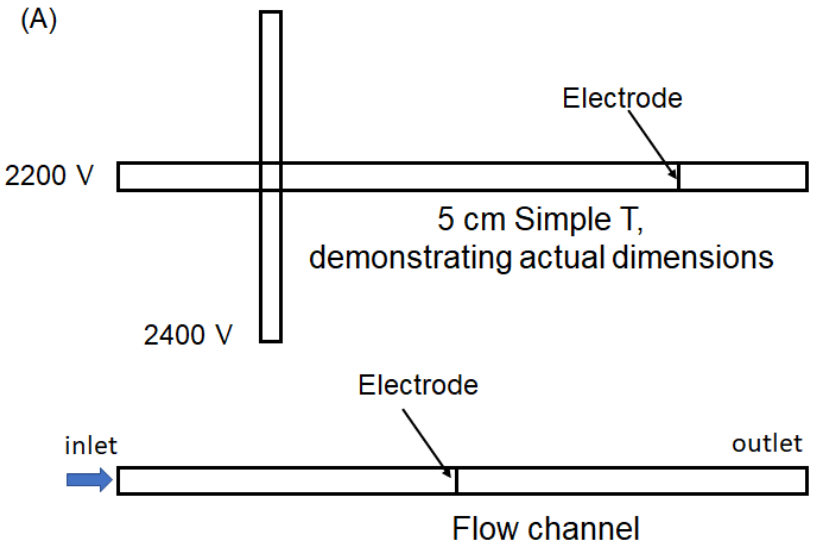

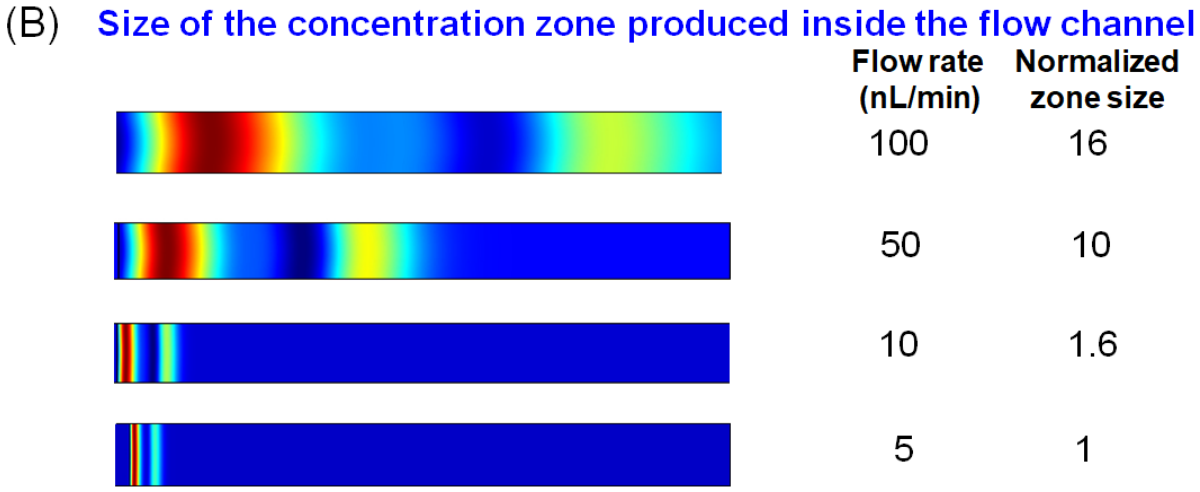

Figure 6.14. Modeling domain representing full experimental setup

6.3 Conclusions

At low flow rates, the zone is more stacked. It is clear from these simulations that the flow rate must be as low as 10 nL/min to avoid spreading of the concentration zone and thus to get the best detection limits. This is in agreement with the fact that the current density should be high to achieve low detection limits. It was observed that the two zones overlap at 1 nL/min.

Linear sweep voltammograms for electrodes in-channel were successfully simulated using COMSOL Multiphysics and they were verified using the limiting current versus flow rate relationship. Also, a program has been developed to generate a bipolar cell voltammogram. Additionally, the injection and separation of species in a simple-t microchannel was modeled successfully. Lastly, the size of the concentration zone produced at the bipolar electrode in the flow channel was simulated successfully.

6.4 References

1. Zoski, C. G.; Wijesinghe, M., Electrochemistry at Ultramicroelectrode Arrays and Nanoelectrode Ensembles of Macro- and Ultramicroelectrode Dimensions. *Isr. J. Chem.* **2010,** *50* (3), 347-359.

2. Ekanayake, C. B.; Wijesinghe, M. B.; Zoski, C. G., Determination of Heterogeneous Electron Transfer and Homogeneous Comproportionation Rate Constants of Tetracyanoquinodimethane Using Scanning Electrochemical Microscopy. *Anal. Chem.* **2013,** *85* (8), 4022-4029.

3. Fernández, J. L.; Wijesinghe, M.; Zoski, C. G., Theory and Experiments for Voltammetric and SECM Investigations and Application to ORR Electrocatalysis at Nanoelectrode Ensembles of Ultramicroelectrode Dimensions. *Anal. Chem.* **2015,** *87* (2), 1066-1074.

4. Kovarik, M. L.; Lai, H. H.; Xiong, J. C.; Allbritton, N. L., Sample transport and electrokinetic injection in a microchip device for chemical cytometry. *Electrophoresis* **2011,** *32* (22), 3180-7.

5. Baker, C. A.; Roper, M. G., A continuous-flow, microfluidic fraction collection device. *J. Chromatogr. A* **2010,** *1217* (28), 4743-8.

6. Ge, Z.; Yang, C.; Tang, G., Concentration enhancement of sample solutes in a sudden expansion microchannel with Joule heating. *Int. J. Heat Mass Transfer* **2010,** *53* (13), 2722-2731.

7. Bottenus, D.; Jubery, T. Z.; Dutta, P.; Ivory, C. F., 10 000-fold concentration increase in proteins in a cascade microchip using anionic ITP by a 3-D numerical simulation with experimental results. *Electrophoresis* **2011,** *32* (5), 550-562.

8. Regel, A. PhD thesis, University of Kansas, 2013.

9. Oborny, N. J. PhD thesis, University of kansas, 2017.

10. Cooper, J. A.; Compton, R. G., Channel Electrodes — A Review. *Electroanalysis* **1998,** *10* (3), 141-155.

11. Cox, J. T.; Guerrette, J. P.; Zhang, B., Steady-state voltammetry of a microelectrode in a closed bipolar cell. *Anal. Chem.* **2012,** *84* (20), 8797-804.

7. Chapter 7 Summary and future directions

7.1 Summary and future directions

In Chapter 1, fundamentals and strategies of amperometric detection are discussed in detail. Different sample injection techniques along with various chip designs are discussed. Also, the typical instrumentation used for microchip electrophoresis with amperometric detection and typical signal-to-noise ratios are also described. Some selected analytical applications of microchip electrophoresis with electrochemical detection (ME-EC) are also described. Electrode configurations and multiple electrode systems that can be used to extend the applications of ME-EC are also mentioned.

The second chapter is dedicated to the development of a dual-channel/dual-parallel electrode microchip configuration to obtain voltammetric information of separated analytes and identify the electroactive species. It was also demonstrated that the developed method can be applied to identify short-lived species, as the detection of the sample at two different potentials is achieved at the same time. Also, the data obtained using this strategy does not need to be corrected as is required for the dual-series electrode configuration. However, the detection limits achieved with this approach were in the micromolar range.

Microchip electrophoresis coupled to fluorescence detection for the detection of superoxide, nitric oxide and total ROS production is described in Chapter 3. The separation capability of ME was successfully used to detect superoxide and nitric oxide, using DAF-FM and MitoSOX, respectively, in a single analysis. Also, the effect of engineered carbon nanoparticles on the production of ROS in microglial cells and lung epithelial cells is shown. All these studies required the addition of fluorescent probe as the detected small molecules were nonfluorescent.

With the successful results obtained with electrochemical detection and fluorescence detection, we were then motivated to explore a new detection method that can preserve the

advantages of both electrochemical and fluorescence detection while limiting their disadvantages. Therefore, the primary goal of this thesis was to develop a novel detection method capable of providing better detection limits for analytes separated by ME. This goal was achieved using a bipolar electrode with fluorescence reporting. An oxidation and a reduction reaction can be made to occur simultaneously on a bipolar electrode by selecting appropriate redox analytes and by applying a suitable bias voltage.

Two modes of bipolar electrode-based fluorescence detection for electroactive species separated by ME were identified, one mode for oxidizable species and the other for reducible species. The reductive mode was selected for this study based on the availability of the non-fluorescent dye dichlorodihydrofluorescein ($DCFH_2$). This molecule is essentially non-fluorescent until oxidation, when a quantum yield of 0.97 is obtained. A simple-t PDMS microchip was aligned on a glass substrate containing a pyrolyzed photoresist film electrode (PPF). A pseudo-in-channel electrode configuration was used for the electrode alignment. A PDMS straight channel was also aligned on the same substrate as that of the simple-t. This straight channel was used to flow the fluorescent probe using hydrodynamic flow. Initially, a vacuum pump was used to generate the hydrodynamic flow. The newly developed method was demonstrated using two model analytes, benzoquinone and resazurin. In this experiment, these two analytes were separated by ME and reduced on the electrode. The current produced due to the reduction of the analytes in the ME-EC separation is used simultaneously at the electrode sitting inside the reporter channel to oxidize the fluorescent probe.

The major challenge of the initial system to achieve better detection limits was the high electrochemical background at the electrophoresis channel. This challenge was addressed by using small channels (5 μm) and small electrodes (10 μm) to decrease the electrochemical background.

Also, a syringe pump (instead of a vacuum) was used to provide a smoother flow. Additionally, the flow channel was aligned on an Au electrode, as these electrodes are more durable than PPF for the irreversible bonding of PDMS with the glass electrode substrate. Bipolar fluorescence of this modified system showed a better signal-to-noise ratio by a factor of 2.5 compared to the bipolar electrochemical response. Calibration curves were successfully generated showing the capability of the method to quantify the analytes. However, the detection limits with this configuration were in the high micromolar range. This was due to the decrease of the electrode response simultaneously with the background current.

An alternative strategy was then utilized to address the electrochemical background issue. The in-channel electrode configuration was used instead of the pseudo-in-channel configuration. The pseudo-in-channel configuration produces higher electrochemical background than the in-channel configuration owing to the exposure of a larger electrode area to the solution. This is mostly not due to a theoretical but experimental reason. Generally, an additional length of the electrode is partially exposed to the solution in the pseudo-in-channel configuration. In addition, ethanol was used instead of methanol to avoid the loss of signal due to the oxidation of solvent instead of the fluorescent probe. A significant amount of solvent oxidation current, combined with analyte oxidation, can decrease the sensitivity of the system. Additionally, a back pressure was applied using a tubing filled with an aqueous background electrolyte to minimize the flow rate as much as possible. This system generated a calibration curve with R^2 values of better than 0.98. With this experimental configuration, detection limits less than 1 μM were obtained.

It is clear that the flow rate plays an important role in the bipolar fluorescence-based detection system. Therefore, it was of interest to study this system using COMSOL Multiphysics to determine the size of the concentration zone that is being produced at the reporter electrode. As

the simulation of the full experimental model is complicated, and can end up with wrong implications, the model was first divided into sections and then modeled. Through this modeling procedure, linear sweep voltammograms were obtained at different flow rates and were verified by plotting the limiting current against the flow rates$^{1/3}$. Also, a program was developed to generate bipolar voltammograms, and the results of the program was verified using $E_{1/2}$ values compared to the analytical equation. This program can be used to generate bipolar cell voltammograms for cells composed of different shapes and sizes of electrodes. In addition, the effect of different electrochemical rate constants can also be studied using this system.

7.2 Future directions

7.2.1 Immediate future goals

7.2.1.1. Applications and further developments of the bipolar detection in the reductive mode

The very first objective should be to evaluate a transparent electrode at the reporter side of the bipolar electrode, *e.g.* an indium tin oxide electrode (ITO). ITO electrodes have been used with microchip electrophoresis with amperometric detection.[1-3] There are also many other reports that use ITO electrodes for electrochemical studies. The use of an ITO electrode will allow the detection of fluorescence on the electrode surface and therefore will help eliminate the peak broadening observed due to the fluorescence detection at the side of the electrode. Narrow peaks will improve separation efficiencies, resolution, and detection limits.

This new method can be applied to the sensitive detection of nitrophenols and nitroaromatic explosives. However, these compounds will require high negative potentials and high electrochemical background may still be a challenge due to oxygen reduction and water reduction taking place at potentials beyond -0.4 V and -0.8 V, respectively. One possible solution would be to use of a deoxygenation system suitable for this analysis. Common degassing procedures to

remove dissolved oxygen before use in a microchip are not effective as the oxygen can dissolves again through the PDMS. Therefore, a 3D printed container that can hold the microchip and Pt leads needs to be developed. The entire container can then be degassed and kept under nitrogen flow. This fabrication should not be difficult with a 3D printer as a design can be drawn with necessary flexibility to hold the microchip and printed.

Alternatively, a solution of a secondary species can be added to the flow channel to increase the available current at the reporting pole. Such a species must totally oxidize at a potential less than that of the onset potential of the fluorescent probe ($DCFH_2$). Sodium borohydride is such a species that shows a steady state plateau at a potential of 0.1 V Ag/AgCl, giving an 8-electron oxidation on a Au electrode.[4] A two-channel system can be used if the oxidation of the fluorescent probe is hindered by the sodium borohydride. The development of this strategy is very important as a similar method can be used for the detection of oxidizable analytes. If this strategy works, the next improvement in the detection limits can be achieved. It was reported[5] that the detector electrode needs to be smaller than the sensor electrode to obtain an optimal electrochemiluminescence signal using a bipolar electrode. Therefore, a smaller electrode can be used as the detector electrode in the bipolar fluorescence detection system developed for ME in Chapter 4 of this dissertation to obtain improved detection limits by increasing the current density.

7.2.1.2 Development of a bipolar electrogenerated chemiluminescence detector

One of the immediate and interesting objectives of this work is to use electrogenerated chemiluminescence instead of fluorescence as the reporting signal. Electrogenerated chemiluminescence has the advantage that it has a negligible and low background compared to fluorescence. This is because the necessary species to excite the luminophore are generated

electrochemically at the electrode. The most common luminophore or the model compound that has been used is the $Ru(bpy)_3^{2+}$with Tri-n-propyl amine (TRA) as the co-reactant. The electrooxidation of TRA and subsequent loss of a hydrogen atom produces a TRA radical that can react with electrooxidized product of $Ru(bpy)_3^{2+}$ to populate the excited state of $Ru(bpy)_3^{3+}$ and produce electrogenerated chemiluminescence.[5]

The coupling of electrogenerated chemiluminescence in the bipolar electrode format is well described, including detailed reviews and book chapters.[5-7] The effect of the size of the electrode on the chemiluminescence signal is also described.[5,8] The bipolar electrogenerated chemiluminescence detection can be integrated to the microchip format in a similar way to fluorescence bipolar detection (Figure 7.1) There is a great potential to obtain better LODs with electrochemiluminescence coupling with microchip format using a bipolar electrode. Initially this system can be used to detect reducible species owing to the availability of many systems to produce electrogenerated chemiluminescence through electrooxidation. Later, the study can be extended to detect oxidizable species separated by ME.

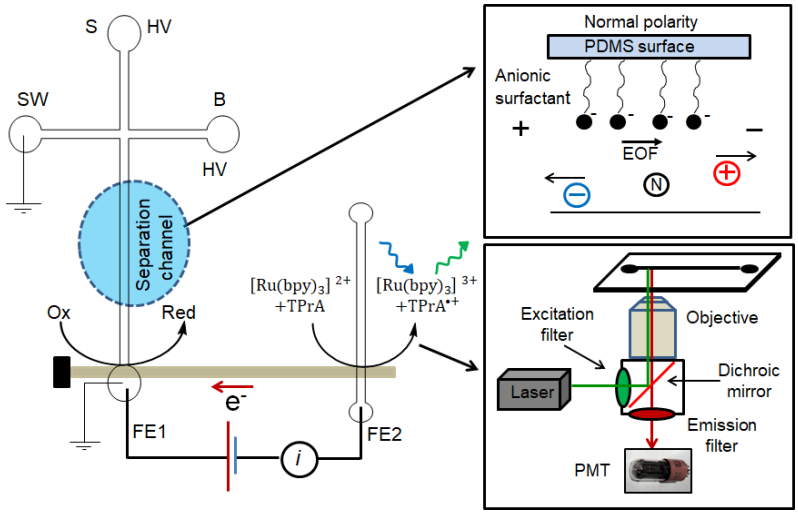

Figure 7.1 Integration of bipolar electrode based electrochemiluminescence detection with microchip electrophoresis

7.3 Long-term goals

7.3.1 Development of the bipolar electrode-based detection in the oxidative mode

The developed bipolar detection method can easily be adopted to detect oxidizable species. The only necessary change is the use of a reducible fluorescent probe. Resorufin is one of the fluorescent probes that can be used for this study as it is converted from a weakly fluorescent molecule (quantum efficiency 0.11) to a highly fluorescent molecule (quantum efficiency 0.42) upon oxidation. This compound has been used extensively in spectro-electrochemical studies, including bipolar reporting and fluorescence-enabled electrochemical imaging. This compound has an absorption maximum at 575 nm and an emission maximum at 585 nm.[9]

The bipolar fluorescence reporter experimental system that can detect oxidizable molecules is shown in Figure 7.2. This system could be used to detect pro-oxidants and antioxidants of interest. The development of the method can be initiated by using a hydrodynamic flow at the flow channel and then can be extended to perform the bipolar fluorescence detection using potentiostat free detection. Resorufin is fairly stable in buffer medium. Therefore, potentiostat-free detection can be performed using a 5 cm-long flow channel.

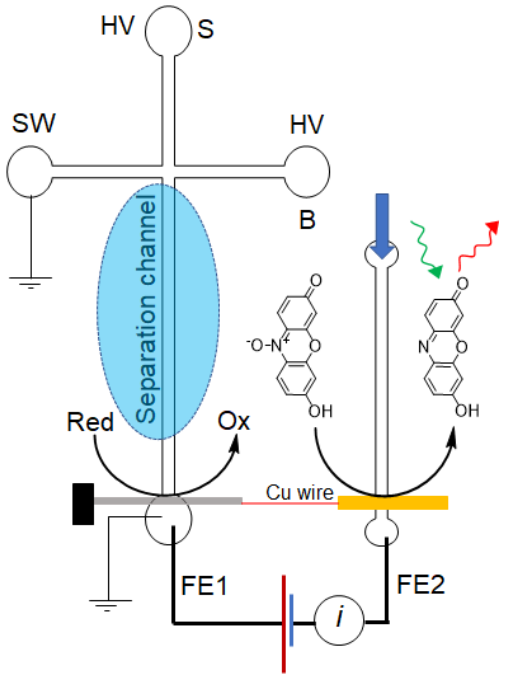

Figure 7.2 Experimental set up to perform bipolar electrode-based fluorescence detection for electrochemically oxidizable molecules

Resazurin is a reversible redox molecule and, therefore, a dual-series electrode configuration may be used to enhance the available current at the reporter end of the bipolar electrode through redox cycling. This may also improve the detection limits. This strategy may be difficult to use in the potentiostat-free mode, as the generator electrode needs to be biased at a positive potential and the collector electrode needs to negatively biased. However, this can be performed with a hydrodynamic flow and with a bipotentiostat.

Once these developments are completed, both native and stimulated cell lysates can be analyzed to quantify the pro-oxidants and antioxidants present. Also, this bipolar detection strategy can be integrated with a single cell analysis system to quantify the pro-oxidants and antioxidants present in a single cell after it is lysed using the electric field. The single cell analysis will provide cellular heterogeneity information and, therefore, be advantageous over the bulk cell analysis.

7.4 References

1. Wang, W.; Xu, X.; Bin, Q.; Ling, J.; Chen, G., A new method for fabrication of an integrated indium tin oxide electrode on electrophoresis microchips with amperometric detection and its application for determination of synephrine and hesperidin in pericarpium citri reticulatae. *Electrophoresis* **2006,** *27* (21), 4174-4181.

2. Wu, M.-S.; Liu, Z.; Shi, H.-W.; Chen, H.-Y.; Xu, J.-J., Visual Electrochemiluminescence Detection of Cancer Biomarkers on a Closed Bipolar Electrode Array Chip. *Anal. Chem.* **2015,** *87* (1), 530-537.

3. Zhang, J.-D.; Yu, T.; Li, J.-Y.; Xu, J.-J.; Chen, H.-Y., An ITO bipolar array for electrochemiluminescence imaging of H2O2. *Electrochem. Commun.* **2014,** *49*, 75-78.

4. Mirkin, M. V.; Yang, H.; Bard, A. J., Borohydride Oxidation at a Gold Electrode. *J. Electrochem. Soc.* **1992,** *139* (8), 2212-2217.

5. Oja, S. M.; Zhang, B., Electrogenerated Chemiluminescence Reporting on Closed Bipolar Microelectrodes and the Influence of Electrode Size. *ChemElectroChem* **2016,** *3* (3), 457-464.

6. Bouffier, L.; Arbault, S.; Kuhn, A.; Sojic, N., Generation of electrochemiluminescence at bipolar electrodes: concepts and applications. *Anal. Bioanal. Chem.* **2016,** *408* (25), 7003-11.

7. Fosdick, S. E.; Knust, K. N.; Scida, K.; Crooks, R. M., Bipolar Electrochemistry. *Angew. Chem. Int. Ed.* **2013,** *52* (40), 10438-10456.

8. Sojic, N.; Arbault, S.; Bouffier, L.; Kuhn, A., Applications of Electrogenerated Chemiluminescence in Analytical Chemistry. In *Luminescence in Electrochemistry: Applications in Analytical Chemistry, Physics and Biology*, Miomandre, F.; Audebert, P., Eds. Springer International Publishing: Cham, 2017; pp 257-291.

9. Oja, S. M.; Guerrette, J. P.; David, M. R.; Zhang, B., Fluorescence-Enabled Electrochemical Microscopy with Dihydroresorufin as a Fluorogenic Indicator. *Anal. Chem.* **2014,** *86* (12), 6040-6048.

Appendix-01 Applications of microchip electrophoresis coupled to amperometric detection

1.1 Environmental Applications

The portability of ME-EC allows for on-site testing, which has proven beneficial for environmental applications. ME-EC based devices have been employed for the determination of analytes such as explosives, chemical warfare agents, and pesticides, in addition to many other compounds.

The need for sensitive, fast, portable and field-executable (fields such as airport security and custom and border regions) analytical devices capable of detecting explosives has increased dramatically during last two decades. Toward this end, the Wang group developed an ME-EC system with an external glassy carbon electrode for the separation and detection of nitrite ester explosives. This class of chemicals is often used in homemade explosives, and the ME-EC device was capable of analyzing a mixture of four nitrite ester explosives in under 3 minutes (Figure 1.12).[1] Additionally, Himi and Luong developed an ME-EC device capable of separating and detecting several different nitroaromatic explosives (including TNT). These researchers employed ME-EC with an external detection cell with a gold working electrode.[2-3]

The detection of chemical warfare agents has also been accomplished with ME-EC. The ability to quickly detect warfare agents, such as nerve gases, would give soldiers and first responders information about the environment allowing, them to make more informed decisions regarding response. V-type nerve agents produce stable thiol degradation products that have been analyzed by ME-EC using screen-printed carbon electrodes.[4] ME-EC devices have also been developed to perform analyses in remote locations using lab-on-a-robot applications.[5]

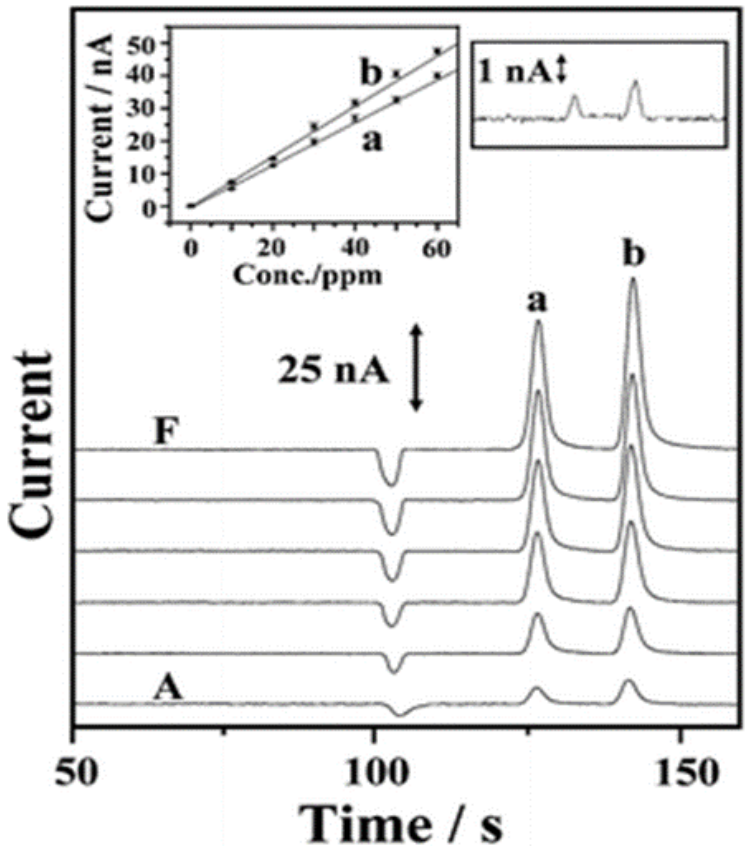

Figure 1.1 ME–EC analysis of nitrate explosives: (a) propylene glycol dinitrate and (b) glyceryl trinitrate. (Reproduced from ref. 1.)

1.2 Food Applications

ME-EC provides an interesting possibility for quality control in the food industry as the devices are portable and could be used to monitor food throughout the journey from farm to the store shelf. Additionally, the small sample size and reagent volume requirements make this technique attractive. Food analysis by microchip electrophoresis has been reviewed previously.[6] ME-EC has been employed for the detection of heavy metals in vegetable juices,[7] nitrite in meats,[8] biogenic amines in beers,[9] and mycotoxin and zearalenone in infant foods,[10] among other applications.

Qualitative and quantitative analysis of antioxidants is a major application of ME-EC. Both natural and synthetic supplements containing antioxidants have been given significant attention recently. ME-EC has been successfully used for quantification of natural antioxidants, phenolic acids and flavonoids (*e.g*., catechin, rutin, and quercetin, and chlorogenic, ferulic, caffeic, protocatechuic, vanillic, and gallic acids) in foods. This technique could also be used to obtain a "class-selective electrochemical index" for the purpose of determining the major antioxidant classes (*e.g.*, flavonoids and phenolic acids) in a food product in a short time period.[11]

A comprehensive survey on applications of microchip electrophoresis coupled with amperometric detection is provided in Table 1.1. This table provides the type of the sample/standard, electrode material, electrode alignment, and LOD.

Table 1.1. Applications of ME-EC

1.3 Biological Applications

Compound	Sample/ Standards	Electrode	Electrode alignment	LOD	Notes/ comments	Ref
Catecholamine neurotransmitters (dopamine , norepinephrine, and catechol)	Standards	Pyrolyzed photoresist film carbon /carbon fiber/carbon ink/Pd	End-channel/ In-channel/ Off-channel	35 nM dopamine-end channel, pyrolyzed photoresist film carbon electrode	Different electrode materials and alignments	12
RNOS and antioxidants (nitrite glutathione, ascorbic acid, and tyrosine)	Standards	Pt film	In-channel	2.6 μM nitrite	Wireless isolated potentiostat	13 and 14
Peroxynitrite	Standards	Pd film	End-channel	2.4 μM Peroxynitrite	First use of ME-EC to detect peroxynitrite	15

Biochemicals/Pharmaceuticals (uric acid and interfering compounds (ascorbic acid, paracetamol, epinephrine, xanthine and theophyline)	Urine samples	Pt film	End-channel	4 μM epinephrine 10 μM uric acid	Micrux portable electrophoresis instrument	16
Vitamins (pyridoxine, ascorbic acid, and folic acid)	Four different pharmaceuticals (Vitafardi, Aspol, Becozyme C Forte, and Hidrosil)	Modified glassy carbon and screen printed electrodes (SCE) with multiwalled carbon nano tubes	End-channel	8 μM pyridoxine 11 μM ascorbic acid 8 μM folic acid with modified SCE	Carbon nano tubes	13
Catechol estrogen-derived DNA adducts (8-Hydroxy-deoxyguanosine (8-OH-dG), 4-OHE2-1-N3Ade, 4-OHE2-1-N7Gua, and 4-OHE2-NacCys)	Standards	Au micro-electrode array (Pd –decoupler)	Off-channel	0.4 μM	PDMS-glass hybrid microchip	14
L-tryptophan metabolites (5-hydroxy-L-tryptophan, 5-hydroxytryptamine and 5-hydroxy-indole-3-acetic acid)	Standards	Pt wire	End-channel	0.84 μM 5-hydroxy-L-tryptophan 0.67 μM 5-hydroxytryptamine 4.2 μM 5-hydroxy-indole-3-acetic acid	Filmy channel microchip	15
Cholesterol	Bovine serum	Au wire	End-channel	1 nM	Enzymatic assay	16
Underivatized carbohydrates ,amino acids, and sulfur-containing antibiotics (fructose, sucrose, lactose, maltose, cysteine, histidine, ampicillin, glucose and penicillin)	Standards	Au wire	End-channel	100 μM cysteine 350 μM histidine 5 μM ampicillin 5 μM penicillin	Pulsed-amperometric detection	17

Mixture of thiols (homocysteine, cysteine glutathione and N-acetylcysteine)	Standards	Palladium/mercury amalgam electrode	Off-channel (Pd decoupler)	9.2 μM	First report of the usage of Pd/Hg for thiols	18
Amino acids (arginine, proline, histidine, valine, and serine)	Standards	Cu wire	End channel	7 μM arginine 6 μM proline 5μM histidine 6 μM valine 6 μM serine	Detection of non electroactive amino acids	19

Environmental Applications

Compound	Sample/ Standards	Electrode	Electrode alignment	LOD	Notes/ comments	Ref
Explosives (ethylene glycol dinitrate, pentaerythritol tetranitrate, propylene glycol, and dinitrate glyceryl trinitrate)	Standards	Glassy carbon	End-channel	0.3 ppm glyceryl trinitrate 0.5 ppm propylene glycol dinitrate	On site explosive analysis	1
Chemical warfare agents (2(dimethylamino) ethanethiol (DMAET), 2-(di-ethylamino)ethanethiol (DEAET), and 2-mercaptoethanol (ME))	Untreated tap and river water samples	Carbon ink	End – channel	5 μM 2-(dimethylamino) ethanethiol 8 μM 2-(di-ethylamino)ethanethiol	Off chip/ on chip derivatization of nerve agents with o-phthaldialdehyde	4
Pollutants (p-aminophenol, o-aminophenol and m-aminophenol)	Standards	Au film	In - channel	14.6 nM p-aminophenol 10.6 nM o-aminophenol 15.3 nM m-aminophenol	Dual channel microchip for noise reduction	20
Anions (chloride, bromide, iodide and thiocyanide)	Standards	Silver film	End-channel	1.23 μM chloride 1.56 μM bromide 0.56 μM iodide 2.03 μM thiocyanide	PDMS/glass hybrid microchip	21

Food Applications

Application	Sample/ Standards	Electrode	Electrode alignment	LOD	Notes/ comments	Ref.
Heavy metals (lead, cadmium and copper)	Standards	Screen-printed carbon	End-channel	1.74 μM Pb^{2+} 0.73 μM Cd^{2+} 0.13 μM Cu^{2+}	First report of heavy metal analysis ME-EC	7
Phenol compounds (tyrosol, hydroxytyrosol and oleuropein Glucoside)	Olive oil	Au wire	End - channel	15 μM tyrosol 36 μM hydroxytyrosol 17 μM oleuropein glucoside	Novel method to quantify phenolics in olive oil	22
Biogenic amines (ethanolamine, tryptamine and tryptophane)	Standards	Ruthenium oxide/hexacyanoruthenate polymeric film modified glassy carbon	End - channel	23 μM ethanolamine 27 μM tryptamine 34 mM tryptophan	Electrocatalytic oxidation ability by a inorganic complex	9
Mycotoxin (zearalenone)	Powdered baby food, cereal milkshakes	Glassy carbon electrode	End - channel	0.4 μgL^{-1} zearalenone	electro-kinetic magnetic bead based immune assay on a Microchip	10
Nitrite	Ham and sausage samples	Copper (3-mercaptopropyl)trimethoxysilane [Cu(II)-MPS] com-plex-modified carbon paste electrode	End - channel	0.35 ppm nitrite	Modified electrode	8
Plant phenols (catechin, rutin, and quercetin, and chlorogenic, ferulic, caffeic, protocatechuic, vanillic, and gallic acids)	Apples, pears, red and white wines, and green tea	Glassy carbon	End-channel	≤6 μM Class selective approach <8 μM Individual antioxidant detection	class selective and individual analysis	11
Monossacharides (glucose and fructose)	Honey samples	Copper nanowires	End - channel	4 μM glucose 23 μM fructose	Usage of nano-materials	23

1.4 References

1. Piccin, E.; Dossi, N.; Cagan, A.; Carrilho, E.; Wang, J., Rapid and sensitive measurements of nitrate ester explosives using microchip electrophoresis with electrochemical detection. *Analyst* **2009,** *134*, 528-532.

2. Hilmi, A.; Luong, J. H. T., Electrochemical detectors prepared by electroless deposition for microfabricated electrophoresis chips. *Anal. Chem.* **2000**, 4677-4682.

3. Hilmi, A.; Luong, J. H. T., Micromachined Electrophoresis Chips with Electrochemical Detectors for Analysis of Explosive Compounds in Soil and Groundwater. *Environ. Sci. Technol.* **2000,** *34*, 3046-3050.

4. Wang, J.; Zima, J.; Lawrence, N. S.; Chatrathi, M. P.; Mulchandani, A.; Collins, G. E., Microchip Capillary Electrophoresis with Electrochemical Detection of Thiol-Containing Degradation Products of V-Type Nerve Agents. *Anal. Chem.* **2004,** *76*, 4721-4726.

5. Felhofer, J. L.; Blanes, L.; Garcia, C. D., Recent developments in instrumentation for capillary electrophoresis and microchip-capillary electrophoresis. *Electrophoresis* **2010,** *31* (15), 2469-2486.

6. Martin, A.; Vilela, D.; Escarpa, A., Food analysis on microchip electrophoresis: An updated review. *Electrophoresis* **2012,** *33*, 2212-2227.

7. Chailapakul, O.; Korsrisakul, S.; Siangproh, W.; Grudpan, K., Fast and simultaneous detection of heavy metals using a simple and reliable microchip-electrochemistry route: An alternative approach to food analysis. *Talanta* **2008,** *74*, 683-689.

8. Shiddiky, M. J. A.; Lee, K.-S.; Son, J.; Park, D.-S.; Shim, Y.-B., Development of Extraction and Analytical Methods of Nitrite Ion from Food Samples: Microchip Electrophoresis with a Modified Electrode. *J. Agric. Food Chem.* **2009,** *57*, 4051-4057.

9. Dossi, N.; Toniolo, R.; Pizzariello, A.; Susmel, S.; Bontempelli, G., A modified electrode for the electrochemical detection of biogenic amines and their amino acid precursors separated by microchip capillary electrophoresis. *Electrophoresis* **2011,** *32*, 906-912.

10. Hervas, M.; Lopez, M. A.; Escarpa, A., Integrated electrokinetic magnetic bead-based electrochemical immunoassay on microfluidic chips for reliable control of permitted levels of zearalenone in infant foods. *Analyst* **2011**, 2131-2138.

11. Kovachev, N.; Canals, A.; Escarpa, A., Fast and Selective Microfluidic Chips for Electrochemical Antioxidant Sensing in Complex Samples. *Anal. Chem.* **2010,** *82* (7), 2925-2931.

12. Fischer, D. J.; Hulvey, M. K.; Regel, A. R.; Lunte, S. M., Amperometric detection in microchip electrophoresis devices: Effect of electrode material and alignment on analytical performance. *Electrophoresis* **2009,** *30* (19), 3324-3333.

13. Gunasekara, D. B.; Hulvey, M. K.; Lunte, S. M., In-channel amperometric detection for microchip electrophoresis using a wireless isolated potentiostat. *Electrophoresis* **2011,** *32* (8), 832-837.

14. Gunasekara, D. B.; Siegel, J. M.; Caruso, G.; Hulvey, M. K.; Lunte, S. M., Microchip electrophoresis with amperometric detection method for profiling cellular nitrosative stress markers. *Analyst* **2014,** *139* (13), 3265-3273.

15. Hulvey, M. K.; Frankenfeld, C. N.; Lunte, S. M., Separation and Detection of Peroxynitrite Using Microchip Electrophoresis with Amperometric Detection. *Anal. Chem.* **2010,** *82* (5), 1608-1611.

16. Fernandez-la-Villa, A.; Bertrand-Serrador, V.; Pozo-Ayuso, D. F.; Castano-Alvarez, M., Fast and reliable urine analysis using a portable platform based on microfluidic electrophoresis chips with electrochemical detection. *Anal. Methods* **2013,** *5* (6), 1494-1501.

17. García, C. D.; Henry, C. S., Direct determination of carbohydrates, amino acids, and antibiotics by microchip electrophoresis with pulsed amperometric detection. *Anal. Chem.* **2003,** *75* (18), 4778-4783.

18. Antwi, C.; Johnson, A. S.; Selimovic, A.; Martin, R. S., Use of microchip electrophoresis and a palladium/mercury amalgam electrode for the separation and detection of thiols. *Anal. Methods* **2011,** *3*, 1072-1078.

19. Liang, R.; Wang, L.; Meng, X.; Wang, J.; Qiu, J., Enhanced electrophoresis separation of non-electroactive amino acids on poly(dimethylsiloxane) microchip coupled with direct electrochemical detection on a copper electrode. *Microfluid. Nanofluid.* **2011,** *11* (2), 227-233.

20. Chen, C.; Hahn, J., Enhanced aminophenols monitoring using in-channel amperometric detection with dual-channel microchip capillary electrophoresis. *Environ. Chem. Lett.* **2011,** *9* (4), 491-497.

21. Yan, J.; Yang, X.; Wang, E., Electrochemical Detection of Anions on an Electrophoresis Microchip with Integrated Silver Electrode. *Electroanalysis* **2005,** *17* (13), 1222-1226.

22. Godoy-Caballero, M. d. P.; Acedo-Valenzuela, M. I.; Galeano-Diaz, T.; Costa-Garcia, A.; Fernandez-Abedul, M. T., Microchip electrophoresis with amperometric detection for a novel determination of phenolic compounds in olive oil. *Analyst* **2012,** *137* (21), 5153-5160.

23. Garcia, M.; Escarpa, A., Microchip electrophoresis-copper nanowires for fast and reliable determination of monosaccharides in honey samples. *Electrophoresis* **2014,** *35* (2-3), 425-432.

Appendix-2 COMSOL method editor coding to generate bipolar cell voltammogram

2.1 Coding

```
int n = 20; double DetectorE = -0.40;
for (int i = 1; i < n; ++i) {
  int Counts = 4;
  double Escan = 0.4;
  double SensorCurrent = 0;
  double SensorCurrentmiddle = 0;
  double SensorCurrentnext = 0;
  boolean foundAll = false;
   double DetectorCurrent = 0.00;
  DetectorE = DetectorE+0.02;
   with(model.param());
    set("E1", DetectorE);
  endwith();
  model.study("std1").run();
  DetectorCurrent = Math.abs(model.result().numerical("int1").getReal()[0][0]);
  DeCurrRep[i] = DetectorCurrent;
  with(model.param());
    set("E2", 0.40);
  endwith();
  model.study("std2").run();
  SensorCurrentnext = Math.abs(model.result().numerical("int2").getReal()[0][0]);
  with(model.param());
```

```
  set("E2", 0.40-(Escan/2));
endwith();
SensorCurrent = SensorCurrentmiddle;
SensorCurrentmiddle = SensorCurrentnext;
  model.study("std2").run();
SensorCurrentnext = Math.abs(model.result().numerical("int2").getReal()[0][0]);
  with(model.param());
  set("E2", 0.40-Escan);
   SensorCurrent = SensorCurrentmiddle;
  SensorCurrentmiddle = SensorCurrentnext;
  model.study("std2").run();
  SensorCurrentnext = Math.abs(model.result().numerical("int2").getReal()[0][0]);
   Escan = Escan/2;
  double AppE2test = 0.2;
  double tempcurrent = 0; double tempnext = 0; int test = 1;
   while (foundAll == false) {
    EscanDis[i] = Escan;
     CountsDis[i] = Counts;
    Sensorcurr[i] = SensorCurrent;
    SensorCurrMid[i] = SensorCurrentmiddle;
    SensorCurrnex[i] = SensorCurrentnext;
      if (Counts > 32768) {
      foundAll = true;
```

```
        EscanDis[i] = Escan*2;
      }
     else if (DetectorCurrent < SensorCurrent && DetectorCurrent > SensorCurrentmiddle &&
Counts > 2) {
        with(model.param());
          set("E2", AppE2test+(Escan/2));
           AppE2test = AppE2test+(Escan/2);
          AppE2[i] = AppE2test;
          tempcurrent = SensorCurrent;
          tempnext = SensorCurrentmiddle;
       endwith();
      }
     else if (DetectorCurrent > SensorCurrentnext && DetectorCurrent < SensorCurrentmiddle
&& Counts > 2) {
        with(model.param());
          set("E2", AppE2test-(Escan/2));
          test = test+1;
          AppE2test = AppE2test-(Escan/2);
          AppE2[i] = AppE2test;
          tempcurrent = SensorCurrentmiddle;
          tempnext = SensorCurrentnext;
          endwith();
```

```
    }
    SensorCurrent = tempcurrent; SensorCurrentnext = tempnext;
    model.study("std2").run();
    SensorCurrentmiddle = Math.abs(model.result().numerical("int2").getReal()[0][0]);
    Escan = Escan/2;
    test = test+1; Counts = Counts*2;
  }
}
```